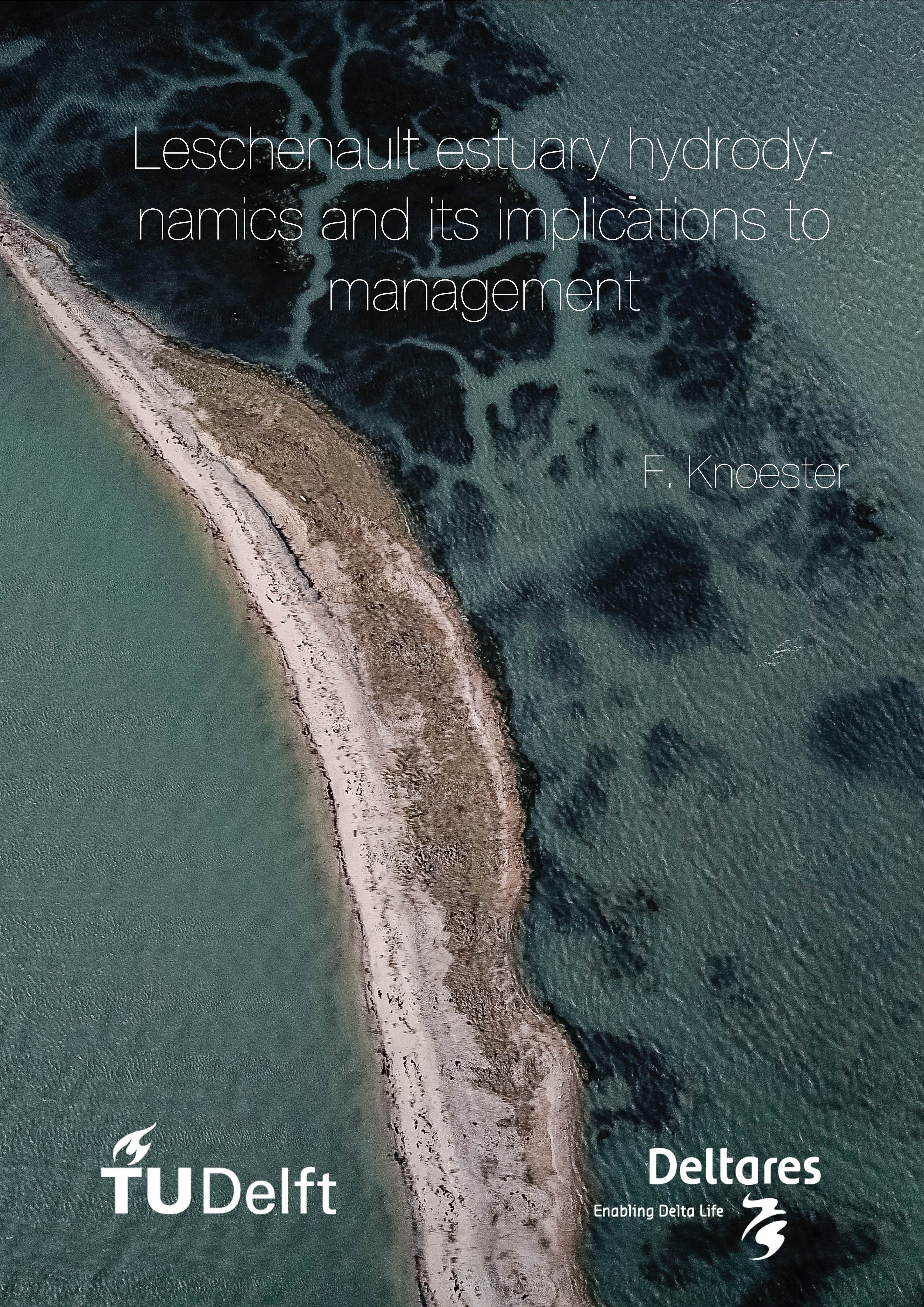

Leschenault estuary hydrodynamics and its implications to management

F. Knoester

TU Delft

Deltares
Enabling Delta Life

Leschenault estuary hydrodynamics and its implications to management

by

F. (Ferdinand) Knoester

October 2, 2020

to obtain the degree of Master of Science
at Delft University of Technology,
to be defended publicly on Friday October 9, 2020 at 09:00.

Student number:	**4299450**	
Thesis committee:	**Prof. dr. ir. Z.B. Wang,**	**TU Delft/Deltares, chair**
	Dr. Qinghua Ye,	**TU Delft/Deltares**
	Dr. ir. P.L.M. de Vet,	**TU Delft/Deltares**
	Dr. ir. J.D. Bricker,	**TU Delft**
	Dr. ir. Alessandra Mantovanelli,	**DWER**

An electronic version of this thesis is available at http://repository.tudelft.nl/.

Cover photo: https://unsplash.com/s/photos/estuary

GOVERNMENT OF WESTERN AUSTRALIA
Department of Water and Environmental Regulation

Deltares
Enabling Delta Life

Preface

This thesis accomplishes the Master of Science programme at Delft University of Technology. The research was partly carried out at Deltares in Delft and partly at the Department of Water and Environmental Regulation in Joondalup, Western Australia.

First of all I would like to thank everyone who have been with me, supported me and helped me in the past 12 months. From the first day of work at Deltares to my last day of work in my own sleeping room, it has been a true roller coaster. The first six months at Deltares I was surrounded by friends, who have made my time at Deltares very pleasant and who have helped me a lot. I would like to thank Qinghua Ye and Lodewijk de Vet for their unconditional help, enthusiasm and the infinite amount of time they have made available for me. I would like to thank Prof. Wang and Jeremy Bricker who helped me to approach my thesis from different perspectives and who always provided me with valuable advice. In the first six months I also became convenient with programs I was not really convenient with at first. This would never have been possible without the help of Herman Kernkamp and Julien Groenenboom of Deltares for which I'm really grateful. I would also thank everyone of Deltares whom I have crossed paths with.

My Master's thesis will always be remembered by the unprecedented outbreak of COVID-19. The moment I departed to Perth, the pandemic just hit the North of Italy. The world, still being a little naive at that time, could not foresee what was still to come. After two weeks in Perth, the situation got worse day-by-day, which urged me to come back to the Netherlands. Despite the major setback of leaving Perth after three weeks, I more than ever realized that there are more important things in live where you should strive for. Nevertheless, the three weeks in Perth have been a fantastic experience and I feel honoured that I have been part of this cooperation. I would therefore like to thank Alessandra Mantovanelli for her inspirational knowledge, enthusiasm, kindness, hospitality and all her help. I would also like to Peta Kelsey and Eduardo da Silva who have made me feel Perth like my home for three weeks. The excursion to the Leschenault Estuary have been very interesting and fruitful. A big thanks to Gayan Gunaratne for his help on the river discharges and my sincere thanks to DWER and everyone involved for all the support.

To my friends and family and most importantly Kien, a big thanks for everything!

Ferdi Knoester
Amsterdam, October 2020

Nomenclature

Abbreviations

DWER	Department of Water and Environmental Regulation
BoM	Bureau of Meteorology
DoT	Department of Transport

Symbols

t	s	Time
m	kg	Mass
$\bigtriangledown$	-	Flux divergence
P	-	Fluid property
ρ	kg/m^3	Density
p	Pa	Pressure
$\overrightarrow{u}$	m/s	Velocity vector u-direction
$\overrightarrow{v}$	m/s	Velocity vector v-direction
$\overrightarrow{w}$	m/s	Velocity vector w-direction
x	m	Coordinate along x-axis
y	m	Coordinate along y-axis
z	m	Coordinate along z-axis
S	PSU	Salinity
K_x	m^2/s	Kinematic eddy diffusion coefficient x-direction
K_y	m^2/s	Kinematic eddy diffusion coefficients y-direction
K_z	m^2/s	Kinematic eddy diffusion coefficients z-direction
M_S	$kg/(ms)$	Salt flux per unit width
h	m	Depth
T	$^{\circ}C$	Temperature
T_d	$^{\circ}C$	Dew point temperature
S_a	PSU	Mean salinity
u_a	m/s	Mean current velocity
S_s	PSU	Steady-state salinity
u_s	m/s	Steady-state velocity
S_t	PSU	Tidal salinity
u_t	m/s	Tidal velocity

Symbols

S'	PSU	Deviation salinity
u'	m/s	Deviation velocity
h_a	m	Time-averaged water depth
$h_t(x,t)$	m	Tidal height
$\overrightarrow{F}$	N	Force vector
$\overrightarrow{a}$	N	Acceleration vector
μ	m^2/s	Absolute or dynamic viscosity
$\overrightarrow{g}$	N	Gravitational force
Ω	rad/s	Angular velocity of the earth
C	kg/m^3	Concentration
V	m/s	Flow velocity
Q	m^3/s	Flow rate
A	m^2	Area
Ri	-	Gradient Richardson number
Ri_L	-	Richardson layer number
ϕ	$\circ$	Tidal phase

Abstract

Estuaries are dynamic partially enclosed water bodies that are constantly or periodically influenced by the ocean and at least occasionally impacted by river discharge. This creates unique but fragile ecosystems that have to be managed with care in order to be recreationally, economically and ecologically valuable. One of the management issues is water quality, which is mainly influenced by hydrodynamic processes and other processes affecting the transport of dissolved or suspended materials. The understanding of the hydrodynamic processes of an estuary and its physical drivers is crucial for management.

One of these fragile ecosystems that have been prone to many human interventions in the past, is the Leschenault Estuary. In this thesis, a 3D-numerical model is developed in D-Flow FM to unravel the governing hydrodynamics of the Leschenault Estuary. Besides, field measurements provided data used as input for the numerical model and more information about the dynamics of the Leschenault Estuary. Most importantly, a methodology is proposed to improve the efficiency in drawing relevant conclusions from observed and modelled data. Efficient and easy-to-apply classification methods are therefore considered that could be powerful management tools. To validate this methodology, a scenario has been considered where the Preston River is aligned to the Bunbury Port.

The governing hydrodynamic processes in the Leschenault Estuary are internal circulation, stratification and turbulence, which are predominantly driven by the freshwater discharge and the tides. However, the dominant physical processes are highly dependent on the seasonal conditions and the specific locations. In general, three different seasonal conditions were distinguished: normal summer, normal winter and peak river discharge conditions.
In summer, freshwater discharge is reduced, which increased the impact of tidal stirring and vertical mixing. In winter, the high river flow generated more stratified flows and under peak discharge conditions some areas of the estuary presented salt-wedge regimes. The Leschenault Estuary can be spatially subdivided in four distinct regions (southern, central, northern and riverine basin), based on the governing hydrodynamic processes. The southern basin is the most dynamic and can not be specified by a single regime due to the influence of the ocean, the Preston River, the Collie River and the northern regions. The central and northern basins were classified as partially-mixed throughout the year and showed weakly to strongly stratified water bodies, depending on the seasonal conditions. Furthermore, a classical estuarine circulation develops under normal winter conditions. In summer, the northern regions become hypersaline, generating an inverse circulation in the central and northern basins. The Collie River is characterized by a partially-mixed water body, with high stratification. Under peak discharge conditions, the salt wedge can be temporally forced out of the river and partially out of the estuary. Winds, waves and Coriolis have a

significant influence on the hydrodynamics of the central and northern basin, due to their shallow and stagnant waters.

The driving forces of the salt transport were obtained by the decomposition of the salt flux. The main physical processes affecting the salt transport between the estuary and the ocean along the transect of the ’Cut’ over the whole year and in winter were freshwater discharge, topographic trapping and Stokes drift. Stokes drift was dominant in summer, followed by freshwater discharge and topographic trapping. This indicates that regardless the season the advective terms were dominant drivers of the salt transport. It also indicates the seasonality of the salt flux at the ’Cut’. The dominant salt flux components at the central basin was the Stokes drift, followed by freshwater discharge and topographic trapping.

The Preston River alignment was compared with its current location to provide useful information for management and to evaluate the efficacy of the adopted classification methods. The scenario results were significantly different than the initial model results and the Preston River alignment had a substantial impact on the hydrodynamics of the Bunbury Port and the southern basin. Bunbury Port circulation became more stratified and its seasonal variation was increased, while the southern basin became less dynamic and partially-mixed, with low to high stratification. The Collie River and central and northern basins however remained almost unaffected. Further, the physical drivers of the salt transport did not vary much but the role of the Stokes drift became relatively more pronounced at the ‘Cut’, due to the decreased influence of freshwater discharge and topographic trapping. At the central basin, the Preston River alignment had a negligible effect on the physical drivers of the salt transport. However, larger spatial and temporal variability of salinity and temperature distributions were observed. It is therefore recommended to conduct an additional ecological valuation of this intervention.

Valuable insights were presented in this thesis that have been critically validated. The used methods have proven to be efficient and valuable tools for management.

Contents

List of Figures

List of Tables

1

Introduction

1.1 Context

In Western Australia, more than 80% of the population lives around estuaries (DWER, 2020). Estuaries are environmentally, ecologically and recreationally valuable ecosystems and require careful management. However, the 166 estuaries in Western Australia are under threat impacted by climate change and human interference like industry, housing, recreation and agriculture (DWER, 2020). The Western Australia State Government therefore launched the Healthy Estuaries WA program, which focuses on improving the health of several important estuaries, amongst others the Leschenault Estuary (DWER, 2020).

The Leschenault Estuary is located at the south-west coast of Western Australia, approximately 180 km south of Perth (Figure 1.1). The estuarine system known today consists of the Leschenault Estuary, the Leschenault Inlet, the Leschenault Peninsula, the Inner Harbour and the Koombana Bay. The Inner Harbour is part of the Bunbury Port, which has exploited this part of the estuary for industry purposes. The Leschenault Estuary is connected to the Indian Ocean via the artificial channel, the 'Cut', which has been constructed in 1951 simultaneously with the development of the Bunbury Port. The 'Cut' has been constructed to guarantee the health of the estuary by stimulating the flow and circulation inside the estuary.

The Leschenault Estuary has a diurnal micro-tidal regime, with a mean spring range of 0.5 m (Semeniuk et al., 2000). The estuary covers a total surface area of 25 km^2 and is approximately 13.5 km long and 2.5 km wide (McKenna, 2007). Furthermore, the estuary functions as a river mouth for multiple rivers surrounding the estuary, e.g. the Parkfield Drain, Wellesley River, Brunswick River, (lower) Collie River, Ferguson River and Preston River (Figure 1.2). The total catchment area of this system is around 1981 km^2 (McKenna, 2007).

The Leschenault Estuary has been quite dynamic in the past 7000 years until it developed into a tide-dominated lagoon (McKenna, 2004). Since then, human interference has been more impactful than ever and altered the estuary's shape, environment and dynamics. Whereas

Figure 1.1: Australian map (Google)

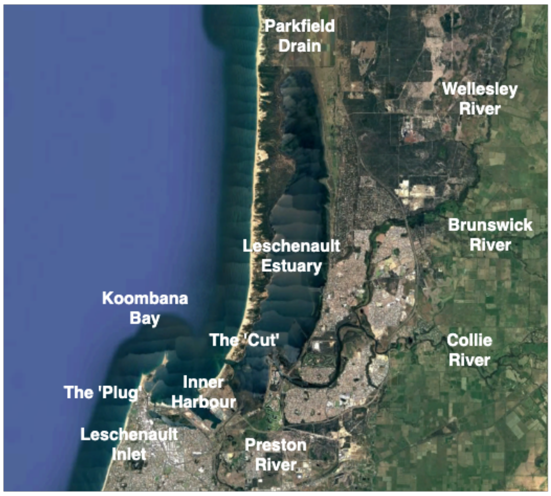

Figure 1.2: Leschenault Estuary region (Google)

changes to the estuary's shape can be observed directly, changes to environment and hydro- and sediment dynamics need decades to adapt. In 1933, the first major alteration was executed by the construction of the Wellington Dam, which altered the freshwater run-off into the Leschenault Estuary (Wooltorton, 2013). An even more impactful event took place with the construction of the of the Bunbury Port, which led to the development of the 'Cut' and the infilling of the natural inlet of the estuary (Wooltorton, 2013). Besides, the construction of the Parkfield Drain and the realignment of the Preston River also had a substantial impact on the Leschenault Estuary. At present the Leschenault Estuary area looks like the aerial overview depicted in Figure 1.2.

1.2 Problem definition

The understanding of the main physical drivers of estuary hydrodynamics is crucial for water quality management in order to make considered and efficient decisions. In the past anthropogenic alterations like the excavation of the 'Cut' and the development of the Inner Harbour have been destructive for the Leschenault Estuary's ecology and drastically changed the estuary's hydrodynamics (Wooltorton, 2013). These are examples of situations in which unsubstantiated judgements have been the foundation of decision-making instead of evidence by observed data or modelled data. This increases the chance of the development of housing, industry, agriculture or recreation in sensitive areas where such development can be detrimental to its environment (Thomson et al., 2017). Moreover, unconsidered management decisions can be cheaper on the first sight, but can at the end be more expensive. In case development causes substantial pressure to its environment, solutions should be investigated to prevent further decline (Thomson et al., 2017). This of course costs more money than forecasted. Besides, a degrading environment also causes a lot of harm to the local community and stakeholders involved in the Leschenault Estuary (Thomson et al., 2017).

As is stated in Thomson et al. (2017), Western Australia's estuary management should have "a stable and enduring, science-based monitoring, modelling and reporting platform" as well as "a modelling platform that can provide robust, auditable results including forecasts and scenarios of potential management options". Before this can be achieved the main drivers of the estuary's hydrodynamics have to be fully comprehended. As soon there is a fundamental understanding in these drivers, impacts of management actions to the Leschenault Estuary can be forecasted. The Bunbury Port will undergo further development in the near future. A major alteration to the system, will be the alignment of the Preston River, which will be aligned to the Bunbury Port. This will insurmountably lead to complications to the estuary's dynamics and therefore also indirectly to the estuary's ecology. The need for a better understanding in the estuary's hydrodynamics is thus crucial to visualise the changes to the system. Numerical models and measurement equipment could therefore be of great help. However, efficient methods are of equal importance as the data should be interpreted quickly by management.

> *"Estuarine environments like the Leschenault Estuary, are sensitive systems that require evidence based management in order to maintain their recreational, ecological and economical value. Due to a lack of fundamental understanding in the main physical drivers of the Leschenault Estuary hydrodynamics, water quality management is limited to judgements which could result in expensive and detrimental situations, may need unnecessary regulation and may does harm to the environment and local economies."*

1.3 Research scope

This research focuses on the physical drivers of the governing hydrodynamic processes of the Leschenault Estuary and the classification of the estuary based on its characteristics. Furthermore, efficient and straightforward methods are used to assess the driving forces and to visualise possible changes in the estuary's hydrodynamics in case of alterations to the system. Insight in the estuary's hydrodynamics is crucial in order to make considered decision for water quality management. A 3D numerical model is developed to complement the observed data in order to increase the understanding in the hydrodynamics. Estuaries are complex systems where salt and fresh water continuously mix. Many physical processes are involved, which makes understanding of these systems difficult. A thorough research should thus be conducted concerning the various processes driving the estuarine circulation, e.g. tidal range, river discharge, wind, waves, Coriolis force and the mixing of salt and fresh water masses (Van Leussen and Dronkers, 1988).

As estuarine systems in Australia and more specific in south-western Australia are at risk, evidence-based management is of paramount importance for these systems. The scope of this research is therefore focused on obtaining a fundamental understanding on the main physical drivers of the Leschenault Estuary hydrodynamics. Besides, hands-on experience is gathered while working at the DWER in Australia during a three month stay. The collaboration with the DWER adds an extra dimension to the thesis by incorporating a management perspective and by obtaining experience in the field. This should enhance the process of drawing relevant conclusions from the research results and adds value to thesis in general. At last, the planned alignment of the Preston River could potentially put pressure on the Leschenault Estuary ecosystem and should therefore carefully be investigated. The Preston River alignment case study is also used to employ different classification techniques that could benefit decision-making on a management level.

1.4 Research objective and questions

The following research objective is defined:

> *"Improve the understanding of the processes governing the hydrodynamics in the Leschenault Estuary relevant for management purposes, and to forecast changes in water quality and enhance environmental regulatory decision-making, by using efficient and easy-to-apply methods for the observed and modelled data"*

In addition to the research objective, the following research questions are formulated:

1. *What are the governing hydrodynamic processes of the Leschenault Estuary and their main physical drivers?*

2. *What are efficient classification techniques for management and how can the Leschenault Estuary be classified?*

3. *What are the main physical drivers of the salt transport in the Leschenault Estuary?*

4. *How will the Preston River Alignment change the hydrodynamics, the classification and the salt transport in the Leschenault Estuary and which conclusion can be drawn from these changes on a management level?*

1.5 Cooperation with Deltares and DWER

This study is conducted in cooperation with Deltares and the Department of Water and Environmental Regulation (DWER). Most of the research is executed at Deltares, who provides a flexible working space, software and a laptop. Qinghua Ye and Lodewijk de Vet from Deltares are the daily supervisors and give advice where needed. Prof. Wang is the chairman of the committee and is also related to Deltares and Jeremy Bricker is related to the DUT. The research is partly conducted at DWER during a three month internship, where Alessandra Mantovanelli is the daily supervisor. In cooperation with DWER new measurements are conducted that complement the available old data. DWER is responsible for the management of the Leschenault Estuary and could thus be of great value in the process of drawing relevant conclusions. The main focus of DWER over the years has been the improvement of water quality and the prevention of further water decline in Western Australia's estuaries. To achieve this, multiple management plans have been drawn up over the years. Besides, DWER provides a working space, accommodation and transfer from and to Perth.

1.6 Approach

This research is approached in four steps that all have their own goal. These steps are noticeable in this report by the different parts, which are summarized in Figure 1.3. First, a system analysis is conducted to obtain a better understanding in the governing hydrodynamic estuaries in general. In Part II, the observed data is analysed and the model set-up is summarized. In Part III, the model results are calibrated and validated against observed data but furthermore the model results are processed in order to draw valuable conclusions. These conclusions are further presented in Part IV. Besides, the overall process and findings are discussed and recommendations are given for follow-up studies. All parts are further subdivided in chapters, which all have a brief discussion and conclusion section at the end of the chapter.

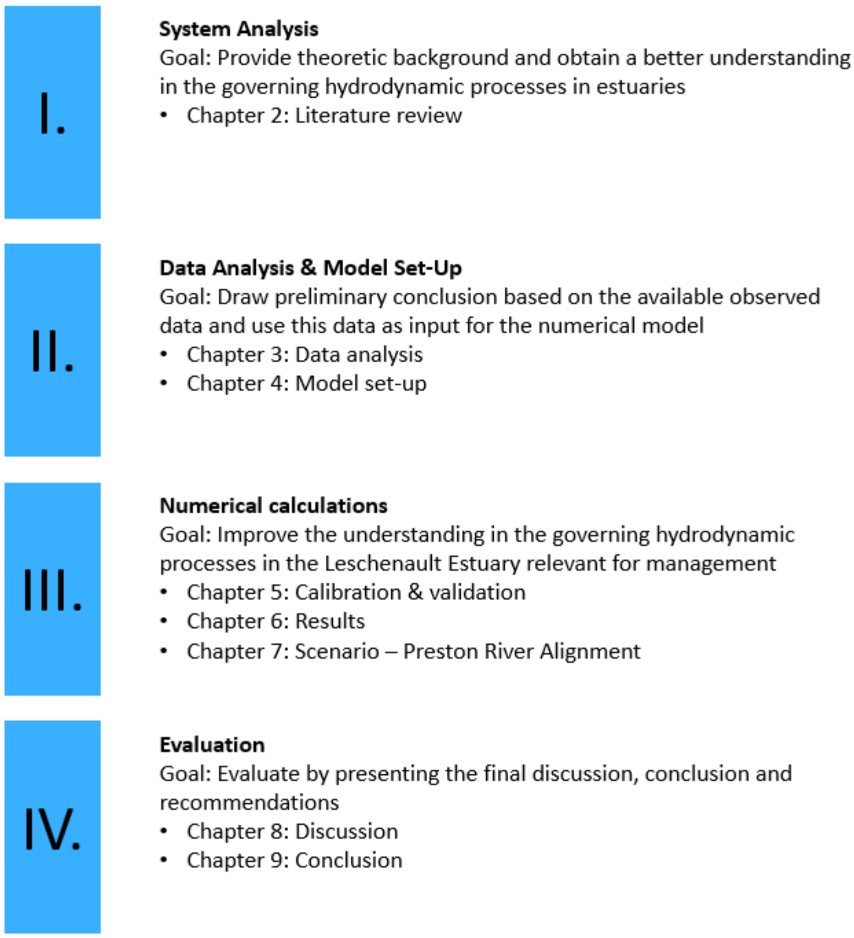

Figure 1.3: The summarized approach of this master thesis

1.6.1 Part I: System analysis

The system analysis only contains Chapter 1 focused on the theoretical background used to conduct this study. Firstly, the basic theory of the hydrodynamics principles is expounded, including the conservation of mass, the conservation of momentum and the hydrodynamic transport of mass. In addition, the theory behind the decomposition of the salt flux is presented. Secondly, the general estuarine hydrodynamics are discussed, which means the definition, the characteristics, the governing hydrodynamics and the driving forces of these dynamics of estuaries are elaborated. Also, a small section is dedicated to the riverine hydrodynamics as this is an important part of the estuarine system. Besides, detailed information is given about the function of temperature and salinity for water quality management purposes. Also, a brief overview is given of the various classification techniques relevant for this thesis. Lastly, the relevant information about the numerical model used for this thesis is provided.

1.6.2 Part II: Data analysis & model set-up

Part II is subdivided in Chapter 3 Data analysis and Chapter 4 Model set-up. Chapter 3 describes the area of study and gives useful information about the developments done in the past and the general processes affecting the hydrodynamics of estuaries, such as the Leschenault Estuary. Furthermore, the key takeaways of previous studies on the Leschenault Estuary are summarized, which should enhance the model set-up of the numerical model for this thesis. Then, all relevant observed data is analysed and processed in order to draw conclusions and to serve as input for the numerical model. Measurements are also conducted in the field during an excursion to the Leschenault Estuary. An impression of this field trip is included in the last section of Chapter 3. Chapter 4, focuses on the model set-up and gives insight in how the model is developed.

1.6.3 Part III: Numerical calculations

Part I is subdivided in three chapters, Chapter 5 Calibration & validation, Chapter 6 Model results and Chapter 7 Scenario - Preston River alignment. The calibration and validation is conducted in order to measure the reliability and accuracy of the developed model. After a thorough calibration process and sensitivity analysis, the model results are validated against observed data. The final model is then used for further research. The model results are processed in order to draw relevant conclusions for management. The analysis of the model results are categorized into a tidal, circulation, flow velocity, temperature and salinity analysis. Furthermore, the estuary is classified by using a set of classification methods. The used methods are the T-S diagram, the Richardson theory, the normalized vertical distribution profiles and the stratification-circulation diagram. A combination of these methods is used in order to guarantee the reliability of the conclusions and to discuss irregularities found for certain methods. Besides, the salt transport is decomposed in order to unravel the governing physical processes driving the salt flux inside estuaries like the Leschenault Estuary. Chapter 7 is added to this thesis to measure the value and efficiency of the methodology proposed to management. In additions, useful insights and information about the Preston River alignment is presented to management.

1.6.4 Part IV: Evaluation

The evaluation consist of the final conclusion, discussion and recommendations and serve as a tool to rethink about certain decisions made and to evaluate on the results, findings, methodology and overall process.

Part I

System analysis

A comprehensive overview of the hydrodynamic processes affecting the estuarine system is drawn up to elaborate on essential hydrodynamic theory needed for this research.

Chapter 2: Literature Review

2

Literature review

This chapter reviews the general hydrodynamic hydrodynamic principles in Section 2.1. Besides, in Section 2.2 the estuarine hydrodynamics are discussed. In Section 2.3, information is given about the numerical model used for this research.

2.1 Hydrodynamic principles

Before the driving forces of estuarine hydrodynamics can be discussed, the main principles of hydrodynamics in general have to be made clear. The study of hydrodynamics is basically the study of water movement and the driving forces of water (Ji, 2017). According to Ji (2017), the theoretical basis of hydrodynamics is founded on the conservation laws, which consist of the conservation of mass, the conservation of energy and the conservation of momentum.

2.1.1 The conservation of mass

The first conservation law, the conservation of mass, is best expressed by Kundu et al. (2016), who stated that "mass can be neither created nor destroyed", when neglecting nuclear reactions and relativistic effects. This means that in case of surface water, which almost is an incompressible fluid (Ji, 2017), the water flux going into a defined area must be equal to the water flux going out of this defined area. This defined area is also called a control volume and can be visualised as an imaginary balloon where mass inside the balloon is conserved when the balloon expands, contracts or deforms (Kundu et al., 2016). The mass balance equation is derived in Equation 2.1 (Ji, 2017).

$$Mass\,accumulation \;=\; mass\,in \;-\; mass\,out \;+\; source \;-\; sink \tag{2.1}$$

Equation 2.1 is a function of the mass balance of a control volume, where variables can enter, leave or be stored inside. However, the shape and position of the water column stays the same and the inflow minus the outflow must equal the volume change over time. Ji (2017) restated Equation 2.1 as Equation 2.2.

$$dm = (m_{in} - m_{out} + m_r) \cdot dt \tag{2.2}$$

In Equation 2.2, the following variables are mentioned: dm = mass accumulation, m_{in} = flux of rate of mass going in, m_{out} = flux of rate of mass going out, m_r = the net rate of production from all source and sink terms and dt = time increment. To be able to calculate the mass balance in terms of mass flux, Equation 2.2 has to be divided by time (Ji, 2017). This generates Equation 2.3, which is widely used in hydrodynamic and water quality studies and serves as a basic equation for mass conservation according to Ji (2017).

$$\frac{dm}{dt} = \frac{\delta m}{\delta t} + \vec{v} \cdot (\nabla m) = m_{in} - m_{out} + m_r \tag{2.3}$$

Equation 2.3 calculates the total variation over time of a certain mass m by summing up the local variation $\delta m/\delta t$ and the variation caused by advection consisting of the fluid velocity and property gradient $\vec{v} \cdot (m\nabla)$. The right part of Equation 2.3 tells how much mass is leaving, entering and produced in the water column. The amount of produced mass by sinks and sources can be influenced by two factors according to Ji (2017): there are other sources that have discharged into the water column or chemical or biological reactions have occurred inside the water column. Equation 2.3 determines the evolution of a certain mass of a fluid in motion over space (x, y, z) and time (t) and can also be used for any other conservative fluid property P that is only dependent of advection and dispersion (De Miranda et al., 2017). Equation 2.3 can thus be rewritten as Equation 2.4, when neglecting any sinks and sources and biological reactions.

$$\frac{dP}{dt} = \frac{\delta P}{\delta t} + \vec{v} \cdot (P\nabla) \tag{2.4}$$

In Equation 2.4: P = fluid property, $\vec{v}$ = velocity vector and ∇ = flux divergence. The flux divergence ∇ represents the net loss of mass at a point due to divergence of a flux (Kundu et al., 2016). This means that when $\vec{v} \cdot (P\nabla)$ is positive, the local density of fluid property P will decrease (Kundu et al., 2016). Kundu et al. (2016) explained furthermore that the flux divergence ∇ is also called a transport term, as it only transfers mass from one region to another and has no effect on the net contribution of an entire field. Equation 2.4 is called the continuity equation and expresses the principle of conservation of mass in a differential way (Kundu et al., 2016). Equation 2.4 can be simplified when considering a steady-state situation with a local variation $\delta P/\delta t$ equals 0 and can even further be simplified to a uniform situation with zero spatial variation (De Miranda et al., 2017). When neglecting molecular and turbulent diffusion the concentration of the adjacent components in a fluid remains constant, which means the total variation of a property over space and time is equal to zero (De Miranda et al., 2017). This situation is derived in Equation 2.5.

$$\frac{dP}{dt} = \frac{\delta P}{\delta t} + \vec{v} \cdot (P\nabla) = 0 \tag{2.5}$$

Equation 2.4 can be redefined in a simplified form to Equation 2.6 for convenient purposes.

$$\frac{d}{dt} = \frac{\delta}{\delta t} + \vec{v} \cdot (\nabla) = 0 \tag{2.6}$$

In the situation defined in Equation 2.6, an equilibrium exists between the local and advective variation. When considering a situation where a fluid is in steady-state, which means $\vec{v} \cdot (\nabla)$ is equal to zero, Equation 2.6 can be redefined in Cartesian coordinates (Ji, 2017) to Equation 2.7. In Equation 2.7, the situation of a property of a fluid in motion that does not vary over time but solely varies in space is mathematically formulated.

$$\frac{\delta u}{\delta x} + \frac{\delta v}{\delta y} + \frac{\delta w}{\delta z} = 0 \tag{2.7}$$

Salt balance

The conservation of salt uses the same principle as the conservation of mass due to the conservative character of salinity, which means the local variation of salt over space and time is only due to advection and dispersion except at the boundaries (De Miranda et al., 2017). The property P (Equation 2.5) can be replaced by the amount of salinity S (Equation 2.8):

$$\frac{dS}{dt} = \frac{\delta S}{\delta t} + \vec{v} \cdot (S\nabla) = 0 \tag{2.8}$$

Equation 2.8 can also be formulated in Cartesian coordinates, which result in Equation 2.9. It should be noted that Equation 2.9 still describes the situation where the dispersion is disregarded.

$$\frac{\delta S}{dt} + u\frac{\delta S}{\delta x} + v\frac{\delta S}{\delta y} + w\frac{\delta S}{\delta z} = \frac{dS}{dt} = 0 \tag{2.9}$$

As is further explained in Section 2.2.2, an important driver of in estuaries is turbulent diffusion, which should therefore be considered when calculating the salt balance in an estuary. Therefore, Pritchard (1952), Cameron and Pritchard (1963) and Sverdrup et al. (1942), developed an equation which also incorporates turbulent diffusion, shown in Equation 2.10.

$$\frac{\delta S}{\delta t} + u\frac{\delta S}{\delta x} + v\frac{\delta S}{\delta y} + w\frac{\delta S}{\delta z} = \frac{\delta}{\delta x}(K_x\frac{\delta S}{\delta x}) + \frac{\delta}{\delta y}(K_y\frac{\delta S}{\delta y}) + \frac{\delta}{\delta z}(K_z\frac{\delta S}{\delta z}) \tag{2.10}$$

In Equation 2.10, the right-hand side of the equation represents the influence of turbulent diffusion, where K_z, K_y and K_x are the kinematic eddy diffusion coefficients. The coefficients determine the cross-correlation between the turbulent fluctuations in velocity (u', v' and w') and the salinity (S') (De Miranda et al., 2017). The diffusion coefficients have been developed by Osborne Reynolds in 1894 according to De Miranda et al. (2017) and are shown in Equation 2.11.

$$K_x = -\frac{\langle u'S'\rangle}{\frac{\delta S}{\delta x}} \; ; \; K_y = -\frac{\langle v'S'\rangle}{\frac{\delta S}{\delta y}} \; ; \; K_z = -\frac{\langle w'S'\rangle}{\frac{\delta S}{\delta z}} \tag{2.11}$$

The diffusion coefficients in $[m^2/s]$ have equal dimensions when multiplying by the density. According to Miranda and Castro Filho (1996) as in Pritchard (1954), the most dominant factors in the salt balance are the horizontal advective salt flux (ρSu) and the vertical non-advective salt flux ($\rho\langle w'S'\rangle$) and the brackets $\langle\rangle$ indicate time averaged values. The latter is dependent on the tidal forcing and the vertical salinity stratification (De Miranda et al., 2017). The same study shows that the mean vertical advective salt flux (ρSw) is less significant and the horizontal non-advective salt flux ($\rho\langle u'S'\rangle$) has only a small influence.

Salt transport

The salt balance is maintained by salt fluxes as already became clear in the previous paragraph. A distinction can be made between factors influencing the landward salt transport in estuaries, namely gravitational circulation and tidal flooding, and the seaward transport of salt, namely the ebb tidal current, the reversal of the tidal oscillation, the gravitational circulation and the freshwater discharge (De Miranda et al., 2017). Hunkins (1981) confirmed the studies on salt transport of Pritchard (1954) by investigating the salt dispersion in the Hudson River. Hunkins (1981) discovered that the mixing in the landward direction is more related to dispersion than diffusion, due to the advective and vertical turbulent diffusion component mainly driven by gravitational circulation, winds and tides. According to De Miranda et al. (2017), measurements of salinity and current velocity are needed to assess the influence of advective and non-advective salt fluxes. Therefore, De Miranda et al. (2017) developed Equation 2.12, which represents the salt flux per unit width averaged over depth and time in $kg/(ms)$ in a simplified laterally homogeneous estuary.

$$M_S \;=\; \int_0^h \rho u S dz \;=\; \langle \overline{\rho u S} h\rangle \tag{2.12}$$

In Equation 2.12, u is the longitudinal velocity component and S is the salinity. The overline above the first three characters of Equation 2.12 indicates depth averaged values. To calculate the non-tidal salt transport T_s, in a time period T of a minimum of one tidal cycle, Equation 2.13 can be used (Miranda and Castro Filho, 1996).

$$T_s \;=\; \langle M_S\rangle \;=\; \frac{1}{T}\int_0^T M_s dt \;=\; \langle \overline{\rho u S} h\rangle \tag{2.13}$$

The mean density in Equation 2.13 is determined by using state equations for sea water (De Miranda et al., 2017). Equations 2.14 and 2.15 are used to calculate the time and space averaged current velocity and salinity respectively (Miranda and Castro Filho, 1996).

$$\langle \overline{u}\rangle \;=\; u_a \;=\; \frac{1}{T}[\frac{1}{h}\int_0^h u(x,z,t)]dt \tag{2.14}$$

$$\langle \overline{S}\rangle \;=\; S_a \;=\; \frac{1}{T}[\frac{1}{h}\int_0^h S(x,z,t)]dt \tag{2.15}$$

Bowden (1963) as in De Miranda et al. (2017) noticed that the advective salt transport also had a dispersive character, despite the advective nature of Equation 2.13. It was therefore key to separate the dominant advective and non-advective components to obtain a better understanding in the landward and seaward salt transport (De Miranda et al., 2017). With the help of studies done by Bowden (1963), Fischer (1976), Hunkins (1981) and Kjerfve (1986), four different salinity and velocity components were identified and two water depth components for a laterally homogeneous estuary or a simplified estuary where the salt transport is calculated of segment perpendicular to the mean flow at time t per unit width. The decomposed current velocity and salinity profiles can be calculated by using Equation 2.16 and 2.17.

$$u(x,z,t) \;=\; u_a(x) \;+\; u_t(x,t) \;+\; u_s(x,z) \;+\; u'(x,z,t) \tag{2.16}$$

$$S(x,z,t) \;=\; S_a(x) \;+\; S_t(x,t) \;+\; S_s(x,z) \;+\; S'(x,z,t) \tag{2.17}$$

In Equation 2.16 and 2.17, four decomposed components can be derived from the subscripts: the mean (a), the tidal (t), the steady-state (s) and the deviation ($'$) term (De Miranda et al., 2017). The mean current velocity u_a and the mean salinity S_a are equal to $\langle\overline{u}\rangle$ and $\langle\overline{S}\rangle$ and can be computed with Equation 2.14 and 2.15 respectively. The tidal and steady-state terms of Equation 2.16 and 2.17 consider the barotropic (tidal) and baroclinic (steady-state component of the gravitational circulation) respectively (Miranda and Castro Filho, 1996). The tidal and steady-state terms can be calculated by using Equation 2.18 to 2.21.

$$u_t \;=\; \overline{u} \;-\; u_a \tag{2.18}$$

$$S_t \;=\; \overline{S} \;-\; S_a \tag{2.19}$$

$$u_s \;=\; \langle u\rangle \;-\; u_a \tag{2.20}$$

$$S_t \;=\; \langle S\rangle \;-\; S_a \tag{2.21}$$

The remainders of Equation 2.16 and 2.17, are the deviation terms and represent the small-scale physical turbulence observed in estuaries and can be calculated by using Equation 2.22 and 2.23 respectively (Miranda and Castro Filho, 1996).

$$u' \;=\; u \;-\; u_a \;-\; u_t \;-\; u_s \tag{2.22}$$

$$S' \;=\; S \;-\; S_a \;-\; S_t \;-\; S_s \tag{2.23}$$

As has already been explained earlier in this section, the water depth profile can be decomposed into two components: the time-averaged water depth $h_a = \langle h\rangle$ and the tidal height $h_t(x,t)$ (Miranda and Castro Filho, 1996). The water depth profile can be computed with Equation 2.24.

$$h(x,t) \;=\; h_a \;+\; h_t(x,t) \tag{2.24}$$

By substituting Equation 2.16, 2.17 and 2.24 into Equation 2.13, 32 advective salt transport terms can be distinguished in a steady-state situation (Miranda and Castro Filho, 1996). However, many of these terms can be neglected after being averaged over time and depth (Miranda and Castro Filho, 1996). Furthermore, other terms can be neglected, because there is no apparent correlation between the tidal, steady-state and deviation components (Miranda and Castro Filho, 1996). After filtering the negligible terms, seven dominant terms remain, which in total cover the total salt transport over one tidal cycle and per unit width. The total salt transport can be calculated according Equation 2.25.

$$\begin{aligned} T_s \ = \ \overline{\rho}[[u_a h_a + \langle h_t u_t \rangle] S_a \ + \ h_a \langle u_t S_t \rangle \ + \ h_a \overline{u_s S_s} \\ + \, h_a \langle \overline{u}' \overline{S}' \rangle \ + \ \langle u_t S_t h_t \rangle \ + \ u_a \langle S_t h_t \rangle] \end{aligned} \tag{2.25}$$

Equation 2.25 can also de redefined as Equation 2.26, where the seven terms are indicated with a capital letter ranging from A to G.

$$T_s \ = \ A \ + \ B \ + \ C \ + \ D \ + \ E \ + \ F \ + \ G \tag{2.26}$$

A brief overview of the seven distinct salt transport terms is presented in Table 2.1. The first component A in Equation 2.26, indicate the advection of salt in seaward direction driven by the mean velocity u. The second component B, represents the salt transport due to tidal wave propagation in a estuarine channel with an inclined topography also known as Stokes' drift (De Miranda et al., 2017). Both terms A and B are advective processes that mainly transport salt in seaward direction and therefore tend to reduce the salinity of estuaries and tend to sharpen the gradient between salt and fresh water (Hunkins, 1981). Both terms are most important for estuaries with macro-tidal regimes according to De Miranda et al. (2017). The influence of term B vanishes in case of a standing wave, where the tidal height and tidal velocity are 90° out of phase, because it is averaged over the tidal cycle (De Miranda et al., 2017). In this case, salt is transported out of the estuary. In case of a long progressive wave, term B drives a negative salt transport in upstream direction. This is counteracted by the advective salt transport of the mean velocity of the freshwater discharge De Miranda et al. (2017).

Salt transport component	**Physical process**	**Formulation**
A - Total freshwater discharge	Freshwater discharge	$\overline{\rho} u_a h_a S_a$
B - Stokes drift/progressive tidal wave	Freshwater discharge	$\overline{\rho}\langle u_t h_t \rangle S_a$
C - Tidal correlation	Topographic trapping	$\overline{\rho} h_a \langle u_t S_t \rangle$
D'- Steady shear dispersion	Gravitational circulation	$\overline{\rho} h_a \overline{u_s S_s}$
E - Steady shear dispersion	Bathymetric tidal pumping and steady wind effect	$\overline{\rho} h_a \langle \overline{u' S'} \rangle$
F - Oscillatory dispersion	Tidal shear	$\overline{\rho}\langle u_t S_t h_t \rangle$
G - Oscillatory dispersion	Wind fluctuations	$\overline{\rho} u_a \langle S_t h_t \rangle$

Table 2.1: Salt transport components and their driving physical process (De Miranda et al., 2017)

Term C, the tidal correlation component, is calculated by the multiplication of the mean correlation of the summation of velocity u_t and salinity S_t with the mean water depth h_a

(De Miranda et al., 2017). The importance of the tidal correlation component depends on the vertical salinity stratification of the estuary as in List et al. (1979). In case of a well-mixed estuary term C can be neglected, as maximum salinity will be observed after the flood tide, which indicates a 90° phase lag between the u_t and S_t. The phase lag can become smaller than 90° and the water is released at an later stage than the tide itself due to topographic trapping (List et al., 1979). In this case, the term C becomes negative, indicating a landward salt transport. It can also be possible that the estuary is partially-mixed, which indicates a lower salinity oscillation in the lower layers of the estuary due to the less sharp salinity gradients at lower depth (De Miranda et al., 2017). In this case term C becomes positive, which indicates a seaward salt transport.

Term D, the steady shear dispersion component driven by vertical gravitational circulation, is counteracted by the circulation induced by the river discharge (De Miranda et al., 2017). According to De Miranda et al. (2017) the term D is most important in partially-mixed estuaries, is the largest salt dispersion component direct landward and experiences the highest fortnightly and seasonal change. In well-mixed estuaries however, term D is less important.

Component E results from turbulent oscillatory shear and has almost no influence on the salt balance (De Miranda et al., 2017). The time scale of the turbulent oscillatory shear is less than the tidal oscillation generated by the wind (De Miranda et al., 2017). The physical processes of term F and G are tidal shear and wind fluctuations and may be of importance for well-mixed estuaries with a meso-tidal regime. Miranda's study also stated that term F is the oscillatory dispersion computed by the triple correlation of the tidal variations of velocity, water depth and salinity. Term G also represents oscillatory dispersion, but is calculated by multiplying the mean correlation of the tidally varying salinity and water depth by the river discharge velocity u_a (De Miranda et al., 2017).

2.1.2 The conservation of momentum

The second conservation law is the conservation of momentum and is developed from Newton's second law, shown in Equation 2.27 (Kundu et al., 2016). Besides, external forces like wind, there are three dominant forces in hydrodynamcis, namely gravitational force due to the gravitational attraction of the earth, water pressure gradient force due to a pressure gradient in a water body and a viscous force due to water viscosity and turbulent mixing (Ji, 2017).

$$\vec{F} = m \cdot \vec{a} \tag{2.27}$$

According to Kundu et al. (2016) and Ji (2017), Equation 2.27 can be rewritten to Equation 2.28 for incompressible fluids by implementing Equation 2.3.

$$\rho\frac{d\vec{v}}{dt} = \frac{\delta\rho\vec{v}}{\delta t} + \nabla \cdot (\rho\vec{v}\vec{v}) = \rho\vec{g} - \nabla p + \mu\nabla^2\vec{v} \tag{2.28}$$

In Equation 2.28, the first term expresses the gravitational factor, where ρ = water density and $\vec{g}$ = gravitational force. The second term represents the water pressure gradient force, where ∇ = divergence flux or gradient operator and p = water pressure. The last and third term indicates the viscous force in case of an incompressible fluid, where μ = absolute or dynamic viscosity (assumed to be constant) and ∇^2 = the Laplacian operator. Equation 2.28 is also called the Navier-Stokes equation and can be changed to Equation 2.29 when considering external forces like the wind and the rotation of the earth (Ji, 2017).

$$\frac{d\vec{v}}{dt} = \frac{\delta\vec{v}}{\delta t} + \nabla \cdot (\vec{v}\vec{v}) = \vec{g} - \frac{1}{\rho}\nabla p + v\nabla^2\vec{v} - 2\vec{\Omega} \cdot \vec{v} + \vec{F}_{fr} \tag{2.29}$$

In Equation 2.29, $\vec{\Omega}$ = angular velocity of the earth, $\vec{F}_{fr}$ = external forces and $v = \frac{\mu}{\rho}$ = kinematic viscosity. The left part of Equation 2.29 represents the acceleration term $\frac{d\vec{v}}{dt}$ and determines how currents change with time and advection of the flow (Ji, 2017). Equation 2.27 expresses the acceleration of the object $\vec{a}$ and the rest of the equation determines the forcing of the acceleration (Ji, 2017). The first term at the right side of Equation 2.29 indicates the gravitational acceleration $\vec{g}$ and always acts towards the centre of the earth (Ji, 2017). The second term is the water pressure gradient term $\frac{1}{\rho}\nabla p$ and expresses the vertical and horizontal water pressure gradient which induces water movement (Ji, 2017). Two pressure gradient components can be derived according to Ji (2017): the barotropic component which is generated by water surface slopes (horizontal) and the baroclinic component which is forced by changes in density (horizontal and vertical). The third term is the viscous term $v\nabla^2\vec{v}$, which includes the impact of water viscosity, but also turbulent mixing (Ji, 2017). The fourth term is the Coriolis force term $2\vec{\Omega} \cdot \vec{v}$, which implies the effects of the rotation of the earth on the movement of water and it is only important for large spatial water surfaces (Ji, 2017). The last term indicates the external force term $\vec{F}_{fr}$ and can consist of all kinds of external forces like wind (Ji, 2017). As mentioned by Ji (2017), it should be noted that the Navier-Stokes equation is too complex to solve analytically and should therefore always be simplified in hydrodynamic models.

2.1.3 Hydrodynamic transport of mass

From a management perspective it is essential to understand the driving forces of transport and fate of contaminants in the environment. These driving forces can be subdivided in four general processes, including advection, dispersion, interphase mass transfer and transformation reactions (Pepper et al., 2011). The first two processes are governed by the conservation of mass and the conservation of momentum. The interphase mass transfer is controlled by the conservation of energy and the last process is regulated by chemical and biological factors.

Advection

Advection is the horizontal bulky mass transport by flows, transporting matter from one region to another without diluting or distorting the material significantly (Ji, 2017). According to Pepper et al. (2011), it is the dominant component in the transport of contaminants and has the same order of magnitude as the rate of a fluid's motion. The movement of the fluid is forced by a horizontal pressure gradient in a water body, e.g. due to temperature or salinity differences (Hardisty, 2007). When water is flowing in a river or estuary, the advection decreases along banks, resulting in a lateral variation of the flow rate across the river or estuary (Ji, 2017). Subsequently, the lateral variation induces turbulent mixing at the frontal areas of the water bodies (Ji, 2017). According to Ji (2017), the lateral advection in rivers is usually small, but the lateral advection might increase in wide and more complex water bodies. Besides advection, there could also be a vertical transport of mass in water bodies (Ji, 2017). This process is called convection and is governed by vertical pressure gradients in the water column (Kothandaraman, 2006). Convection is the main process influencing oceanic currents (Tomczak, 1998), but is usually small in lakes, rivers or estuaries (Ji, 2017).

Dispersion

Dispersion can best be described by the spreading of a material from the centre of a concentration to the outside (Pepper et al., 2011). If a contaminant is disposed in a water body, the patch of material or also called the 'plume' will be transferred mostly by advection. However, the size of this 'plume' is determined by dispersion, as the 'plume' increases in size as it moves. The concentration of the material is decreased by dispersion due to this spreading and mixing effect (Ji, 2017). Dispersion is caused by two phenomena of different magnitude, namely molecular and diffusion turbulent mixing (Pepper et al., 2011). According to Pepper et al. (2011), the first phenomenon, molecular diffusion, is caused by the random movement of molecules and only plays a role on a microscopic level. Here, one can think of a drop of dye in a glass of water who tends to spread until the whole glass is uniformly filled with dye. The material thus tends to move from a region with a high concentration of material towards a region with a lower concentration (Ji, 2017). Because, the small scale of molecular diffusion, the effect is only felt in regions with very low currents, such as at the riverbed (Ji, 2012). On the other hand, turbulent mixing has a higher impact on the transport of matter due to its higher order of magnitude (Pepper et al., 2011). Turbulent mixing is the dominant factor causing dispersion, which is due to the momentum exchange between different parts in a water body (Pepper et al., 2011). Turbulent mixing is a non-uniform process and does not propagate uniformly. Instead, different parts in a water body flow at different velocities (Ji, 2017).

Interphase mass transport and transformation reactions

Other processes that could have impact on the fate and transport of contaminants in water bodies are interphase mass transport and transformation reactions (Pepper et al., 2011). According to Pepper et al. (2011), the interphase mass transport is the process in which a material is transferred from its original phase to other phases. The four most important interphase mass transport processes are stated by Pepper et al. (2011), namely dissolution, evaporation, volatilization and sorption. Dissolution is the process in which materials get dissolved in water, evaporation is the process in which a material is transferred from a solid to a gas, volatilization is the process in which a material is transferred from the water to the atmosphere and sorption is the process in which materials get absorbed by a porous medium (Pepper et al., 2011). At last, transformation reactions could lead to an increase and a decrease of contaminants in a water body, depending on the material Pepper et al. (2011).

Mass balance equation

All these processes have an effect on the distribution of a substances like salinity, dissolved oxygen, nutrients, contaminants, etc. Water quality is qualified according to these substances and it would therefore be of great value to calculate these matters. This can be done with Equation 2.30, as Ji (2012) and De Miranda et al. (2017).

$$\frac{\delta C}{\delta t}+u\frac{\delta C}{\delta x}+v\frac{\delta C}{\delta y}+w\frac{\delta C}{\delta z} = \frac{\delta}{\delta x}(K_{xC}\frac{\delta S}{\delta x})+\frac{\delta}{\delta y}(K_{yC}\frac{\delta C}{\delta y})+\frac{\delta}{\delta z}(K_{zC}\frac{\delta C}{\delta z})+S+R+Q \quad (2.30)$$

The term $\delta C/\delta t$ represents the change in concentration over time. The change in concentration in space due to advection is formulated as $u\frac{\delta C}{\delta x}+v\frac{\delta C}{\delta y}+w\frac{\delta C}{\delta z}$. The change in concentration in space due to dispersion is formulated as $\frac{\delta}{\delta x}(K_{xC}\frac{\delta S}{\delta x})+\frac{\delta}{\delta y}(K_{yC}\frac{\delta C}{\delta y})+\frac{\delta}{\delta z}(K_{zC}\frac{\delta C}{\delta z})$. The S in Equation 2.30 indicates the amount of settling particles and the resuspended particles from the bed in the water. The R in Equation 2.30 has a chemical and/or biological character and refers to the transformation reactions discussed earlier. Terms R and S are out of the scope of this thesis and will not be discussed. The last term represents the load due to external factors like atmospheric forcing, point and non-point sources and open boundary forcing. Atmospheric forcing includes wind, air temperature, solar radiation and precipitation, representing the major components of external forces (Ji, 2017). However, properties like atmospheric humidity, cloud cover and atmospheric pressure can also have a significant influence on the mass balance (Ji, 2017).

2.2 Estuarine hydrodynamics

In this section, the estuarine hydrodynamics is discussed. First, the definition of an estuary is presented in Section 2.2.1. Then, the estuarine hydrodynamics and their driving forces are outlined in Section 2.2.2. In Section 2.2.3, the driving forces of river hydrodynamics and their driving forces are presented. Next, the importance of the water properties temperature and salinity on estuarine systems is highlighted in Section 2.2.4. Lastly, a overview of the different classification methods relevant for estuaries is presented in Section 2.2.5.

2.2.1 Definition of an estuary

The correct definition of an estuary has been largely discussed (Semeniuk et al., 2000). Semeniuk et al. (2000) described that the definition of an estuary has gradually developed over time from its original hydro-chemical concept stated by Ketchum and Rawn (1951). Ketchum and Rawn (1951) defined an estuary as "a body of water where river water mixes with and measurably dilutes sea water". This roughly explains the basic concept of an estuary, but does not consider any exceptions. According to Potter et al. (2010), the first definitions of an estuary considered mostly estuaries located in temperate regions of the northern hemisphere. These northerly located estuaries lack two main features that characterize numerous estuaries on the southern hemisphere. The southern hemisphere estuaries are often periodically separated from the sea due to the formation of sand bars across their mouths and these estuaries can become hypersaline due to dry periods when freshwater input from rivers is low and evaporation is high (Potter et al., 2010). Potter et al. (2010) proposed a renewed definition, namely: "an estuary is a partially enclosed coastal body of water that is either permanently or periodically open to the sea and which receives at least periodic discharge from a river(s), and thus, while its salinity is typically less than that of natural sea water and varies temporally and along its length, it can become hypersaline in regions when evaporative water loss is high and freshwater and tidal inputs are negligible". Estuaries are thus the place where the oceans and the continents overlap, and where saline ocean water and freshwater mix, creating unique environments.

2.2.2 Driving forces of estuarine hydrodynamics

Estuaries are complex water systems influenced by oceans. The understanding of oceanic dynamics is therefore essential to comprehend the estuarine hydrodynamics. A brief overview of oceanic dynamics and its driving forces is provided in Appendix A.1. Estuarine hydrodynamics differs from oceanic dynamics for various reasons. The interaction between tides, freshwater discharge and the estuary's geometry generate currents and mixing inside the estuary. The driving forces of the tidal and sub-tidal currents are friction, barotropic influences, baroclinic forces, wind and Coriolis, depending on the geometry and conditions of the specific estuary (Fugate and Jose, 2019).

Tidal motion

The gravitational attraction between the moon, the earth and the sun generates tides, which are continuously falling and rising water levels (Tomczak, 1998). Differences in tidal elevation generate tidal currents, the repeatedly horizontal flow back and forth according to the tide (Ji, 2017). Tides are long waves (a few hundred to thousands of kilometres) formed by the summation of different tidal constituents, which are harmonic oscillations with an amplitude, a period and a phase (Bosboom and Stive, 2012). Tidal oscillations can be classified as diurnal (a high tide and a low tide per day), semi-diurnal (two high tides and two low tides per day) and mixed (two high tides and two low tides with varying water levels) (Bosboom and Stive, 2012). Whereas in deep oceans the effect of the tide is negligible due to its long wave length and small amplitude, the tidal effect becomes more relevant towards the coast (Tomczak, 1998). This is due to the decreased water depth towards the coast, which increases the tidal amplitude and delays the propagation of the tidal wave crest (Tomczak, 1998). Tidal motion is especially important for estuaries for various reasons. According to Ji (2017), tides are one of the major factors impacting the flushing time of estuaries. Besides, tides are responsible for a large part of the estuary's mixing and produce a residual flow influencing the transport of pollutants over the long term (Ji, 2017). Tides are important for the hydrodynamic, morphologic and water quality processes in estuaries (Ji, 2017). The main factors that have impact on the amplitude and propagation of the tides are the bottom friction, the water depth and the Coriolis force (Ji, 2017). As water depths decrease the effect of friction becomes more substantial, which results in the decrease of the tidal current near the bed. This decrease in tidal current results in an increase in the responsiveness of the currents near the bed to tidal elevation, causing vertical phase differences over the water depth (Ji, 2017). In wide estuaries and oceans, the Coriolis force can have a significant effect on ebb and flood currents as the currents are deflected by the Coriolis effect. In narrow estuaries, the flow is often bidirectional and goes back and forth along the channel (Ji, 2017).

Terrestrial influences

Estuaries are highly influenced by evaporation, precipitation and river discharge (Tomczak, 1998). River discharge strongly affects temperature and salinity values in estuaries producing horizontal density gradients and generating buoyancy-driven flows (Tomczak, 1998). Buoyancy-driven flows are generated by density gradients along the estuary and mixing is induced by velocity shear caused by tides and winds (De Miranda et al., 2017). Stratification depends on the balance between the buoyancy force and the velocity shear (De Miranda et al., 2017). In estuaries, stratification is mainly controlled by thermohaline gradients, which can vary seasonally (Tomczak, 1998). Estuaries are shallow water bodies with small volumes, which increases fluctuations in temperature and salinity. Estuaries can also become hypersaline when the salt flux is insufficient to remove the accumulated salt by evaporation (Tomczak, 1998). According to (Pawlowicz, 2013), density is the most important thermodynamic property in marine environments, depending on water temperature, salinity and pressure. The level of stratification or vertical salinity structure determines the estuary classification, which can be salt wedge, strongly stratified, weakly stratified or vertically mixed ((Prichard, 1955); (Cameron and Pritchard, 1963)). This classification considers the competition between buoyancy forcing from river discharge and mixing from tidal forcing. The estuary classification is further explained in Section 2.2.5.

Friction force

Whereas the friction force in deep oceans can be disregarded, the friction force is important in shallow waters. The friction force, produced by the bed, is directed against the flow and gradually decreases the current velocity to zero near the bed (Huang, 2015).

Barotropic force

Barotropic forces are generated by barotropic pressure gradients caused by water level slopes (Fugate and Jose, 2019). In estuaries, the water level slope is mostly dominated by water level differences between the ocean and the estuary (Fugate and Jose, 2019). However, water level slopes are also created by the freshwater discharge out of the estuary (Fugate and Jose, 2019). The water level slopes force water from the higher pressure zone under the top of the slope to the lower pressure zone with lower water level (Fugate and Jose, 2019).

Baroclinic force

Baroclinic forces are generated by baroclinic pressure gradients caused by differences in water density (Fugate and Jose, 2019). In estuaries, the effect of pressure on water density is negligible, which means the density is determined by salinity and temperature (Fugate and Jose, 2019). Baroclinic pressure gradients increase with depth in the water column (Fugate and Jose, 2019). In partially-mixed estuaries, the water is least dense at the fresher estuary head and the water is denser at the saline estuary mouth. Considering both baroclinic and barotropic forces, this leads to a two-layered sub-tidal current (tidally-averaged), with freshwater flowing out of the estuary at the surface and saline ocean water flowing into the estuary at the bed (Figure 2.1).

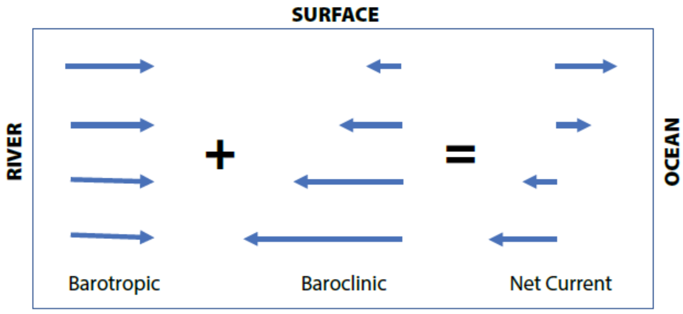

Figure 2.1: Barotropic and baroclinic currents and the net current over the vertical axis of a partially-mixed estuary (Fugate and Jose, 2019)

Wind

Wind can be a dominant force in controlling the estuarine bidirectional circulation and in decreasing or increasing the vertical density stratification (Scully et al., 2005). Wind can play an important role in straining the along-channel density gradient (Scully et al., 2005). Down-estuary winds might increase the tidally-averaged vertical shear and up-estuary winds might reduce or even reverse the vertical shear (Scully et al., 2005). For down-estuary winds this means the vertical density stratification is increased and for up-estuary winds this means the vertical density stratification is reduced (Scully et al., 2005).

Coriolis

The Coriolis effect is the deflection of moving objects due to the Earth's rotation to the right on the Northern Hemisphere and to the left on the Southern Hemisphere (Ji, 2017). The Coriolis force might be an important factor in estuaries, depending on the time and length scales of the physical properties (Fugate and Jose, 2019). In larger estuaries, the effect of Coriolis can be significant, but in smaller estuaries the effect of Coriolis is negligible (Fugate and Jose, 2019). The effect of Coriolis can be determined by applying the Rossby number (Equation 2.31).

$$Ro = |\frac{U}{Wf}| \tag{2.31}$$

Where Ro represents the Rossby number, U is the mean downstream velocity, W is the estuary width and f is the Coriolis parameter. For Ro « 1, the effect of Coriolis becomes more important and for Ro » 1, the effect of Coriolis is negligible (Cossu et al., 2010). The Coriolis parameter is calculated by using Equation 2.32, where Ω is the rotation rate of the earth and θ is the latitude (Cossu et al., 2010).

$$f = 2\Omega sin(\theta) \tag{2.32}$$

2.2.3 Driving forces of river hydrodynamics

The hydrodynamics of rivers differ from those of estuaries and lakes. Flow velocities in rivers are often higher than in lakes and rivers (Ji, 2012). While the flow direction in rivers is mainly downstream, estuarine circulation is complex and water can move in different directions due to the combined influence of the tides, wind and freshwater forcing (Ji, 2012). River hydrodynamics can vary tremendously due to differences in river geometry, bed roughness, flow rates and flow velocity (Ji, 2017). Furthermore, dispersion and advection are the dominant processes of transport of matter in rivers (Ji, 2012).

Type of channel	**Manning roughness coefficient (n)**
Smooth concrete	0.012
Ordinary concrete lining	0.013
Earth channels in best conditions	0.017
Straight unlined earth canals in good condition	0.020
Natural rivers and canals	0.020 – 0.035
Mountain streams with rocky beds and rivers with variable sections and some vegetation along banks	0.040 – 0.050
Alluvial channels without vegetation	0.011 – 0.035

Table 2.2: Manning coefficient for various bottom types in rivers and channels (Ji, 2012)

Manning coefficient and flow rate

Estuaries receive most of their freshwater inflow from rivers. Subsequently, flow rates in rivers are determined by groundwater inflow and precipitation (Ji, 2017). The flow rate $Q[m^3/s]$ can be determined once the cross-sectional area $A[m^2]$ of the river and the flow velocity $V[m/s]$ are known (Equation 2.33).

$$V = \frac{Q}{A} = \frac{R^{2/3} \cdot I^{1/3}}{n} \tag{2.33}$$

According to Ji (2017), flow velocity, flow rate and water depth are usually calculated by means of momentum and continuity equations. However, Manning formulated an equation, which linked the average flow velocity V and the hydraulic slope I, the hydraulic radius R and the Chézy coefficient C to each other (Dyakonova and Khoperskov, 2018). The hydraulic radius is determined by dividing the cross-sectional area of the river A with the wetted perimeter P, which is the length of the river in meters normal to the flow direction. The Chézy coefficient C can be replaced by the Manning roughness coefficient n, by applying the Pavlosky formula, $C = R/n$ (Dyakonova and Khoperskov, 2018). This results in the empirical Equation 2.33. According to Dyakonova and Khoperskov (2018), the Manning coefficient, considers inhomogeneity in the water column, braking due to vegetation, meandering channels, changes in channel width, turbulence, sediment transport and impurity transfers. The various roughness values for different types of river bed can be observed in Table 2.2. Berlamont (2020) explained that the Manning equation (Equation 2.33) can be applied for wide-shallow estuaries with a width-depth ratio of 10 or higher.

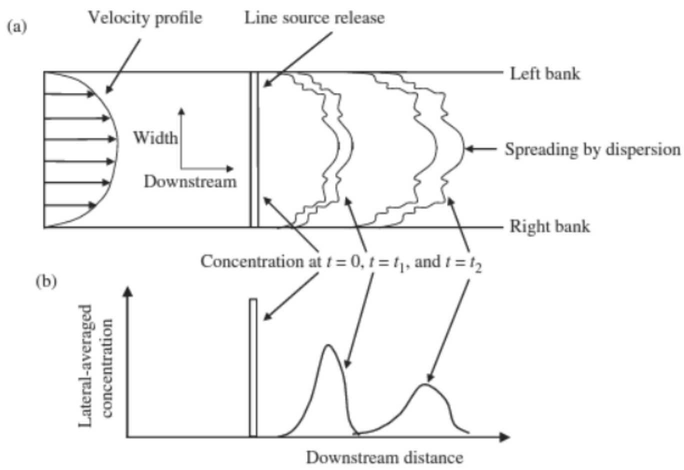

Figure 2.2: (a) Plan view of transport of dye in river (b) Laterally averaged dye concentration in river (Ji, 2017)

Advection and dispersion

According to Ji (2012), two main features of transport of mass in rivers are flow advection and turbulence dispersion. The latter one is mostly due to longitudinal dispersion in rivers and describes the amount of mixing in a river (Ji, 2012). Both features are mathematically described by the first and second term respectively in Equation 2.30. In Figure 2.2 two schematisations are depicted of an idealized situation where a certain material, in this case dye, is released into the river. The dye will be transported by advection and dispersion and can therefore give insight in how for instance salt or pollutants are transported through a river. In Figure 2.2 (a), the a plan view of the experiment can be observed. At the moment of release the concentration of dye can be simplified as a line source, which propagates downstream over time due to advection. What also becomes evident is that the dye becomes less concentrated and starts to spread in both lateral and longitudinal direction due to varying flow velocities across the river. As the river banks induce higher friction values on the adjacent water column, the dye propagates slower along the banks than in the middle. In Figure 2.2 (b), the laterally-averaged dye concentration is plotted over time and distance from the location of release. Here, the velocity shear and turbulence dispersion have a prevailing influence on the distribution of the dye concentration in the river.

2.2.4 Importance of temperature and salinity

Temperature and salinity are perhaps the most important water properties according to Hardisty (2007). They both are measures of hydrodynamics and water quality (Liu, 2018), which make them ideal properties to research from a management perspective. Another advantage is that they are physical parameters, so that they can be measured directly (Pawlowicz, 2013) and are affordable and technically straightforward (NRMRL (U.S.) and EMPACT Program (U.S.), 2002). From Figure 2.3 it becomes clear that by monitoring salinity and temperature conclusions can be drawn on the total water quality of a water body, as salinity and temperature have impact on all dominant water quality properties. Salinity and temperature will be increasingly affected by future climate change (Pachauri et al., 2014). Changes in salinity and temperature can have dramatic impact on estuaries. It is therefore key to understand their dynamics.

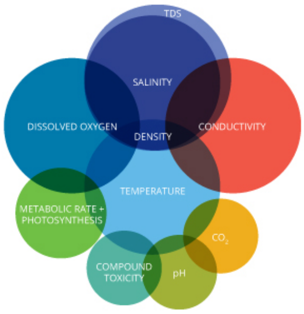

Figure 2.3: Water quality properties and their interdependency (Fondriest Environmental, Inc., 2014)

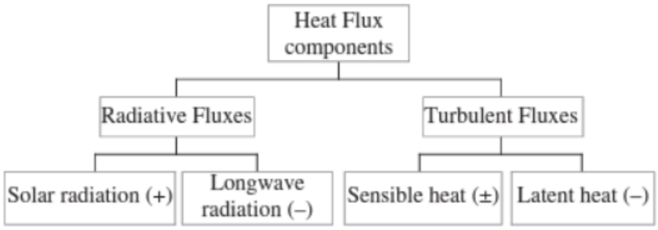

Figure 2.4: Heat flux components (plus (+) sign means heat input and minus (-) sign means heat output) (Ji, 2017)

Definition of temperature

Temperature is "a measure of the heat content of a physical body" (Ji, 2017). Water temperature varies as a function of the surface heat flux and the transport of water into and out of the system (Ji, 2017). The surface heat flux of a water body is mainly driven by the heat exchange with the atmosphere and can be divided in radiative and turbulent fluxes, as shown in Figure 2.4 (Ji, 2017):

1. Solar radiation is a positive radiative heat flux component generated by the sun. It consists of short-wave radiation heating the water surface.

2. Long-wave radiation is a negative radiative heat flux component and is emitted by the atmosphere and the water surface.

3. Sensible heat can be either a positive or a negative turbulent heat flux component and is the heat transfer between the atmosphere and the water body.

4. Latent heat is a negative turbulent heat flux component and is the heat transfer forced by evaporation.

There are also other factors influencing the surface heat flux like, chemical and biological reactions, transfer of heat between the water body and bed, and current friction (Ji, 2017). However, these factors play a minor role in the total amount of heat in the water body and can therefore be neglected (Ji, 2017). Temperature is an important factor when assessing water quality as it has impact on physical and chemical properties like, water density, conductivity and salinity, pH, oxidation reduction potential, dissolved oxygen and other dissolved gas concentrations, compound toxicity and metabolic rates and photosynthesis production (Fondriest Environmental, Inc., 2014). The different water quality properties and their interdependency are depicted in Figure 2.3. Temperature thus has a direct effect on water quality and hydrodynamics and is therefore essential in assessing the dynamics of estuaries.

Definition of salinity

Salinity basically defines the amount of dissolved salts in the water column (Pawlowicz, 2013). These dissolved salts, also known as electrolytes, consist mostly of elements like chloride, sodium, magnesium, sulfate, calcium, potassium and bromine (Fondriest Environmental, Inc., 2014). Ionic particles, with each particle containing cations and anions, are formed as these electrolytes are dissolved(Fondriest Environmental, Inc., 2014). The ionic particles determine the conductivity, the ability of water to pass an electrical flow (CWT, 2004). Originally, the term salinity came from oceanography and never had an exact chemical definition (Ji, 2017). Salinity can therefore be calculated in different ways. According to Association et al. (1915) as in Fondriest Environmental, Inc. (2014), one of the most straightforward ways of calculating salinity is measuring the complete chemical analysis. This method however is too complicated as the water column consists of too many elements (Pawlowicz, 2013). Pawlowicz (2013) also stated that the ratio of dissolved salts in sea water is more or less constant, which means salinity can be determined linearly on a single element. The chloride ion is often used to calculate the salinity in parts per trillion or ppt (Pawlowicz, 2013). However, as conductivity is directly determined by salinity, but also temperature and density, the Practical Salinity Scale or Practical Salinity Unit (PSS or PSU) was developed in 1978 (Arulananthan, 2000). The Practical Salinity Scale thus depends on conductivity, pressure and temperature and is unit less. As can be seen in Figure 2.3, salinity has influence on conductivity, temperature, density and dissolved oxygen. Salinity should therefore be assessed from a management perspective as it has direct impact on water quality and hydrodynamics.

2.2.5 Estuarine classification

Due to the complexity of coastal waterways it is sometimes difficult or even impossible to generalize these coastal waterways on oceanographic principles (De Miranda et al., 2017). However, according to Nichols and Biggs (1985), despite the fact that estuaries around the world are prone to different environments and tidal regimes and have widely varying characteristics, they can be categorized into specific classes. This enables managers to easily compare different estuaries and to quickly obtain a profound understanding in the dynamics of estuaries (Ryan et al., 2003). In Appendix A.2, the geomorphic classification methods are summarized, which are used in Chapter 3. The focus in this section is to explain the relevant hydrodynamic classification methods.

Salinity stratification

Salinity stratification is extensively applied as a classification characteristic in oceanography and considers the dominant factors in the salt balance discussed in Section 2.1.1 (De Miranda et al., 2017). When considering a positive steady-state estuary with invariable salt content, the freshwater volume R that enters the estuary over one tidal cycle, has also to leave the estuary (Tomczak, 1998). This is due to a balance between advection of the freshwater volume R and diffusion of salt (De Miranda et al., 2017). In Section 2.1.3, it became clear that diffusion in coastal waters is caused by turbulence. Subsequently, tidal forcing is one of the driving forces of turbulence in estuaries and can therefore be predicted by the strength of the tide ((Tomczak, 1998)). The tidal forcing can be expressed as tidal volume

V, which is the total volume of water that enters and leaves the estuary in one tidal cycle (Tomczak, 1998). The comparison between the freshwater volume over one tidal cycle R and the tidal volume over one tidal cycle V, gives an indication of the circulation patterns, mixing processes and salinity stratification. By using the R/V-ratio described by Tomczak (1998), who referred to pioneering research done by Pritchard (1952, 1967) and Cameron and Pritchard (1963), seven estuary types can be distinguished, which are enumerated below:

1. Salt wedge estuaries, with a large R/V-ratio, are known for their highly stratified character. As the tidal influence is negligible, not much mixing is observed, which results in freshwater floating on ocean water. Salty ocean water is therefore able to intrude the estuary at the bottom, whereas freshwater flows out of the estuary at the surface (Tomczak, 1998). Salt wedge estuaries are mostly found in regions with micro or meso tides and high river discharge (De Miranda et al., 2017).

2. Highly stratified estuaries, with a R/V-ratio of 0.1 to 1, are known for entrainment, which is the transport of mass from a less turbulent medium to a more turbulent one and therefore only propagates in one direction (Tomczak, 1998). Entrainment is present at the interface of a stronger tidal current at the bottom and a weaker freshwater current at the surface, which causes local turbulent mixing (Tomczak, 1998). Due to entrainment, salt water is transported into the fresh surface layer, which increases the volume transport in the upper layer, which is depicted in Figure 2.5. Due to mass continuity the net volume transport at the estuary's mouth must be equal to the river discharge R, which indicates that the volume transport input of the ocean should be $(n-1)R$ when considering a volume transport due to entrainment of n. According to Tomczak (1998), the volume transport in highly stratified estuaries can go up to thirty times the river discharge. This type of estuaries are often found in fjords where a large saline lower layer and a small fresh upper layer, generate a perfect environment for entrainment (Tomczak, 1998).

3. Slightly stratified estuaries, with a R/V-ratio of 0.005 to 0.1, are known for their partially-mixed character according to Tomczak (1998). The tidally-induced turbulence in this case is strong enough to destabilize the buoyancy forces and the bottom friction of the water column and to produce turbulent diffusion at the interface (De Miranda et al., 2017). Subsequently, the turbulent vortices reduce the vertical salinity gradients and generate the mixing of fresh and salt water (De Miranda et al., 2017). The mixing results in the transport of salt from the salty bottom layer to the fresh surface layer, which increases the volume transport of the upper layer (De Miranda et al., 2017). Due to mass continuity, the opposite occurs in the bottom layer. This can lead to large volume transports in estuaries, as can be seen in Figure 2.6. According to (De Miranda et al., 2017), the volume transport can increase up to twenty times the river discharge.

4. Well-mixed estuaries, with a R/V-ratio of less than 0.005, are known for their vertically mixed character (Tomczak, 1998). Due to the weak freshwater input by the river and the strong tidal current, the mean flow is directed towards the ocean with a gradual increase in salinity towards the ocean (Tomczak, 1998). Salinity intrusion is only generated by turbulent diffusion against the mean flow and salinity does not

vary over depth (Tomczak, 1998). De Miranda et al. (2017) distinguishes two kinds of well-mixed estuaries: laterally stratified estuaries and non-laterally stratified estuaries. The former mainly occurs in estuaries with a large width/depth ratio generated by the deflection induced by Coriolis and the latter has already been described (De Miranda et al., 2017). In the Southern Hemisphere this deflection intensifies the circulation of the estuary to the left. Well-mixed estuaries are often observed in former shallow river valleys with low river discharge and a micro or meso tide that is able to generate sufficient bottom shear stress to vertically mix the water (De Miranda et al., 2017).

5. Inverse estuaries, with a negative R/V-ratio, are known for their reversed bidirectional flow induced by evaporation (Tomczak, 1998). Whereas in positive stratified estuaries the bottom layer and surface layer tends to flow into the estuary and into the ocean respectively, negative estuaries tend to have a reversed circulation (Tomczak, 1998). This is due to the denser hypersaline freshwater that sinks below the less dense and less saline ocean water. Consequently, the hypersaline water flows out of the estuary along the bottom and the ocean water intrudes the estuary on top. This kind of estuaries are mostly found in arid regions where the input of freshwater is way smaller than the amount of evaporation (Tomczak, 1998).

6. Salt plug estuaries can be recognized by their simultaneous positive and negative character (Tomczak, 1998). According to Tomczak (1998), the freshwater input is weak, indicating a slightly stratified water column near the estuary head. Further downstream the estuary becomes more prone to evaporation, increasing the salinity values (Tomczak, 1998). Consequently, the estuary tends to have a more inverse estuarine character towards the estuary's mouth (Tomczak, 1998). The combination of a slightly stratified estuary upstream and an inverse estuary downstream, results in the salt plug estuary, where the highest salinity values are obtained at the interface of the two circulation systems (Tomczak and Godfrey, 1994). At the interface, the only form of transport is caused by turbulent diffusion, which restricts the ability of the estuary to flush properly (Tomczak, 1998). As a consequence fluids tend to accumulate at the interface, which can have dramatic effects for the environment (Tomczak, 1998).

7. Intermittent estuaries can be distinguished by the disappearance of the thermohaline forcing, which causes the estuary to change from an estuary to an embayment and back on a regular basis (Tomczak, 1998).

As is also mentioned by Tomczak (1998), the elaborated schemes only serve as a concept of the different circulation types in estuaries, but should not be taken for granted. The circulation behaviour of estuaries differ both spatially and temporally and can therefore hardly be described by one of the seven estuary types (Tomczak, 1998). Nevertheless, when comparing estuaries based on their estuarine classification, sometimes clear assumptions can be made on particular circulation types (Tomczak, 1998).

Richardson

According to De Miranda et al. (2017) as in Dyer (1977), an important process in estuaries is the balance between the exchanges of motion and the vertical density gradient, which determines the order of vertical stratification and mixing. One method to determine the order

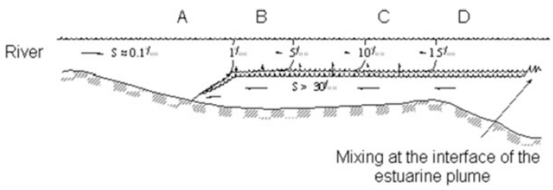

Figure 2.5: Longitudinal circulation pattern of a highly stratified estuary with entrainment (De Miranda et al., 2017)

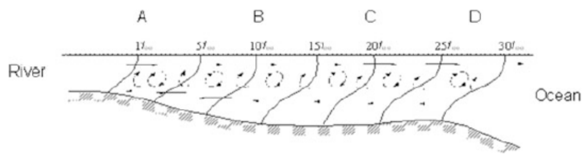

Figure 2.6: Longitudinal circulation pattern of a slightly stratified estuary (De Miranda et al., 2017)

of mixing and vertical stratification is by using the Richardson number (De Miranda et al., 2017). In this thesis, two different Richardson numbers are used, the gradient Richardson number and the Richardson layer number. The former indicates the occurrence of turbulence in a fluid flow by comparing the vertical density gradient ($\delta\rho/\delta z$) (stabilizing factor) with the vertical velocity shear ($\delta u/\delta z$) (destabilizing factor). The gradient Richardson number is calculated by D-Flow FM using Equation 2.34.

$$Ri \; = \; \frac{-g \, \frac{\delta\rho}{\delta z}}{\rho \, \left[(\frac{\delta u}{\delta z})^2 \; + \; (\frac{\delta v}{\delta z})^2 \right]} \tag{2.34}$$

The gradient Richardson number thus gives information about the relationship between buoyancy stabilizing factor to the destabilizing factor but also about the order of stratification in a fluid flow (De Miranda et al., 2017). According to De Miranda et al. (2017), the transition between laminar and turbulent regimes takes place approximately at Ri = 0.25. For values lower than 0.25 the turbulence becomes dominant and overpowers the vertical density stratification causing mixing in the fluid flow (De Miranda et al., 2017). Note that the gradient Richardson can also become negative, indicating vertical instability and therefore vertically mixed fluid flows. For Ri > 0.25, the fluid flow becomes stable indicating less vertical mixing and increased stratification. Obviously, higher positive values indicate higher stratification and higher negative values indicate more vertical mixing. The Richardson layer number is developed in order to calculate the varying Richardson numbers over the vertical water column. However, the Richardson layer number can also be used for depth-averaged value. The Richardson layer number can be calculated by using Equation 2.35 as in Dyer and New (1986).

$$Ri_L(t) \; = \; \frac{gh(t)\Delta\rho_V(t)}{\overline{\rho}(t)(\overline{u}^2(t))} \tag{2.35}$$

Where, $h(t)$ is the local depth, $\Delta\rho_V(t)$ is the difference between bed and surface densities, $\overline{\rho}(t)$ is the depth-averaged density and $\overline{u}(t)$ is the depth-averaged velocity. For Richardson layer numbers of more than 20 ($Ri_L > 20$), almost no vertical mixing is encountered and the fluid flow is highly stable (Dyer and New, 1986). For $Ri_L < 20$, the fluid flow becomes less stable due to the higher influence of the turbulence at the bed level initiating vertical mixing (Dyer and New, 1986). For $Ri_L < 2$, the fluid flow becomes unstable caused by the dominant influence of the turbulence (Dyer and New, 1986).

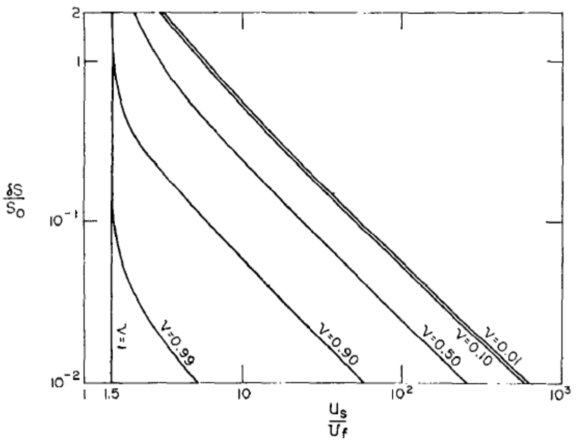

Figure 2.7: Original stratification-circulation diagram (Hansen and Rattray Jr, 1966)

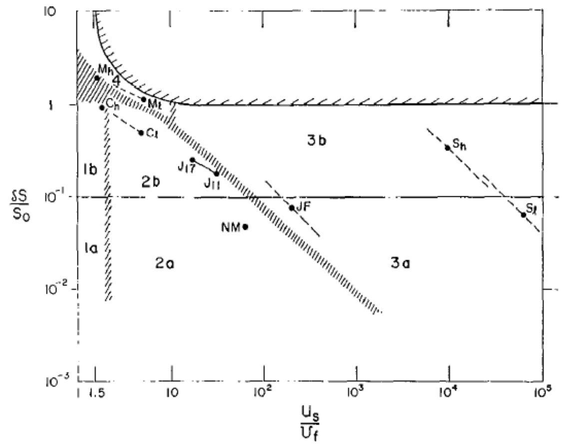

Figure 2.8: Stratification-circulation diagram with different estuary types (Hansen and Rattray Jr, 1966)

Stratification-circulation diagram

Hansen and Rattray Jr (1966) concluded that it can be useful to classify the estuaries bu using two parameters, stratification and circulation. However, it should be noted that not all dynamics of the estuarine properties in the vertical can be described by these parameters (Hansen and Rattray Jr, 1966). Nevertheless, differences in the vertical regime of an estuary can easily and quickly be visualised. Hansen and Rattray Jr (1966) developed the stratification-circulation diagram depicted in Figure 2.7. The x-axis in Figure 2.7 represents the order of circulation in the estuary and the y-axis represents the order of stratification in the estuary. The former is called the circulation parameter p_c and is calculated by Equation 2.37. The latter is called the stratification parameter p_e and is calculated by Equation 2.36.

$$p_e = \frac{\delta S}{S_0} \tag{2.36}$$

$$p_c = \frac{\delta u}{u_0} \tag{2.37}$$

Hansen and Rattray Jr (1966) distinguished seven different estuary types based on the circulation and stratification parameter: Type 1a, 1a, 2a, 2b, 3a, 3b and 4. The regions of these estuary types are depicted in Figure 2.8. Type 1 estuaries can be characterized by their seaward unidirectional flow over the vertical and their upstream salt transport driven by diffusion (Hansen and Rattray Jr, 1966). The difference between a and b is characterized by the order of stratification, which is low for Type a estuaries and high for Type b estuaries (Hansen and Rattray Jr, 1966). For Type 2 estuaries a different circulation regime is observed over the vertical, with reversed flows over the depth (Hansen and Rattray Jr, 1966). According to Hansen and Rattray Jr (1966), the upstream salt transfer is mostly effected by advection and diffusion. In Type 3 estuaries the influence of advection becomes dominant (>99%) for the upstream upstream salt transfer (Hansen and Rattray Jr, 1966). In Type 3b estuaries, the lower layers are so deep that the salinity gradient will not extend to the bottom, which is encountered in fjords for example (Hansen and Rattray Jr, 1966). In Type 3a, the halocline is more mixed, with lower stratification as a result Hansen and Rattray Jr (1966). Type 4 estuaries are specified as salt wedge estuaries and can be recognized by a thick upper layer that flows over a thin lower layer to a shallow upper layer flowing over a deep lower layer (Hansen and Rattray Jr, 1966). In both situations, the layer have negligible effect on each other.

2.3 D-Flow Flexible Mesh

Hydrodynamic models are useful tools to understand current velocities, circulation patterns, mixing, dispersion, water temperature, and density stratification (Ji, 2017). These processes provide essential information to a wide range of other numerical models, including water quality, wave, ecology and morphology models (Ji, 2017). Deltares therefore developed a hydrodynamic simulation program, D-Flow Flexible Mesh, which is part of the Delft3D Flexible Mesh Suite, a multi-disciplinary software suite that can execute wave, water quality, ecology, morphology and hydrodynamic flow simulations in 1D, 2D and 3D (Deltares, 2020).

2.3.1 Applicability

D-Flow FM is capable of modelling 2DH (depth-averaged) and 3D hydrodynamic processes generated by forces like meteorology, tide and density-gradients (Deltares, 2020). The DFM-module is especially applicable to areas where the horizontal length and time scales are larger than the vertical dimensions like coastal areas, estuaries, lakes, lagoons, rivers, and shallow seas (Deltares, 2020). The applicability of 2DH-models depends on the vertical homogeneity of the specific fluid. If a fluid is well-mixed 2DH-models can be used to simulate the hydrodynamic processes. 3D-models are used for situations where the hydrodynamic processes vary significantly over the vertical plane driven by, for example bed shear stress, bed topography, density-gradients, wind forcing and/or Coriolis force. Salt intrusion is an example of a situation where 3D-modelling is recommended by Deltares (2020).

2.3.2 Flexibility

The flexibility of the program is enabled by the use of unstructured grids in the horizontal plane, where a grid can be build by using triangular and rectangular cells. The flexibility in the vertical plane is guaranteed by offering two vertical grid systems: the σ-model and the z-model (Deltares, 2020). The former model is illustrated in Figure 2.9 (left) and the latter in Figure 2.9 (right). In the σ-model the vertical layers are defined by two σ planes that follow the free surface and the bed topography. This means the vertical layers in the σ-model are in general non-uniform (Deltares, 2020). The vertical layers in the z-model have specified depths and are parallelly distributed (Deltares, 2020).

2.3.3 Physical processes

According to Deltares (2020), the theoretical basis of D-Flow FM is founded on the unsteady shallow water equations, which are solved in 2DH or in 3D. The unsteady shallow

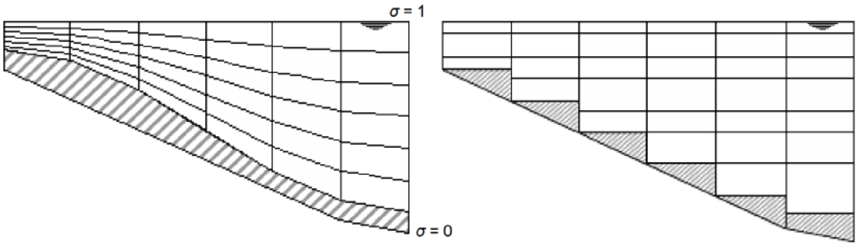

Figure 2.9: Examples of the two applicable vertical grid systems: σ-model (left) and the z-model (right) (Deltares, 2020)

water equations consider the continuity equation, the transport equations and the horizontal equations of motion and can be either formulated in Cartesian or in spherical coordinates. In the former, the bathymetry and free surface level have a flat horizontal plane of reference and in the latter, the bathymetry and free surface level have the Earth curvature as reference. The considered physical processes included in the D-Flow FM model are numerous but are briefly listed. In Chapter 4 a more extensive explanation of the considered physical processes in this thesis research can be found. The D-Flow FM model takes into account the tide (forced at the open boundaries), the density gradients (baroclinic), the pressure gradients (barotropic) and the wind stress at the free surface (Deltares, 2020). Besides, discharges can be applied to the open boundaries as well to simulate rivers and sink and source terms can be included to model smaller discharges and sinks of water (Deltares, 2020).

Part II

Data analysis & model set-up

A thorough data analysis is conducted to supply the numerical model with the essential data needed for calculation and to draw up preliminary conclusions on the hydrodynamic processes of the system. A detailed description of the model set-up is added to motivate the taken decisions and the considered strategy in the numerical model.

3

Data Analysis

Data analysis is conducted to understand the dominant hydrodynamic processes in the Leschenault Estuary and its main physical drivers. First, the Leschenault Estuary is investigated in Section 3.1. Secondly, the takeaways of previous developed numerical models of the Leschenault Estuary are summarized in Section 3.2. All relevant data are summarized in Section 3.3, is processed and analysed to serve as input for the numerical model and to draw preliminary conclusions. Lastly, the field measurements conducted at the Leschenault Estuary are briefly described.

3.1 Area description

The area of interest in this research is the Leschenault Estuary, which is located approximately 180 km south of Perth, Western Australia. To obtain a comprehensive understanding of the processes affecting the estuary, the estuary's history and developments are briefly discussed in Section 3.1.1 and 3.1.2. Section 3.1.3, 3.1.4 and 3.1.5 present a geomorphic characterization and highlight the dominant hydrodynamic processes.

3.1.1 Historical background

The Leschenault Estuary was created in the Holocene, approximately 7000 years by the development of a natural sand dune barrier in front of the original open coast (McKenna, 2004). A schematization of the evolution of the Leschenault Estuary during various stages of the Holocene is presented in Figure 3.1. According to research conducted by Semeniuk et al. (2000), continuously changing sea levels and a retreating sand barrier led to the creation of one large estuarine lagoon. Studies by Semeniuk et al. (2000), showed that the shape of the lagoon was more elongated and wider between approximately 7000 years and 2500 years BP. Their research indicated a lagoon three times as wide and covering an area from the Leschenault Inlet to the northern part of Lake Preston. During that time the lagoon was interconnected with the sea via the former Leschenault Inlet on the south side of the lagoon. The landward retreating sand dunes eventually led to the segmentation of the lagoon into two different systems, Lake Preston and the Leschenault Estuary (McKenna,

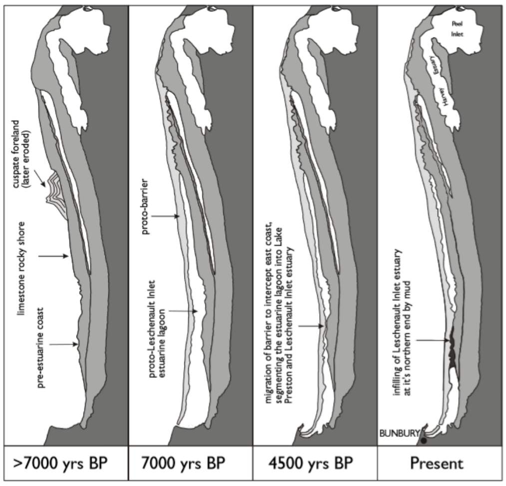

Figure 3.1: Leschenault Estuary evolution (Semeniuk et al., 2000)

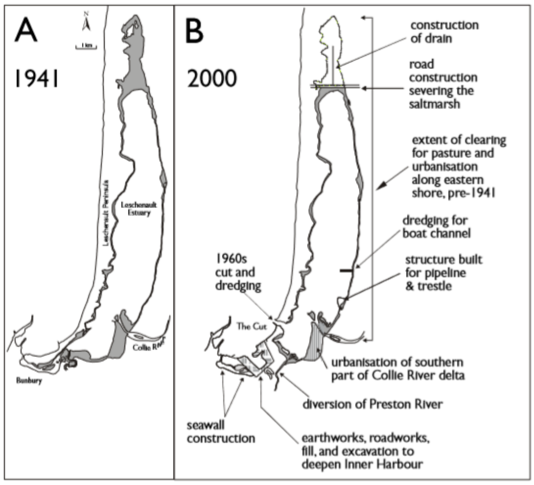

Figure 3.2: Anthropogenic impacts to the Leschenault Estuary (Semeniuk et al., 2000)

2004). McKenna's research implied that due to the segmentation, Lake Preston was no longer connected with the sea and lost its initial estuarine characteristics. As a result of the ongoing retrograding sand dunes, decreasing sea levels and the infilling of mud on the north side of the Leschenault Estuary the size of the estuary decreased significantly until it finally reached its current shape (McKenna, 2004). A schematization of the Leschenault Estuary prior to anthropogenic changes is depicted in Figure 3.2.

3.1.2 Developments

Since the first Europeans set foot on the Australian continent many developments have taken place. According to a historical summary of the Leschenault Estuary's developments provided by Hugues-dit-Ciles et al. (2012) and slightly altered by Wooltorton (2013), the first settlers arrived around 1838 and were mainly farmers. Hugues-dit-Ciles et al. (2012) research indicated that during the early stages of the first settlement of the farmers the clearing of vegetation commenced to provide space for agriculture. Around 1910 - 1912 the first major clearing of vegetation occurred around the Leschenault rivers to improve drainage and reduce flooding what affected the hydrology and ecology of the area (Hugues-dit-Ciles et al., 2012). The Wellington Dam was constructed in 1933 to increase the availability of fresh water for agricultural purposes and to mitigate flood risk. This significantly reduced the freshwater input of the Collie River to the estuary. An even more drastic development took place in 1951 with the excavation of the 'Cut' and the filling of the initial Leschenault Inlet. This resulted in the separation of the Leschenault Estuary and the Leschenault Inlet. According to Semeniuk et al. (2000), the construction of the 'Cut' altered the estuarine landforms, hydrodynamics and hydrochemistry. Semeniuk et al. (2000) mentioned furthermore that before the 'Cut' was excavated, the whole Leschenault estuarine system was called the Leschenault Inlet. However, Semeniuk et al. (2000) stated that from a technical perspective the name 'Leschenault Inlet' should have been given to the connection between the ocean and the lagoon and the name 'Leschenault Lagoon' to the lagoon itself. After the 'Cut' had been constructed the original inlet was called 'Leschenault Inlet' and the lagoonal water body was named 'Leschenault Estuary' (Semeniuk et al.,

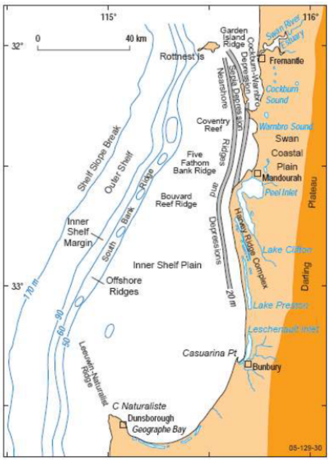

Figure 3.3: Morphology of Naturaliste to Rottnest Shelf (Damara, 2016)

2000). The summary provided by Hugues-dit-Ciles et al. (2012) described that between 1941 and 1989 the Leschenault area urbanized rapidly with a destructive impact on fringing vegetation, the area lost almost half of its vegetation. Hugues-dit-Ciles et al. (2012) mentioned furthermore that in 1967 the construction of the Inner Harbour commenced and in 1976 the harbour was finished. Consequently, large areas of samphire were destroyed (Hugues-dit-Ciles et al., 2012). Moreover, the Preston River had to be realigned in order to reclaim the old inlet channel near the Inner Harbour and to start the development of the Inner Harbour. The land reclamation, dredging and construction necessary for the development of the harbour destroyed much of the Preston River Delta (Semeniuk et al., 2000). In 1977, the Parkfield Drain was constructed to enhance water drainage of agricultural land use, which had significant impact on hydrodynamics and biogeochemistry of the northern part of the estuary (Hugues-dit-Ciles et al., 2012). From 1990 onwards, increased urbanisation around the Leschenault Estuary destroyed another 50% of its vegetation with major impacts on the hydrology and ecology (Hugues-dit-Ciles et al., 2012). Urbanisation also caused the destruction of the southern Collie River Delta (Semeniuk et al., 2000). Most of the previous described anthropogenic changes are summarized in a schematization depicted in Figure 3.2.

3.1.3 Morphological classification

The definition of an estuary described in Section 2.2.1 is genuinely applicable for the Leschenault Estuary. Namely, the estuary is partially enclosed by a peninsula sand barrier, always open to the sea due to the 'Cut', influenced by a periodic river discharge and periodically hypersaline during dry periods. Semeniuk et al. (2000) described the Leschenault Estuary as a wave dominated and wind current driven lagoonal water body with an open connection to the sea and a micro-tidal regime with a mean spring tidal range of 0.5 m. Boyd et al. (1992) developed a ternary classification based on dominant processes for deltas, estuaries, lagoons, strand plains and tidal flats. The classification, illustrated in Figure 3.4, contains three axes. The first axis (horizontal axis) illustrates the relative power of the waves and tide. The second axis (vertical axis) indicates the influence of fluvial processes.

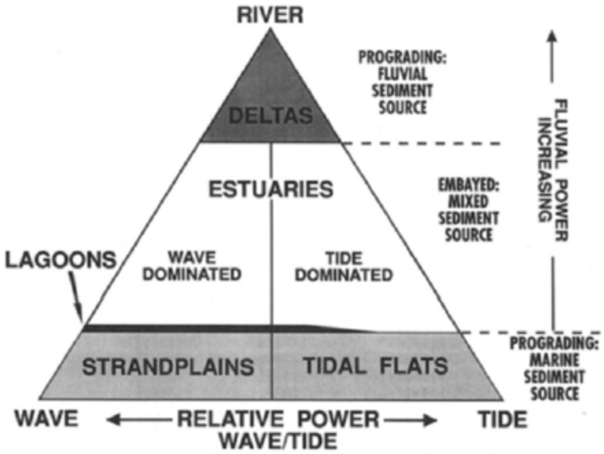

Figure 3.4: Estuarine classification (Boyd et al., 1992)

Ryan et al. (2003) slightly changed the classification by dividing the delta section into a wave dominated delta and a tide dominated delta. The same report also categorizes all Australian coastal waterways including the Leschenault Estuary. According to Ryan et al. (2003), the Leschenault Estuary can be described as a wave dominated estuary. This means that the coast is influenced by waves and rivers, but the tide plays a minor role in local morphology. These descriptions of the Leschenault Estuary can be confirmed by implementing a generalized diagram developed by Hayes (1979), which gives the relationship between mean wave height and mean tidal range. The diagram is pictured in Figure 3.5 and is only applicable for regions with mild wave conditions and a microtidal regime (Hayes, 1979). Davies (1964) was the first to distinguish different coastal regimes on their tidal range: microtidal coasts with a tidal range of $0-2$ m, mesotidal coast with a tidal range of $2-4$ m and macrotidal coasts with a tidal range of > 4 m. Hayes (1979) later subdivided these three classes into five coastal types, because they all had specific characteristics. This led to the final table listed in Table 3.1.

Class	**Tidal Range**
Microtidal	$0-1$ m
Low-mesotidal	$1-2$ m
High-mesotidal	$2-3.5$ m
Low-macrotidal	$3.5-5$ m
Macrotidal	> 5 m

Table 3.1: Coastal types – medium wave energy ($H_s = 60 - 150$ cm)

According to Semeniuk et al. (2000), the mean spring tidal range is 0.5 m in the Leschenault region, which satisfies the first requirement of a microtidal regime. The second requirement, mild wave conditions or medium wave energy, is satisfied for the mean significant wave height lays between $0.6-1.5$ m (Bosboom and Stive, 2012). With a mean significant wave height of 0.8 m, this perfectly satisfies the second requirement. This means, Hayes' diagram can be applied to assess the relationship between tidal range and wave height. In Figure

3.5 it becomes clear that the Leschenault Estuary is wave dominated according to Hayes' diagram, with a mean spring tidal range of 0.5 m and a mean significant wave height of 0.8 m. It therefore confirms the classification done by Semeniuk et al. (2000) and Ryan et al. (2003).

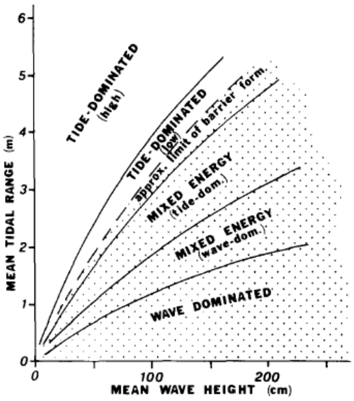

Figure 3.5: Influence of tidal range and wave height to coastal morphology (Hayes, 1979)

Figure 3.6: Leschenault Estuary aerial photo (Google)

3.1.4 Wave dominated estuary

Hayes (1979) concluded "that barrier island shorelines are most abundant on coastal plains located on trailing edges of continents and on marginal sea coasts". The Western Australian coast is a trailing edge coast, which means the centre of the tectonic plate is diverging (Bosboom and Stive, 2012). In Figure 3.3, a map is shown of the coast south of Perth, which depicts the continental shelf along the shore. Continental shelves are shallow ($0 - 200$ m) coastal plains, typically found in protected coastal areas and on trailing edge coasts (Bosboom and Stive, 2012). The Leschenault coast has a microtidal regime and mild wave climate with a long elongated sand barrier peninsula with numerous washovers as can be seen in Figure 3.6. Wave dominated coastal regions can be distinguished by their rather smooth shoreline with well-developed beaches and dunes (Bosboom and Stive, 2012). According to Bosboom and Stive (2012), their are two different shapes of wave dominated coastline. The first shape is rather symmetrical and usually has a small delta due to the higher wave impact than the fluvial impact. The second shape has elongated sand spits created by a strong longshore current. The latter shape can be recognized in the Leschenault Estuary, where the Leschenault Peninsula protects the estuary from the Indian Ocean. Ryan et al. (2003) stated that "a wave dominated estuary represents a coastal bedrock embayment that has been partially infilled by sediment derived from both the catchment and marine sources, in which waves are the dominant force shaping the gross geomorphology". This sort of estuaries usually has a supra-tidal barrier near the mouth separating the central basin from the open ocean (Ryan et al., 2003). It can therefore be concluded that the description of a wave dominated estuary is in good agreement with the observations in the Leschenault Estuary.

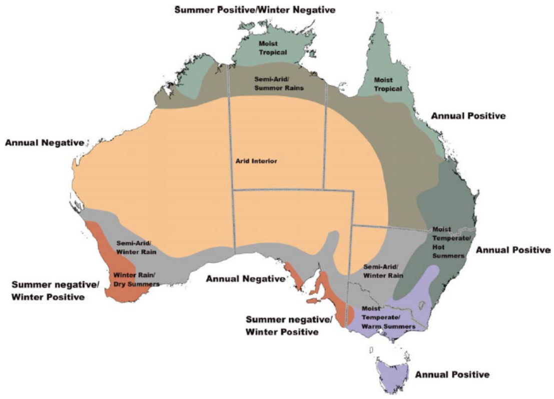

Figure 3.7: Climatic zones (Ryan et al., 2003)

3.1.5 Hydrodynamics in wave dominated estuaries

Ryan et al. (2003) described six important hydrodynamic processes that influence wave dominated estuaries: freshwater input, stratification, mixing, marine exchange, internal circulation and evaporation. These processes are dependent on local climate and behave differently under dry and wet circumstances. Therefore, Ryan et al. (2003) made a distinction between Australia's varying climatic zones. The six climatic zones shown in Figure 3.7, can be subdivided in four climate types: annual positive, annual negative, summer-positive and winter-positive. If a region is positive or negative depends on the water balance. This means that a positive region has a positive freshwater balance and thus has a higher freshwater input than output. For a negative region this is exactly reversed, which means there is a higher freshwater output than input. Obviously, there are also regions with a seasonal influence with both positive and negative seasons. This can clearly be seen in Figure 3.7, where the south west of Australia has a seasonal climate with dry hot summers and rainy winters. This indicates that Australia's south west is prone to typical wet periods with a relatively higher river flow in winter and dry periods with a relatively higher evaporation in summer. This might indicate that in winter a lower salinity and temperature could be observed inside the Leschenault Estuary and a higher salinity and temperature in summer. The six hydrodynamic processes are illustrated by Ryan et al. (2003) in Figures 3.8 and 3.9. Namely:

1. **Freshwater** input from the estuary's surroundings is one of the major processes influencing estuaries. During summer the influence of freshwater input is less significant in the Leschenault Estuary according to Ryan et al. (2003), due to the lower rainfall rates. This is illustrated by the smaller arrow with number sign 1 in Figure 3.9.

2. The degree of **stratification** in an estuary is important for ecology and determines the circulation patterns. In Figure 3.8 and 3.9, stratification is marked with number sign 2. In Figure 3.8, a strongly stratified estuary is illustrated, where at moments of extreme rainfall or river flow the entire estuary can be flushed, typical for winter conditions in the Leschenault Estuary according to Ryan et al. (2003). In Figure 3.9, the less stratified situation is illustrated, typical for summer conditions with reduced freshwater input.

3. In wave dominated estuaries two types of **mixing** occur, one for positive estuaries and one for negative estuaries (Ryan et al., 2003). During winter, the estuary has positive characteristics with a classical estuarine circulation, illustrated in Figure 3.8 with number sign 3. Freshwater from the rivers is less dense than the salty ocean water and floats on top of the ocean water in a seaward direction. During summer, the estuary has negative characteristics with an inverse estuarine circulation, illustrated in Figure 3.9 with number sign 3. Surface water in the estuary heats up, increasing the evaporation rates and therefore also increasing the salinity values. In arid climates estuarine waters could even become saltier and denser than the ocean water, resulting in a floating ocean water layer directed landwards. The hypersaline bottom layer flows in a seaward direction.

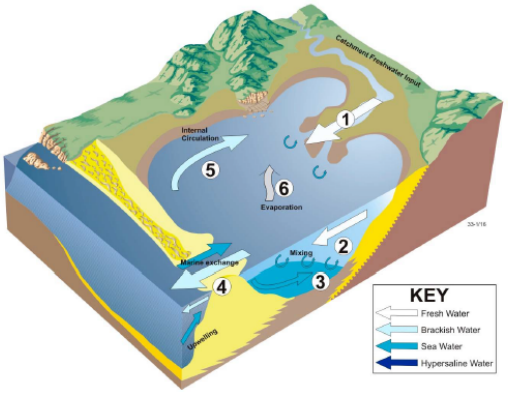

Figure 3.8: Hydrodynamic processes in a positive wave dominated estuary (Ryan et al., 2003)

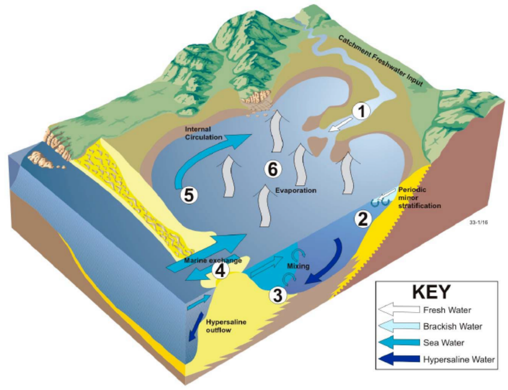

Figure 3.9: Hydrodynamic processes in a negative wave dominated estuary (Ryan et al., 2003)

4. **Marine exchange** takes place at the estuary's mouth and is dependent on the size and length of the mouth's channel (Ryan et al., 2003). Moreover, the seasonal circulation mechanisms explained in the previous paragraph determine the marine exchange in the estuary. Positive estuaries with a higher freshwater inflow than outflow tend to have an inflowing ocean water layer at the bed and an out-flowing freshwater layer at the top, depicted in 3.8 with number sign 4. This type of marine exchange causes upwelling in the adjacent sea. Negative estuaries tend to have an out-flowing hypersaline water layer at the bed and an inflowing ocean water layer at the top, depicted in 3.9 with number sign 4. This type of marine exchange causes downdwelling in the adjacent sea.

5. The major driver for **internal circulation**, indicated in Figure 3.8 and 3.9 with number sign 5, in wave dominated estuaries is wind according to Ryan et al. (2003). Other significant factors are the tide and the Coriolis' force (Ryan et al., 2003). The Coriolis' force is only of importance in very large basins. Besides, tidal ranges inside the estuary could be small for wave dominated estuaries compared to tidal ranges in the ocean (Ryan et al., 2003). This should be investigated in further detail for the Leschenault Estuary. Due to the size of the 'Cut', the tidal range could still be significant inside the Leschenault Estuary. However, a significant phase lag might be present due to the length of the estuary. These assumptions are motivated in further detail in Chapter 6.

During extreme weather events with high rainfall and river flow, internal circulations driven by wind, tides and Coriolis' effects, are occasionally disrupted (Ryan et al., 2003).

6. As stated by Heggie et al. (1999), **evaporation** is encountered in positive wave dominated estuaries, but does not exceed the freshwater inflow. In negative estuaries however, this process is reversed due to the occurrence of a drier and warmer climate (Ryan et al., 2003). More freshwater is evaporating than the amount of freshwater that is flowing into the estuary. As a consequence, the estuary tends to have less freshwater inflow and thus tends to have a larger residence time than positive estuaries (Ryan et al., 2003). The difference between evaporation rates in a positive and negative wave dominated estuary is illustrated in Figure 3.8 and 3.9 with number sign 6.

3.2 Results previous models

Two numerical models of the Leschenault Estuary were developed in advance of the DFM-model developed during this research. The first model was developed by Charteris and Deeley (2000), who investigated different circulation pattern scenarios in the Leschenault Estuary forced by different tidal, wind and river flow input. The second numerical model was developed by the Environmental Modelling group at the Marine research Division of CSIRO (Commonwealth Scientific and Industrial Research Environmental), who investigated the 3D-hydrodynamics of the Leschenault Estuary, including circulation patterns, salinity and temperature (Gillibrand et al., 2012). The conclusions of the first model and second model are described in Section 3.2.1 and 3.2.2 respectively.

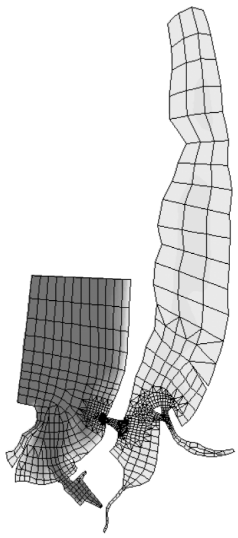

Figure 3.10: The numerical model developed by Charteris and Deeley (2000)

3.2.1 Charteris & Deeley

Charteris and Deeley (2000) used finite element techniques of the RMA suite of software to model the different circulation patterns based on different scenarios. The model grid developed by Charteris and Deeley (2000) is depicted in Figure 3.10. Scenarios ranged from tidal characteristics, seasonal variation (summer and winter), ebb and flood variations and an afternoon sea breeze typical for summer conditions with a parallel flooding tide (Charteris and Deeley, 2000). Unfortunately, their research results were not validated against measured data. However, their outcomes can be useful to compare with the model results generated in this research. Charteris and Deeley (2000) concluded that the 'Cut' is responsible for a four to seven hours tidal phase lag for flood and ebb tide between the ocean and the estuary, due to the hydraulic restrictive characteristic of the 'Cut'. Moreover, peak flood flow velocities in the 'Cut' occur about one to two hours before high water in the ocean and peak ebb flow velocities occur two to three hours before low water in the ocean (Charteris and Deeley, 2000). Charteris and Deeley (2000) used the four main constituents (M2, S2, O1 and K1) to reproduce the diurnal tidal wave existent in the Bunbury Port. Besides the tidal influence, Charteris and Deeley (2000) found out that the water level inside the Leschenault Estuary is also dependent on the freshwater input from the adjacent rivers, like the Collie, Preston, Brunswick and Ferguson River. This causes higher water levels inside the estuary during the wet winter months with higher river flow. According to Charteris and Deeley (2000), circulation patterns inside the Leschenault Estuary do not vary under summer and winter conditions and the summer sea breeze has only minor influence on the circulation pattern. Conversely, circulation patterns in the Koombana Bay varied significantly under winter and summer and ebb and flood conditions.

3.2.2 CSIRO

The environmental modelling team of CSIRO used SHOC (Sparse Hydrodynamic Ocean Code) to develop the numerical model for the Leschenault Estuary (Gillibrand et al., 2012), which is a 3D finite difference hydrodynamic model built on primitive equations. It is applicable as a general purpose model with scales ranging from estuaries to regional oceans (Gillibrand et al., 2012). The output of the SHOC-model is very similar to the DFM-output and contains data like temperature, velocity, density, salinity, mixing coefficients, water level and passive tracers (Gillibrand et al., 2012). The model grid and bathymetry of CSIRO are depicted in Figure 3.11. The CSIRO-team investigated the hydrodynamics in the Leschenault Estuary in the April 2011 to April 2012 period, focusing mainly on stratification, mixing and flushing time processes. The model was verified against observed salinity and temperature data and showed good agreement with the observed data, except the poorly modelled salt wedge dynamics in the Collie River (Gillibrand et al., 2012).

Tides

The tide appeared to be the dominant forcing of the circulation in the Leschenault Estuary, especially in the southern parts close by the 'Cut' (Gillibrand et al., 2012). Tidally-driven flow velocities in the 'Cut' exceeded 1.5 m/s at certain moments (Gillibrand et al., 2012). The estuary's entrance causes a phase lag between high water and low water at Bunbury Harbor and the estuary of respectively two and six hours (Gillibrand et al., 2012). Circulation patterns typical for flood periods generate northward currents inside the estuary and a anti-clockwise swirl south of the estuary (Gillibrand et al., 2012). Circulation patterns typical for ebb periods generate reversed currents in the estuary, with a southward-flowing current in the northern part and a clockwise circulation in the southern part (Gillibrand et al., 2012). Gillibrand et al. (2012) also concluded that the currents quickly became weaker, away from the estuary's entrance. During high freshwater flow events, the currents induced by the flow outcompeted the tidally induced currents, which generated unidirectional currents out of the estuary (Gillibrand et al., 2012).

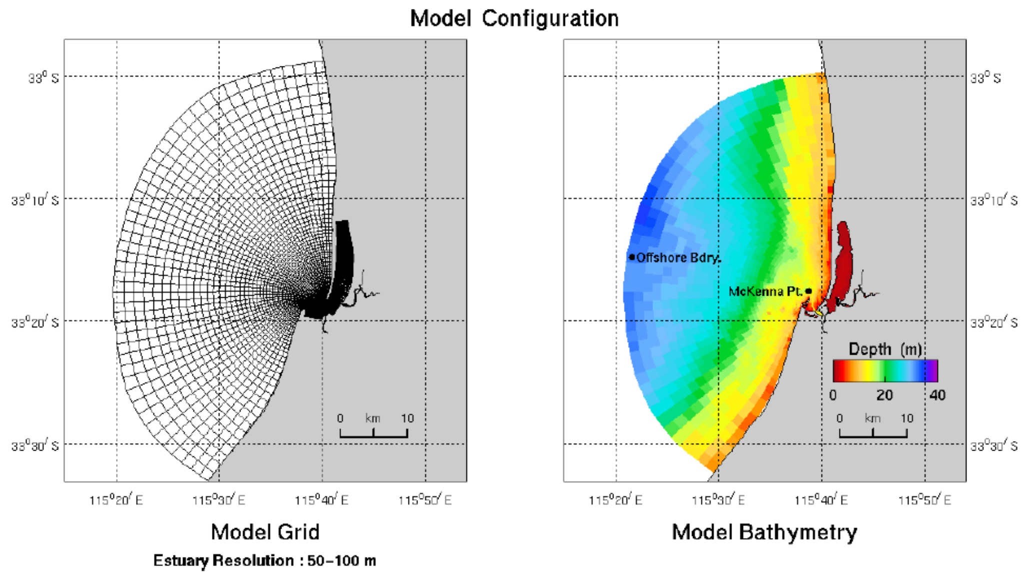

Figure 3.11: The numerical model developed by CSIRO (Gillibrand et al., 2012)

Seasonality

Gillibrand et al. (2012) investigated the seasonal variation in circulation type of the Leschenault Estuary. Gillibrand et al. (2012) discovered that during winter the estuary showed a classical estuarine circulation, with the mean winter surface flow in a seaward direction and the mean winter flow near the bed in a landward direction. This could be explained by the high river flow during winter with increased precipitation. Typical surface current speeds averaged 1 cm/s in the estuary with bed current speeds of the same order of magnitude (Gillibrand et al., 2012). Flow velocities in the southern part of the estuary were slightly higher, with 3 to 4 cm/s on average. In summer, the estuarine circulation was inverse, with a landward-moving surface flow and a seaward-moving bed flow for the largest part of the estuary, excepting the southern region (Gillibrand et al., 2012). This is probably due to the low river flow and high evaporation in the northern region of the estuary. Averaged flow velocities appeared to be around 2 cm/s, which is slightly higher than during winter. The southern part of the estuary showed a classical estuarine circulation, due to the higher influence of the rivers (Gillibrand et al., 2012).

Peak flow events

In August 2011, a high river flow event took place, which had a tremendous effect on the dynamics of the southern part of the estuary (Gillibrand et al., 2012). The discharged freshwater from the rivers accumulated in the southern part of the estuary, where it gradually flowed out of the estuary through the 'Cut' (Gillibrand et al., 2012). This produced a freshwater flume into the adjacent bay with flow velocities of 0.5 m/s or higher (Gillibrand et al., 2012). Impact in the northern and central parts of the estuary was not as significant, but also decreased the salinity values drastically (Gillibrand et al., 2012).

Flushing times

Gillibrand et al. (2012) also conducted research into the mixing characteristics and flushing time of the Leschenault estuary. Gillibrand et al. (2012) subdivided the estuary in three compartments: a northern region influenced by the Parkfield Drain and weak tidal currents, a central region influenced with weak tidal currents and no direct influence of rivers, and a southern region influenced by the 'Cut', the Collie River and the Preston River. Gillibrand et al. (2012) applied passive tracers in the SHOC-model to inspect the flushing times. The southern compartment turned out to be the most dynamic one, with the shortest flushing time of around 9 days (Gillibrand et al., 2012). The flushing times in the entire estuary varied from 9 to 32 days (Gillibrand et al., 2012).

Collie River salt wedge

Whereas the modelled salinity values in the Leschenault Estuary were in good agreement with the observed salinity data, the modelled salinity values in the Collie River did not reproduce the observed data well, what was attributed to the coarse grid resolution (Gillibrand et al., 2012). Gillibrand et al. (2012) applied a vertical resolution of 0.5 m in the Collie River, because finer resolutions dramatically increased the calculation time. The model showed the general salt wedge dynamics of the Collie River, where at moments of high river flow the salt wedge was pushed out of the estuary through the 'Cut' and at moments of low river flow the salty ocean water was able to penetrate all the way up the Collie River along the bed (Gillibrand et al., 2012). However, the model lacked accuracy in modelling the correct salinity over the depth of the Collie River. This led to a lower modelled salinity gradient over depth than observed. A refined vertical resolution could be the key to improved salt wedge dynamics in the rivers.

3.3 Data

The data analysed in this section covers precipitation and freshwater discharge in Section 3.3.1, wind in Section 3.3.2, tide and surface elevation in Section 3.3.3, temperature and salinity in Section 3.3.5, evaporation in Section 3.3.6 and waves in Section 3.3.7.

3.3.1 Precipitation and freshwater flow

Two datasets were provided by DWER: one dataset contains modelled rainfall data used by CSIRO while developing the SHOC-model (Figure 3.13) and one dataset contains measured rainfall data provided by the Bureau of Meteorology (Figure 3.12). The former dataset was extracted from the atmospheric model of the Bureau of Meteorology named ACCESS. The latter dataset contains observed rainfall data collected at the Bunbury Power Station weather station, being more reliable. The average of the daily rainfall over the analysed period was 2.76 mm/day for the ACCESS model and 2 mm/day for the measured data. The modelled ACCESS data overestimates the rainfall by 38 %. Therefore, the measured data was applied in the DFM model.

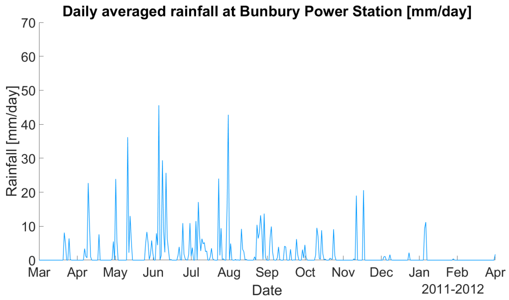

Figure 3.12: Daily averaged rainfall in mm/day measured at the Bunbury Power Station (17-03-2011 to 01-04-2012)

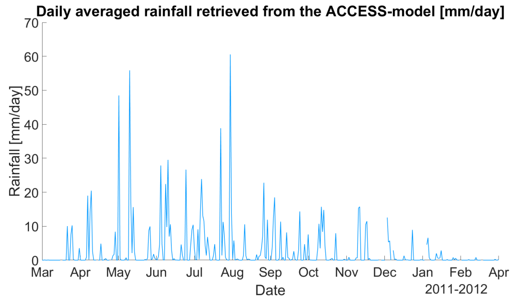

Figure 3.13: Daily averaged rainfall in mm/day retrieved from the ACCESS-model (17-03-2011 to 01-04-2012)

Peak rainfall event

Two peak rainfall events are visible in Figure 3.12: one in June and one in August. Both rainfall events have the same order of magnitude, with a rainfall rate of more than 40 mm/-day. The peak rainfall events could have drastic impact on the estuarine hydrodynamics due to the coinciding peak river flow discussed in Section 3.3.1.

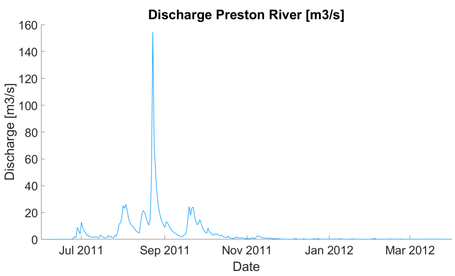

Figure 3.14: Modelled discharge of the Preston River in m^3/s

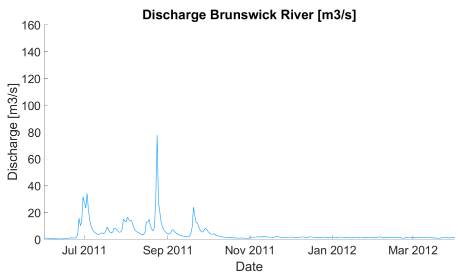

Figure 3.15: Modelled discharge of the Brunswick River in m^3/s

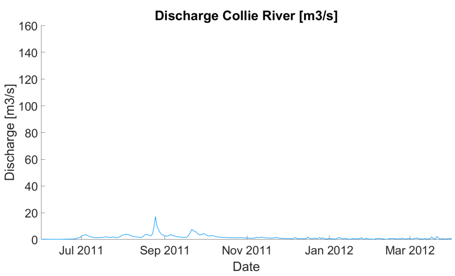

Figure 3.16: Modelled discharge of the Collie River in m^3/s

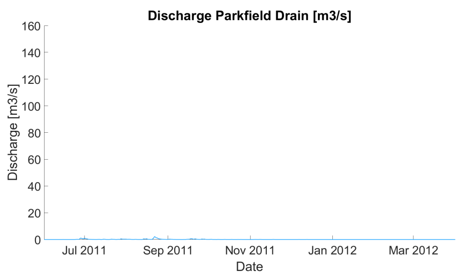

Figure 3.17: Modelled discharge of the Parkfield Drain in m^3/s

Freshwater discharge

The river discharge data of the Parkfield Drain (Figure 3.17), Collie (Figure 3.16), Brunswick (Figure 3.15), Ferguson and Preston River (Figure 3.14) in 2011 and 2012 are modelled by

DWER in 2020 and are verified against observed river discharge data. The peak discharge for all rivers occurs just after the peak rainfall event of the 21^{st} and 22^{nd} of August 2011 and persists for a couple of days. The intensity of the peak rainfall event described in Section 3.3.1, caused the large river discharge rates after August 21.

River	Full period	Summer	Winter
Collie	1.56	0.65	2.20
Brunswick	4.11	1.43	8.52
Preston	4.31	0.19	9.71
Parkfield Drain	0.08	0.001	0.20

Table 3.2: Mean river discharges $[m^3/s]$

Mean freshwater discharge

The mean discharges over the summer period (01/12/2011 to 29/02/2012) and the winter period (01/06/2011 to 31/08/2011) for each river are listed in Table 3.2. Winter river flow is one to two orders of magnitude higher than summer river flow due to higher and more frequent rainfall.

3.3.2 Wind

Wind data (from the Bureau of Meteorology at the Bunbury Power Station) were decomposed into east-west (Figure 3.18) and north-south (Figure 3.19) components. On average, south-easterly winds dominate in summer while north-westerly winds prevailed in winter (Figure 3.20). This observations correspond with the findings of Pearce et al. (2015), who stated that in winter winds are predominant north-westerly and in summer winds are predominant south-easterly. The mean for the whole period is a southerly wind (Figure 3.20).

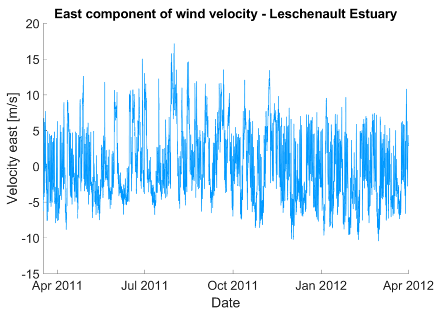

Figure 3.18: East (+) and West (-) component of wind velocity measured at Bunbury Power Station

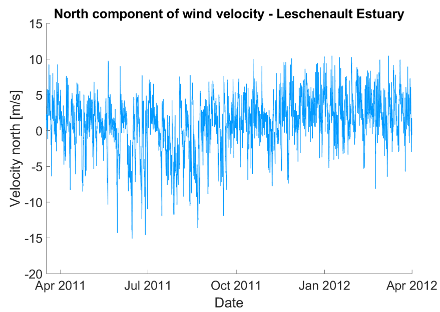

Figure 3.19: North (+) and South (-) component of wind velocity measured at Bunbury Power Station

Alongshore current

According to Pearce et al. (2015), the alongshore current at the west coast of Australia is mainly influenced by the Leeuwin current primarily driven by a pressure gradient with a

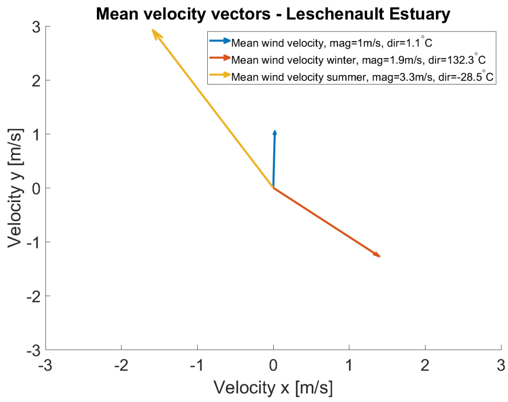

Figure 3.20: Mean wind velocity vector measured at the Bunbury Power Station of the full period, winter period and summer period (arrow points the direction the wind is blowing to)

range from south-east Asia to Tasmania. The Leeuwin current is caused by thermohaline forcing and the Indonesian Throughput, which is the large-scale oceanic current flowing through the Indonesian archipelago (Feng et al., 2009). The direction of the surface current of the Leeuwin current is southward along the west coast of Australia and flows eastward along the south coast of Australia towards Tasmania (Pearce et al., 2015). The Leeuwin current is modulated by seasonally varying wind currents and is strongest during winter when the southerly winds are less prevailing (Pearce et al., 2015). Moreover, as can be seen in Figure 3.20, the wind direction in winter is pointed towards the south-east and therefore strengthen the Leeuwin current. In the summer months the southerly winds prevail, which overpowers the southward directed Leeuwin current, resulting in northward alongshore currents (Pearce et al., 2015). According to Pearce et al. (2015) minimum wind speeds of 3-5 m/s are needed to counteract the pressure gradient of the Leeuwin current and change the direction of the alongshore current in shallow coastal regions and wind speeds of 6.2 m/s or higher on the outer shelf. In estuaries, the effect of winds on the current is different due to their shallow depths, which underlines the influence of the wind stress relative to the effects of the horizontal density gradient (Geyer, 1997).

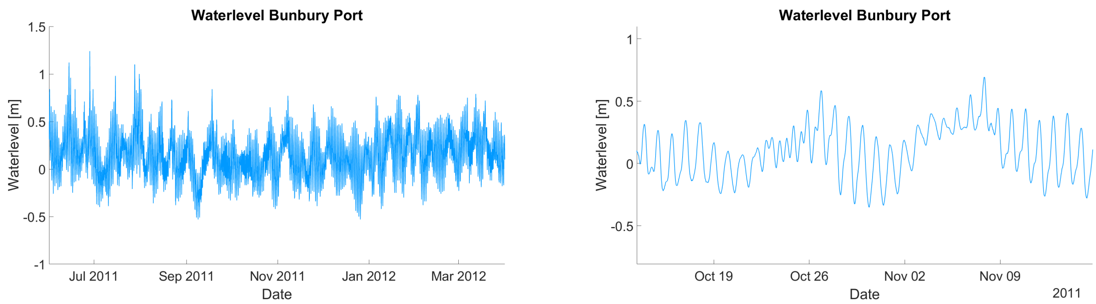

Figure 3.21: Observed water level collected at Bunbury Port between March 2011 and April 2012 with an open air non-contact microwave radar gauge, full period (left), zoomed in (right)

3.3.3 Tide and surface elevation

Water level measurements from March 2011 until April 2012 at the Bunbury Port are performed by the DoT (Figure 3.21, left). The water levels show a clear tidal influence. The main tidal constituents for Bunbury Port are summarized in Table B.1 and those calculated by Gillibrand et al. (2012) in Table B.2. By applying the tidal constituents of Table B.1 and B.2 in Equation 3.1 a value of 2.7 - 2.8 is obtained, indicating a mixed tidal regime for the Leschenault region but mainly diurnal (Bosboom and Stive, 2012). As shown in Figure 3.21, tides are mainly diurnal during spring and become more semi-diurnal during the neap period.

$$F = \frac{K1 + O1}{M2 + S2} \tag{3.1}$$

Category	Value of F
Semi-diurnal	$0 - 0.25$
Mixed, mainly semi-diurnal	$0.25 - 1.5$
Mixed, mainly diurnal	$1.5 - 3$
Diurnal	> 3

Table 3.3: The tidal character indicated by the form factor F (Bosboom and Stive, 2012)

3.3.4 River temperature and salinity

Air temperature and water temperature for the Ferguson and Collie river measured by DWER during 2011 and 2012 are shown in Figure 3.24. A clear difference between summer and winter is noticed, which expresses the high sensitivity of the water temperature to the atmospheric forcing. The cooler climate in winter lowers the water temperature of the rivers. In summer, this process is reversed, with a warmer climate heating the water of the rivers. River salinities are near zero and do not exceed values of 1 PSU. The salinity values in the Collie River and Ferguson River are therefore not shown.

3.3.5 Meteorology

Meteorology data relevant for the Leschenault Estuary area are continuously monitored by BoM at weather station Bunbury. Air pressure, cloud cover, air temperature and dew-point data are collected. The cloud cover monitored by BoM is expressed in okta, which represents the cloud amount in numbers between 0 and 9 (Ahmad et al., 2017). A value of 0 indicates a clear sky without the presence of clouds and a value of 8 represents a totally covered sky (Ahmad et al., 2017). A value of 9 indicates fog or other phenomena that could obstruct the sky from view (Ahmad et al., 2017). The cloud cover in okta can be rewritten to cloud cover in percentages by multiplying the cloud cover in okta by 12.5. The daily averaged cloud cover in percentages is depicted in Figure 3.23. More clear skies are detected in the summer period than in the winter period. Air pressure and air temperature data are shown in Figure 3.22 and 3.24 respectively. The relative humidity presented in Figure

3.25 is calculated according the August-Roche-Magnus formula (Equation 3.2) explained by Lawrence (2005).

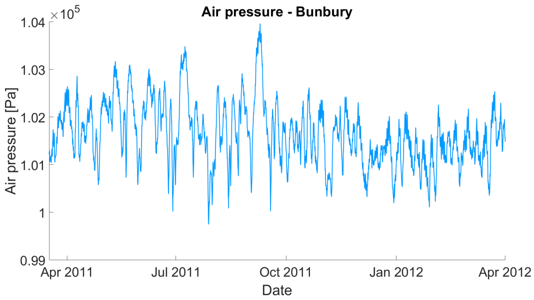

Figure 3.22: Measured air pressure at weather station Bunbury

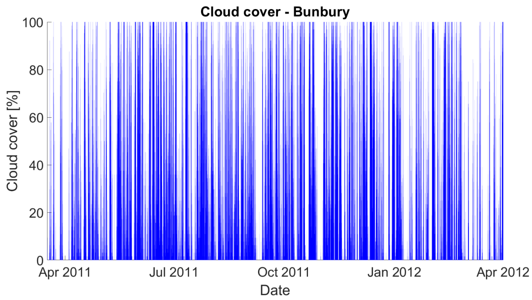

Figure 3.23: Cloud cover at weather station Bunbury

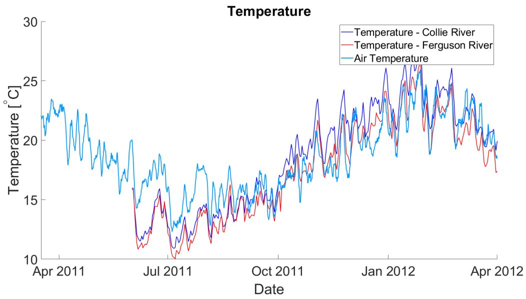

Figure 3.24: Measured air temperature at weather station Bunbury

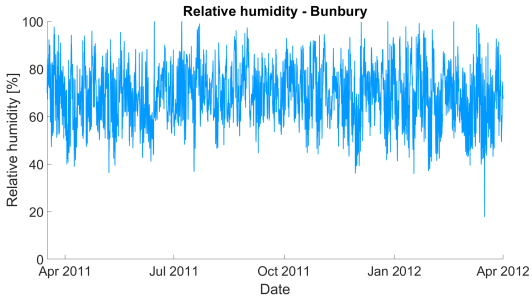

Figure 3.25: Relative humidity at weather station Bunbury

$$RH = 100 \frac{exp(\frac{aT_d}{b+T_d})}{exp(\frac{aT}{b+T})} \tag{3.2}$$

Where Rh represents the relative humidity in %, T is air temperature in $°C$, T_d is dew-point temperature in $°C$, a is a constant with a value of 17.625 and b is a constant with a value of 243.04.

3.3.6 Evaporation

In Figure 3.26 (left), the daily evaporations rates measured at the weather station Bunbury Power Station are depicted. A clear distinction between winter and summer rates is noticeable. Evaporation rates are typically lower in winter and higher in summer. This is due to many factors including cloud cover, humidity and air temperature. In Figure 3.26 (right), the evaporation is plotted against these factors. From Figure 3.26 (right), it becomes clear that the air temperature is following the same trend as the evaporation, which indicates their correlation. Moreover, lower humidity and cloud cover values, result directly in higher evaporation rates. After a maximum evaporation rate is achieved, evaporation

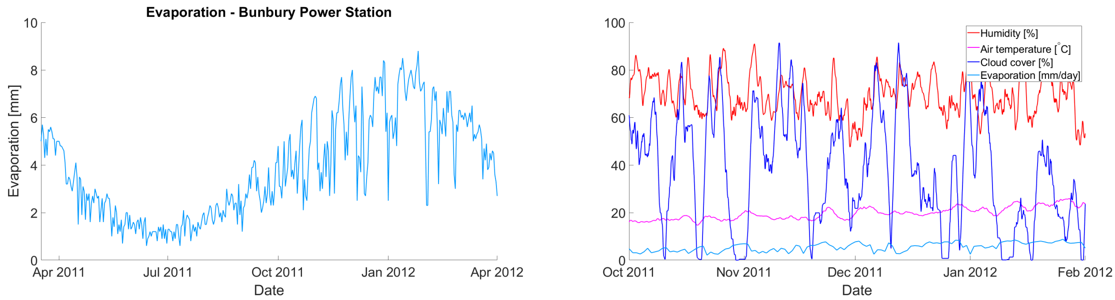

Figure 3.26: Evaporation measured at weather station Bunbury Power Station (left), evaporation assessed with cloud cover and humidity (right)

rates suddenly drop as a result of an increase in humidity and cloud cover. It is therefore suggested that the higher evaporation rates in summer, generate more clouds and humidity, which eventually decreases the evaporation. This pattern is recognizable in Figure 3.26 (left), where the evaporation rates are more volatile in summer and more constant in winter.

3.3.7 Tides inside the estuary

RBR-pressure sensors were deployed in 2020 to measure the water level inside the Leschenault Estuary with a 2Hz frequency. This sampling frequency includes gravity waves on the pressure measurements. The pressure measurements were conducted from February 14, 2020 to April 23, 2020. In Figure 3.27, the water level is presented from February 20 to March 6. This period is chosen, as it contains the highest high-frequency waves in the 2.5 month period. The waves are all less than 10 cm in height and it could therefore be argued if these will play a significant role in the hydrodynamics of estuaries like the Leschenault Estuary. However, the measurements are conducted in the summer/autumn period and higher waves are expected in the winter period.

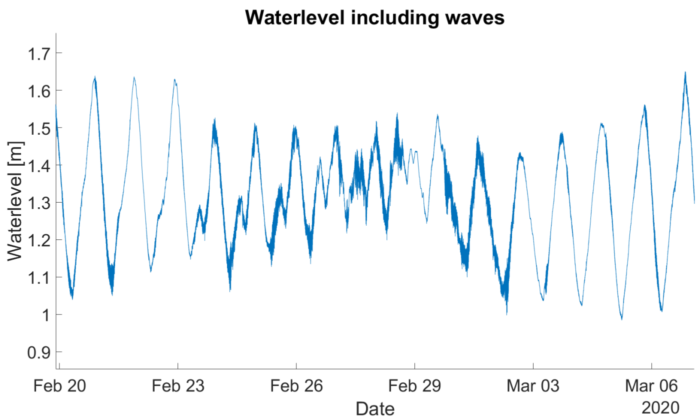

Figure 3.27: Water level at ESTUARY4 including high-frequency waves

3.4 Field Measurements

During this thesis, DWER conducted measurements at the Leschenault Estuary. An overview of the used instruments, location and observation points is summarized in Table 3.4. The new data were collected at almost similar locations as the data measured in 2011/2012 (Figure 3.28). EXO-sensors measure a wide range of water quality properties including temperature and salinity. RBR-sensors measure pressure, which can be used to calculate water depth, water level, wave height and wave period. ADCP-sensors measure flow velocities and direction. In Figure 3.29 and 3.30, several pictures are added to illustrate the field trip to the Leschenault Estuary. In Figure 3.29 (left), the boat used for the measurements is shown. In Figure 3.29 (right) and Figure 3.30 (right), the dismantling and deploying respectively of the EXO-sensor frame are shown. The sensors were attached to a heavy steel frame with enough weight in order to not be moved by currents. In Figure 3.30 (left), the data has been extracted from the instruments. All data were referenced and quality-controlled.

Site	Latitude	Longitude	Depth (m)	Instruments
LECUTN The Cut – NEW SITE	-33.3042	115.6781	~4	Two EXOs (CTD) at the surface and bottom and an ADCP (doppler flow meter) at the bottom.
LECOL1A Collie River – NEW SITE	-33.3123	115.7149	~2	An EXO (CTD) at the bottom/mid depth and an ADCP (doppler flow meter) at the bottom/mid depth.
Est6 AWRC 6121254 (Leschenault Estuary - Mid Estuary)	-33.2706	115.700	~1.5	An EXO (CTD) at the bottom/mid depth. And two RBR pressure sensors at the bottom/mid depth attached to a metal frame.
Est3 AWRC 6121206 (Leschenault Estuary - Est3)	-33.2323	115.7095	~1	An EXO (CTD) at the bottom/mid depth.

Table 3.4: Overview of the observation points of 2020

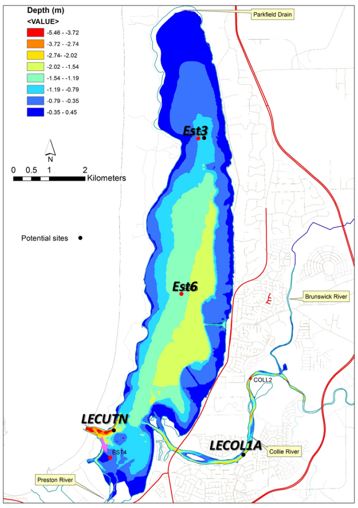

Figure 3.28: Map overview with observation points used for the measurements in 2020 (DWER, 2020)

Figure 3.29: Boat used to conduct measurements (left), collecting EXO-sensor (right)

Figure 3.30: Extracting data (left), deploying EXO-sensor (right)

4

Model set-up

In this chapter, the model set-up of the Leschenault estuary is briefly discussed, details about the model calibration and validation are presented in Chapter 5.

4.1 General

The general specifications of the model contain the vertical layer set-up, the model coordinate system and the angle of latitude. For the vertical layer specification the z-model is chosen with uniform z-layers of 0.2 m thick from the free surface level of 0 m until a depth of 3 m. Below 3 m depth, the vertical grid size grows with a factor of 1.2 until the lowest vertical point is reached. The z-model is chosen in order to reduce the chance of modelling errors in salinity and/or temperature in the vertical. The z-model has specified layer depths in contrast with the σ-model. The σ-model can therefore have to much artificial mixing, which is unwanted. Besides, it is easier to compare the stratification in the estuary. The model coordinate system used by DWER for Western Australia is GDA94 / MGA zone 50 with EPSG code 28350. This is a Cartesian (x, y, z) coordinate system that has a horizontal plane of reference. All spatial datasets are converted to GDA94 / MGA zone 50. The angle of latitude is specified in the model to calculate a fixed Coriolis force for the model domain. The applied angle of latitude and longitude have values of -33.267° and 115.7° respectively.

4.2 Area

The model area consists of all geographical features that are not based on grid coordinates but xy-coordinates and can therefore exist without or outside the grid (Deltares, 2020). If the grid is changed for example this will not alter the location of the geographical features. The features used in this research are the observation points and cross-sections, a fixed weir and land boundaries. The land boundaries only served as a reference for the development of the grid and are therefore not discussed.

4.2.1 Observation points

The observation points of the DFM-model are located on the same geographic positions as the measurement points of 2011 and 2012 (Figure 4.1). The observation points of 2011 and 2012 are depicted in Figure 4.1 as white dots. The names of the specific observation points are attached to the corresponding white dots. Figure 4.1 also shows four red dots, which indicate the new measurement points of 2020. The new positions should be considered when comparing 2011/2012 data with 2020 data.

4.2.2 Observation cross-sections

The observation cross-sections are illustrated as white lines in Figure 4.2. The names of the cross-sections are attached to the corresponding lines. The positions of the nine cross-sections are strategically chosen to enhance the ability to draw valuable conclusions.

4.2.3 Fixed weirs

In the central basin of the Leschenault Estuary, an emerged dam is built that only serves a recreational purpose. The emerged dam is connected with the mainland by a jetty and is modelled as a fixed weir. A thin dam would be less realistic in this case, being infinitely thin and high. A fixed weir takes into account the chance of overtopping in case of extreme water levels or waves. The fixed weir applied in the Leschenault Estuary model is depicted in Figure 4.3 (left) as a purple line in the central basin. The dimensions of the fixed weir are specified in Table 4.1.

Parameter	**Value**	**Unit**
X-coordinate 1	379070	m
X-coordinate 2	379541	m
Y-coordinate 1	6315956	m
Y-coordinate 2	6315279	m
Crest level	1	m
Ground height left	2.5	m
Ground height right	2.5	m
Crest width	15	m
Slope left	3	–
Slope right	3	–
Roughness code	0.05	–

Table 4.1: Dimensions of fixed weir of DFM-model

4.3 Computational grid

The computational grid of the final version of the Leschenault Estuary is depicted in Figure 4.3 (left). The grid is unstructured and developed by combining triangular and rectangular grid cells. During the set-up of the model a trade-off had to be made between computation

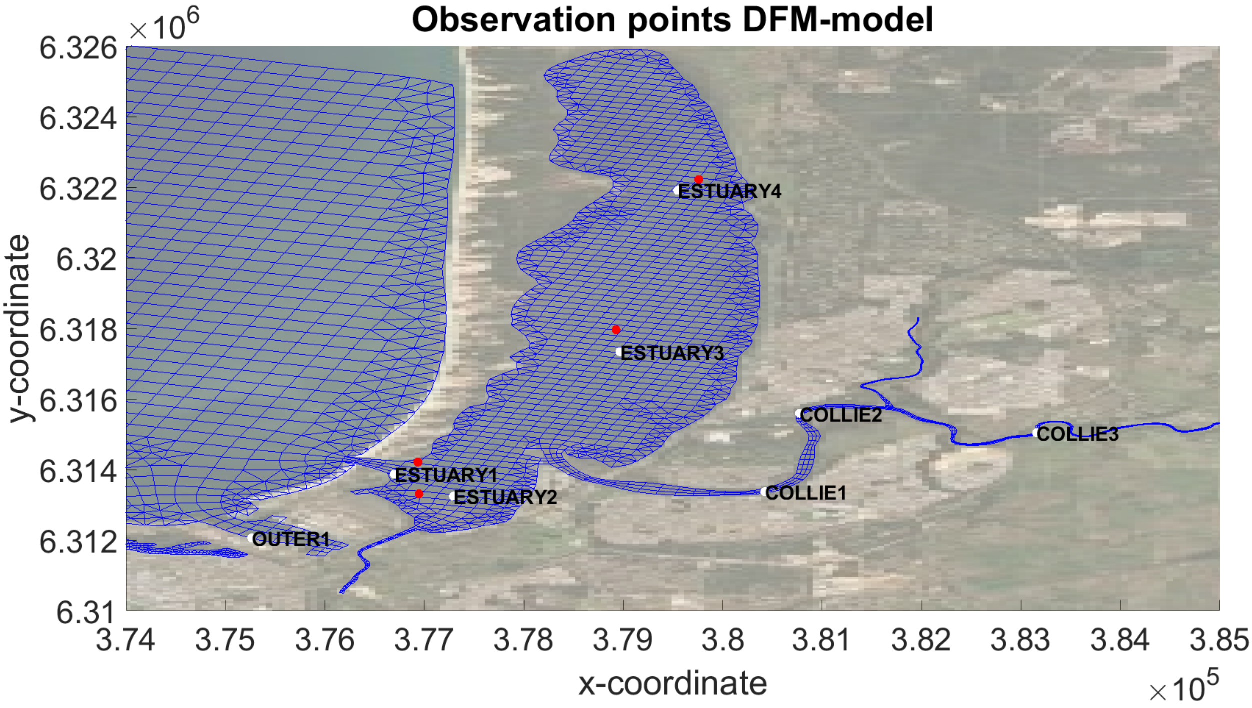

Figure 4.1: Observation points indicated with white dots, red dots indicate new observation points

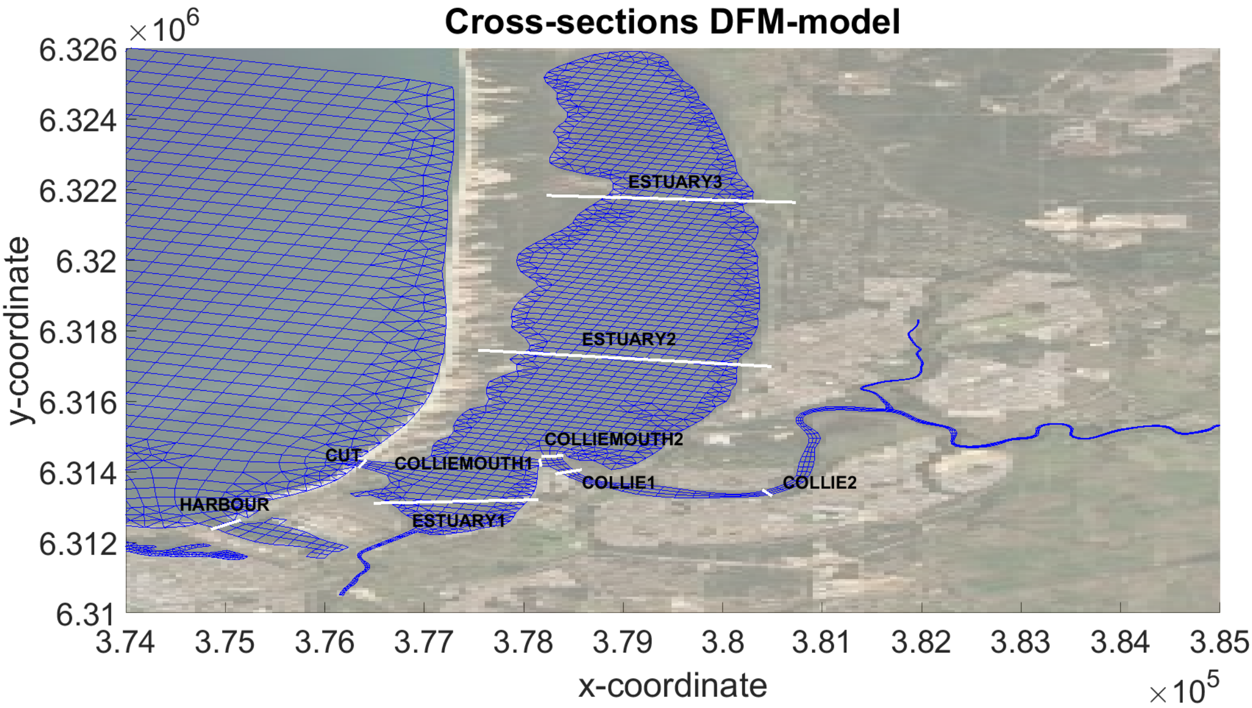

Figure 4.2: Cross-sections in DFM-model indicated with white lines

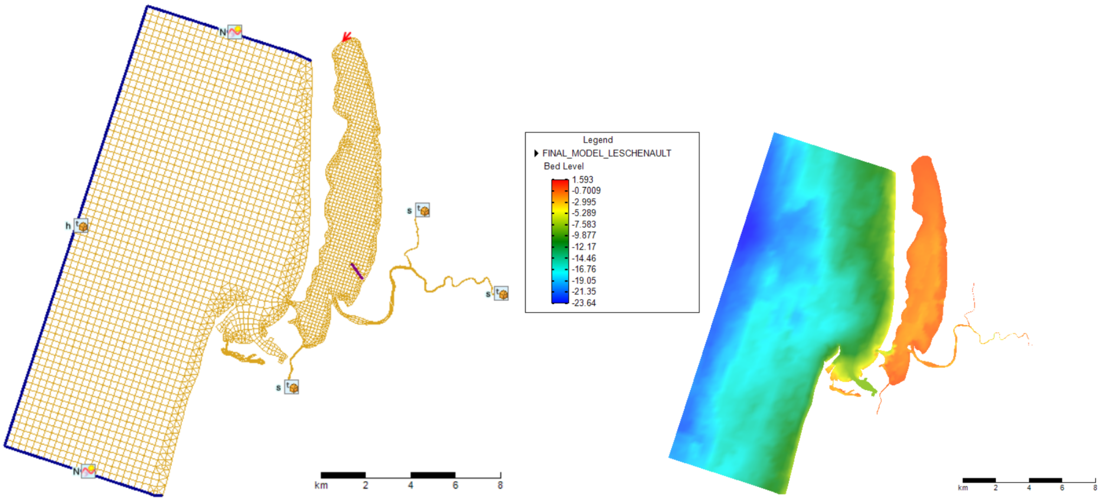

Figure 4.3: Grid of final DFM-model (left), bathymetry interpolated over grid (right)

time and accuracy. After a thorough calibration process, the final version of the grid is developed, which is depicted in Figure 4.3 (left). The final version has the most ideal balance between accuracy and computation time. The offshore grid cells have a dimension of 300 m by 300 m, the rectangular grid cells in the estuary are 150 m by 150 m and the smallest grid cells can be found in the rivers (min. 30 m by 10 m).

4.4 Bed level

The bathymetry data used in the Leschenault-model were compiled by DWER in 2016 using different datasets. The bathymetry data consists of block filled data, data from a survey conducted by DoT in 2005, estuary LiDAR data from 2015, in-filled focal statistics, interpolated data, marine LiDAR data from 2009 and terrestrial LiDAR data from 2008. The geodetic model used by DWER is GDA 94 and the vertical coordinate system used is AHD 71. The bathymetry is added to the model by interpolating the data over the grid points. The best option proved to be averaging the bathymetry data by their minimum value. This resulted in the bed level depicted in Figure 4.3 (right). Lowest bed levels are encountered offshore (as low as -25 m) and gradually rise until the coast is reached. The Bunbury Port and the connecting channel to the sea have a constant bed level of -8 m and are periodically dredged to maintain the depth. In the estuary bed levels typically lie between -0.5 m and -2.5 m and lowest values are observed in the ‘Cut’ (around 3-5 m deep). The bed level in the Preston River has a constant value of -0.7 m and bed levels in the Collie and Brunswick River vary between -2.5 m and 0.5 m. The Collie and Brunswick River were gradually risen upstream to mimic observations.

4.5 Time frame

The time frame is set up with a maximum Courant number of 0.7, user time step of 2 minutes, nodal update interval of 6 hours, maximum time step of 60 s and initial time step of 60 s. The start and stop time are chosen based on the available data and are 01-06-2011

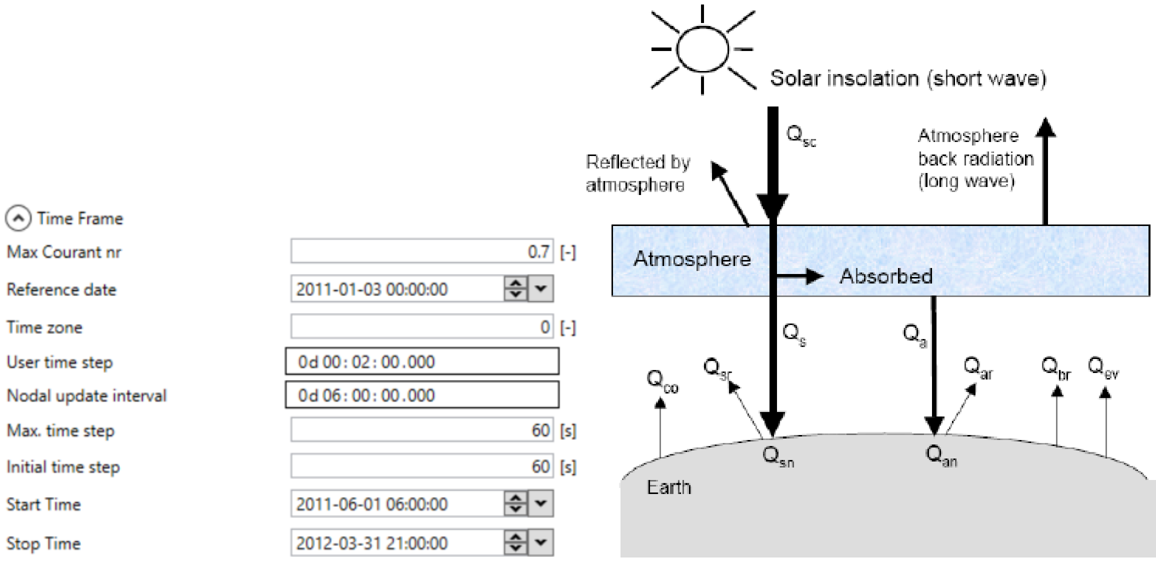

Figure 4.4: Time frame of Leschenault-model (left), heat exchange system (Deltares, 2020) (right)

06:00:00 and 31-03-2012 21:00:00 respectively. All applied time frame input are summarized in Figure 4.4.

4.6 Processes

The processes included in the Leschenault-model are tide generating forces, salinity and temperature. Secondary flow is not considered as the focus of the hydrodynamics is on the estuarine water body and not on the rivers. The secondary flow would therefore play a minor role in the hydrodynamics of the model and would only increase the computation time without improving the accuracy. Waves are not considered, as wave data were not available for the 2011/2012 period. However, 2020 data presented in Chapter 3, shows that wave heights are less than 10 cm. This indicates the minor role of the waves on the hydrodynamics inside the estuary. However, extreme weather events could disrupt the hydrodynamics. Morphological processes were not considered in this research due to time constraints but including them in future research is highly recommended. The composite model (heat flux model - number 5) is chosen to calculate the temperature in the model and makes use of Equation 4.1 as in Deltares (2020). A schematization of Equation 4.1 is depicted in Figure 4.4 (right).

$$Q_{tot} = Q_{sn} + Q_{an} + Q_{br} + Q_{ev} + Q_{co} + Q_{evfree} + Q_{cofree} \tag{4.1}$$

Where, Q_{sn} is the net incident solar radiation (short wave), Q_{an} is the net incident atmospheric radiation (long wave), Q_{br} is the back radiation (long wave), Q_{ev} is the evaporative heat flux (latent heat), Q_{co} is the convective heat flux (sensible heat), Q_{evfree} is the evaporative heat flux (free convection latent heat) and Q_{cofree} is the convective heat flux (free convection sensible heat).

4.7 Initial and boundary conditions

The initial conditions seem not to be very important for the model results as is seen in Chapter 5. Due to the short spin-up time of approximately two weeks, the model is able to adapt quickly. Uniform initial values for water level, salinity and temperature of respectively 0 m, 36 PSU and 21 °C were applied. The boundaries applied in the model are depicted in Figure 4.3 (left). Three different boundary types can be distinguished in Figure 4.3: one boundary indicated with an h represents the western offshore boundary, two boundaries indicated with a N represent the northern and southern offshore boundary and three boundaries indicated with a s represent the river boundaries.

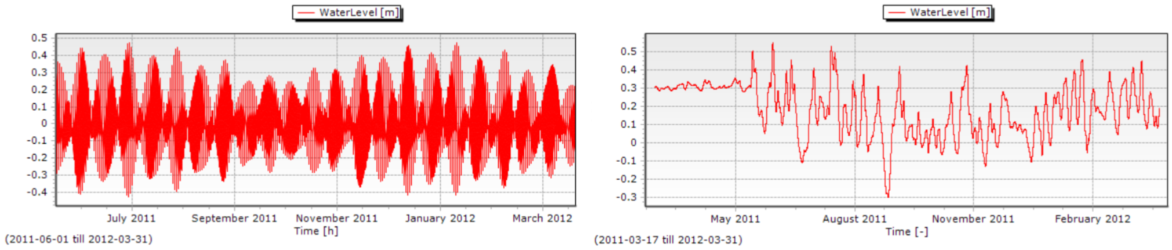

Figure 4.5: Tidal forcing (left) and sub-tidal forcing (right) at western offshore boundary

4.7.1 Western offshore boundary

The western offshore boundary is forced with tidal and sub-tidal water levels, salinity and temperature data at two data points at the corners of the model grid. No spatial flow velocity data were included in the model, since the velocity data have a coarse (10 km) resolution. Further, the Leschenault Estuary is located 10 km from the northern and southern boundaries and 7 km from the western boundary. As the estuary is only connected with the ocean by the 'Cut', the influence of the flow velocity at the boundaries is expected to be negligibly small. This is confirmed in Chapter 5 and 6. The northern and southern data points of the western boundary have slightly different values for the sub-tidal data to simulate the barotropic gradient along the coast. The sub-tidal forcing, also used in the CSIRO-model, is the residual water level after filtering the tide from the water level observations depicted in Figure 3.21, using a low-pass filter with half amplitude period of 33 hours and a half power period of 38 hours (Beardsley et al., 1983). The tidal time-series and sub-tidal time-series are depicted in Figure 4.5 (left) and (right) respectively. The spatial salinity and temperature data were retrieved from the OFAM-model operated by CSIRO and are depicted in Figure 4.6 (left) and (right) respectively. The data shown in Figure 4.5 and 4.6 belong to the southern data point of the western offshore boundary. The data of the northern data point are not shown as the data only differ slightly an are not worth depicting.

4.7.2 Northern and southern offshore boundary

The northern and southern offshore boundaries are forced with a Neumann gradient of 0, which simulates a uniform water level from the western offshore boundary to the coast. A Neumann gradient is chosen for these boundaries to reduce the chance of unrealistic and unphysical flow velocities modelled along the boundaries. Unfortunately, this solution also

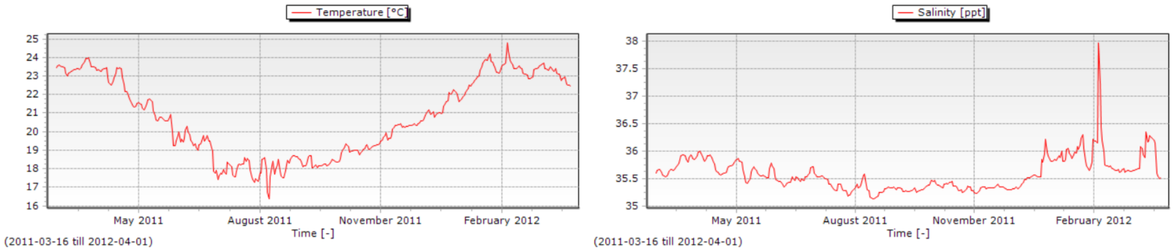

Figure 4.6: Temperature (left) and salinity (right) at western offshore boundary

might introduce strange circulation patterns and often reduces the reduction quality of the water level. However, as the focus area is the Leschenault Estuary, which is sufficiently far from the boundaries, this did not influence the hydrodynamics inside the estuary.

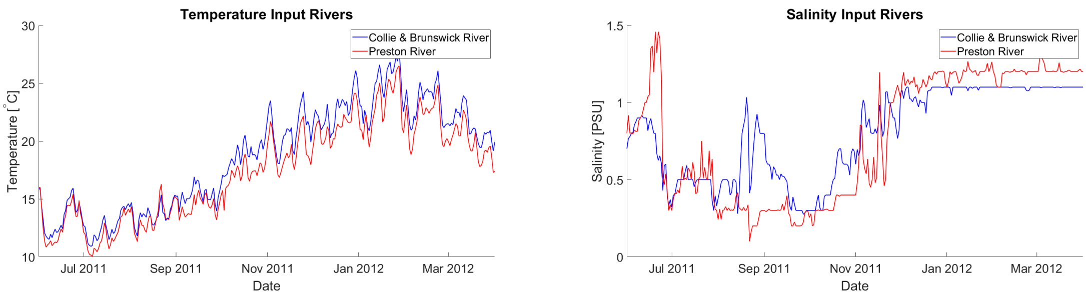

Figure 4.7: Temperature (left) and salinity (right) at river boundaries

4.7.3 River boundaries

The river boundaries at the Collie River, Preston River and Brunswick River were forced with discharge, salinity and temperature measured for the Ferguson River and Collie River. Salinity and temperature data of the Ferguson River and Collie River were also used for the Preston River and Brunswick River respectively. The temperature input of the river boundaries is depicted in Figure 4.7 (left) and the salinity input of the river boundaries is depicted in Figure 4.7 (right). Note that the Ferguson River is not considered in the model, as bathymetry data is lacking for this river. The discharge input of the river boundaries is shown in Figure 4.8 and is provided by DWER in 2020. The data are generated by a model developed by the SOURCE model that forecasts river discharge based on catchment characteristics and meteorological forcing.

4.8 Physical parameters

Different coefficients and parametrization were applied for temperature, gravity, density, roughness, viscosity and wind. These parameters and coefficients are summarized in Table 4.2.

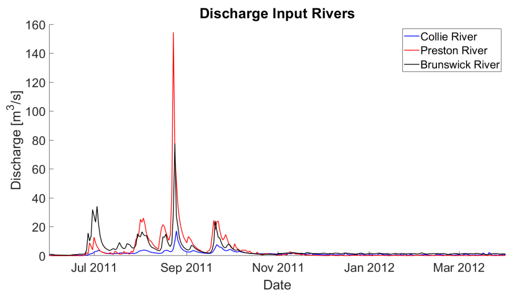

Figure 4.8: Discharge at river boundaries

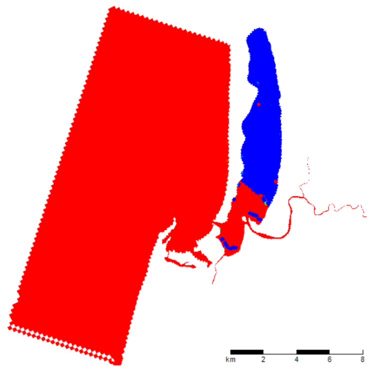

Figure 4.9: Spatial roughness data

Parameter	Process	Specification	Unit
Secchi depth	Temperature	1	m
Stanton number	Temperature	-1	–
Dalton number	Temperature	-1	–
Gravitational acceleration	Gravity	9.81	m^2/s
Water density	Density	1000	kg/m^3
Equation of state	Density	UNESCO	–
Manning friction coefficient	Roughness	0.02-0.023 (Figure 4.9)	–
Wall-behaviour	Roughness	Free-slip	–
Wall k_s for partial slip	Roughness	0	–
Uniform linear friction coefficient	Roughness	0	–
Linear friction U_{mod}	Roughness	0	–
Uniform horizontal eddy viscosity	Mixing	10	m^2/s
Uniform horizontal eddy diffusivity	Mixing	1	m^2/s
Uniform vertical eddy viscosity	Mixing	0.0001	m^2/s
Uniform vertical eddy diffusivity	Mixing	10^{-6}	m^2/s
Smagorinsky	Mixing	0.45	–
Wind drag coefficient	Wind	ICdtyp 6 (Wuest, 2005)	–
Air density	Wind	1.2	kg/m^3

Table 4.2: Physical parameters DFM-model

4.9 Sources and sinks

The Parkfield Drain source indicated as a red arrow in Figure 4.3 is forced with temperature, salinity and discharge data shown in Figure 4.10 (a), (b) and (c) respectively. The temperature and salinity data of the Parkfield Drain are similar as the data of the Collie and Brunswick River. The discharge of the Parkfield Drain is modelled by DWER in 2020, similar to the discharge data of the Collie, Brunswick and Preston River.

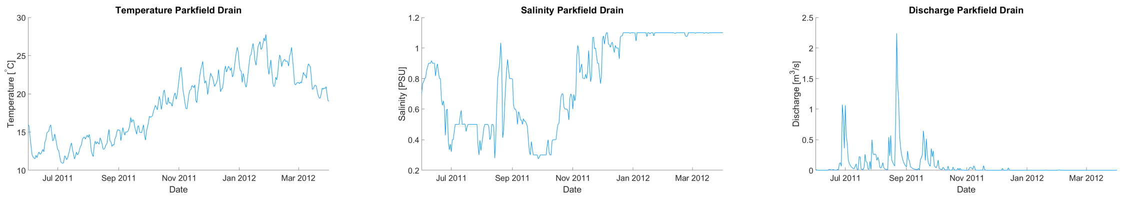

Figure 4.10: Temperature (a), salinity (b) and discharge (c) of Parkfield Drain

4.10 Numerical and output parameters and miscellaneous

The numerical parameters used in the Leschenault-model have default settings and are summarized in Figure 4.11. The output parameters are listed in Figure C.1 and C.2 of Appendix C. The his-file output is stored with an interval of 4 minutes and the map-file output is stored with an interval of 3 hours. The miscellaneous parameters are summed up in Figure C.3 and C.4. The model makes use of the k-ϵ turbulence model, which calculates the turbulence in 3D. Furthermore, a fully implicit step reduce is used as time step type and the turbulence advection is calculated by using horizontally explicit and vertically implicit schemes.

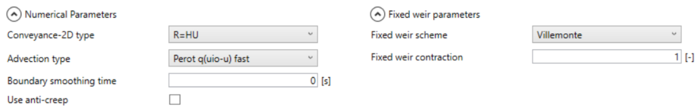

Figure 4.11: Numerical parameters of the DFM-model

4.11 Post-processing

To post-process the model results multiple programs are used including TextPad, Matlab, Python, Excel, QuickPlot, QGIS and more. Especially Matlab seemed very helpful in analysing and post-processing the data. Deltares has developed an open source Matlab-tool that can easily be of help when processing the data. This Matlab-tool is called EHY and has many features, as EHY-statistics, EHY-getmodeldata, etc.

Part III

Numerical calculations

A numerical model is developed to support the understanding in the governing hydrodynamic processes in the Leschenault Estuary relevant for water quality management. The model is calibrated and validated, but also valued by incorporating a realistic scenario and by retrieving important knowledge on hydrodynamic processes relevant for management.

5

Calibration & validation

The DFM-model was modified from its initial set-up to achieve an optimal version of the model. Model development consisted of three steps: the initial calibration, the sensitivity analysis and the validation. In the calibration phase, the model is stepwise adjusted to improve the model and to improve the understanding in the dominant factors affecting the model results. A brief and structured outline of this phase including the most important findings is summarized in Section 5.1. Secondly, a sensitivity analysis is conducted to better understand the dominant processes found in Section 5.1. The sensitivity analysis is outlined in Section 5.2. Lastly, the model results were validated against observed and modelled reference data to objectively assess the model's performance, elucidated in Section 5.3.

5.1 Calibration

The model is calibrated against observed water level, temperature and salinity data collected in 2011 and 2012 by the DWER and the DoT at eight individual observation points. To objectively assess the model's performance, specific statistics are used, which are expounded in Section 5.1.1. The calibration process briefly summarized in Section 5.1.2, is categorized according the specific variables that are modified step-by-step. To enhance the understanding in the dominant physical processes of the model, only one modification is executed at a time. The final validation of the model results is elucidated and depicted in Section 5.3.

5.1.1 Statistics

To objectively assess the DFM-model output, four statistical analyses are used: the bias, the standard deviation, the root mean squared error and the index of agreement of Willmott et al. (1985). The first three analyses are calculated with the EHY-statistics tool developed by Deltares in Matlab and the index of agreement of Willmott et al. (1985) is also calculated in Matlab. The bias is formulated in Equation 5.1.

$$bias = \frac{\sum_{j=1}^{n} (p_j - o_j)}{N} \tag{5.1}$$

Where, subscript j refers to the location in time or/and space, p_j refers to the model-predicted variable, o_j refers to the observed variable and N refers to the number of data points. Obviously, a smaller bias indicates a well-performing model, as the errors between modelled and observed data are small. The standard deviation used in this research is formulated in Equation 5.2.

$$std = \sqrt{\frac{\sum_{j=1}^{n} (p_j - o_j - bias)^2}{N}} \tag{5.2}$$

The standard deviation also gives information about the comparison between modelled and observed data. However, the standard deviation itself does not indicate the performance of the model. The standard deviation can best be interpreted by dividing it by the weighted average of the observed data. The root mean squared error is slightly different than the standard deviation and is formulated in Equation 5.3.

$$rmse = \sqrt{\frac{\sum_{j=1}^{n} (p_j - o_j)^2}{N}} \tag{5.3}$$

The root mean squared error can also be interpreted by dividing it by the weighted average of the observed data, which results in the ratio between the *rmse* and the weighted average of the observed data. The lower this ratio, the better performs the model. Gillibrand et al. (2012) classified ratios of 10% as well-performing models. Lastly, the index of agreement of Willmott et al. (1985) is formulated in Equation 5.4.

$$d_2 = 1 - \frac{\left[\sum_{j=1}^{n} (p_j - o_j)^2\right]}{\left[\sum_{j=1}^{n} (|p_j - \overline{o}| + |o_j - \overline{o}|)^2\right]} \tag{5.4}$$

Where d_2 represents the index of agreement of Willmott et al. (1985) and $\bar{(}o)$ refers to the weighted mean of the observed variable. The index of agreement indicates the performance of the model with a value between 0 and 1. A value of 1 represents a perfectly performing model and decreasing values towards 0 indicate worse performing models (Willmott et al., 1985).

5.1.2 Calibration process

The calibration process is summarized in this Section and subdivided in the physical processes that force the model and those calibrated during the development of the model. Furthermore, the the importance of these processes in the estuarine hydrodynamics were evaluated based on the changes in the model results.

Vertical and horizontal resolution

Several model runs were executed with different layer types and vertical resolution. Model runs with σ-layers take less time than model runs with z-layers. So, with regard to computation time, models with σ-layers are superior. However, z-layers perform better to assess stratification in shallow estuaries. Gillibrand et al. (2012) applied a vertical layer height of 0.5 m to the CSIRO-model. With a depth of max. -2.5 m in the estuary and the rivers, this layer height seemed to be to coarse to correctly simulate the salt transport dynamics inside the rivers according to Gillibrand et al. (2012). Here z-layers with a vertical grid height of 0.2 m for the top 3 m of the water column were applied. The layer size of 0.2 m gave the most optimal accuracy/computation time ratio. Below the upper layer of 3 m, the layer size grows with a factor of 1.2. The growth factor is chosen in cooperation with Herman Kernkamp, an experienced Delft3DFM-developer from Deltares, who stated that the growth factor should not exceed values of 1.2. Also a growth factor is considered of 1.1, which did not result in a better model performance but increased the computation time. Horizontal grid cell resolution appears to be an important factor in terms of computation time but is less of influence in the accuracy of the model than the vertical resolution. Several experiences are conducted with different grid cell sizes varying from coarse (300 m x 300 m) to fine (30 m x 30 m). The model with the coarser horizontal resolution and same vertical resolution as the model with the finer horizontal resolution has similar model outcomes. This confirms that it is better to have a vertically fine and horizontally coarse gird with regard to optimal computation time and accuracy.

River boundaries

Several model runs used different positions of the upstream river boundaries and different river discharge input to assess the influence of the position of the estuary and the estuary's discharge. First of all, three different boundary positions are tested: (a) boundary locations of the final model, (b) boundary locations at the estimated maximum salt wedge intrusion provided by DWER and (c) extended boundaries located further upstream. Changes in the position of the boundaries drastically alter the salt transport inside the rivers but not in the estuary. In the situation with the extended boundaries, the highest salt transport occurs in the rivers. The salt wedge configuration also generated a higher salt transport in the rivers than the final boundary locations. However, no bathymetry data were available for these extended river stretches. Moreover, the model runs with extended boundaries and salt wedge boundaries were run with default viscosity and diffusivity values and the salt transport in the rivers is therefore not in good agreement with the observed data. Bathymetric data for the stretch of the rivers are required to investigate the salt transport and salt wedge intrusion in the rivers. Despite the different salinity values per model scenario in the rivers, the salinity in the estuary did not change significantly. Therefore, the final model locations were chosen based on the reach of the bathymetry data. The influence of the freshwater discharge was assessed by reducing its value by 50%. This change increased the salinity in the rivers. However, to keep the model as realistic as possible the most recent developed discharge data of DWER were used.

Bathymetry

The bathymetry data used for the DFM-model, is developed by DWER in 2016. Different methods of interpolation of the bathymetry data to the model grid were tested. First, the bathymetry is interpolated by triangulation. However, problems were encountered to guarantee sufficient depth in the rivers to enable salt transport. To safeguard the depth in the rivers, the bathymetry was interpolated by averaging over the minimum depth in a grid cell. This resulted in slightly overestimated bed levels in the estuary but better agreement of the salinity values in the rivers.

Water level

The water level of the estuary comprises of tidal and sub-tidal forcing at the western offshore boundary. The sub-tidal data was extracted from Gillibrand et al. (2012). The tidal forcing on the other hand is thoroughly analysed. The tidal constituents, listed in Table B.2 and B.1, were implemented in different versions of the model. The best fit was obtained by using the tidal constituents of Table B.1 less J1 and MSM and using the phase and amplitude of the corresponding constituents of Table B.2.

Viscosity and diffusivity

The degree of mixing in the estuary is for a great extent determined by the viscosity and diffusivity parameters. Using the default vertical and horizontal viscosity and diffusivity coefficients prevented the salt transport inside the rivers. This led to salinity values in the rivers of 0 year-round. During the calibration process, higher horizontal diffusivity values were applied (10 to 100 m^2/s) to increase the horizontal mixing and therefore the salt transport in the rivers. However, the stratification is overpowered by increasing the mixing in the estuary, which is unrealistic for the Leschenault Estuary. To see whether something was wrong with the forcing in the model or with the mixing parameters, the vertical diffusivity was set to 0. In this case no vertical mixing is possible, which leads to highly stratified flows. This immediately generated better 3D salinity and temperature results in the river but also in the estuary. Besides, experiences are conducted with the smagorinsky value, which calculates the horizontal diffusivity for different locations. The mixing parameters seemed of significant influence and are therefore also used in the sensitivity analysis of Section 5.2.

Roughness

The roughness input of the model was determined by using Table 2.2. Firstly, constant roughness and Manning coefficients were applied to the model. Models with different roughness values were compared to the default model with roughness of 0.023. A lower roughness value of 0.020 produced a better salinity agreement in the rivers, the 'Cut' and the southern and central basin of the estuary. A higher roughness value of 0.026 promoted better matching of the salinity values in the northern basin of the estuary. A value of 0.035 for the Manning coefficient resulted in worst agreement and a value of 0.011 led to unstable model results. The roughness parameter is further assessed in the sensitivity analysis of Section 5.2.

Rainfall and evaporation

Rainfall and evaporation data were provided by DWER. Whereas salinity was more sensitive to variations in mixing parameters, temperature was not. Therefore, different methods were tested to model the temperature and salinity. Heat flux model 1, with prescribed rainfall and evaporation data, gave worse results for salinity and temperature. The salinity was underestimated throughout the estuary and temperature results were completely off. Therefore, heat flux model 5 (composite model) was used in the final DFM-model to calculate the temperature.

Miscellaneous

Other parameters that are calibrated are the baroclinicity function *idensform*, the water density, the *logprofkeps* function and the secondary flow. The first parameter *idensform* considers the baroclinicity in the model. The model results were not better by implementing the *idensform* function but it should be included to consider the baroclinic flow. Model runs with different uniform water densities had similar outcomes as the default value of 1000 kg/m^3. The implementation of the secondary flow also does not alter the hydrodynamics of the estuary. Lastly, the use of the *logprofkeps* function, which should improve the stability of the turbulence along the boundaries does not change the model output.

Parameter	Initial Model	Final Model
Horizontal diffusivity	0.1 m^2/s	1 m^2/s
Horizontal viscosity	1 m^2/s	10 m^2/s
Vertical diffusivity	0 m^2/s	10^{-6} m^2/s
Vertical viscosity	$5 \cdot 10^{-5}$ m^2/s	10^{-4} m^2/s
Roughness	0.023	Spatial
Smagorinsky	0	0.45

Table 5.1: Parameters of initial and final model

5.2 Sensitivity analysis

In the sensitivity analysis the most impactful parameters are considered to improve the salinity and temperature results of the DFM-model. These parameters include the horizontal diffusivity, the horizontal viscosity, the vertical diffusivity, the vertical viscosity, the bed roughness and the Smagorinsky value. The different sensitivity scenarios, including their values and units, are listed in Table 5.2. The salinity and temperature data generated by DFM were validated against observed data and compared with the initial model results by using the D2 skill number. The parameter values of the initial model are summarized in Table 5.1. All D2 skill numbers of the different stations in the different sensitivity models are shown in Table 5.3 for salinity and in Table 5.4 for temperature. The station names are: C1S (COLLIE1SURFACE), C1B (COLLIE1BED), E1 (ESTUARY1), E4 (ESTUARY4), E2 (ESTUARY2), E3 (ESTUARY1).

Model	Parameter	Value	Unit
M1	Horizontal diffusivity	1	m^2/s
M2	Horizontal diffusivity	0.01	m^2/s
M3	Horizontal viscosity	10	m^2/s
M4	Horizontal viscosity	0.1	m^2/s
M5	Vertical diffusivity	10^{-6}	m^2/s
M6	Vertical diffusivity	10^{-8}	m^2/s
M7	Vertical viscosity	10^{-4}	m^2/s
M8	Vertical viscosity	10^{-7}	m^2/s
M9	Roughness	0.02	-
M10	Roughness	0.026	-
M11	Smagorinsky	0.15	-
M12	Smagorinsky	0.3	-
M13	Smagorinsky	0.45	-

Table 5.2: Sensitivity analysis scenarios

5.2.1 Horizontal diffusivity

M1 and M2 have horizontal diffusivity values of 1 m^2/s and 0.01 m^2/s and were compared with the initial model with a horizontal diffusivity of 0.1 m^2/s. With regard to salinity, the M1 and M2 results were not significantly different. M1 has a slightly worse agreement at C1S but a slightly better agreement at E4 and E3. M2 has similar D2-values as the initial model but a slightly worse value at E2. The slightly better D2-values for M1 could indicate that the horizontal diffusivity is higher in the estuary. However M1 generated better results for temperature. Therefore a horizontal diffusivity of 1 m^2/s is considered in the final model.

5.2.2 Horizontal viscosity

M3 and M4 have horizontal viscosity values of 10 m^2/s and 0.1 m^2/s and were compared with the initial model with a horizontal viscosity of 1 m^2/s. With regard to salinity, M3 gave much better D2-values at C1S, C1B, E1 and E2 but slightly worse values at E4 and E3. M4 only produced a better D2-value at E4 for salinity but generated significantly worse values for temperature. In contrast, the M3 temperature results have similar agreements with observed data as the initial model. It is therefore suggested that the Leschenault Estuary had a higher horizontal viscosity of 10 m^2/s.

5.2.3 Vertical diffusivity

M5 and M6 have vertical diffusivity values of 10^{-6} m^2/s and 10^{-8} m^2/s and were compared with the initial model with a vertical diffusivity of 0 m^2/s. With regard to salinity, M5 gave much better D2-values at C1S, C1B, E1 but slightly worse values at E4 and E2. M6 only had a better D2-value at E3 for salinity but performed a lot better than the initial model in terms of temperature. In contrast, the M5 temperature results were slightly worse. However, due to the significant improvement of M5 in the salinity results a vertical diffusivity was chosen of 10^{-6} m^2/s.

	INITIAL	M1	M2	M3	M4	M5	M6	M7	M8	M9	M10	M11	M12	M13
C1S	0.85	0.84	0.84	0.88	0.84	0.89	0.75	0.85	0.84	0.84	-	0.84	0.84	0.84
C1B	0.89	0.89	0.89	0.91	0.88	0.91	0.51	0.88	0.89	0.89	-	0.89	0.89	0.89
E1	0.86	0.86	0.86	0.87	0.86	0.87	0.84	0.85	0.86	0.85	-	0.86	0.86	0.87
E4	0.93	0.94	0.93	0.92	0.94	0.92	0.91	0.93	0.94	0.94	-	0.94	0.94	0.93
E3	0.78	0.8	0.78	0.77	0.78	0.78	0.81	0.81	0.78	0.79	-	0.78	0.79	0.81
E2	0.81	0.81	0.8	0.82	0.8	0.8	0.79	0.81	0.8	0.79	-	0.81	0.82	0.82

Table 5.3: D2 of salinity values per model of the sensitivity analysis scenarios

	INITIAL	M1	M2	M3	M4	M5	M6	M7	M8	M9	M10	M11	M12	M13
C1S	0.94	0.94	0.94	0.94	0.94	0.95	0.94	0.94	0.94	0.93	-	0.94	0.94	0.94
C1B	0.95	0.95	0.95	0.95	0.95	0.95	0.95	0.95	0.95	0.95	-	0.95	0.95	0.95
E1	0.84	0.84	0.84	0.85	0.84	0.83	0.86	0.84	0.84	0.84	-	0.84	0.84	0.84
E4	0.94	0.94	0.94	0.94	0.94	0.94	0.95	0.95	0.94	0.94	-	0.94	0.94	0.94
E3	0.93	0.93	0.93	0.93	0.93	0.91	0.95	0.94	0.93	0.93	-	0.93	0.93	0.93
E2	0.55	0.57	0.55	0.55	0.54	0.47	0.62	0.57	0.55	0.55	-	0.55	0.55	0.56

Table 5.4: D2 of temperature values per model of the sensitivity analysis scenarios

5.2.4 Vertical viscosity

M7 and M8 have vertical viscosity values of $10^{-4}\ m^2/s$ and $10^{-7}\ m^2/s$ and were compared with the initial model with a vertical diffusivity of $5 \cdot 10^{-5}\ m^2/s$. With regard to salinity, M7 gave a better D2-value at E3 but slightly worse values at C1B and E1. M8 only had a better D2-value at E4 for salinity and performed slightly worse than M7 but similar to the initial model in terms of temperature. The vertical viscosity is therefore suggested to be higher than initially thought with a value of $10^{-4}\ m^2/s$.

5.2.5 Roughness

M9 and M10 used bed roughness values of 0.020 and 0.026 which were compared with the initial model with a bed roughness of 0.023. With regard to salinity, M9 gave better D2-values at E3 and E4 but slightly worse values at C1S, E1 and E2. With regard to temperature, M9 only gave a slightly lower D2-value at C1S. M10's computation time took incredibly longer and a Manning coefficient of 0.026 caused unstable and unphysical model results and increased computation time. The model results of M9 contradict the findings of Section 5.1.2, which suggested higher bed roughness values for the northern basin. With the correct stratified flow in the estuary, the bed roughness becomes of less importance in the areas with lower flow velocities. The final model applies a spatially varying bed roughness with a value of 0.020 in the northern basin and 0.023 in the rest of the domain.

5.2.6 Smagorinsky

M11, M12 and M13 have Smagorinsky values of 0.15, 0.30 and 0.45 respectively, which were compared with the initial model with a Smagorinsky value of 0. With regard to salinity, M13 performs much better in the estuarine water body (E1, E2, E3, E4) than M11, M12 and the initial model. M13 performs slightly better for temperature as well. A higher Smagorinsky value of 0.45 was applied, indicating the grid-size dependence on the horizontal diffusivity.

5.3 Validation

The DFM-model results were validated for water level, salinity, temperature and flow velocity output.

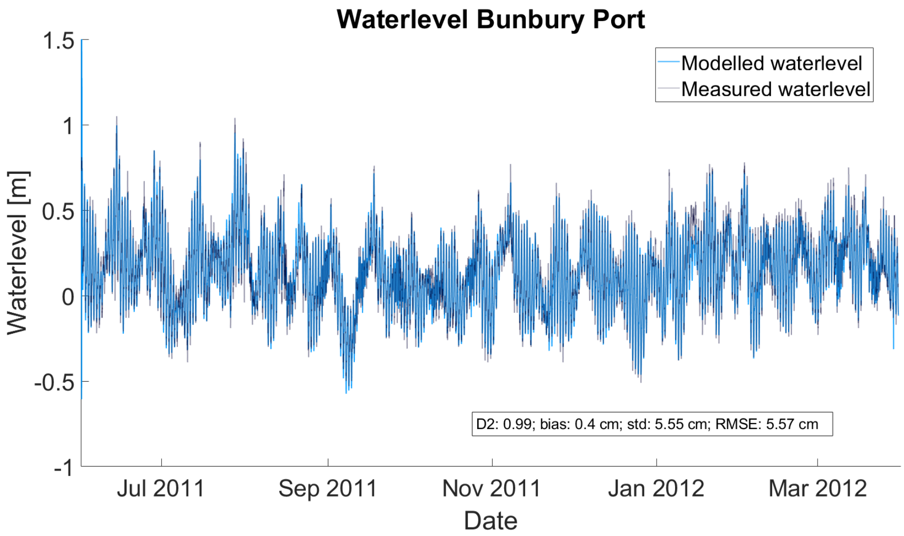

Figure 5.1: Modelled and observed water level values for observation point OUTER1

5.3.1 Water level

The modelled water levels of the DFM-model were verified against the observed water level data collected at two different time periods and two different locations. First, the modelled water level was verified against the water level observed in the Bunbury Port (observation point OUTER1) in 2011/2012 by the DoT. This is elucidated in Section 5.3.1. Secondly, the modelled water level at observation point ESTUARY3 is validated against the water level observed in 2020 by the DWER, which is expounded in Section 5.3.1. However, the latter validation was only conducted to assess the order of magnitude of the water level inside the estuary, as no water level data inside the estuary was collected in 2011/2012. The water level inside the estuary was not properly verified, which is recommended for future research.

Bunbury Port

The observed and modelled water level of observation point OUTER1 is depicted in Figure 5.1. The modelled water level is in good agreement with the observed water level (d_2 of 0.99). The standard deviation and RMSE are 5.55 cm and 5.57 cm respectively and the bias is 0.4 cm. These values are similar to the d_2 and RMSE found for the CSIRO-model (a d_2 of 0.99 and a RMSE of 5 cm) as can be seen in Appendix D.1.1.

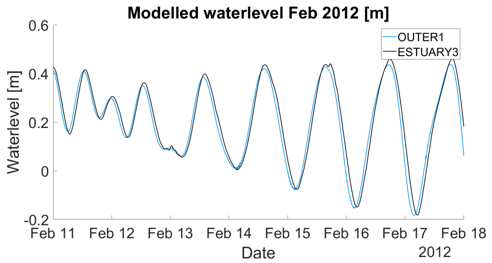

Figure 5.2: Modelled water level at OUTER1 and ESTUARY3 in February 2012

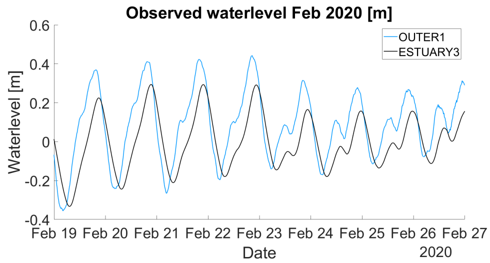

Figure 5.3: Observed water level at OUTER1 and ESTUARY3 in February 2020

Leschenault Estuary

The water level inside the estuary is validated based on the order of magnitude of the phase lag and the attenuation of the tidal wave of the observed water level at observation point OUTER1 and ESTUARY3 in 2020. Figure 5.2 represents the modelled water level of the OUTER1 and ESTUARY3 in February 2012 and Figure 5.3 represents the measured water levels of the OUTER1 and ESTUARY3 in February 2020. The phase lag between high and low tides at OUTER1 and ESTUARY3 of the modelled tidal wave in 2012 was 0.5-1 hours and 1-2 hours, respectively. The attenuation of the tidal wave inside the estuary is almost negligible and has a similar pattern as the water level observed at OUTER1. The phase lag between high and low tide at OUTER1 and ESTUARY3 of the measured tidal wave in 2020 was 1-1.5 hours and 2-3 hours, respectively. The attenuation of the tidal wave observed inside the estuary in 2020 is significantly higher than the modelled attenuation. This results in a tidal range of approximately 25% lower at ESTUARY3 than at OUTER1. The tidal phase lag is also more significant for the observed water levels than the modelled water levels. Compared to the Charteris & Deeley-model (4 and 7 hours phase lag for high and low tide) and the CSIRO-model (2 and 6 hours phase lag for high and low tide), the DFM-model shows a better agreement with the observed tidal phase lag in 2020. The modelled water levels of the Charteris & Deeley-model and CSIRO-model are depicted in Figure 5.4 and 5.5 respectively. Besides the tidal phase lag, the attenuation of the tidal range in the Charteris & Deeley-model and the CSIRO-model is higher than the observed attenuation of the tidal range of the observed water levels in 2020. However, the DFM-model does not show a clear sign of tidal damping, which could indicate that the tidal volume of the estuary and the dimensions of the 'Cut' are overestimated in the DFM-model.

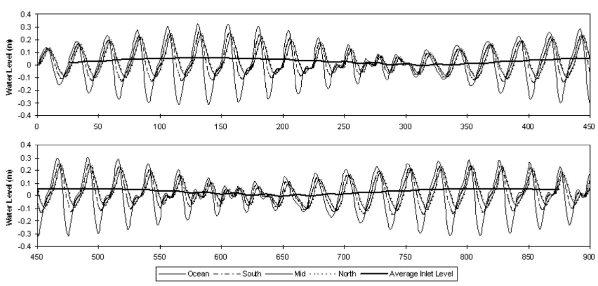

Figure 5.4: Modelled water level Charteris & Deeley (Charteris and Deeley, 2000)

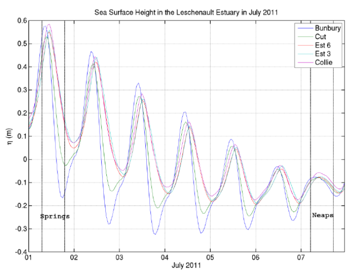

Figure 5.5: Modelled water level CSIRO (Gillibrand et al., 2012)

5.3.2 Salinity

In Appendix D.2, a detailed salinity validation is presented for each observation point shown in Figure 4.1. The RMSE and D_2 coefficients for the salinity validation are summarized in Table 5.5. The RMSE and D_2 for the salinity values show significantly better results for the DFM-model than for the CSIRO-model. Great improvements were made at COLLIE1BED, COLLIE1SURFACE and ESTUARY4. At ESTUARY3 and ESTUARY4, the salinity values are slightly underestimated for the second half of the period. At ESTUARY1, the salinity values are in good agreement with the measured salinity. In the Collie River, the salt intrusion is much better simulated than in the CSIRO-model. In general, the DFM-model represents the salinity of the Leschenault Estuary correctly.

Model	Coefficient	EST1	EST2	EST3	EST4	COL1BED	COL1SURF
CSIRO	RMS	2.57	6.35	4.17	4.81	11.85	12.99
DFM	RMS	2.49	5.99	4.61	2.66	7.03	9.65
CSIRO	D_2	0.87	0.85	0.79	0.84	0.68	0.72
DFM	D_2	0.97	0.92	0.92	0.94	0.95	0.9

Table 5.5: Validation of salinity values based on statistics

5.3.3 Temperature

In Appendix D.3, a detailed temperature validation is presented for each observation point. The statistical coefficients (RMSE and D_2) obtained by validating the modelled temperature values with the measured temperature values, are summarized in Table 5.6. In general, no major anomalies between the DFM-model and CSIRO-model are observed. However, the RMSE is slightly higher for the DFM-model but this difference is small. Overall, the modelled temperature values are in good agreement with the observed temperature.

Model	Coefficient	EST1	EST2	EST3	EST4	COL1BED	COL1SURF
CSIRO	RMS	0.78	0.95	1.08	0.95	1.04	1.58
DFM	RMS	1.32	1.56	1.36	1.6	1.35	2.38
CSIRO	D_2	0.96	0.79	0.97	0.98	0.97	0.94
DFM	D_2	0.95	0.63	0.97	0.97	0.98	0.93

Table 5.6: Validation of temperature values based on statistics

5.3.4 Flow velocities

Current velocities are measured near the ‘Cut’ and in the Collie River from February 14, 2020 to April 22, 2020 at 20 min time interval (Figure 3.28). The measured current velocity and direction were decomposed into u- and v-components. Unfortunately, no flow velocity measurements were conducted in 2011 and 2012. The modelled current velocities can therefore only be validated based on the order of magnitude of the current velocities measured in 2020 in the ‘Cut’ and the Collie River. The depth-averaged current velocities in u-and v-direction at the 'Cut' (Figure 5.6 and 5.7) and the Collie River (Figure 5.6 and 5.7) represent moving averages with a 3 hours interval. The modelled 2012 current velocities are plotted over the 2020 time period to facilitate comparison. Blue lines represent modelled current velocities from 2012 and black lines represent measured current velocities from 2020.

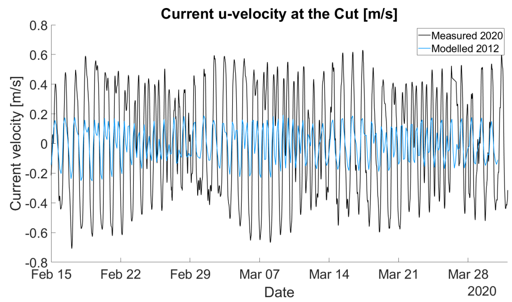

Figure 5.6: Depth-averaged current velocity (u-component) at Cut in m/s (+ represents eastward flow and - represents westward flow)

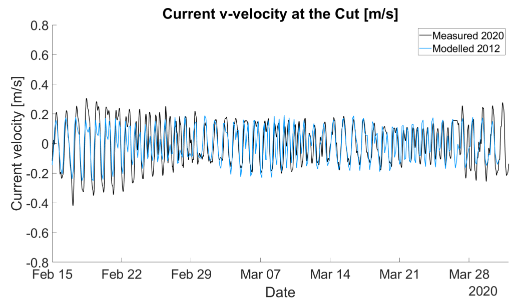

Figure 5.7: Depth-averaged current velocity (v-component) at Cut in m/s (+ represents northward flow and - represents southward flow)

The order of magnitude of the modelled depth-averaged current velocity in u-direction at the 'Cut' is approximately two to three times lower than the measured depth-averaged current velocity in u-direction (Figure 5.6). The modelled depth-averaged current velocity in v-direction at the 'Cut' is in good agreement with the measured data (Figure 5.7). The order of magnitude of the modelled depth-averaged current velocity in u-direction in the Collie River is approximately one to two times lower than the measured depth-averaged current velocity in u-direction (Figure 5.8). The modelled depth-averaged current velocity in v-direction in the Collie River is in good agreement with the measured data (Figure 5.9). The differences in magnitude between the measured and modelled current velocity in u-direction could be due to differences in climatic and meteorological conditions between the 2012 and 2020 period. Nevertheless, the modelled current velocity signal is in line with the measured current velocity signal. Measured and modelled current velocities switch between east and west and north and south at the same moments in time. Moreover, the good agreement between the modelled and measured current velocities in v-direction gives confidence in the correct simulation of the current velocities in the Leschenault Estuary.

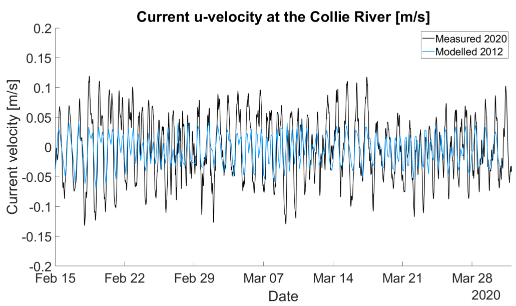

Figure 5.8: Depth-averaged current velocity (u-component) at Collie River in m/s (+ represents eastward flow and - represents westward flow)

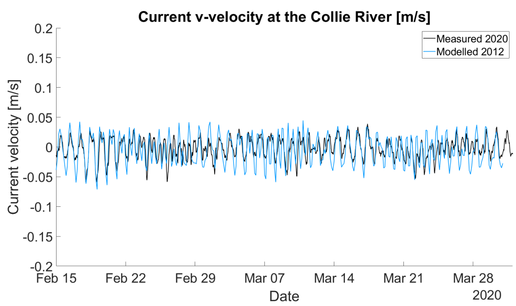

Figure 5.9: Depth-averaged current velocity (v-component) at Collie River in m/s (+ represents northward flow and - represents southward flow)

5.3.5 Evaporation

The daily-averaged modelled evaporation rates (Figure 5.10) did not match the measurements well during winter. From October onwards the modelled evaporation rates agreed better with observations, but still differ a lot from the measured evaporation rates. The daily-averaged measured evaporation tends to be more fluctuating than the daily-averaged modelled evaporation (Figure 5.10). As explained in Section 4.6, evaporation rates are calculated internally in the DFM-model with heat-flux model 5. Several experiments with different evaporation rates or heat-flux models, expounded in Section 5.1.2, did not result in intentional improvements of the salinity and temperature output of the DFM-model. In fact, the salinity and temperature output only worsened. Improved investigation into the application of correct heat-flux models or evaporation rates in the DFM-model is recommended for future research.

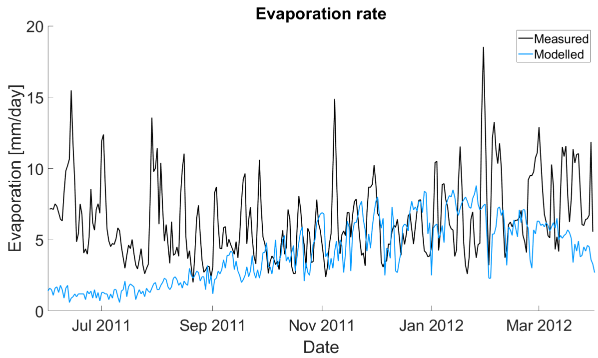

Figure 5.10: Modelled and measured evaporation rates are not in good agreement

6 Model results

In this Chapter, the model results using the set-up of Chapter 4 are presented. First, the typical circulation patterns and flow velocities of summer, winter and flood conditions are discussed. Secondly, the seasonality of the circulation patterns and the flow velocities are assessed. Thirdly, the temperature and salinity values are given and analysed for various conditions. Next, the estuary is classified according to the degree of stratification, depending on area and conditions. Lastly, the salt transport is decomposed to analyse the physical processes driving the salt fluxes between the ocean and the estuary.

6.1 Circulation

Analysis of the circulation patterns in the Leschenault Estuary and the Koombana Bay allows the understanding of the driving forces of the hydrodynamics. Firstly, it is interesting to look into moment in time under normal winter and summer conditions without the presence of extreme rainfall or extreme discharge events. Secondly, the circulation patterns under extreme rainfall and discharge conditions were investigated. Lastly, the seasonality of the circulation patterns is discussed.

6.1.1 Temporal conditions

To assess the circulation patterns of the Leschenault Estuary, snapshots are taken containing spatially varying depth-averaged current velocities and vectors at eight moments in time with different conditions (Table 6.1). The moments in time represent maximum rising (flooding tide) or falling (ebbing tide) neap and spring tides, when current velocities are highest. The magnitude of the current velocities is specified in the colour bars. Three types of vectors can be distinguished: yellow arrows (current velocities lower than 0.05 m/s), black arrows (current velocities between 0.05-0.5 m/s) and red arrows (current velocities higher than 0.5 m/s). The three vector types are independently scaled to improve the visibility of the circulation patterns in the plots.

Season	Tide	Moment	Time
Winter	Spring	Rising	15-07-2011 03:00:00
Winter	Spring	Falling	15-07-2011 15:00:00
Winter	Neap	Rising	20-07-2011 21:00:00
Winter	Neap	Falling	21-07-2011 15:00:00
Summer	Spring	Rising	24-12-2011 15:00:00
Summer	Spring	Falling	25-12-2011 03:00:00
Summer	Neap	Rising	30-12-2011 12:00:00
Summer	Neap	Falling	31-12-2011 03:00:00
Winter	Spring	Rising	17-08-2011 21:00:00
Winter	Spring	Falling	18-08-2011 15:00:00
Winter	Neap	Rising	23-08-2011 21:00:00
Winter	Neap	Falling	24-08-2011 12:00:00

Table 6.1: Moments of time applied to spatial current snapshots

Winter (15-Jul-2011 03:00:00 & 15-Jul-2011 15:00:00)

High rainfall and freshwater discharge occurs during the wet season in winter (see Section 3.3.1). The tidal influence in the hydrodynamics of the Leschenault Estuary is therefore lessened by the freshwater discharge. At rising tide the estuary is flooding, increasing the water level inside the estuary. The circulation pattern inside the estuary is shaped by the tidal and freshwater influence and shows a northward current at rising spring tide in the central and northern part of the estuary (Figure 6.1). Besides, a southward current is obtained along the estuary's boundaries at rising spring tide (Figure 6.1), potentially generated by northerly winds and/or Coriolis effects (investigated in Section 6.1.3 and 6.1.4, receptively). In the southern part, the circulation is clockwise at rising spring tide (Figure 6.1). At falling spring tides, the circulation is reversed, generating a southward flow in the central and northern basin (Figure 6.2) and an anti-clockwise circulation in the southern basin (Figure 6.2). In the most northern part of the estuary, a clockwise circulation is ob-

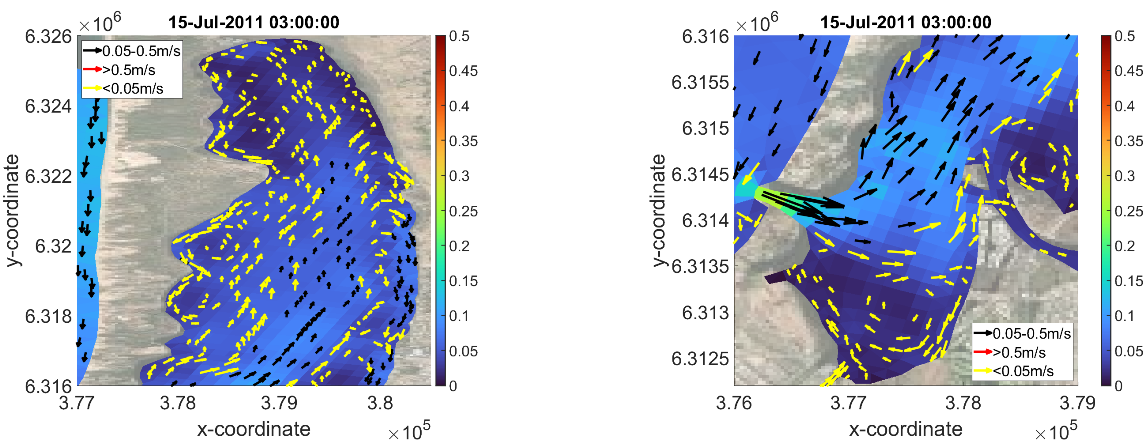

Figure 6.1: Top view of modelled depth-averaged current velocities at rising spring tide in winter (15-Jul-2011 03:00:00) - north (left) and south (right)

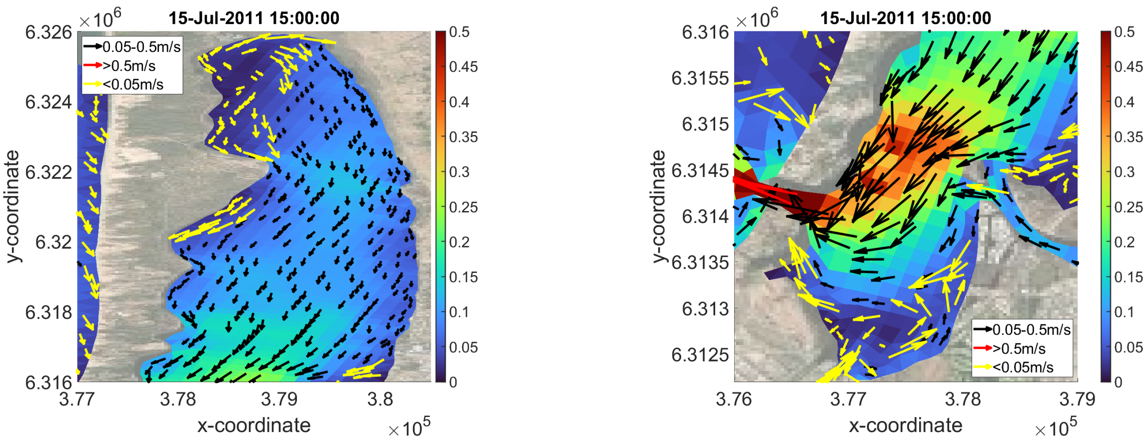

Figure 6.2: Top view of modelled depth-averaged current velocities at falling spring tide in winter (15-Jul-2011 15:00:00) - north (left) and south (right)

served, which could be generated by Coriolis effects that deflects currents to the left at the Southern Hemisphere (Figure 6.2). Also, along the boundaries, where the current velocities are low, currents seem to be deflected to the left in the central and northern basins. In the southern basin, the influence of the freshwater discharge dominates the Coriolis effects. Highest current velocities are generated at the 'Cut' at falling spring tide (Figure 6.2).

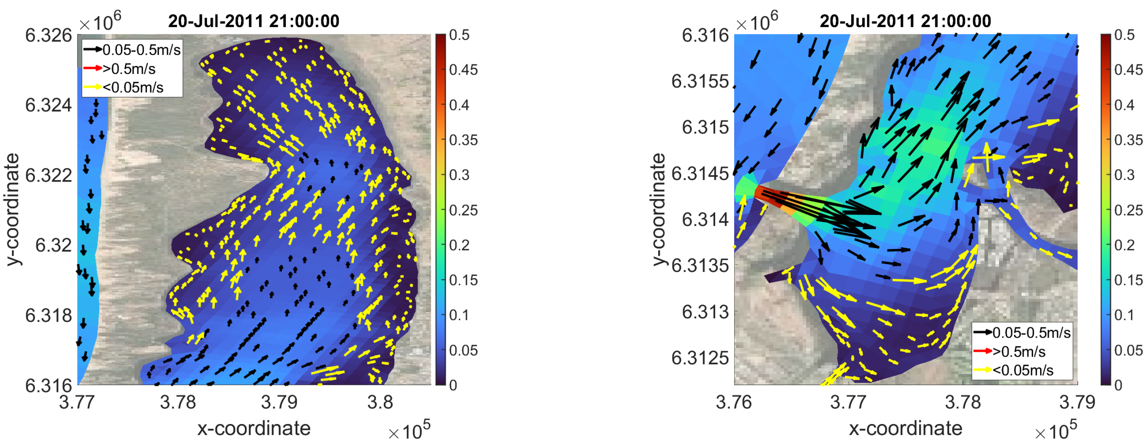

Figure 6.3: Top view of modelled depth-averaged current velocities at falling neap tide in winter (20-Jul-2011 21:00:00) - north (left) and south (right)

Winter (20-Jul-2011 21:00:00 & 21-Jul-2011 15:00:00)

At neap tide, the tidal flow is weaker generating different circulation patterns than at spring tide. At rising and falling neap tide, the circulation in the southern basin is counter-clockwise (Figure 6.3 and Figure 6.4). The circulation pattern in the central and northern basin has a northward direction at rising neap tide (Figure 6.3) and a southward direction at falling neap tide in winter (Figure 6.4). Current velocities are significantly lower at neap tide than at spring tide.

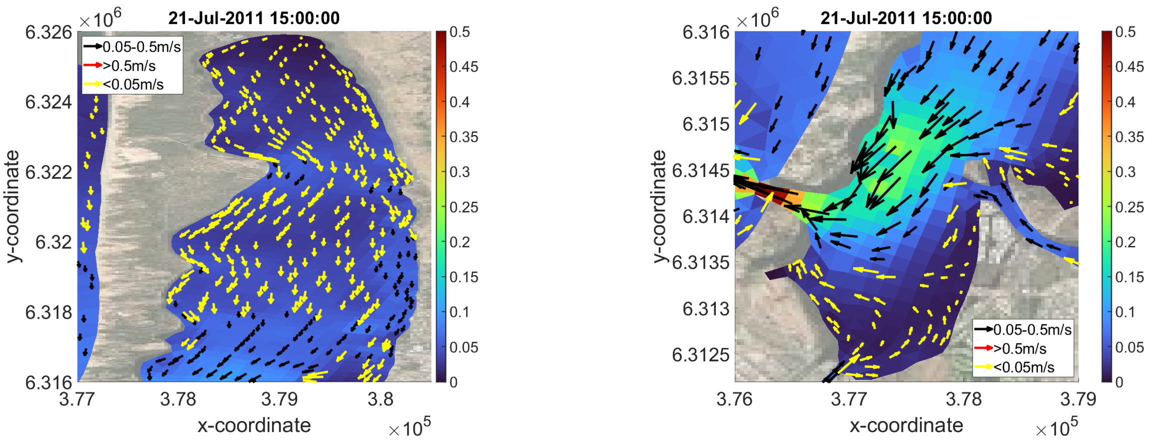

Figure 6.4: Top view of modelled depth-averaged current velocities at falling neap tide in winter (21-Jul-2011 15:00:00) - north (left) and south (right)

Summer (24-Dec-2011 15:00:00 & 25-Dec-2011 03:00:00)

During the dry summer period the freshwater discharge is reduced, and estuarine hydrodynamics is dominated by tides. At rising spring tide, the tidally-driven flows overpower the river flows, generating landward currents in the downstream portion of the rivers (Figure 6.5). This also causes an anti-clockwise circulation in the southern basin, contrary to the winter pattern (Figure 6.5). At falling spring tide, the weak river flow and the stronger tidal current generated a clockwise circulation in the southern basin (Figure 6.6). In the central basin, circulation was equal to the one observed in winter, with northward currents at rising spring tide (Figure 6.5) and southward currents at falling spring tide (Figure 6.6). In the northern basin, a clockwise circulation is obtained at rising spring tide (Figure 6.5) and a counter-clockwise circulation at falling spring tide (Figure 6.6). Besides, the higher current velocities along the estuary's boundaries at rising spring tide are probably wind-driven.

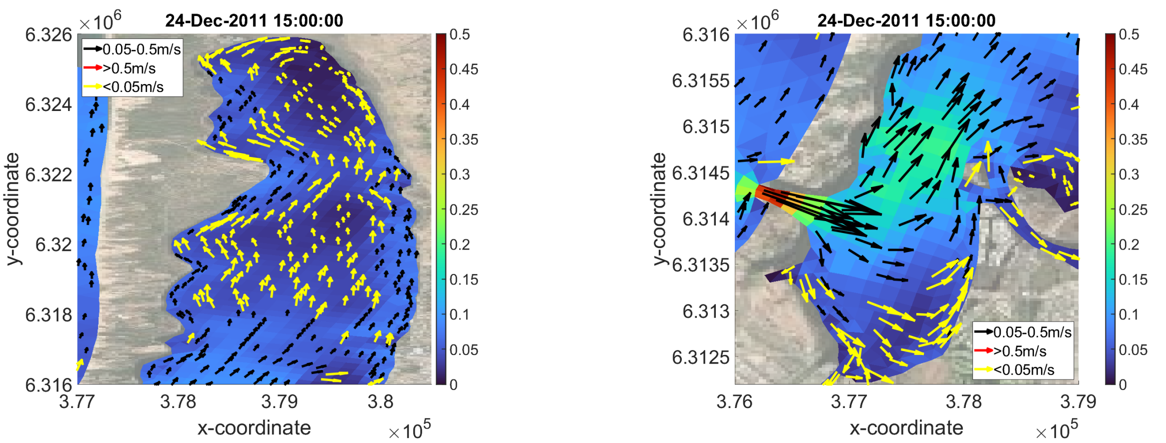

Figure 6.5: Top view of modelled depth-averaged current velocities at rising spring tide in summer (24-Dec-2011 15:00:00) - north (left) and south (right)

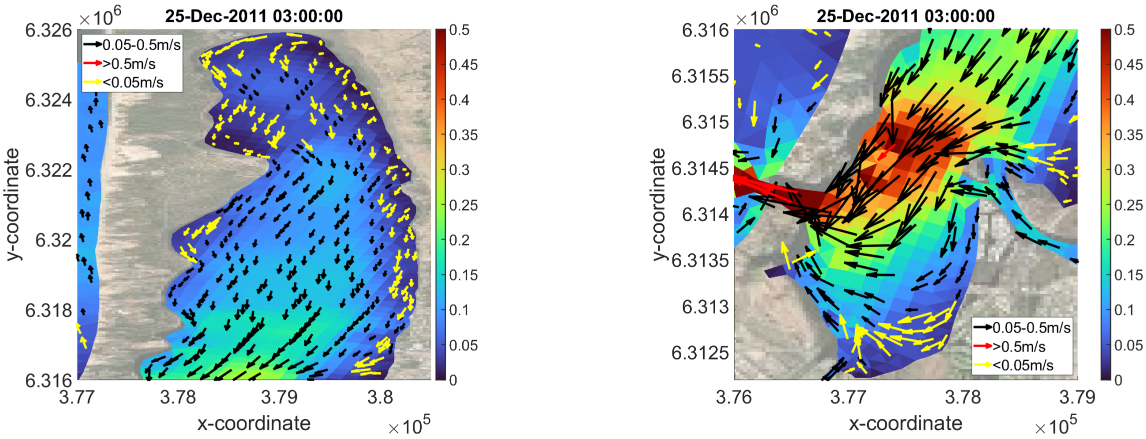

Figure 6.6: Top view of modelled depth-averaged current velocities at falling spring tide in summer (25-Dec-2011 03:00:00) - north (left) and south (right)

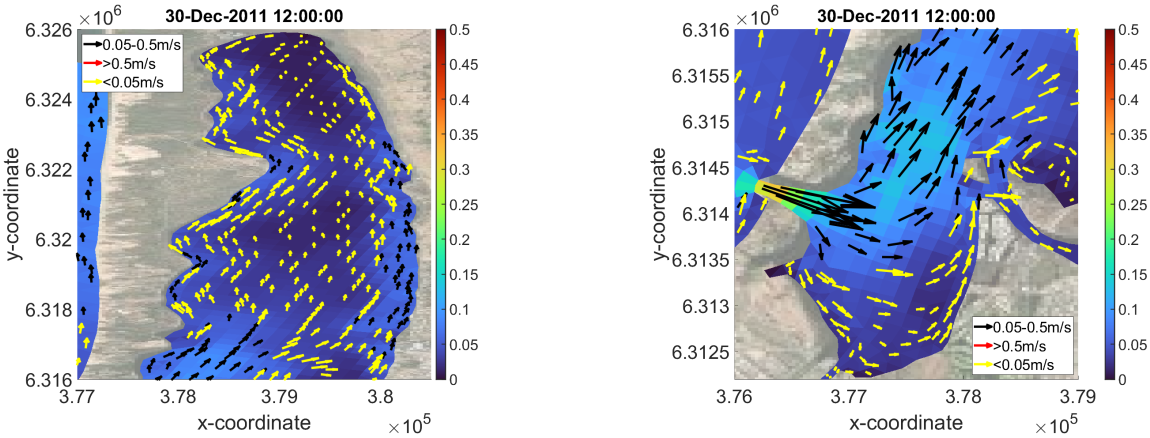

Figure 6.7: Top view of modelled depth-averaged current velocities at falling neap tide in summer (30-Dec-2011 12:00:00) - north (left) and south (right)

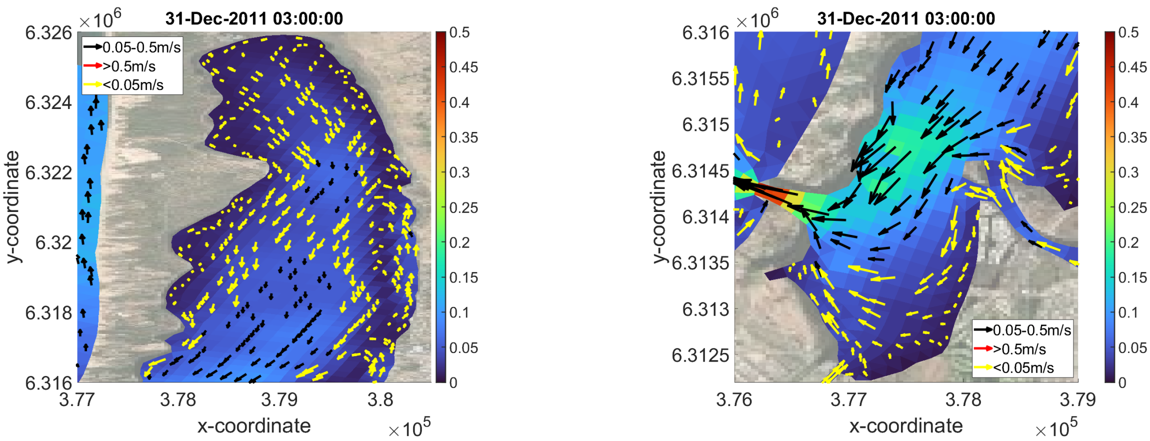

Figure 6.8: Top view of modelled depth-averaged current velocities at falling neap tide in summer (31-Dec-2011 03:00:00) - north (left) and south (right)

Summer (30-Dec-2011 12:00:00 & 31-Dec-2011 03:00:00)

Neap circulation patterns in the southern basin at rising and falling tides were similar to those observed at spring tide (Figure 6.7 and 6.8). In the central and northern basin, the depth-averaged current velocities are lower in the main body at rising neap tide than at falling neap tide (Figure 6.7 and 6.8). At falling neap tide, the current in the main body is southward, but the current along the eastern boundary is northward (Figure 6.7).

Extreme discharge conditions (17-Aug-2011 21:00:00 & 18-Aug-2011 15:00:00)

Before the extreme discharge event, the freshwater discharge was already higher than normal winter conditions, increasing the influence of the freshwater discharge relative to the the tide. The typical winter circulation patterns in the southern basin are interrupted by the increased freshwater flow, generating seaward currents at falling neap tide (Figure 6.9) and counter-clockwise currents at rising neap tide (Figure 6.10). The current in the central and northern basin has a northward direction at rising neap tide (Figure 6.9) and a southward direction at falling neap tide (Figure 6.10). The wind drives the southward alongshore currents, counteracts the northward currents along the estuary's boundaries at rising neap tide (Figure 6.9) and superimposes the currents along the estuary's boundaries at falling neap tide (Figure 6.10). At rising neap tide high flow velocities are obtained at the Cut and a clockwise circulation is generated in the northern parts of the estuary (Figure 6.9).

Extreme discharge conditions (23-Aug-2011 21:00:00 & 24-Aug-2011 12:00:00)

During the extreme discharge event, currents in the southern basin are mostly directed to the north at rising spring tide due to the increased freshwater discharge (Figure 6.11). The central and northern basin become more dynamic generating strong northward currents in the main body and strong southward currents along the estuary's boundaries (Figure 6.11). At falling spring tide, the current in the southern basin is mostly forced out of the estuary (Figure 6.12). The peak flow event coincided with the spring tides generating strong currents near 'Cut'.

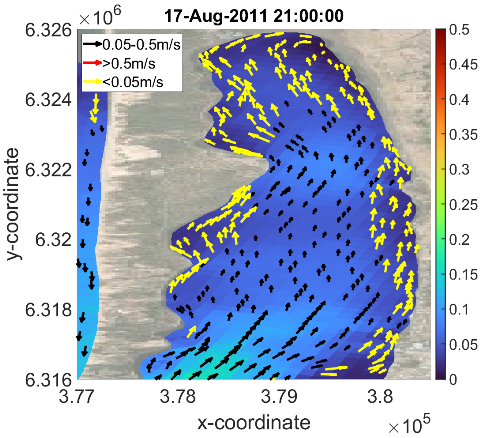

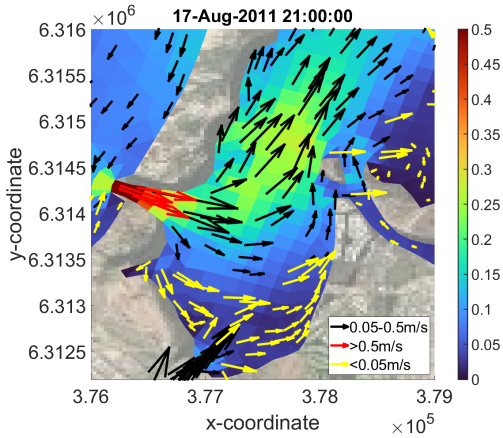

Figure 6.9: Top view of modelled depth-averaged current velocities at rising neap tide before extreme discharge event (17-Aug-2011 21:00:00) - north (left) and south (right)

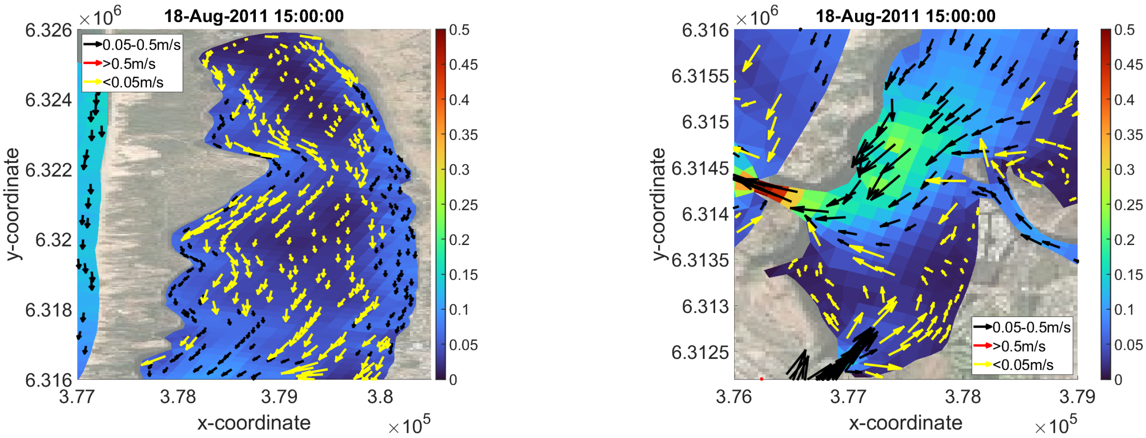

Figure 6.10: Top view of modelled depth-averaged current velocities at rising neap tide before extreme discharge event (18-Aug-2011 15:00:00) - north (left) and south (right)

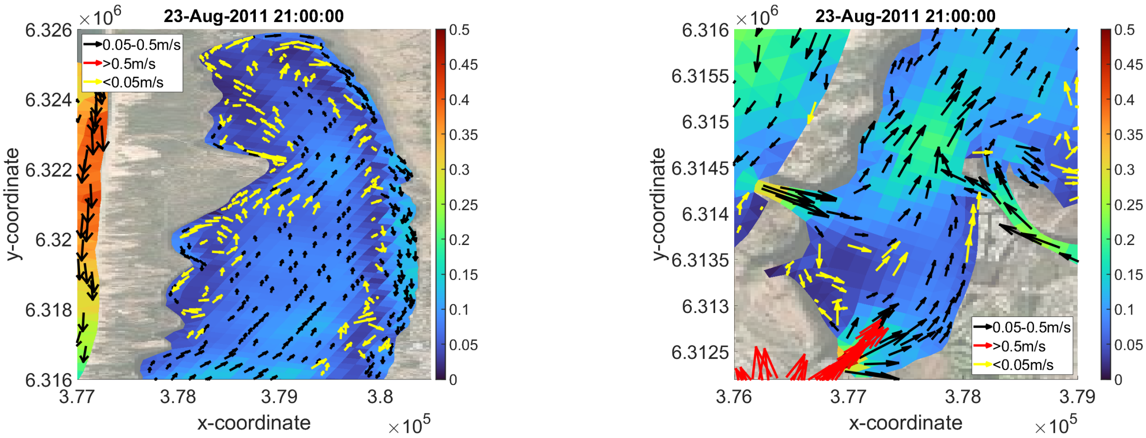

Figure 6.11: Top view of modelled depth-averaged current velocities at rising spring tide at extreme discharge event (23-Aug-2011 21:00:00) - north (left) and south (right)

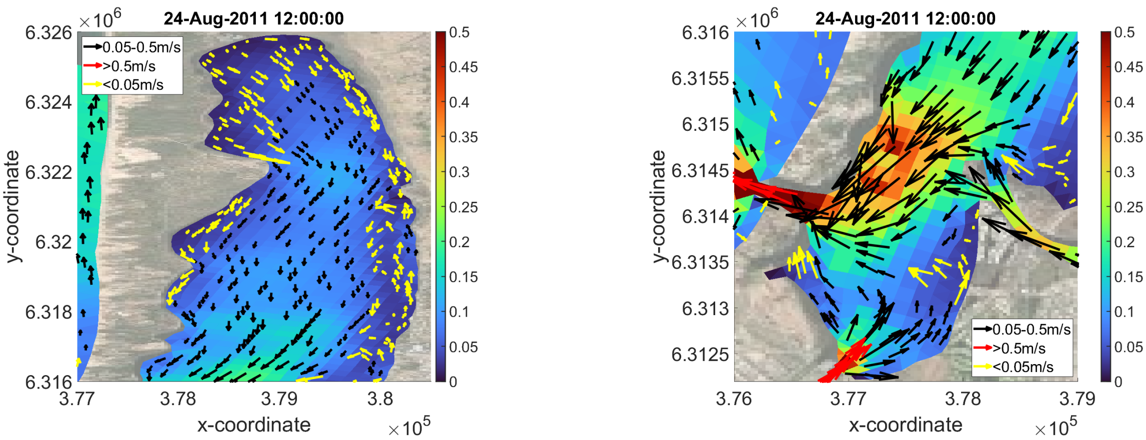

Figure 6.12: Top view of modelled depth-averaged current velocities at rising spring tide at extreme discharge event (24-Aug-2011 12:00:00) - north (left) and south (right)

6.1.2 Seasonal conditions

To assess the seasonal variation of the water circulation in the Leschenault Estuary, two periods are considered: winter and summer. The winter period at the Leschenault Estuary starts on June 1, 2011 and ends on August 31, 2011. The summer period start on December 1, 2011 and ends on February 29, 2012. The time averaged water levels and time and depth-averaged flow velocities of the winter and summer period are depicted in Figure 6.13 and 6.14 respectively. The water levels and depth-averaged flow velocities were time averaged to filter the influence of the tide on the water circulation and assess the seasonal differences.

Winter

Figure 6.13 shows dominant southward currents along the coast in winter. This alongshore current is typical for winter conditions as is explained in Section 3.3.2. The flow near the 'Cut' had a jet-like shape with strong outflow velocities. Rivers presented a strong downstream flow. In the central and upper basin of the Leschenault Estuary, the flow was mainly northward in the main body but southward along the estuary's boundaries (Figure 6.13). Current velocities are higher along these boundaries, likely driven by the prevailing northerly winds in winter. Time and depth-averaged flow velocities were highest in the rivers and the 'Cut'. In the southern basin, the circulation pattern was anti-clockwise, with dominant outflow in the 'Cut' (Figure 6.13). In the northern basin, a clockwise circulation prevailed in winter (Figure 6.13). Mean water levels were highest near the river mouths and gradually decreased towards the northern boundary of the estuary. This is in line with the prevailing northerly winds that causes fetch across the estuary, with lower waterlevels in the northern basin. In winter, the mean water level of the estuary was around 2-3 *cm* higher than the ocean level, generated by the river discharge and fetch.

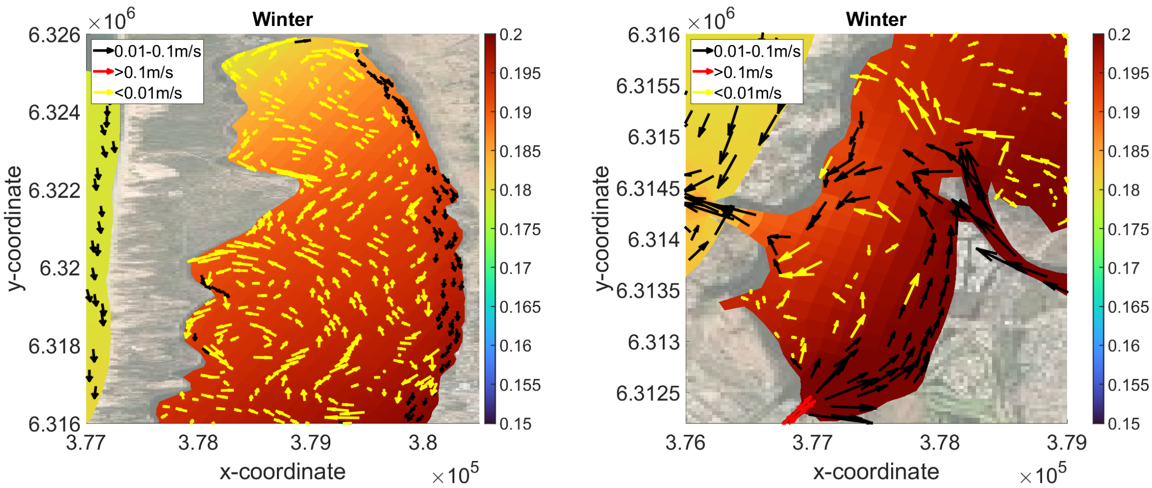

Figure 6.13: Time averaged water levels and time and depth-averaged current velocities for the winter period (1-Jun-2011 to 31-Aug-2011) - north (left) and south (right)

Summer

A northerly alongshore current prevailed in summer (Figure 6.14), as expected (see Section 3.3.2). The southward offshore Leeuwin current is influenced by winds, generating stronger southward currents in winter due to northerly winds and weaker northward currents in summer due to southerly winds. Compared to winter conditions the flow velocities along the rivers were also seaward but weaker. The time and depth-averaged current velocities at the ‘Cut’, were much weaker and are not entirely seaward (Figure 6.14), which could indicate bidirectional lateral currents (investigated in Section 6.1.5). The central and northern basin showed southward averaged currents in the main body (Figure 6.14). However, the mean current velocities along the estuary’s boundaries were southward and stronger, likely due to the stronger wind effects over shallower areas. The southern basin circulation is significantly different from winter conditions, as two main circulation patterns are distinguished (Figure 6.14): a clockwise and an anti-clockwise cell. In the northern basin, a counter-clockwise circulation prevailed in winter (Figure 6.13). Mean water levels were higher in the northern region and gradually decreased towards the south of the estuary, in line with the fetch generated by the prevailing southerly winds in summer. Mean sea level was 5 cm lower than the estuary.

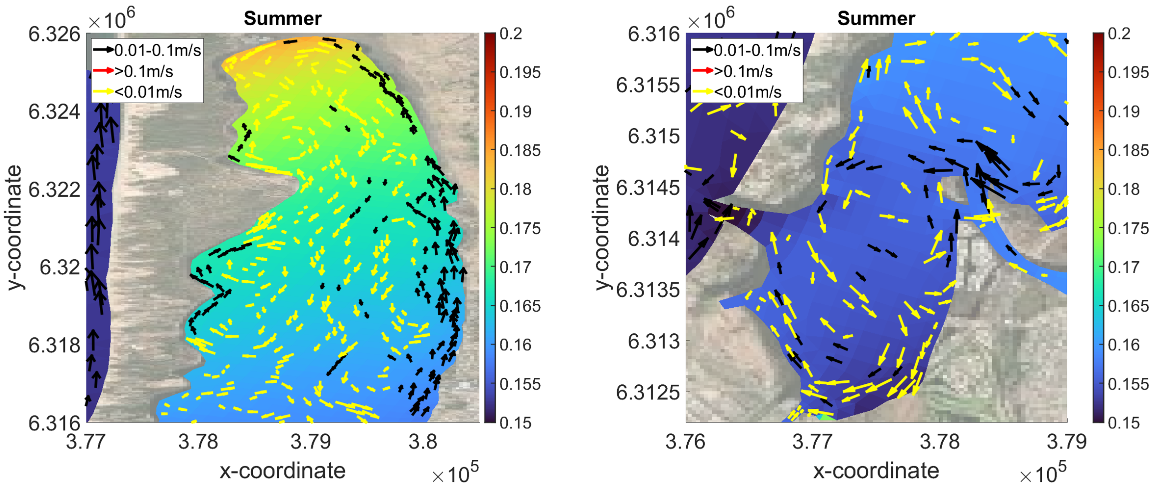

Figure 6.14: Time averaged water levels and time and depth-averaged current velocities for the summer period (1-Dec-2011 to 29-Feb-2011) - north (left) and south (right)

6.1.3 Wind influence

In Section 3.3.2, the dominant influence of the wind on the alongshore current already became clear. The influence of the wind increases in shallow regions ((Pearce et al., 2015)). This becomes evident in Figure 6.13, where the currents along the estuary’s boundaries were southward, while northward currents prevailed in the central basin. The southward current along the boundaries are likely generated by prevailing northerly winds in winter. In summer, the reversed phenomenon occurred, with strong southward currents along the estuary’s boundaries and a weaker northward current in the main body (Figure6.14), likely generated by prevailing northerly winds in summer. It is therefore assumed that winds are an important driver of the water circulation in the Leschenault Estuary in the shallow regions.

6.1.4 Coriolis

Figure 6.15 shows the Rossby numbers based on depth-averaged velocities for winter (15-Jul-2011 15:00:00; left), summer (25-Dec-2011 03:00:00; centre) and peak river discharge (23-Aug-2011 21:00:00; right). The Rossby number is calculated by Equation 2.31. The considered times are all taken at falling spring tide, when current velocities in the Leschenault Estuary were the highest. For Rossby numbers lower than 1, Coriolis might play a role in the hydrodynamics of the estuary (Cossu et al., 2010). Rossby numbers in the Leschenault Estuary were high ($Ro > 1$), in the southern basin, 'Cut', bay and rivers (Figure 6.15). The Rossby numbers were lowest in the northern basin and near the estuary's boundaries, with values far below 1 ($Ro << 1$) (Figure 6.15). This might indicated that Coriolis has influence on the circulation pattern of the Leschenault Estuary. However, the shallow regions in which Coriolis might be important, winds are also more impactful. From Section 6.1, it is assumed that winds have a stronger influence on the circulation patterns than Coriolis. Furthermore, no clear deflections to the left were observed in the spatial circulation plots of Section 6.1.

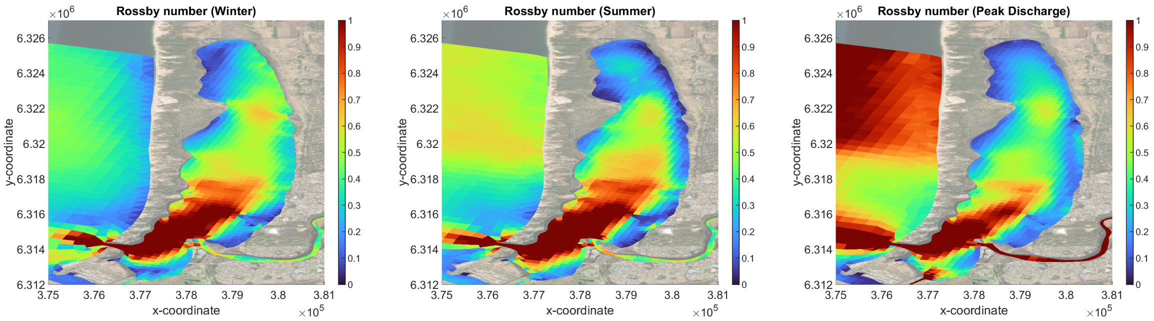

Figure 6.15: Rossby number: winter (15-Jul-2011 15:00:00; left), summer (25-Dec-2011 03:00:00; centre) and peak discharge event (23-Aug-2011 21:00:00; right)

6.1.5 Lateral variations - The 'Cut'

Lateral cross-section plots with current velocities in u-direction (east-west) at the 'Cut' were generated to investigate the circulation patterns in lateral and vertical direction. Three single tidal cycles (24 hours) are considered with 3-hour interval: winter neap (20-Jul-2011 21:00:00 to 21-Jul-2011 21:00:00), summer neap (30-Dec-2011 12:00:00 to 31-Dec-2011 12:00:00) and peak river discharge spring (23-Aug-2011 21:00:00 to 24-Aug-2011 21:00:00 (shown in Figure 6.67).

Winter neap

Figures 6.16 and 6.17 show the u-components of the current velocity along the cross-section during winter neap and a clear difference between the two sides of the channel. During rising tide (Figure 6.16, left), the flow into the estuary was substantially higher at the channel's south side than at its north side, with landward currents. A similar pattern was observed during flood tide (Figure 6.16, centre), with higher seaward currents at the south side of the ’Cut’. In Figure 6.16 (right, 6 hours later), a two-layered current velocity structure occurred, with landward bottom currents and seaward surface currents. Figure 6.17 (left) shows lateral variable currents, with higher velocities observed at the south side during ebb. In Figure 6.17 (right), the waters at the ‘Cut’ started rising again, with higher inflowing currents ar the south side.

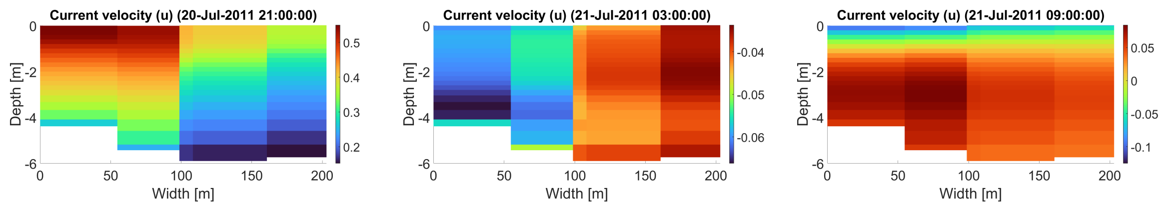

Figure 6.16: Lateral variation current velocity (u-component) at transect the ‘Cut’ during winter neap (east (+); west (−))

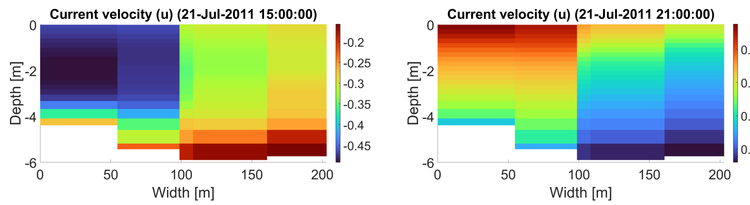

Figure 6.17: Lateral variation current velocity (u-component) at transect the ‘Cut’ during winter neap (east (+); west (−))

Summer neap

Figures 6.18 and 6.19 show the u-components of the current velocity along the cross-section during summer neap. A similar difference between the higher velocities at the south side and lower velocities at the north side was observed during summer neap (Figures 6.18 and 6.19). However, no two-layered current velocity structures were observed during the summer neap (Figures 6.18 and 6.19). Current velocities were significantly higher during falling tide than rising tide (Figures 6.18 and 6.19). Besides, the currents did not change in direction laterally (Figures 6.18 and 6.19).

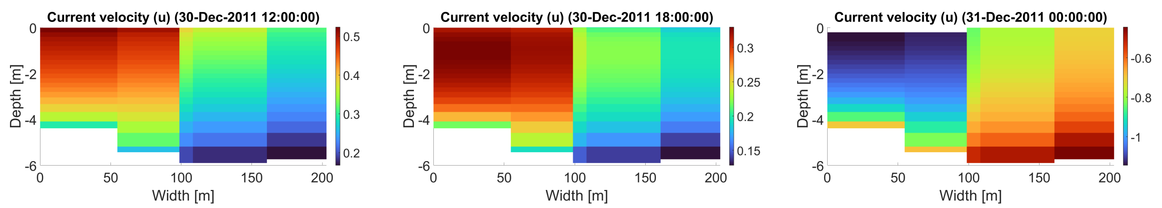

Figure 6.18: Lateral variation current velocity (u-component) at transect the ‘Cut’ during summer neap (east (+); west (−))

Peak river discharge spring

Figures 6.20 and 6.21 show the u-components of the current velocity along the cross-section during peak river discharge spring. Two main lateral variations could be distinguished:

a vertical (Figure 6.20, left and centre) and horizontal (Figure 6.20, right and 6.21) two-layered current velocity structure. Again, higher current velocities occurred at the south side of the 'Cut' (Figure 6.20, right and 6.21) and currents did not change in direction laterally.

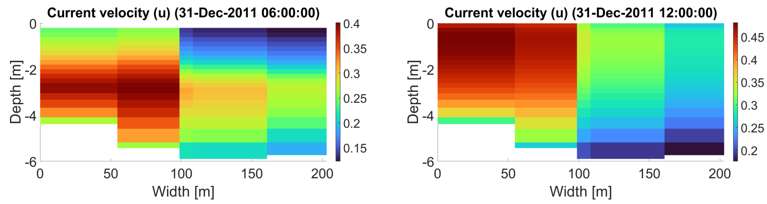

Figure 6.19: Lateral variation current velocity (u-component) at transect the 'Cut' during summer neap (east (+); west (−))

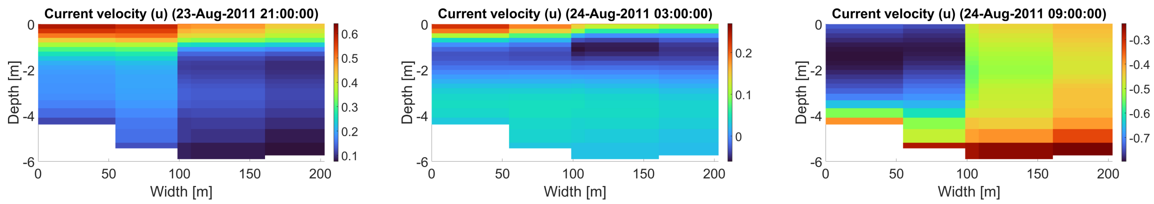

Figure 6.20: Lateral variation current velocity (u-component) at transect the 'Cut' during peak river discharge spring (east (+); west (−))

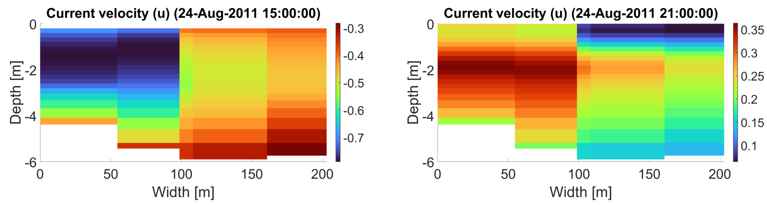

Figure 6.21: Lateral variation current velocity (u-component) at transect the 'Cut' during peak river discharge spring (east (+); west (−))

6.2 Flow velocities

Flow velocity data are extracted at the observation points and cross-sections, including u- and v-components and flow magnitude. To assess the dominant processes affecting the currents in the estuary, the same periods are considered as in Section 6.1: a typical winter and summer week with seven tidal cycles including both neap and spring tides to assess the differences.

6.2.1 U-component of flow velocity

Figure 6.22 shows the u-components of the flow velocity at the different stations during summer (right) and winter (left). The peaks and troughs of the u-components correspond with the steepest curves of the tidal wave and the zero velocity values correspond with ebb and flood slack. The out-flowing water at the 'Cut' (ESTUARY1) in winter and summer was smooth. The inflowing water on the other hand seemed to be counteracted by the

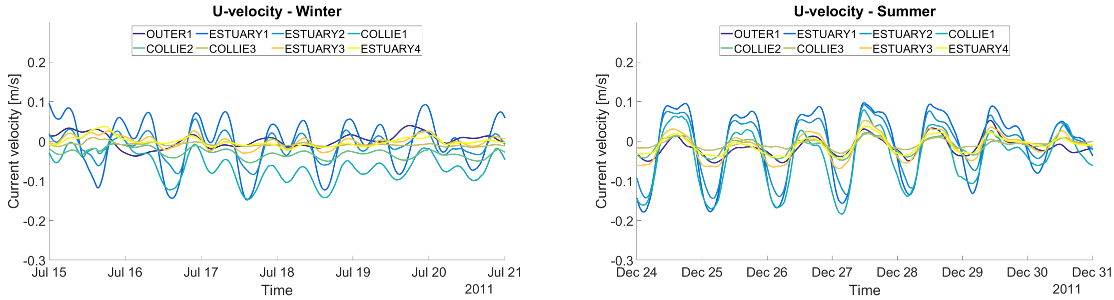

Figure 6.22: Modelled flow velocity (u-components) at the different stations during winter (left) and during summer (right) - (+ represents eastward flow and − represents westward flow)

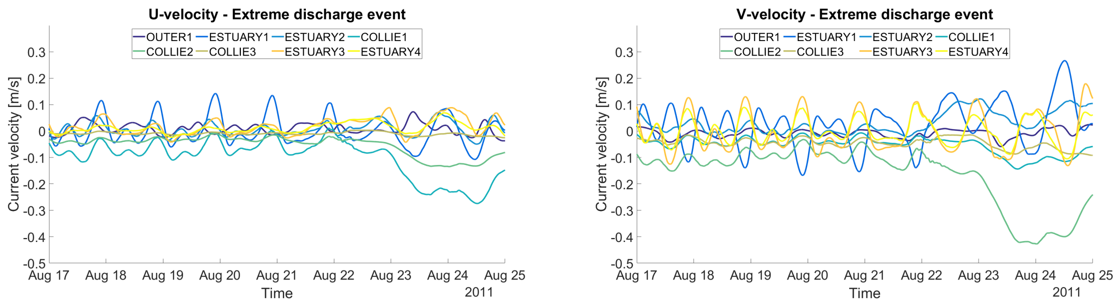

Figure 6.23: Modelled flow velocity u-component (left) (+ = east & − = west) and v-component (right) (+ = north & − = south) at the different stations during the extreme discharge event

freshwater discharge, which reduced the flow velocity during rising tide. This can clearly be seen in Figure 6.22, where at the ‘Cut’ (ESTUARY1) two small peaks with lower values than the troughs are observed. Compared with the u-component of the flow velocity during summer, the winter currents suffered higher influence of the freshwater discharge, with weaker ebb and flood tidal flow velocities. The u-velocities at the Collie River (COLLIE1, COLLIE2) were negative in winter, indicating freshwater outflow. In summer, the freshwater discharge was reduced, allowing the ocean water to flow upriver during flood tides. The higher influence of the tide in summer is clear at all locations, being more in phase and less disrupted. During winter, incoming tides at the ‘Cut’ (ESTUARY1) opposed the freshwater outflow, generating more complex circulation patterns (Figure 6.22). An explanation can be found in the considered periods that start with a spring tide and end with a neap tide. The extreme discharge event starts with a neap tide and ends with spring tide. The u-component showed a semi-diurnal pattern during the neap (Figure 6.22). A more diurnal pattern was observed during rising tide in the neap and a more semi-diurnal pattern during falling tide in the neap. Figure 6.23 shows that the extreme rainfall event (August, 21/22) had maximum currents at the Collie River (COLLIE1, COLLIE2, COLLIE3) but the flow also increased in other parts of the estuary.

6.2.2 V-component of flow velocity

In Figure 6.24, the v-components of the flow velocity at the different stations are shown. The highest values occurred at the ‘Cut’ (ESTUARY1), reaching 0.3 m/s. Values of the v-components of the flow velocity were higher during summer, when the freshwater discharge was reduced, showing the dominant influence of the tide on the v-component in summer. The v-component of the flow velocity in the central basin (ESTUARY3) and the northern basin (ESTUARY4) had opposite directions compared to those at the 'Cut' (ESTUARY1) and the southern basin (ESTUARY2). This could be attributed to the phase lag of the flow velocity induced by the tide. The same phenomenon as in Section 6.2.1 is encountered at the 'Cut' (ESTUARY1), with a diurnal behaviour for positive values of the v-component and a semi-diurnal behaviour for negative values (Figure 6.24). During neap tide, this phenomenon was reversed, resulting in diurnal peaks for negative v-components of the flow velocity and semi-diurnal peaks for positive v-components (Figure 6.24). This pattern can be clearly seen during the extreme discharge event (Figure 6.23 (right)). Spring tide coincided with the extreme discharge event, generating strong currents across the 'Cut' (ESTUARY1) and Collie River (COLLIE1, COLLIE2, COLLIE3).

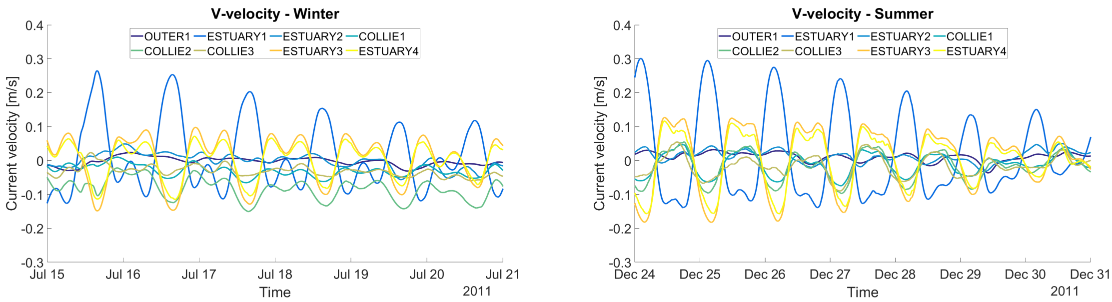

Figure 6.24: Modelled flow velocity (v-components) at the different stations during winter (left) and during summer (right) - (+ represents northward flow and − represents southward flow)

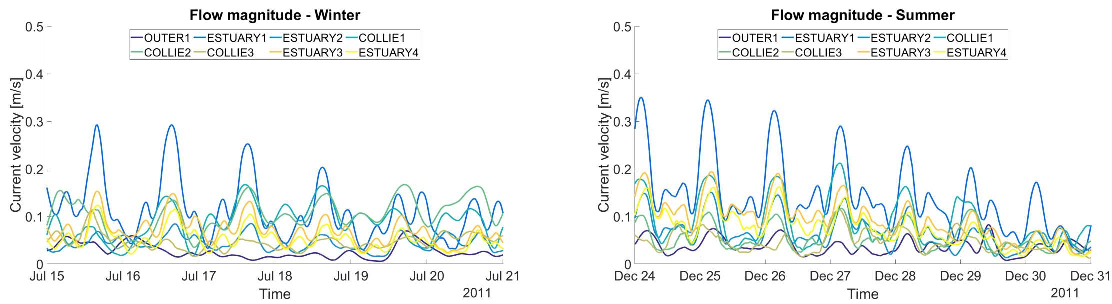

Figure 6.25: Modelled flow magnitude at the different stations during winter (left) and during summer (right)

6.2.3 Magnitude of flow velocity

Current speeds are shown at the different stations and as resultant values along the different cross-sections. The former data type represents positive magnitudes of the flow velocity observed at the different stations and the latter data type assumes negative or positive values for averaged flows along a cross-section. The same periods were considered as in Section 6.2.1 and 6.2.2 and the magnitudes of the flow velocity at the different stations are depicted in Figure 6.25 and 6.27 (left). The result flows in the cross-sections are shown in Figure 6.26 and 6.27 (right). In typical summer periods (Figure 6.25, right) the flow velocities were higher than in winter (Figure 6.25, left), generated by tides. The higher freshwater discharge during winter does not generate higher flow velocities. During the extreme discharge event (Figure 6.27), high current velocities were observed in the Collie River (COLLIE1, COLLIE2, COLLIE3), with values exceeding 0.4 m/s. However, the flow velocities at the 'Cut' (ESTUARY1) during the extreme discharge event were lower than under typical summer conditions (Figure 6.26). This could be due to the lower tidal range at the extreme discharge event, which was around 0.5 m at the extreme discharge event during spring and 0.8 m under typical summer and winter conditions at spring (Appendix E.1). Current velocities were highest in the Preston River (PRESTON1), reaching a peak of 1.2 m/s after the flood event (Figure 6.27, right).

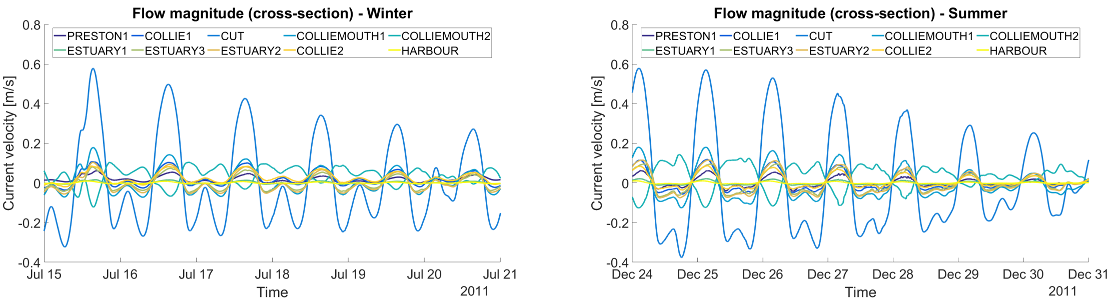

Figure 6.26: Modelled flow magnitude at the different stations during winter (left) and during summer (right)

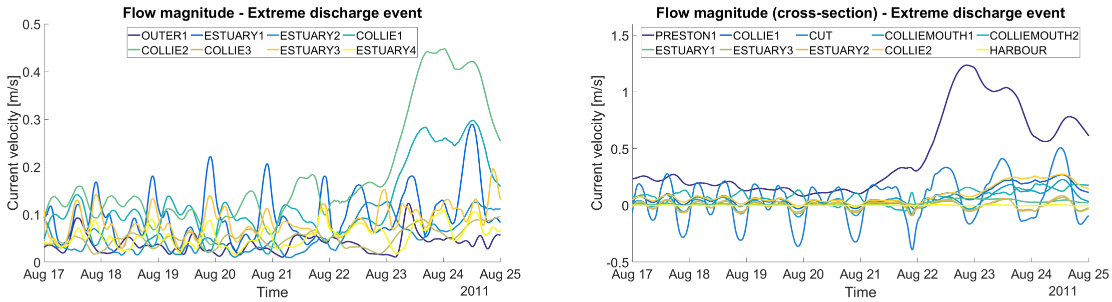

Figure 6.27: Modelled flow magnitude at the different stations (left) and cross-sections (right) during the extreme discharge event

6.3 Temperature

Similar to Section 6.1, temperature results are assessed for a typical summer and winter week (Section 6.3.1) and a week associated with extreme river discharge (Section 6.3.2). Seasonal variations between summer and winter were evaluated in Section 6.3.3 and the vertical variations of temperature were analysed in Section 6.3.4.

6.3.1 Normal conditions

Similar periods as in Section 6.1 were considered to evaluate temperature results: (a) rising spring tide in winter (Figure 6.28), and in summer (Figure 6.32), (b) falling spring tide in winter (Figure 6.29), and in summer (Figure 6.33), (c) rising neap tide in winter (Figure

6.30), and in summer (Figure 6.34), (d) falling neap tide in winter (Figure 6.31), and in summer (Figure 6.35). All temperatures were depth-averaged.

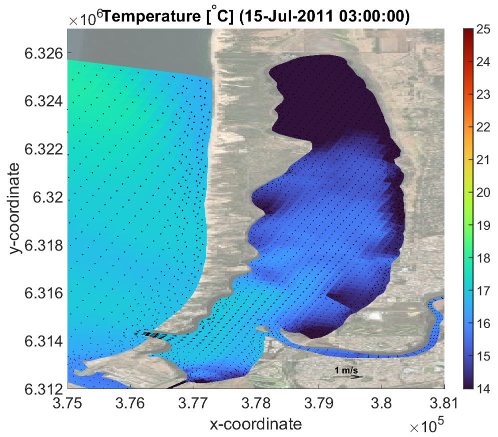

Figure 6.28: Depth-averaged temperature observed in a typical winter week (15-07-2011 03:00 - rising spring tide)

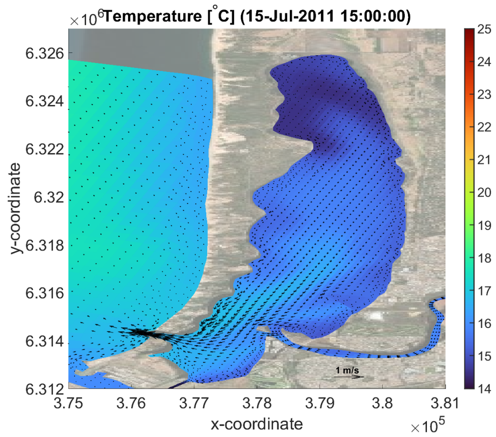

Figure 6.29: Depth-averaged temperature observed in a typical winter week (15-07-2011 15:00 - falling spring tide)

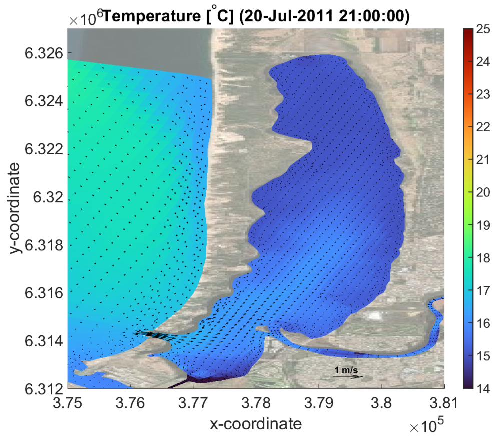

Figure 6.30: Depth-averaged temperature observed in a typical winter week (20-07-2011 21:00 - rising neap tide)

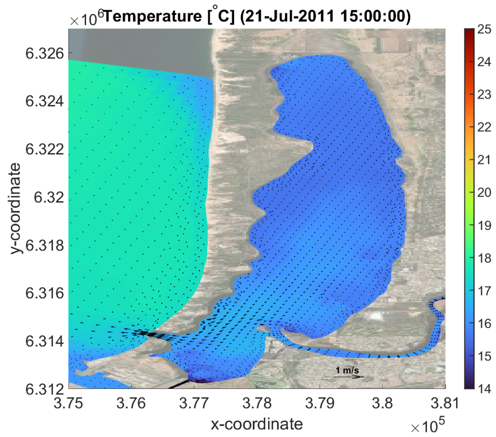

Figure 6.31: Depth-averaged temperature observed in a typical winter week (21-07-2011 15:00 - falling neap tide)

Winter

Figures 6.28, 6.29, 6.30 and 6.31 show the depth-averaged water temperatures of four moments in time in winter. Winter water temperatures for these moments varied between 12 and 17 $°C$. Warmest water temperatures occurred offshore ($\approx$18/ 19 $°C$) and coolest water temperatures were observed in the northern basin of the estuary (<14 $°C$). Moreover, the northern basin is less affected by river flow and ocean water, which makes the atmospheric forcing dominant. As the estuary is shallower than the ocean, it is more sensitive to heating and cooling. The northern basin is also less affected by river flow and ocean water, which makes the atmospheric forcing dominant. The water in the northern basin was cooler than in other parts of the estuary. During rising tide warmer ocean water penetrates the estuary, heating up the estuary's water temperature by mixing and water circulation. This is evident when Figures 6.28 and 6.30 are compared against Figures 6.29 and 6.31. At ebb tide the cooler estuarine water, cools the coastal waters. The opposite process occurs during rising tide, when warmer ocean waters were observed nearshore.

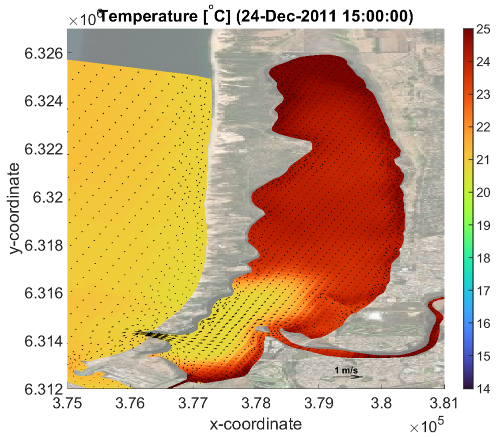

Figure 6.32: Depth-averaged temperature observed in a typical summer week (24-12-2011 15:00 - rising spring tide)

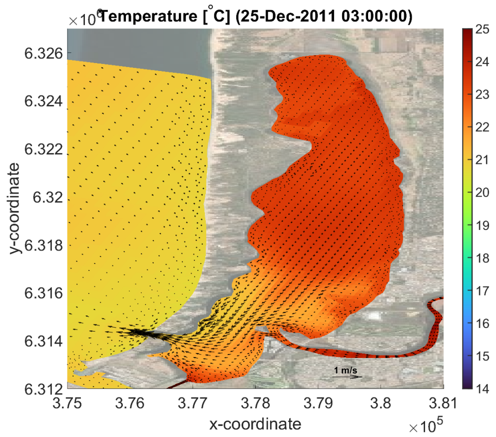

Figure 6.33: Depth-averaged temperature observed in a typical week summer week (25-12-2011 03:00 - falling spring tide)

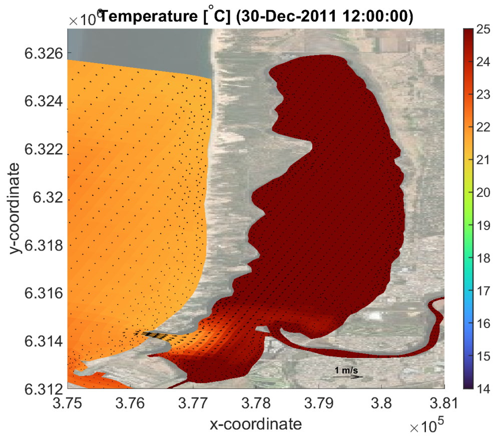

Figure 6.34: Depth-averaged temperature observed in a typical summer week (30-12-2011 12:00 - rising neap tide)

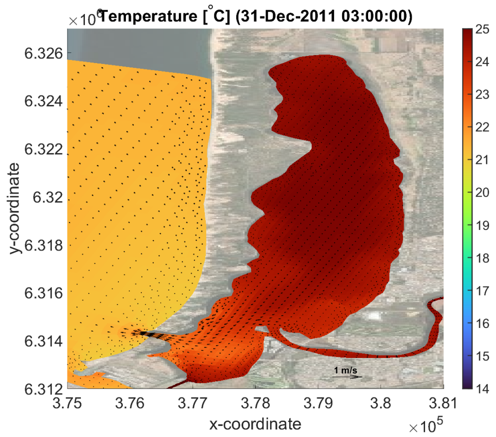

Figure 6.35: Depth-averaged temperature observed in a typical summer week (31-12-2011 03:00 - falling neap tide)

Summer

Figures 6.32, 6.33, 6.34 and 6.35 show the depth-averaged water temperatures of four moments in time in summer. Typical summer water temperatures in the estuary varied between 20 and 27 $°C$. Warmest water temperatures were observed in the northern basin of the estuary (>26 $°C$) and coolest water temperatures occurred offshore (≈20 $°C$). The reversed phenomenon of the winter situation happened in summer, with colder ocean waters penetrating the estuary during rising tide and cooling down the estuarine waters. The northern basin was less affected by water circulation and mixing generated by the tide, and typically presented higher water temperatures than the rest of the estuary. The water in the northern basin was predominantly affected by heat transfer between water and atmosphere. During falling tide, warmer estuary water heats up nearshore waters.

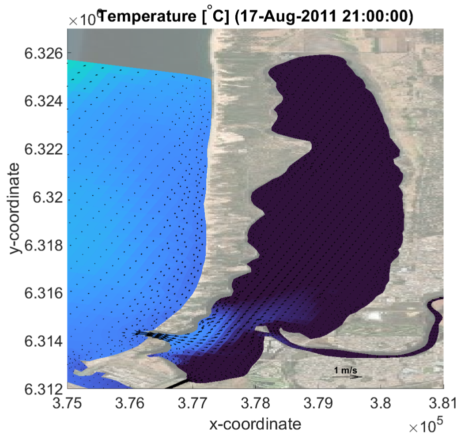

Figure 6.36: Depth-averaged temperature during rising neap tide before the extreme rainfall event of August 22 (17-08-2011 21:00)

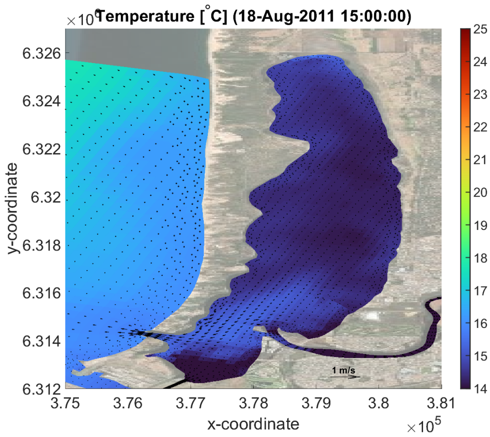

Figure 6.37: Depth-averaged temperature during falling neap tide before the extreme rainfall event of August 22 (18-08-2011 15:00)

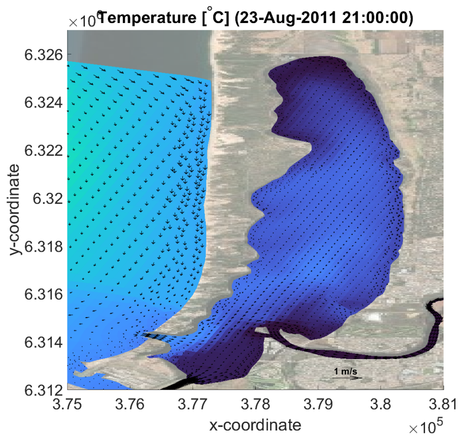

Figure 6.38: Depth-averaged temperature during rising spring tide after the extreme rainfall event of August 22 (23-08-2011 21:00)

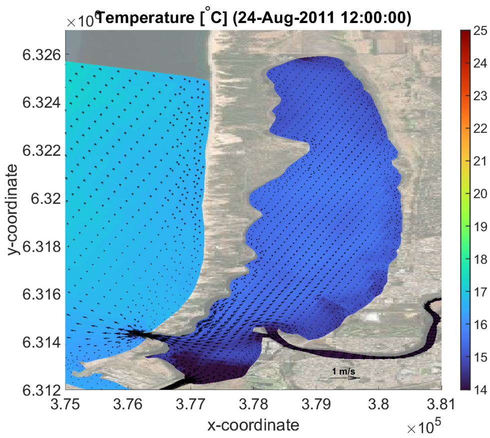

Figure 6.39: Depth-averaged temperature during falling spring tide after the extreme rainfall event of August 22 (24-08-2011 12:00)

6.3.2 Extreme discharge conditions

Figures 6.36, 6.37, 6.38 and 6.39 show the depth-averaged water temperatures a few days before and after the extreme rainfall event (August, 21/22). Temperatures in the estuary had values between 12 and 16 $°C$, with the lowest temperatures observed in the northern basin (<14°). Maximum nearshore temperatures were around 18 °. Similarly to the winter conditions, warmer ocean water penetrated the estuary during rising tide and heating up the estuary's water. A higher variation in water temperature was observed in winter, highlighting the influence of the freshwater. During falling tide, the colder estuary water cooled the nearshore waters.

6.3.3 Seasonal variation

The seasonal difference in the Leschenault water temperature between winter and summer periods is shown clearly in Figure 6.40. In winter, the depth-averaged water temperatures were lower than in summer, with values between 14 and 18 $°C$. Warmest estuary water occurred near the 'Cut'($\approx$18$°C$) and coldest estuary water was observed in the northern basin. Offshore waters had temperatures of 18/19 $°C$ in winter and around 22 $°C$ in summer. Higher water temperatures were observed inside the estuary in summer(22-24 $°C$). A higher variation in water temperature was observed in winter, highlighting the influence of the freshwater. In the northern basin of the estuary, the water temperature was mainly influenced by atmospheric forcing.

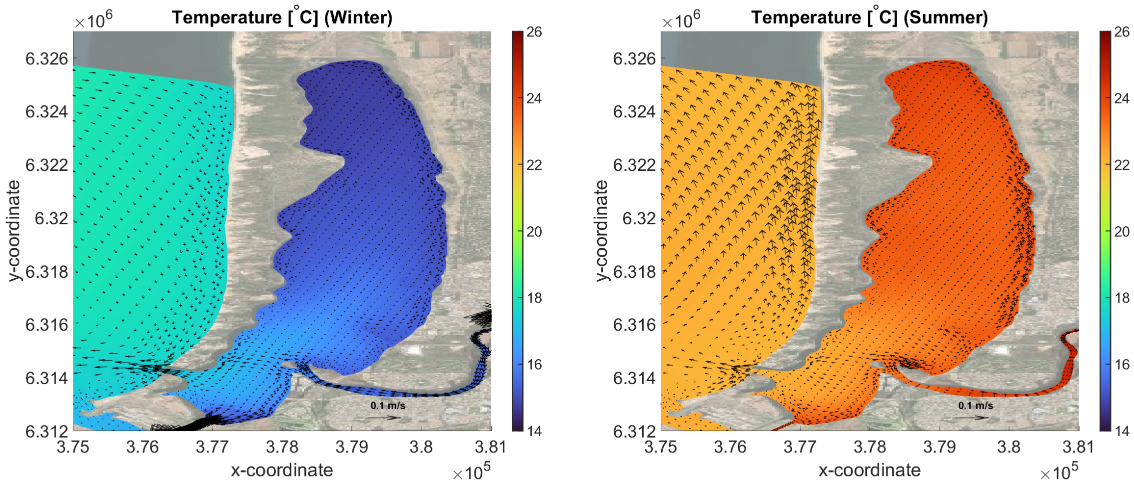

Figure 6.40: Time- and depth-averaged modelled temperature in winter [June 2011 - August 2011] (left) and summer [December 2011 - February 2012] (right)

6.3.4 Temperature profiles

To assess the variations of temperature along the water column, four different cross-sections were considered: Cut-Collie, Cut-Parkfield, Cut-Preston and Bay-Bunbury Port-Preston (only assessed in Chapter 7). The cross-sections are shown in Figure 6.41. Three snapshots were taken (winter (21-July-2011 21:00), summer (31-December-2011 12:00) and extreme discharge conditions (24-August-2011 21:00)) for each cross-section to evaluate seasonal temperature stratification patterns in the Leschenault Estuary, the rivers and the Bunbury Port. Besides, the time-averaged vertical temperature values are shown for the winter and summer seasons.

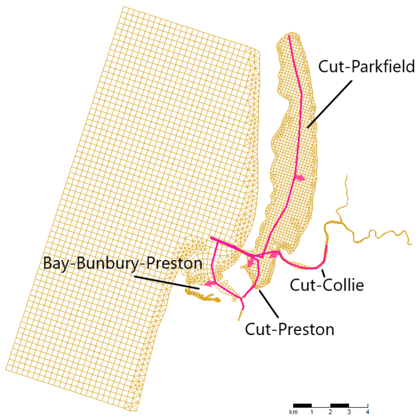

Figure 6.41: Cross-sections Leschenault Estuary DFM-model

The Cut-Collie profile

The Cut-Collie profiles for winter, summer and extreme discharge conditions are shown in Figure 6.42. At the distance between 2000 and 3000 m, the bed level starts to fall, indicating the Leschenault Estuary mouth (Figure 6.42). In winter, the ocean waters penetrated up to the Collie River close to the river bed and underneath the freshwater (Figure 6.42, left). This upriver bed flow brings warmer ocean water further upstream, resulting in a strong temperature gradient and a highly stratified flow. In summer (Figure 6.42, centre), this process was reversed, with colder ocean water penetrating up the Collie River. However, this process was weaker as well as the vertical temperature gradient. The estuary is therefore less stratified in summer in terms of temperature. During the extreme discharge event (Figure 6.42, right), the thermocline was pushed out of the estuary by the freshwater discharge. The thermocline occurred in Koombana Bay, generating temperature stratification in the upper layers of the water body.

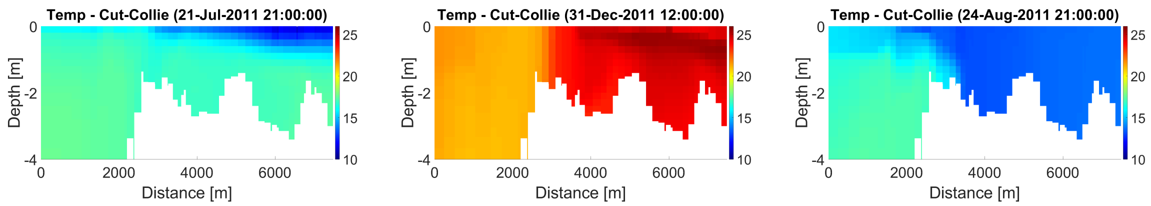

Figure 6.42: Along estuary temperature profile in $^{\circ}C$ from the mouth of the Leschenault Estuary to the Collie River (21-July-2011 21:00 - winter, left), (31-December-2011 12:00 - summer, centre) and (24-August-2011 21:00 - extreme discharge event, right)

The Cut-Preston profile

The Cut-Preston profiles (Figure 6.43) show the same phenomena as seen in the Cut-Collie profiles (Figure 6.42). However, the thermocline in the Preston River did not penetrate all the way upriver in winter but only around 1 km upstream. Nevertheless, a strong thermocline was observed in the estuary in winter (Figure 6.43, left). In summer, the vertical temperature stratification was weak and the largest gradients occurred in the horizontal, with temperatures gradually decreasing from Preston River to Koombana Bay (Figure 6.43, centre). During the peak flow event (Figure 6.43, right), the thermocline is pushed far out of the estuary.

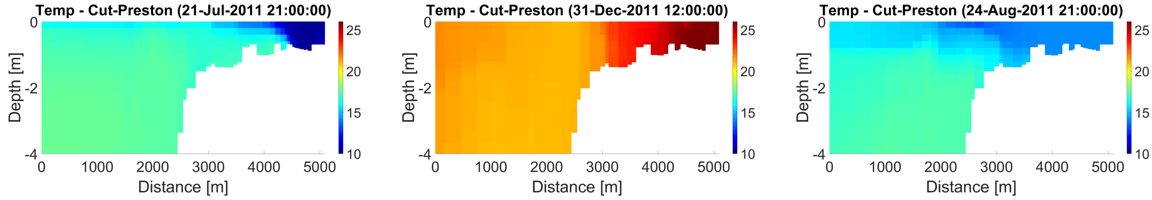

Figure 6.43: Along estuary temperature profile in $^{\circ}C$ from the mouth of the Leschenault Estuary to the Preston River (21-July-2011 21:00 - winter, left), (31-December-2011 12:00 - summer, centre) and (24-August-2011 21:00 - extreme discharge event, right)

The Cut-Parkfield profile

The Cut-Parkfield profiles (Figure 6.44), indicate that the central and northern basins were less stratified than the southern basin. In winter (Figure 6.44, left), strong stratification was observed in the southern basin, indicating the influence of the freshwater flow, which is considerably less in the central and northern basin. During the extreme discharge event, increased temperature stratification occurred in the southern basin and partly in the central basin (Figure 6.44, right). Water temperatures gradually decreased in the estuary in a northerly direction in winter (Figure 6.44, left). In summer (Figure 6.44, centre), no stratification was observed and water temperatures were higher in the northern basin, gradually decreasing towards the ocean.

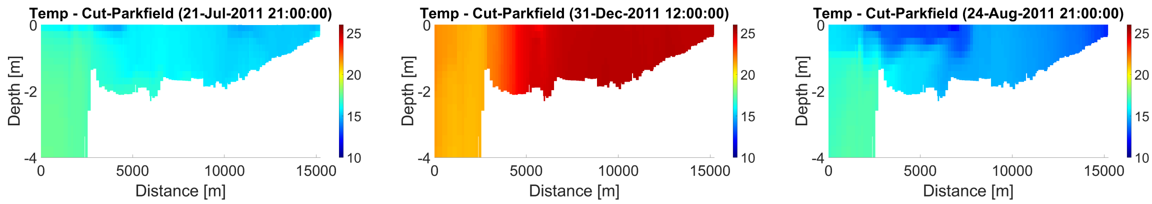

Figure 6.44: Along estuary temperature profile in $^{\circ}C$ from the mouth of the Leschenault Estuary to the Parkfield Drain (21-July-2011 21:00 - winter, left), (31-December-2011 12:00 - summer, centre) and (24-August-2011 21:00 - extreme discharge event, right)

Seasonally averaged profile - Cut-Collie

In Figure 6.45 and 6.45, the mean winter and summer temperatures of cross-section Cut-Collie are shown. In winter, the average water temperature varied from 15 $^{\circ}C$, in the Collie River, to 17.5 $^{\circ}C$ in the Koombana Bay (Figure 6.45, left). In summer, temperatures around 25 $^{\circ}C$ were observed in the Collie River and 22 $^{\circ}C$ in the Koombana Bay (Figure 6.45, right). In both situations, the water body was stratified with a sharper temperature gradient being observed in winter. Besides, the thermocline seemed to be located in the southern basin of the estuary in winter (Figure 6.45, left) and more upstream the Collie River in summer (Figure 6.45, right).

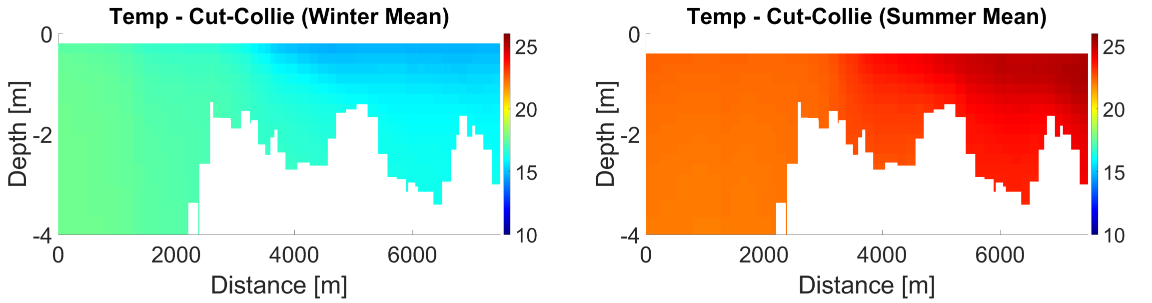

Figure 6.45: Along estuary temperature profile in $^{\circ}C$ from the mouth of the Leschenault Estuary to the Collie River (winter (left) and summer (right) mean)

Seasonally averaged profile - Cut-Preston

In Figure 6.46, the mean winter and summer temperatures of the Cut-Preston profile are shown. In winter, the average water temperature varied from 14 $^{\circ}C$, in the Preston River, to 17.5 $^{\circ}C$ in the Koombana Bay (Figure 6.46, left). In summer, values lied between 25 $^{\circ}C$ in the Preston River to 22 $^{\circ}C$ in the Koombana Bay (Figure 6.46, right). Whereas the thermocline in the Collie River was present far upstream the river, the thermocline in the Preston River showed a minor reach. In winter, the thermocline was visible in the southern basin of the estuary, with highly stratified conditions (Figure 6.46, left). In summer however, the temperature was almost uniform along the water column and gradually decreased from upriver towards the 'Cut' (Figure 6.46, right).

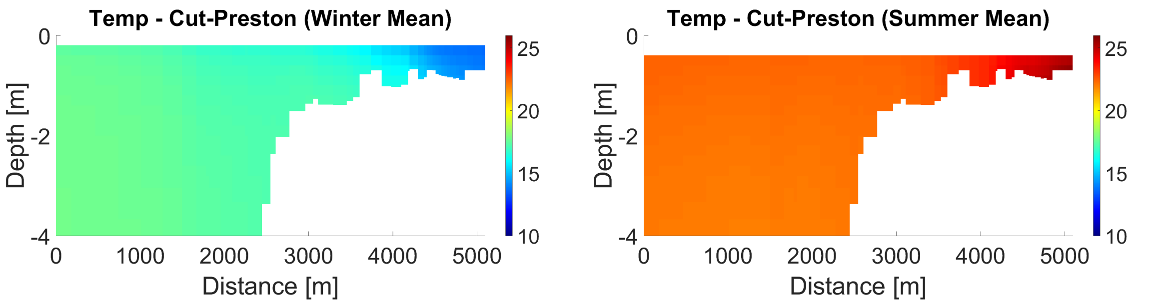

Figure 6.46: Along estuary temperature profile in $^{\circ}C$ from the mouth of the Leschenault Estuary to the Preston River (winter (left) and summer (right) mean)

Seasonally averaged profile - Cut-Parkfield

In Figure 6.47, mean winter and summer temperatures for the Cut-Parkfield section are shown. In winter, the average water temperature varied from 15 $^{\circ}C$, in the northern basin, to 17.5 $^{\circ}C$ in the Koombana Bay (Figure 6.47, left). In summer, it varied between 24 $^{\circ}C$, in the northern basin, and 22 $^{\circ}C$ in Koombana Bay (Figure 6.47, right). Stratification was less pronounced in the central and northern basin, even in winter when the freshwater discharge was higher (Figure 6.47, left). The thermocline is observed in the southern basin in summer and winter but had a sharper gradient in winter (Figure 6.47). In winter, the temperature gradually increased from the 'Cut' towards the north and in summer, the temperature gradually decreased from the 'Cut' towards the north (Figure 6.47).

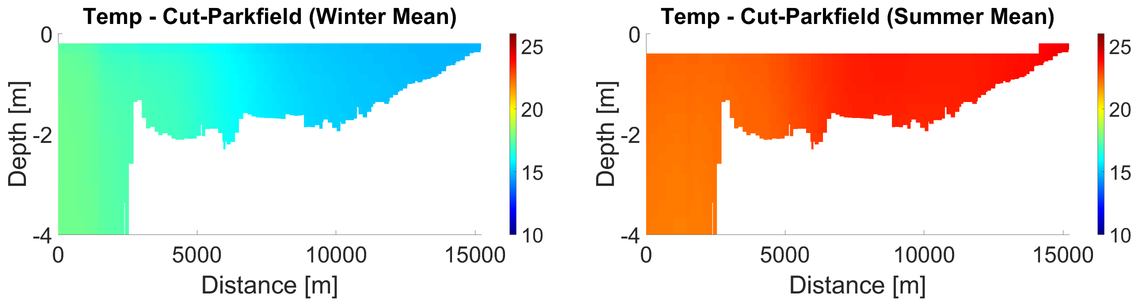

Figure 6.47: Along estuary temperature profile in $^{\circ}C$ from the mouth of the Leschenault Estuary to the Parkfield Drain (winter (left) and summer (right) mean)

6.4 Salinity

Similar to Section 6.1 and Section 6.3, salinity results were evaluated for a typical summer and winter week (Section 6.4.1) and a week associated with extreme river discharge conditions (Section 6.4.2). The seasonal variation between summer and winter is evaluated in Section 6.4.3 and the vertical variation of salinity is analysed in Section 6.4.4. Salinity values are specified with PSU (practical salinity unit).

6.4.1 Normal conditions

Similar periods were considered to evaluate the salinity results as for the circulation results (Section 6.1): (a) rising spring tide in winter (Figure 6.48), and in summer (Figure 6.52), (b) falling spring tide in winter (Figure 6.49), and in summer (Figure 6.53), (c) rising neap tide in winter (Figure 6.50), and in summer (Figure 6.54), (d) falling neap tide in winter (Figure 6.51), and in summer (Figure 6.55). All salinity results are depth-averaged.

Winter

Figures 6.52, 6.53, 6.54 and 6.55 show the depth-averaged salinity under typical winter conditions. Salinity values in the Leschenault Estuary reached 35 around the ‘Cut’ but as low as 0 near the river mouths. In winter, the estuary was influenced both by the tides and freshwater discharge. This can be noticed when comparing Figure 6.52 against Figure 6.53 and Figure 6.54 against Figure 6.55. At rising spring and neap tide, the salinity inside the estuary increased, indicating that saline ocean waters penetrated the estuary during rising tide (Figures 6.52 and 6.54). During falling tide, the brackish water flowed out of the estuary, decreasing the nearshore salinity (Figures 6.53 and 6.55). During falling tide, freshwater reached the central and northern basin of the estuary, decreasing the salinity in those regions. The southern basin was the most dynamical area, being influenced by the ‘Cut’ and the Preston Collie rivers. The highest salinity gradient occurred in the southern basin with values from 0 at the river mouths to 35 at the ‘Cut’. The central basin was less affected by the tide and freshwater discharge, showing a lower salinity gradient (values between 25 and 31). The northern basin was mainly influenced by Parkfield Drain discharge and less affected by tides.

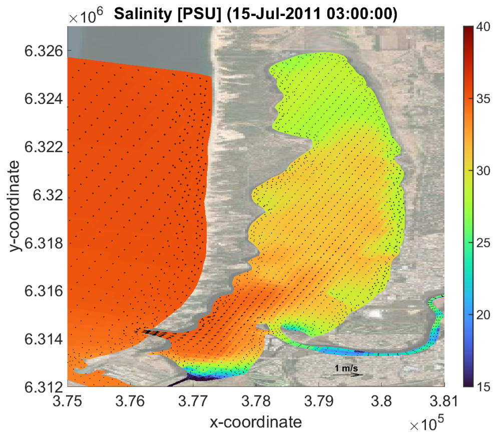

Figure 6.48: Depth-averaged salinity observed in a typical winter week (15-07-2011 03:00 - rising spring tide)

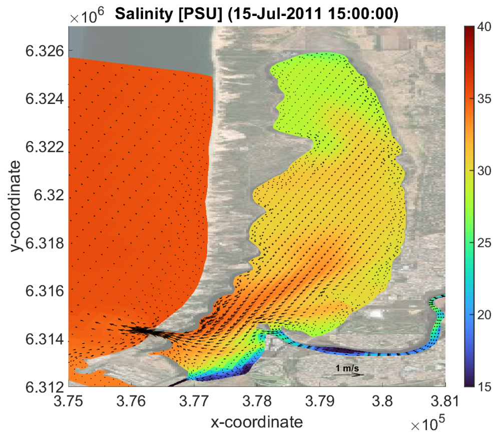

Figure 6.49: Depth-averaged salinity observed in a typical winter week (15-07-2011 15:00 - falling spring tide)

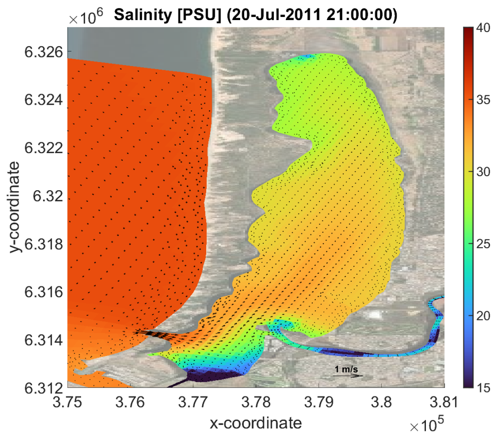

Figure 6.50: Depth-averaged salinity observed in a typical winter week (20-07-2011 21:00 - rising neap tide)

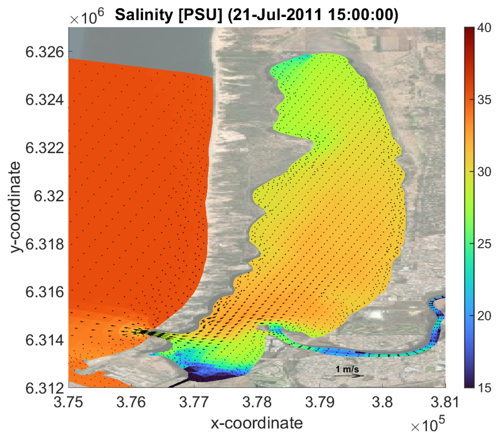

Figure 6.51: Depth-averaged salinity observed in a typical winter week (21-07-2011 15:00 - falling neap tide)

Summer

The typical summer salinity values are shown in Figures 6.56, 6.57, 6.58 and 6.59. Ocean salinity was around 35 and in the Leschenault Estuary, salinity values reached 40 in the northern basin, with hypersaline conditions in summer. Salinity values were significantly lower near the river mouths ($\approx$28). In winter, ocean water penetrated the estuary, mixing up with the brackish estuary water and therefore increased the salinity inside the estuary. This phenomenon can be clearly seen while assessing Figure 6.56 against 6.57 and Figure 6.58 against Figure 6.59. The freshwater discharge played a minor role in summer in the dynamics and the freshwater input of the Parkfield Drain was almost negligible. The northern basin was less affected by tides and freshwater discharge from the Preston and Collie rivers, becoming hypersaline in summer.

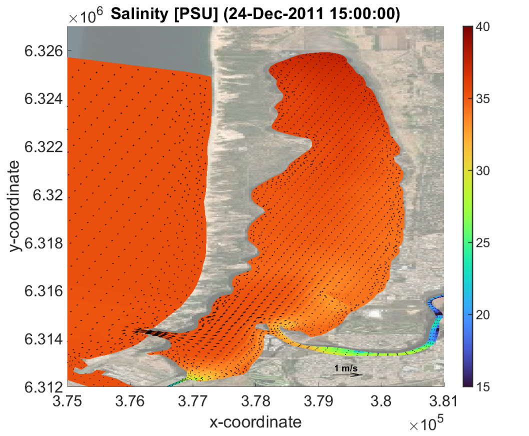

Figure 6.52: Depth-averaged salinity observed in a typical summer week (24-12-2011 15:00 - rising spring tide)

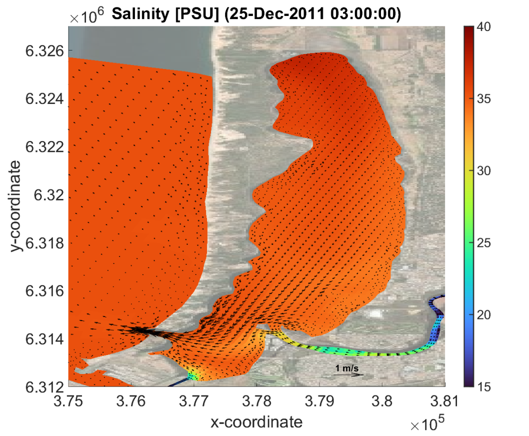

Figure 6.53: Depth-averaged salinity observed in a typical summer week (25-12-2011 03:00 - falling spring tide)

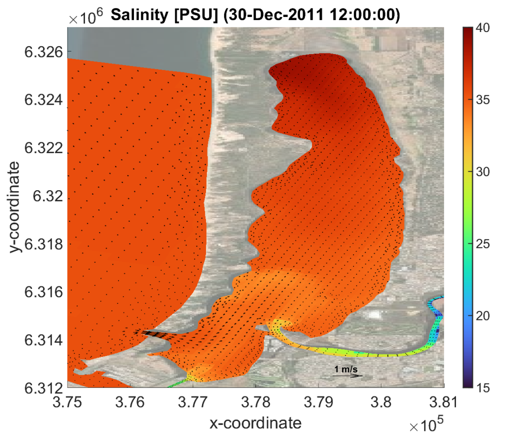

Figure 6.54: Depth-averaged salinity observed in a typical summer week (30-12-2011 12:00 - rising neap tide)

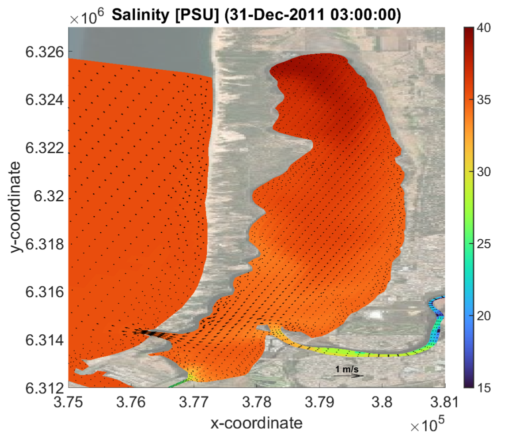

Figure 6.55: Depth-averaged salinity observed in a typical summer week (31-12-2011 03:00 - falling neap tide)

6.4.2 Flood conditions

Figures 6.56 and 6.57 show estuarine salinities before the August 22 extreme discharge event and Figures 6.58 and 6.59 show the salinity distributions after the extreme discharge event. A extreme discharge event lowers the Leschenault salinities considerably compared to the normal conditions (Section 6.4.1), indicating the increased influence of the freshwater discharge on the salinity. Discharges were higher in the days before the extreme discharge event than during typical winter days. Saline ocean water penetrated the estuary during rising tide (as is seen in Section 6.4.1), increasing estuarine salinities (Figures 6.56 and 6.58). During falling tide, the process is reversed and saline waters were pushed out of the estuary (Figures 6.57 and 6.59). Under extreme discharge conditions this process was strengthened and the southern region of the estuary became totally fresh (Figure 6.59).

Freshwater was flowing out of the estuary, decreasing the nearshore salinities (Figures 6.58 and 6.59). In the northern basin, the peak discharge of the Parkfield Drain had a considerable impact on the salinity reduction. Salinity values in the adjacent bay before the flood event were around 35 but dropped to minimum values of 25 after the extreme discharge event (Figures 6.56 and 6.57). Salinities in the central basin situated around 25-27 but decreased to 0 in the northern basin (Figures 6.56 and 6.57). After the extreme discharge event, salinity values of the entire southern and partly of the central basin dropped to 0, indicating the dominant influence of the freshwater discharge under extreme discharge conditions (Figures 6.58 and 6.59).

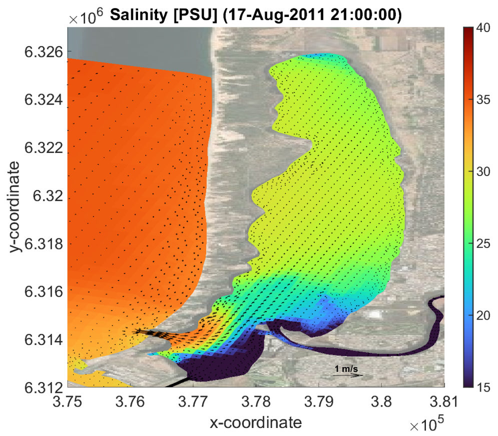

Figure 6.56: Depth-averaged salinity during rising neap tide before the extreme rainfall event of August 22 (17-08-2011 21:00)

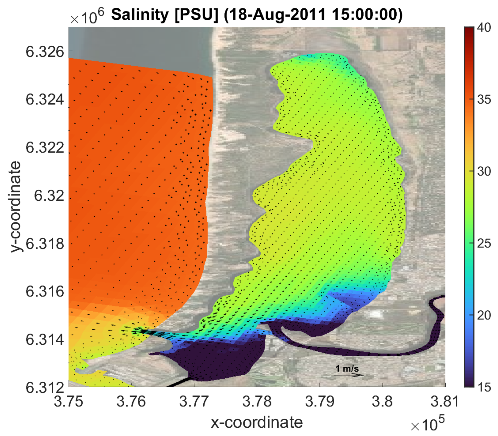

Figure 6.57: Depth-averaged salinity during falling neap tide before the extreme rainfall event of August 22 (18-08-2011 15:00)

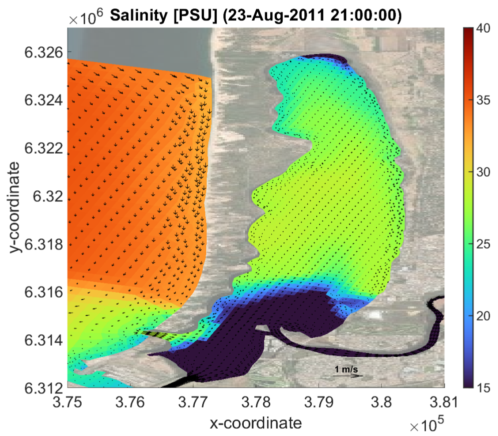

Figure 6.58: Depth-averaged salinity during rising spring tide after the extreme rainfall event of August 22 (23-08-2011 21:00)

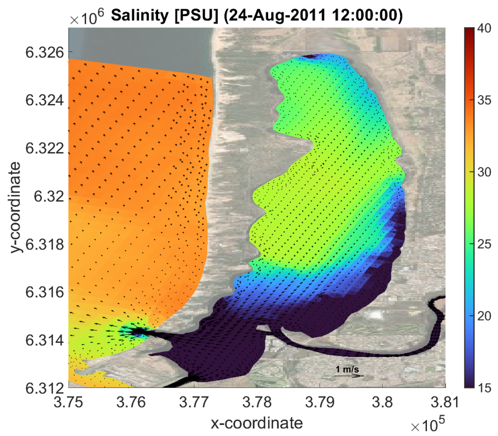

Figure 6.59: Depth-averaged salinity during falling spring tide after the extreme rainfall event of August 22 (24-08-2011 12:00)

6.4.3 Seasonal variation

Figure 6.60 show the time- and depth-averaged salinities in winter (left) and summer (right). The salinity values represent averages over the entire winter and summer periods, filtering out the tidal influence on salinity. Observed salinities in summer (between 30 and 40) were much higher than in winter (between 15 and 32). Coastal salinities were around 35, with slightly higher values being observed in summer. Highest salinity values were found in winter in the northern basin (around 40) and gradually decreased towards the south. The impact of the freshwater discharge on the salinity was clearly more pronounced in winter (Figure 6.60). Salinity values near the river mouths were 0 in winter and in summer, river salinities were considerably higher than in winter (Figure 6.60).

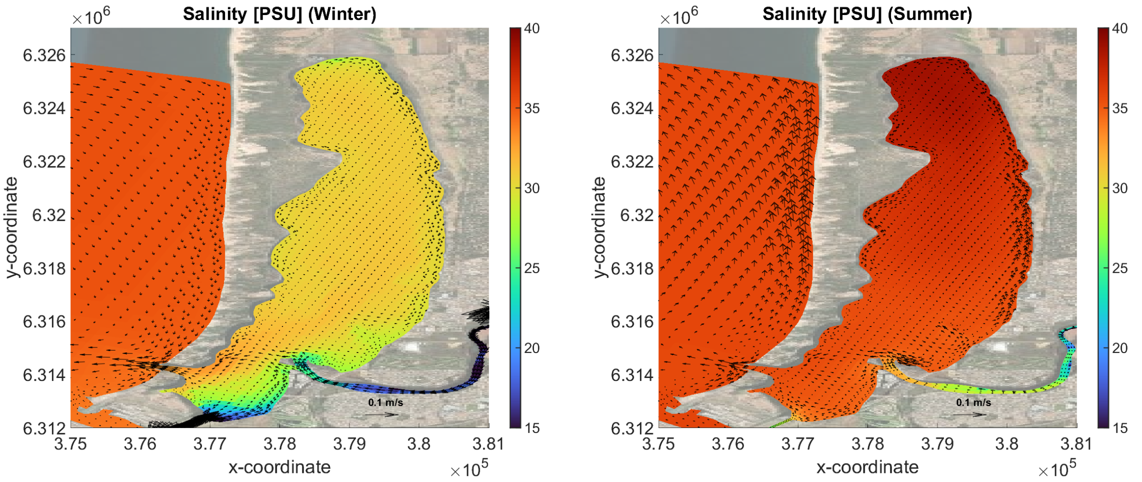

Figure 6.60: Time- and depth-averaged modelled salinity in winter [June 2011 - August 2011] (left) and summer [December 2011 - February 2012] (right)

6.4.4 Salinity profiles

The same cross-sections adopted for temperature were used to show longitudinal salinity variations (Figure 6.41). Three snapshots of moments in time (winter (21-July-2011 21:00), summer (31-December-2011 12:00) and extreme discharge conditions (24-August-2011 21:00)) were taken for each cross-section to evaluate seasonal variations of salinity stratification in the Leschenault Estuary, the rivers and the Bunbury Port. Also, the time-averaged vertical salinity values are shown for winter and summer.

The Cut-Collie profile

In the Collie River, freshwater flows on top of ocean waters that intrude the estuary near the bottom. This salinity stratification happened both in winter (Figure 6.61, left) and summer (Figure 6.61, centre) but it was higher in winter (Figure 6.61, left). The sharp halocline is still observed near the entrance of the estuary. This halocline is less sharp in summer and is pushed back up the Collie River. Saline ocean water penetrates the Collie River along the river bed. However, under extreme flood conditions the halocline is forced out of the estuary (Figure 6.61, right). The halocline has a sharp gradient despite the season with varying salinity values between 0 and 35.

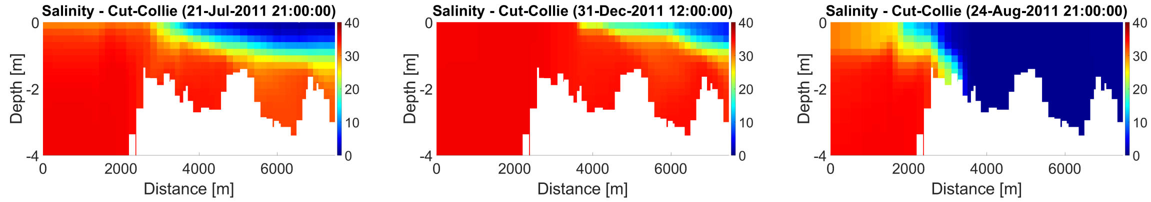

Figure 6.61: Along estuary salinity profile in PSU from the mouth of the Leschenault Estuary to the Collie River (21-July-2011 21:00 - winter, left), (31-December-2011 12:00 - summer, centre) and (24-August-2011 21:00 - extreme discharge event, right)

The Cut-Preston profile

The Cut-Preston profiles (Figure 6.62) show similar patterns to the Cut-Collie profiles (Figure 6.61). The halocline was observed in the southern basin in winter, indicating highly stratified waters (Figure 6.62, left). In summer, the halocline was pushed upriver (Figure 6.62, right), and had a relatively reduced salinity gradient. Under extreme flood conditions, the halocline was forced out of the estuary (Figure 6.62, right).

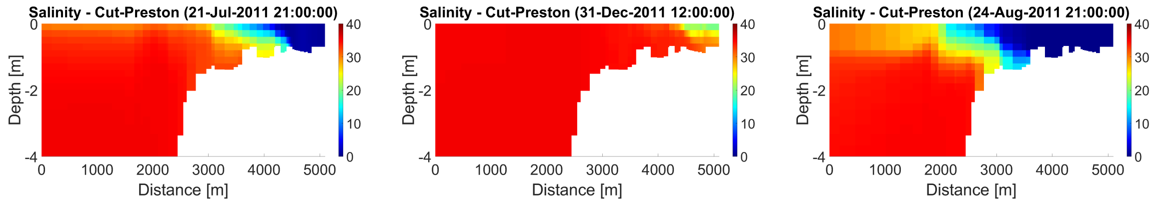

Figure 6.62: Along estuary salinity profile in PSU from the mouth of the Leschenault Estuary to the Preston River (21-July-2011 21:00 - winter, left), (31-December-2011 12:00 - summer, centre) and (24-August-2011 21:00 - extreme discharge event, right)

The Cut-Parkfield profile

The Cut-Parkfield profiles (Figures 6.63) showed better mixing than the Cut-Collie and Cut-Preston profiles (Figures 6.61 and 6.62). During winter, the salinity was almost homogeneous along the estuary, with highest stratification observed in the southern regions of the estuary (Figure 6.63, left). In summer, the salinity was almost vertically uniform and reached hypersaline values (≈40) in the northern reach of the estuary (Figure 6.63, centre). During the extreme discharge event, the northern regions were well-mixed and high salinity stratification occurred south of the estuary (Figure 6.63, right).

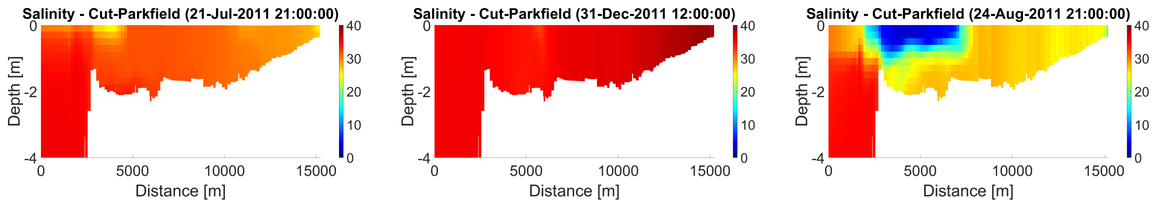

Figure 6.63: Along estuary salinity profile in PSU from the mouth of the Leschenault Estuary to the Parkfield Drain (21-July-2011 21:00 - winter, left), (31-December-2011 12:00 - summer, centre) and (24-August-2011 21:00 - extreme discharge event, right)

Seasonally averaged profile - Cut-Collie

Winter and summer mean salinities for the Cut-Collie profiles are shown in Figure 6.64. In winter, the averaged salinity varied from 0 in the Collie River to 35 in the Koombana Bay (Figure 6.64, left). In summer, this variation was the same but the halocline was located further upriver, with a much weaker salinity gradient (Figure 6.64, right). In winter, more freshwater flowed into the estuary (Figure 6.64, left) and in summer, ocean water intruded further upriver (Figure 6.64, right).

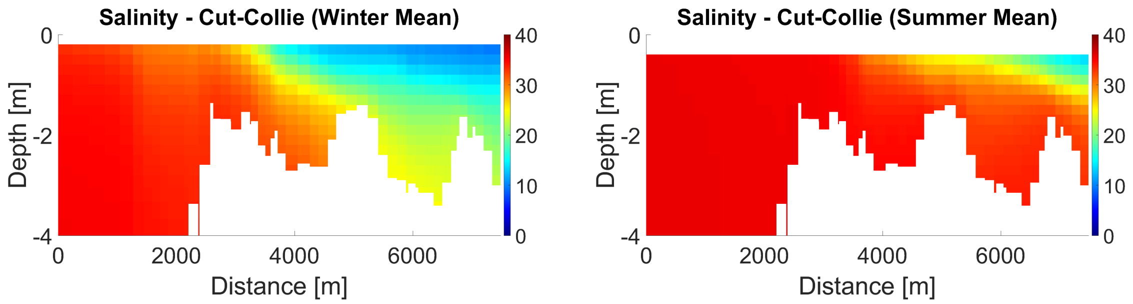

Figure 6.64: Along estuary salinity profile in PSU from the mouth of the Leschenault Estuary to the Collie River (winter (left) and summer(right) mean)

Seasonally averaged profile - Cut-Preston

In Figure 6.65, the mean winter and summer salinities are shown for the Cut-Preston profile. In winter, the averaged salinity varied between 10 in the Preston River and 35 in the Koombana Bay (Figure 6.65, left). In summer, this variation lied between 20 in the Preston River to 35 in the Koombana Bay (Figure 6.65, right). In winter, a higher stratification occurred (Figure 6.65, left), whereas in summer, the salinity homogeneously decreased upriver (Figure 6.65, right).

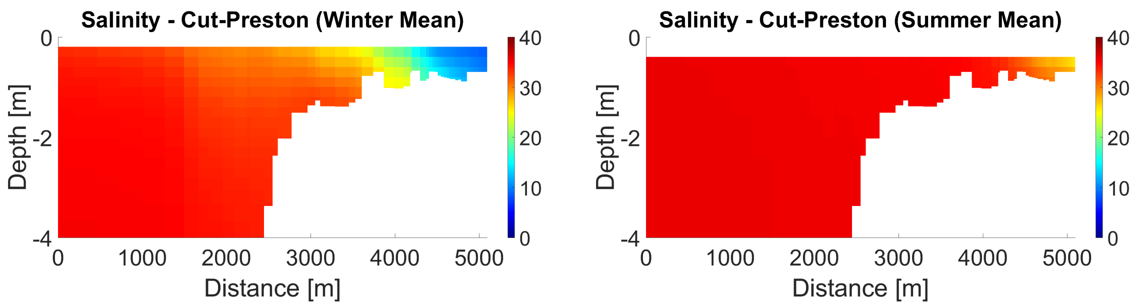

Figure 6.65: Along estuary salinity profile in PSU from the mouth of the Leschenault Estuary to the Preston River (winter (left) and summer (right) mean)

Seasonally averaged profile - Cut-Parkfield

Even less stratification was observed for the Cut-Parkfield profile (Figure 6.66). In winter, the average water salinity varied between 31 in the central and northern basin of the estuary and 35 in the Koombana Bay (Figure 6.66, left). In summer, this variation lied between 40 in the northern basin and 35 in the Koombana Bay (Figure 6.66, right). In the

Cut-Parkfield profile in winter (Figure 6.66, left), the range of salinity variation was much less than in other cross-sections, which already indicates that the salinity varied less over depth. Most of the salinity stratification occurred in the southern basin in winter (Figure 6.66, left). In summer, the salinity gradually increased along the estuary, with hypersaline salinity in the northern regions (Figure 6.66, right).

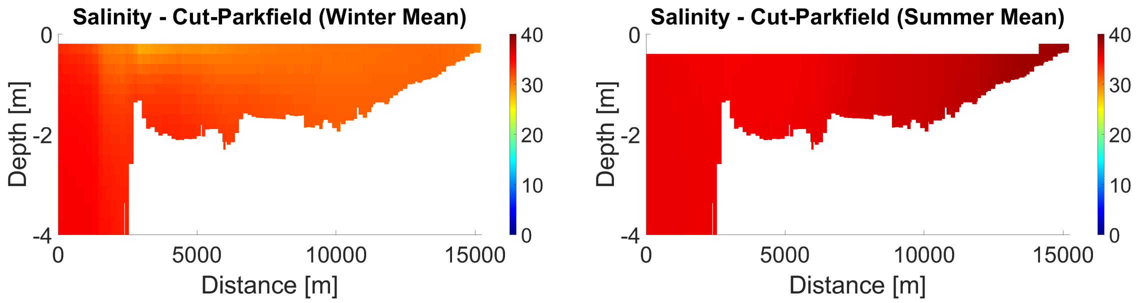

Figure 6.66: Along estuary salinity profile in PSU from the mouth of the Leschenault Estuary to the Parkfield Drain (winter (left) and summer (right) mean)

6.5 Estuarine classification

The Leschenault Estuary was classified by assessing the thermohaline characteristics, the vertical variations of salinity and current velocity, the Richardson layer number and the circulation and stratification parameter of Hansen and Rattray Jr (1966). Each parameter was calculated for the variability per parameter for both a neap and spring tidal cycle under winter, summer and peak river flow conditions. The neap and spring tidal cycles all have a duration of 24 hours, for dominant diurnal tides, including ebbing and flooding periods. Note that the neap tidal cycle is mainly diurnal with a slight semi-diurnal characteristic. The start and end dates and times of the considered tidal cycles are summarized in Table 6.2 and shown in Figure 6.67.

Period	Start	End
Neap Winter	15-Jul-2011 03:00:00	16-Jul-2011 03:00:00
Spring Winter	20-Jul-2011 21:00:00	21-Jul-2011 21:00:00
Neap Summer	24-Dec-2011 15:00:00	25-Dec-2011 15:00:00
Spring Summer	30-Dec-2011 12:00:00	31-Dec-2011 12:00:00
Neap Peak Flow	17-Aug-2011 21:00:00	18-Aug-2011 21:00:00
Spring Peak Flow	23-Aug-2011 21:00:00	24-Aug-2011 21:00:00

Table 6.2: Start and end dates and times of the winter, summer and flood neap and spring tidal cycles

6.5.1 Thermohaline character

The T-S diagrams show the thermohaline characteristics of the Leschenault Estuary at the different stations, and were built using depth-averaged salinity and temperature data, generated by the DFM-model. The considered time periods are listed in Table 6.2 and shown in Figure 6.67. According to De Miranda et al. (2017), the water is more homogeneous if

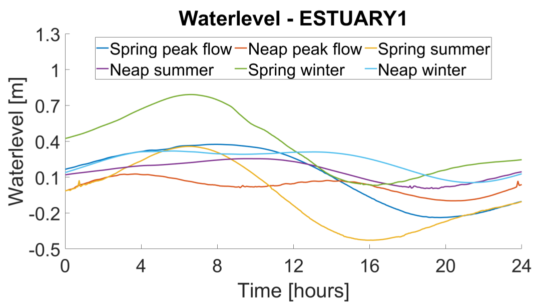

Figure 6.67: Tidal cycles at the 'Cut' (ESTUARY1) considered in Section 6.5

the set of data points are clustered, indicating no variation in the advective and diffusive properties. More scattered datasets represent non-homogenous water bodies with variation in these properties (De Miranda et al., 2017).

Bunbury Port

The T-S diagram at the Bunbury Port (OUTER1) shows temperatures ranging from 15.3-16 $°C$ in winter to 21-22.5 $°C$ in summer, and salinities ranging from 31.4-33.8 in winter to 35.4 in summer (Figure 6.68, left). However, the variations between neap and spring were small. This is probably due to reduced influence of the estuarine waters in the Bunbury Port, considering the long distance between the 'Cut' and the harbour. However, significant variations in salinity were observed under flood conditions, ranging between 22-30 at spring and 28-34 at neap. A possible explanation is the high freshwater discharge at this time of year generating highly variable salinities, although with almost constant temperatures. Further, higher temperatures occurred at summer neap and winter spring. This indicates more intense mixing during spring tides, resulting in warmer water in the harbour in winter and cooler water in the harbour in summer. Coastal shallow water bodies are more sensitive to atmospheric heat exchanges and are generally colder than ocean waters in winter and warmer in summer. The same trend is observed at all other stations.

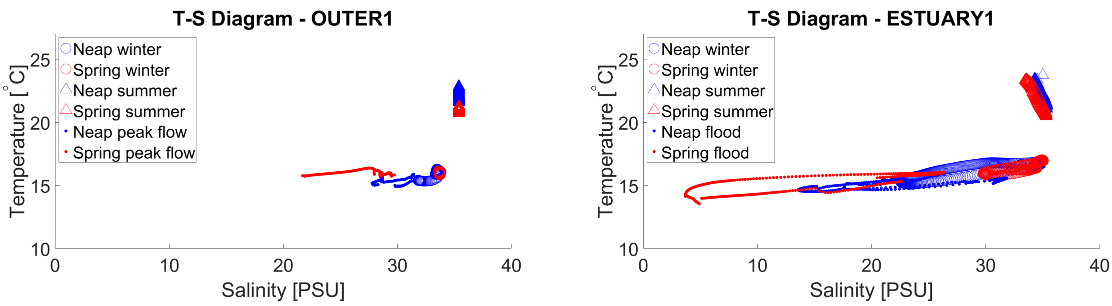

Figure 6.68: T-S Diagram of OUTER1 (left) and ESTUARY1 (right) for winter, summer and flood spring and neap tidal cycles

The 'Cut'

The T-S diagram at the 'Cut' (ESTUARY1) shows temperatures ranging from 15-17 $°C$ in winter to 20.5-23 $°C$ in summer, and salinities ranging from 22.5-35 in winter to 33.7-35.3

in summer (Figure 6.68, right). During the peak river flow event, salinities ranged from 3.7 to 31.8 and the temperatures ranged from 13.5 to 16.3 $°C$. The highly variable salinity at the 'Cut' (ESTUARY1) indicates that the station is located in a mixing zone (Figure 6.68, right). The positive correlation between the temperature and the salinity under flood and winter conditions represents the influence of both the tide and the freshwater discharge according to De Miranda et al. (2017). However, a different pattern was recognized in summer, with a negative correlation. A possible explanation could be the increased influence of the tide under drier summer conditions with low river flow. The hypersaline conditions in the estuary in summer could only be reduced by mixing of ocean water induced by the tide. Another phenomenon that can be noticed in Figure 6.68 (right) is the lower salinity at spring tide during the peak river flow event. Overall, salinities were higher in winter spring than at winter neap due to increased mixing (Figure 6.68, right). Conversely, salinities were higher in summer inside the estuary and lower salinities occurred at spring than at neap tide (Figure 6.68, right). On the other hand, the lower salinity values at spring during the peak flow event were caused by the extreme freshwater flow just before spring tide, diminishing the influence of the tide.

Central basin

The T-S diagram at the central basin of the estuary (ESTUARY3) shows temperature ranges of 15-17 $°C$ in winter, and 20.5-25.5 $°C$, in summer (Figure 6.69, left). Salinities varied between 29.3-33.8 in winter, and 34-35.8, in summer (Figure 6.69, left). During the peak river flow event, the salinity ranged from 8.9 to 27.6 and the temperature ranged from 12.5 to 16 $°C$ (Figure 6.69, left). Compared to the 'Cut' (ESTUARY1), the salinity variation was reduced under peak freshwater discharge conditions and almost negligible under normal winter conditions. Again, a positive correlation can be noticed for the flood and winter situation. Under summer conditions, the salinity variation was almost nil and temperatures varied only slightly at spring tide (Figure 6.69, left), indicating the dominant tidal influence in the central basin in summer. In winter, a more balanced influence was observed between tides and freshwater discharge.

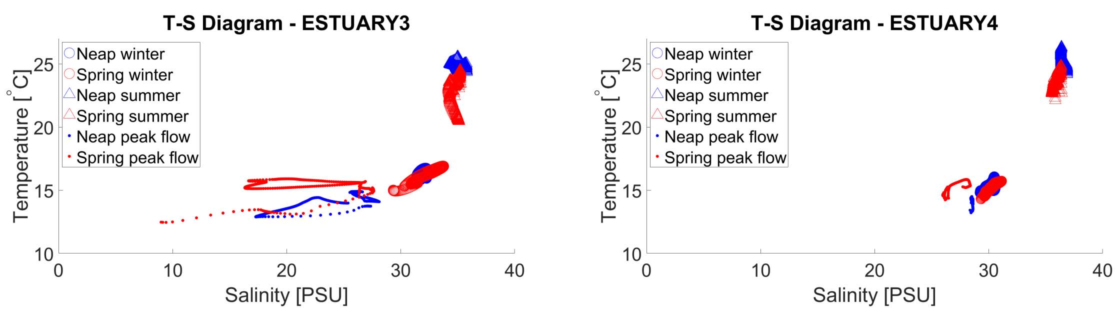

Figure 6.69: T-S Diagram of ESTUARY3 (left) and ESTUARY4 (right) for winter, summer and flood spring and neap tidal cycles

Northern basin

At the northern basin (ESTUARY4) the T-S diagram (Figure 6.69, right) shows temperature ranges of 14.3-16 $°C$ in winter, and 22.1-26.3 $°C$ in summer. Salinities varied between 29.3-31.1 in winter and 35.5-36.9 in summer. During the peak river flow event, salinities ranged between 26.1-28.7 and temperatures ranged between 13.2-15.9 $°C$. Compared to the central basin (ESTUARY3), the salinity variation was less marked, even during the peak river flow event. Positive correlations were observed for peak river flow and winter conditions (Figure 6.69, right). As a result of the remote location of the northern basin (ESTUARY4), it suffers less influence of tides and freshwater discharge. In summer, salinities were almost constant and water temperatures varied slightly (Figure 6.69, right). Tidal influence dominated in the northern basin in summer over freshwater inflow. During winter and the peak river flow event, both tidal and freshwater discharge influence were important.

Southern basin

The T-S diagram at the southern basin of the estuary (ESTUARY2) shows temperatures between 13.1-17.1 $°C$ in winter, and between 20.3-25 $°C$ in summer (Figure 6.70, left). Salinity varies between 17-34 in winter, and 33.2-35.3 in summer (Figure 6.70, left). During the peak river flow event, salinities ranged between 0.2-6.2 and temperature ranged between 12-15 $°C$ (Figure 6.70, left). Temperature and salinity distributions in summer at the southern basin (ESTUARY2) had similar patterns to those observed at the 'Cut' (ESTUARY1), due to the proximity of these two stations (Figure 6.68, right). Temperature and salinity distributions in winter had higher variations, indicating a higher influence of the freshwater discharge in winter at the southern basin (ESTUARY2) (Figure 6.70, left). During the peak river flow event, the southern basin (ESTUARY2) water behaved more like a river. Both salinity and temperature variations were considerably lower (<6 PSU) than at other stations, what indicates the dominant influence of the river discharge under peak flow conditions.

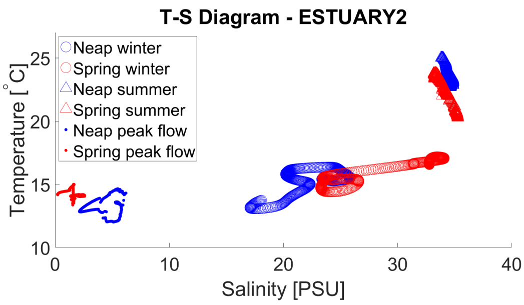

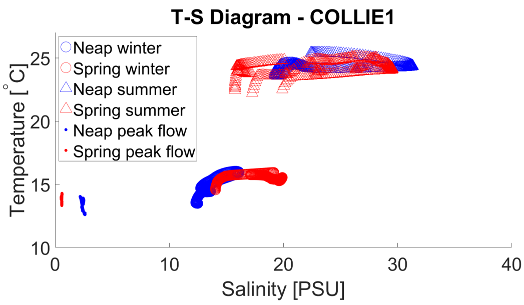

Figure 6.70: T-S Diagram of ESTUARY2 (left) and COLLIE1 (right) for winter, summer and flood spring and neap tidal cycles

Collie River

The T-S diagram at the Collie River (COLLIE1) shows temperatures ranging between 13.5-16 $°C$ in winter and between 22.2-25.4 $°C$ in summer (Figure 6.70, right). Salinities varied between 12.5-20 in winter to 15.7-31.3 in summer (Figure 6.70, right). During the peak flow event, salinities ranged between 0.5-2.6 and temperatures ranged between 12.6-14.3 $°C$. The pattern of the temperature and salinity distribution at the Collie River (COLLIE1) differed significantly from the other stations. The highest variation in salinity and temperature occurred in summer (Figure 6.70, right), indicating the decreased freshwater discharge in the Collie River and the higher influence of the tide. It also implies that the mixing zone extends beyond this point in summer with saline ocean water intruding far into the Collie

River. In winter, the variation was less pronounced with lower salinity values than inside the estuary (Figure 6.70, right), implying the higher influence of the freshwater discharge at COLLIE1 in winter. During the peak flow event, the water in the Collie River (COLLIE1) is solely affected by the freshwater discharge (Figure 6.70, right), which pushes the salt wedge out of the Collie River and partly out of the estuary.

6.5.2 Richardson

The depth-averaged Richardson layer number is used to evaluate the mixing intensity at the different stations per tidal cycle (specified in Table 6.2 and shown in Figure 6.67). Diurnal neap and spring tidal cycles started at rising tide and ended at falling tide (Figure 6.67). For Richardson layer number of more than 20 ($Ri_L > 20$), almost no vertical mixing occurs in the water column and the water column can be classified as highly stratified (De Miranda et al., 2017). For Richardson layer numbers of 2 or lower ($Ri_L < 2$), turbulence becomes dominant and the the water column can be classified as well-mixed (De Miranda et al., 2017). For Richardson layer numbers in between 2 and 20 ($2 \leq Ri_L \leq 20$) , the water column can be classified as partially-mixed with slight stratification (De Miranda et al., 2017).

Bunbury Port

The Ri_L of the different tidal cycles at Bunbury Port (OUTER1) are shown in Figure 6.71 (left). Bunbury Port waters can be classified as highly stratified ($Ri_L > 20$) for neap winter, neap peak flow and spring peak flow tidal cycles (Figure 6.71, left). For spring summer, neap summer and spring winter tidal cycles, the water at Bunbury Port was mainly partially-mixed ($2 \leq Ri_L \leq 20$), with some outliers in the well-mixed zone (Figure 6.71, left). The size of the box-plots are small indicating small variations in richardson later numbers over a single tidal cycle (Figure 6.71, left). The higher Richardson layer numbers at neap tide than at spring tide for winter and summer conditions at Bunbury Port indicates the dominant tidal influence on vertical mixing during spring. During the peak flow event, the influence of the spring tides was dominated by the freshwater discharge, generating stratified flows in the Bunbury Port (Figure 6.71, left). During summer, the weak freshwater discharge was dominated by tides, generating partially-mixed to well-mixed flows in the Bunbury Port (Figure 6.71, left).

The 'Cut'

The Ri_L of the different tidal cycles at the 'Cut' (ESTUARY1) show that estuarine waters at the 'Cut' have very dynamic conditions (Figure 6.71, right). In winter, the waters at the 'Cut' (ESTUARY1) were partially-mixed to highly stratified at neap and well-mixed to partially-mixed at spring (Figure 6.71, right), indicating the higher influence of the freshwater discharge during neap and the higher influence of tides during spring in winter. In summer, the water at the 'Cut' (ESTUARY1), was mainly well-mixed, indicating the weak freshwater discharge dominated by tides (Figure 6.71, right). During the peak river flow event, the water at the 'Cut' can be classified as partially-mixed to highly stratified at spring and highly stratified at neap (Figure 6.71, right), indicating increased vertical mixing generated by spring tides.

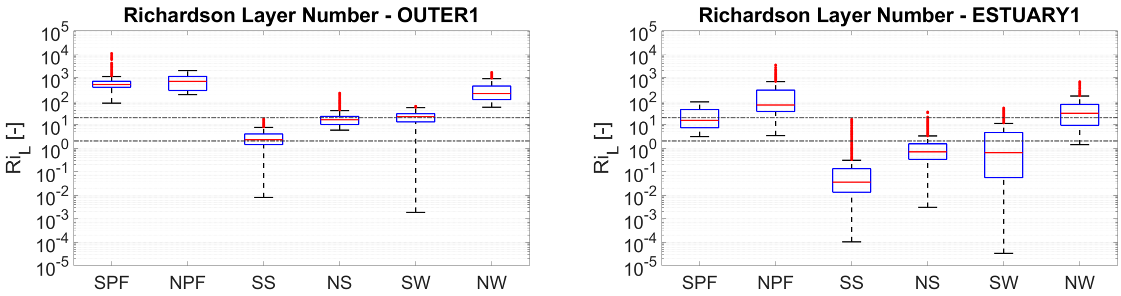

Figure 6.71: Richardson layer number at Bunbury Port (OUTER1) (left) and the 'Cut' (ESTUARY1) (right); SPW = Spring Peak Flow, NPW = Neap Peak Flow, SS = Spring Summer, NS = Neap Summer, SW = Spring Winter and NW = Neap Winter; $Ri_L < 2$ = well-mixed, $2 \leq Ri_L \leq 20$ = partially-mixed and $Ri_L > 20$ = highly stratified

Southern basin

Figure 6.72 (left) shows the Ri_L of the different tidal cycles at the southern basin (ESTUARY2). In winter, the waters in the southern basin were highly stratified during neap and partially to well-mixed during spring (Figure 6.71, left), indicating stratified flows generated by freshwater discharge at neap and increased mixed flows due to dominant tidal influence. In summer, the waters in the southern basin were well-mixed during spring and partially to well-mixed during neap (Figure 6.71, left), which indicates the reduced influence of the freshwater discharge in summer. During the peak river flow event, the southern basin waters were highly stratified during neap and partially-mixed during spring (Figure 6.71, left). This indicates that the southern basin waters are still significantly mixed during the peak discharge event at spring tide.

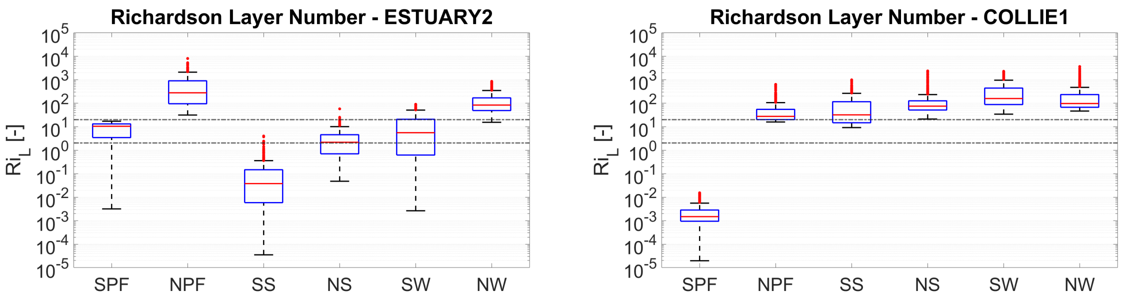

Figure 6.72: Richardson layer number at the southern basin (ESTUARY2) (left) and the Collie River (COLLIE1) (right); SPW = Spring Peak Flow, NPW = Neap Peak Flow, SS = Spring Summer, NS = Neap Summer, SW = Spring Winter and NW = Neap Winter; $Ri_L < 2$ = well-mixed, $2 < Ri_L < 20$ = partially-mixed and $Ri_L > 20$ = highly stratified

Collie River

The turbulence regime in the Collie River (COLLIE1) was rather uniform, with highly stratified flows for almost all tidal cycles, except the spring tidal cycle during the peak river flow event (Figure 6.72, right). Ri_L-values were well above the limits of the transition zones, which indicated highly stable water bodies with high stratification at the Collie River (COLLIE1) (Figure 6.72, right). However, during the peak flow event, the situation changed with extreme river flow pushing the salt wedge out of the rivers, resulting in a well-mixed water body (Figure 6.72, right). The fact that the peak river flow event occurred a few days after neap tide explains why the water body at neap tide was still highly stratified. Hence, the chosen neap tide for the peak river flow event occurred before spring tide. In summer, the influence of the tides became higher in the Collie River, due to the decreased influence of the freshwater discharge in summer (Figure 6.72, right).

Central basin

The estuarine waters in the central basin (ESTUARY3) are less influenced by the freshwater discharge from the south, which can be noticed by the lower Ri_L shown in Figure 6.73 (left). The central basin waters can be classified as well-mixed for spring summer, neap summer and spring winter tidal cycles (Figure 6.73, left), indicating weak influence of freshwater discharge and higher influence of tides. During neap in winter, the central basin became partially-mixed at moments of dominant freshwater discharge over tides (Figure 6.73, left). partially-mixed flows were also observed during the peak river flow event, when more freshwater flowed into the central basin (Figure 6.73, left).

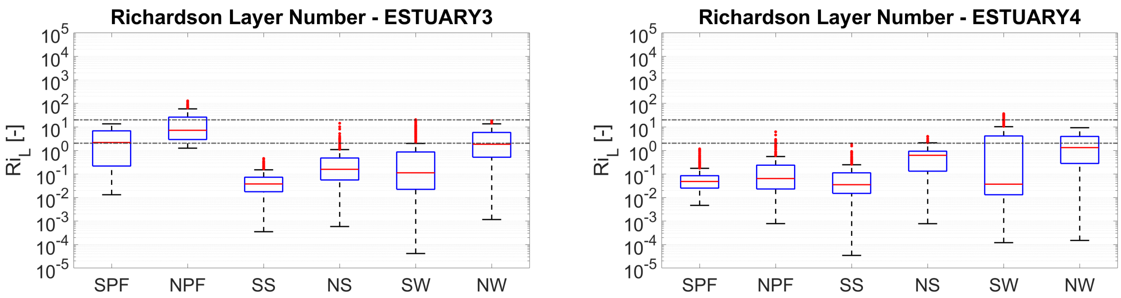

Figure 6.73: Richardson layer number at the central basin (ESTUARY3) (left) and the northern basin (ESTUARY4) (right); SPW = Spring Peak Flow, NPW = Neap Peak Flow, SS = Spring Summer, NS = Neap Summer, SW = Spring Winter and NW = Neap Winter; $Ri_L < 2$ = well-mixed, $2 < Ri_L < 20$ = partially-mixed and $Ri_L > 20$ = highly stratified

Northern basin

The northern basin of the estuary (ESTUARY4) showed even less stratification than the central basin (ESTUARY3) (Figure 6.73). Only under winter conditions, the Richardson layer number sometimes was high enough to provide vertical stability and increased stratification to become partially-mixed (Figure 6.73, right). The partially-mixed characteristics in winter were potentially caused by the Parkfield Drain discharge. In summer and during the peak river flow event, the northern basin waters were well-mixed (Figure 6.73, right). It is therefore expected that the northern basin is almost unaffected by the freshwater discharge from the southern rivers.

6.5.3 Vertical distribution profiles

Vertical variations of time-averaged salinity and current velocity were assessed by plotting salinities and current velocities against the normalized depth. The considered tidal cycles for each station are summarized in Table 6.2 and shown in Figure 6.67. As the Leschenault

Estuary has many flow directions due to the different flow regimes along the estuary, both u- and v-components of the current velocity were assessed. The considered currents are residual, net flows averaged over single tidal cycles under different (tidal) conditions (Table 6.2 and Figure 6.67).

Salinity - Bunbury Port

Figure 6.74 (left) shows the vertical salinity distributions at Bunbury Port (OUTER1). In summer, the salinity was well-mixed at neap and spring tide with values of 35 in the Bunbury Port (OUTER1) (Figure 6.74, left). In winter, the vertical salinity variation was about 1 at spring and slightly higher at neap (Figure 6.74, left). During the peak river flow event however, the surface salinity was 22 at spring tide and 26 at neap tide, and the bottom salinity was about 35 in both cases (Figure 6.74, left). This indicates that the Bunbury Port is influenced by the freshwater output of the Leschenault Estuary during extreme river flow events.

Salinity - The 'Cut'

Figure 6.74 (right) shows the vertical salinity distributions at the 'Cut' (ESTUARY1). In summer, the salinity values were nearly homogeneous, indicating well-mixed flows (Figure 6.74, right). In winter, the water column at the 'Cut' (ESTUARY1) was vertically mixed at spring tide and weakly stratified at neap tide ($S_{surf} = 27$ and $S_{bed} = 34$) (Figure 6.74, right). During the peak river flow event, a sharp halocline developed at the 'Cut' (OUTER1) ((Figure 6.74, right)), with salinities ranging between 10-25 at spring tide and 27-32 at neap tide.

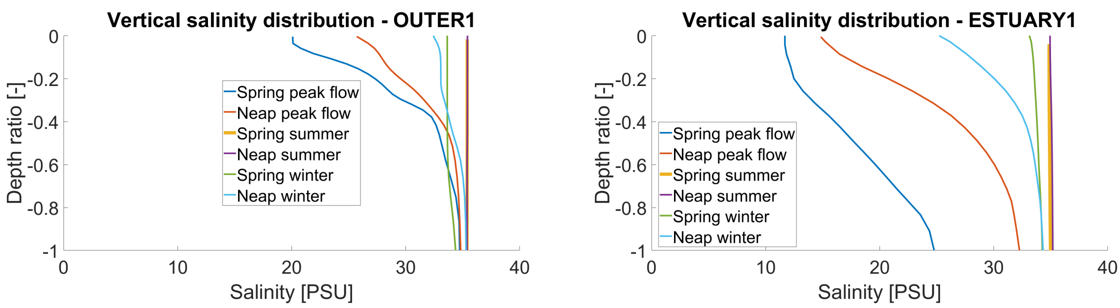

Figure 6.74: The vertical salinity distribution at OUTER1 (left) and the vertical salinity distribution at ESTUARY1 (right)

Salinity - Central Basin

Figure 6.75 (left) shows the vertical salinity distributions at the central basin (ESTUARY3). Partially to well-mixed conditions occurred in the central basin (ESTUARY3) (Figure 6.75, left). In winter and summer, the central basin waters were well-mixed and during the peak river flow event, the waters became weakly stratified (Figure 6.75, left). The central basin (ESTUARY3) waters were strongly affected by the freshwater discharge during the peak river flow event, and strongly affected by tides under typical winter and summer conditions.

Salinity - Northern Basin

Figure 6.75 (right) shows the vertical salinity distributions at the northern basin (ESTUARY4). Well-mixed salinities occurred for all tidal cycles (Figure 6.75, right), indicating the negligible effect of the southern freshwater discharge on the salinity stratification. The influence of tidal stirring became more important at the central (ESTUARY3) and northern basin (ESTUARY4). In the northern basin (ESTUARY4), estuarine waters became hypersaline (> 35 PSU) in summer. In winter, the northern basin waters were very weakly stratified in winter, indicating a high Parkfield Drain discharge (Figure 6.75, right).

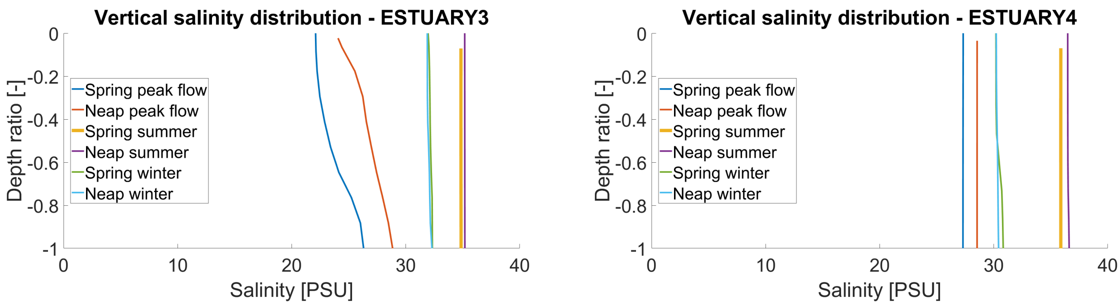

Figure 6.75: The vertical salinity distribution at ESTUARY3 (left) and the vertical salinity distribution at ESTUARY4 (right)

Salinity - Southern Basin

Figure 6.76 (left) shows the vertical salinity profiles of the southern basin (ESTUARY2). The southern basin waters (ESTUARY2) were strongly affected by the freshwater discharge under winter and peak river flow conditions, as the salinities were low and the vertical variations were high (Figure 6.76, left). During the peak river flow event, salinities ranged between 0-10 at spring tide and 4-26 at neap tide (Figure 6.76, left). In winter, the salinity stratification was also significant with values ranging between 22-31 at neap tide and between 30-32 at spring tide (Figure 6.76, left). In summer, the water in the southern basin (ESTUARY2) was well-mixed (Figure 6.76, left).

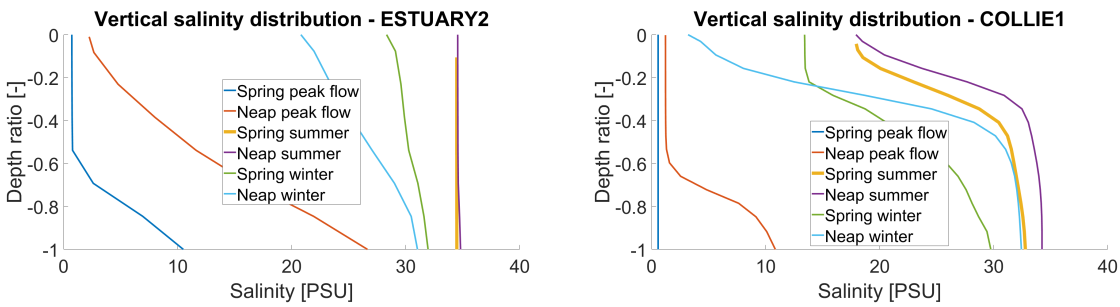

Figure 6.76: The vertical salinity distribution at ESTUARY2 (left) and the vertical salinity distribution at COLLIE1 (right)

Salinity - Collie River

Figure 6.76 (right) shows the vertical salinity profiles of the Collie River (COLLIE1). Fierce stratification was observed throughout the year, with highest stratification under normal winter conditions (Figure 6.76, right). In winter at neap, the highest salinities occurred along the river bed of the Collie River (≈33) and the lowest salinities were observed at the surface (≈5). During the peak flow event, the halocline was forced out of the river, generating well-mixed, fresh conditions along the water column of the Collie River (COLLIE1). Note, that the peak flow event occurred during the spring.

Current velocity - Bunbury Port

Figure 6.77 shows the u- and v-components of the current velocities obtained at Bunbury Port (OUTER1). In summer, the surface current velocities had values of -0.06 m/s in u-direction and values of 0.05-0.06 m/s in v-direction (Figure 6.77). Current velocities at the bed were reversed, with values of 0.02 m/s in u-direction and -0.02 m/s in v-direction (Figure 6.77). The flow was therefore, bidirectional under normal summer conditions, with a surface current directed to the north-west, coincident with the wind direction in summer (Figure 6.77). This resulted in a countercurrent near the bed (Figure 6.77). In winter, the averaged wind velocities were lower and winds were coming from the north-west. This caused a reversed flow direction at Bunbury Port (OUTER1) in winter, with lower values (u_{bed} = -0.005 m/s and u_{surf} = 0.02 m/s). During the peak river flow event, the Bunbury Port (OUTER1) was also affected by the freshwater discharge from the Leschenault Estuary, generating a flow in opposite direction to the wind below the surface and a flow in the direction coincident with the wind in the lower half of the water column (Figure 6.77).

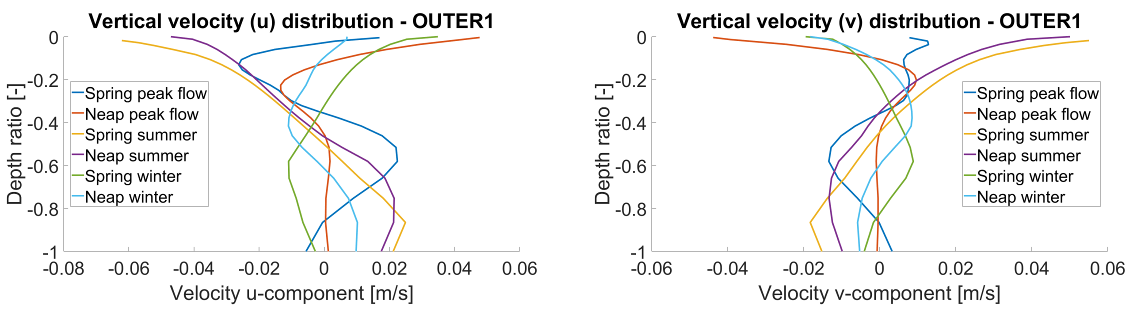

Figure 6.77: The vertical velocity u-component distribution (left) (+ = east; - = west) and vertical velocity v-component (right) (+ = north; - = south) at OUTER1

Current velocity - The 'Cut'

Figure 6.78 shows the u- and v-components of the current velocities of the 'Cut' (ESTUARY1). Negative u-components and slightly positive y-components indicate outflow. In Figure 6.78 (left), the surface currents are westward (leaving the estuary) during the peak river flow event and in winter, and eastward (entering the estuary) during summer. Currents in the main body have opposite directions for these tidal cycles (Figure 6.78, left). These current directions over depth, suggest that a classical estuarine circulation would occur in summer and a inverse circulation in winter and during peak river flow. However, this is exactly the opposite of what should be expected. A classical estuarine circulation represents an inflowing bottom ocean layer and an out-flowing surface freshwater layer and an inverse circulation represents an inflowing surface ocean layer and an out-flowing bottom hypersaline estuary layer. The prevailing winds in summer (south-westerly) and winter (north-easterly), provide an explanation for the observed vertical current profiles at the 'Cut' (COLLIE1). It is likely that the surface currents at the 'Cut' (ESTUARY1) are strongly influenced by the winds, generating residual currents underneath the surface layer (Figure 6.78, left). The v-components of the current velocities (Figure 6.78, right) are northward for all spring tidal cycles and northward for the upper layer for the neap summer tidal cycle. For neap peak flow and neap winter tidal cycles the upper layer is directed to the south. It can be concluded that the flow at the 'Cut' (ESTUARY1) becomes more stratified under winter and flood conditions and under summer conditions the water becomes more mixed (Figure 6.78).

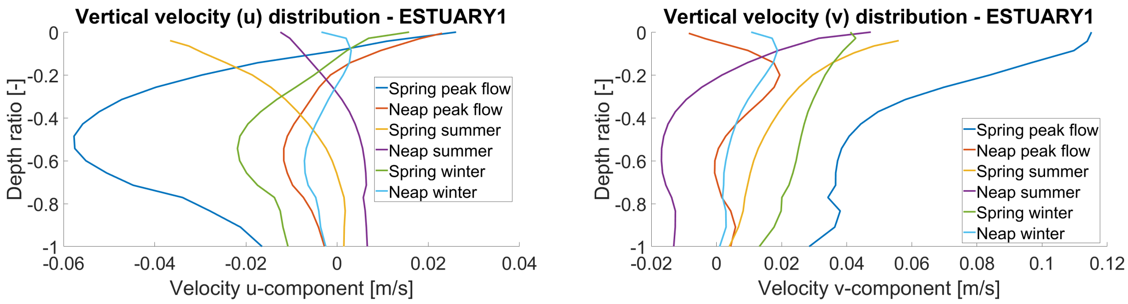

Figure 6.78: The vertical velocity u-component distribution (left) (+ = east; - = west) and vertical velocity v-component (right) (+ = north; - = south) at ESTUARY1

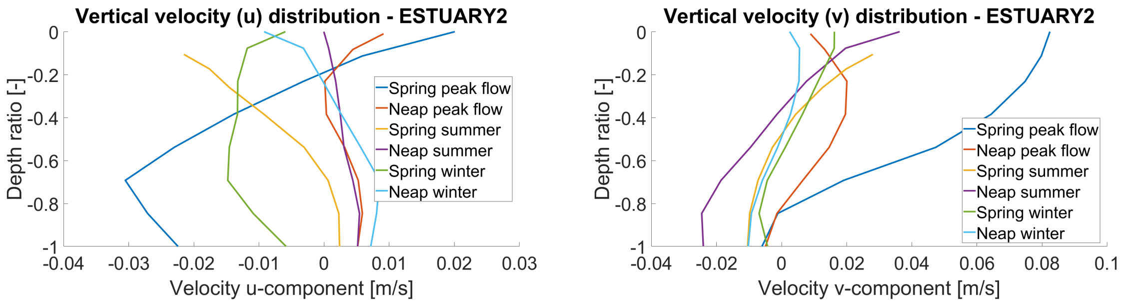

Figure 6.79: The vertical velocity u-component distribution (left) (+ = east; - = west) and vertical velocity v-component (right) (+ = north; - = south) at ESTUARY2

Current velocity - Southern Basin

Figure 6.79 shows the current velocities in u- and v-direction at the southern basin (ESTUARY2) along the water column. The southern basin waters are suffering the influence of many different processes, resulting in highly variable (east-west) current velocities. In summer, the u-velocity at spring tide varied from -0.02 m/s near the surface to 0.04 m/s near the bed and the v-velocity varied from -0.01 near the bed to 0.03 m/s near the surface (Figure 6.79). During neap tide, a similar trend was observed but with a unidirectional u-velocity and a bidirectional v-velocity (Figure 6.79). In winter, the neap and spring tide situation showed different current regimes in u-direction, with a unidirectional flow of about 0.01 m/s towards the west at spring tide and a slightly bidirectional flow of -0.005 m/s at the surface and 0.01 at the bed during neap tide (Figure 6.79). This indicates a lower vertical current stratification during spring than neap. Under extreme river discharge conditions, the flow became bidirectional indicating a two layer structure.

Current velocity - Collie River

Figure 6.80 shows the u- and v-components at the Collie River (COLLIE1). The Collie River (COLLIE1) lies approximately in the east-west direction, with the u-component representing the main flow along the river. The vertical current structure was typical shape for a stratified river with salt-wedge intrusion. The surface flow velocity is directed to the west (downriver) and the bed flow was directed to the east (upriver) (Figure 6.80). This is an indication of saline ocean water that flows upriver underneath the out-flowing freshwater. The same pattern was observed for winter and summer conditions but changed to a unidirectional shape under extreme discharge conditions. In this case the salt wedge was pushed out of the river, generating uniform conditions in the Collie River (COLLIE1) (Figure 6.80).

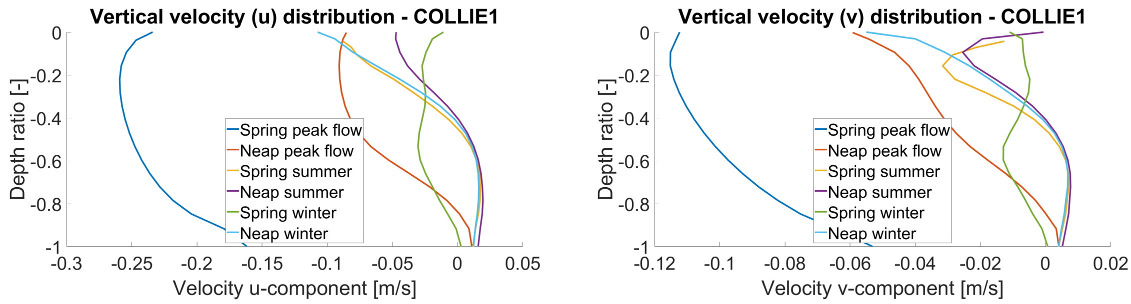

Figure 6.80: The vertical velocity u-component distribution (left) (+ = east; - = west) and vertical velocity v-component (right) (+ = north; - = south) at COLLIE1

Current velocity - Central Basin

Figure 6.81 shows the u- and v-components of the current velocity along the water columns at the central basin (ESTUARY3), with longitudinal flow along the v-direction. Central basin waters (ESTUARY3) showed both the classical stratified circulation and the inverse circulation. The former was evident during the winter neap, winter spring and neap peak flow for the v-component (Figure 6.81, right). Here, a slight southerly current is observed near the surface and a modest northward current near the bed. The salinity stratification is weak for the the central basin in summer and winter (Figure 6.75), which could indicate that the seasonal wind direction are the dominant driver of the surface currents. A reversed circulation was observed in summer, with northward flow velocities near the surface layer and southward direct flow velocities near the bed layer (Figure 6.75). This pattern could be related to the hypersaline waters in summer in the north of the estuary, which sank below the northward flowing ocean waters and flowed out of the estuary near the bed. However, the salinity stratification was very weak, which could argue of this was its driving force. In summer, southerly winds prevailed, which could be the reason for the northward surface currents. The longitudinal salinity gradient could be the driving force of the southward bottom currents. The only exception occurred during spring tide under extreme river flow conditions, when the water body at the central basin (ESTUARY3) was affected by the fresh waters from the south. The freshwater floated on top of the more saline estuary water towards the north and generated a countercurrent in the lower layers (Figure 6.75).

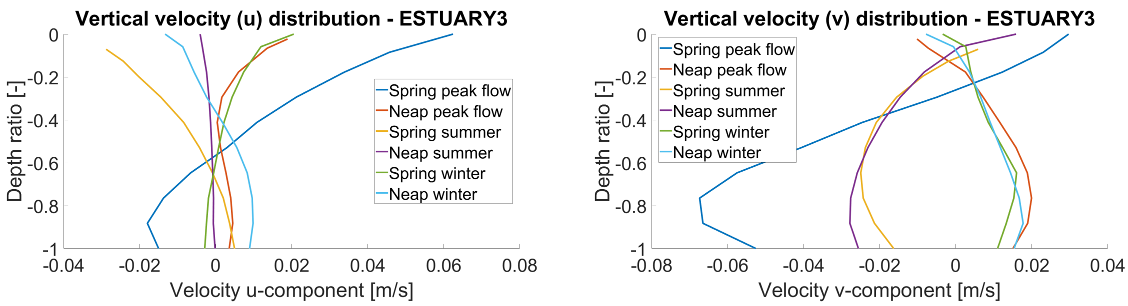

Figure 6.81: The vertical velocity u-component distribution (left) (+ = east; - = west) and vertical velocity v-component (right) (+ = north; - = south) at ESTUARY3

Current velocity - Northern Basin

Figure 6.82 shows the flow velocities over the normalized depths at the northern basin (ESTUARY4), with longitudinal flows along v-direction. Similar circulation patterns were observed for the northern basin (ESTUARY4) and for the central basin (ESTUARY3) (Figures 6.81 and 6.82). In winter, a classical estuarine circulation was observed with southward directed surface velocities and northward directed bed velocities. In summer, an inverse circulation occurred. Conversely to the central basin (ESTUARY3), the flow during the extreme discharge event during spring was unidirectional and southward directed (Figure 6.82). This could be due to smaller influence of the freshwater discharge in the northern portion of the estuary.

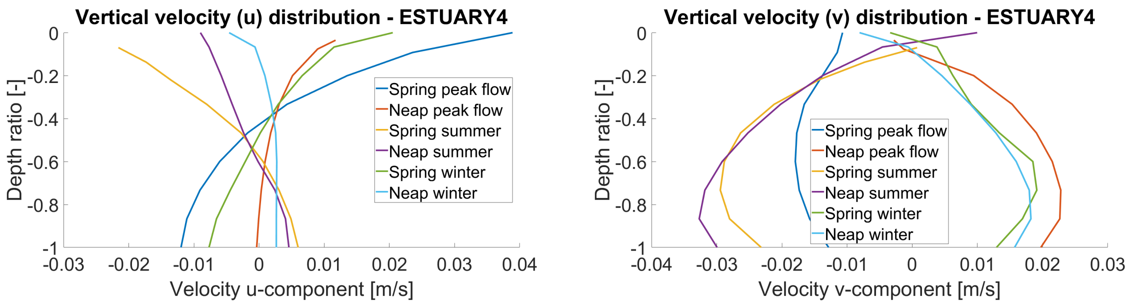

Figure 6.82: The vertical velocity u-component distribution (left) (+ = east; - = west) and vertical velocity v-component (right) (+ = north; - = south) at ESTUARY4

6.5.4 Circulation and stratification parameter

The stratification-circulation diagram proposed by Hansen and Rattray Jr (1966) (see Section 2.2.5) was used to classify the Leschenault Estuary under different conditions, considering both the u- and v-components. The Leschenault Estuary has many different orientations. Therefore, the stratification-circulation diagram is based on both u- and v-components and the circulation parameter p_c is calculated for both u- and v-direction.

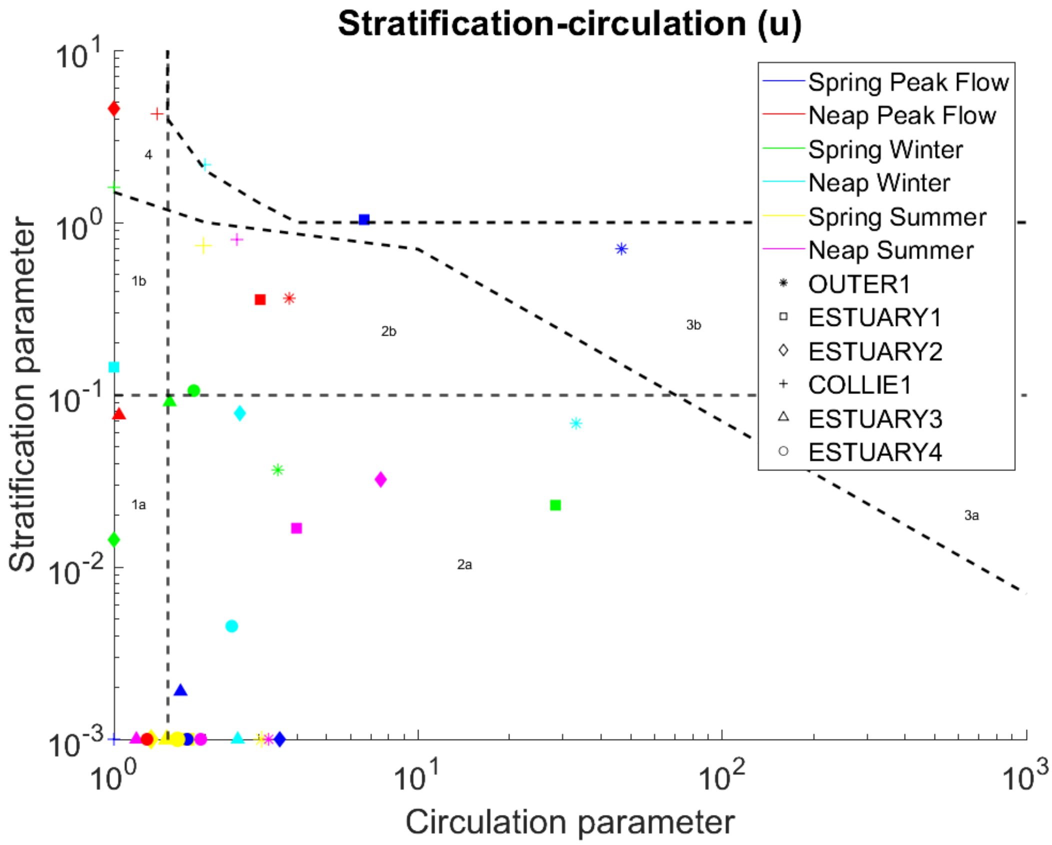

Figure 6.83: Circulation-stratification diagram for the x-component of the current velocity

Bunbury Port

Water at the Bunbury Port (OUTER1) is indicated by an asterisk in Figures 6.83 and 6.84. A general distinction can be made between the estuary class at Bunbury Port (OUTER1) under normal winter and summer conditions and under extreme discharge conditions. Under normal summer conditions, the very low stratification parameters ($p_e < 10^{-3}$) and modest circulation parameters ($p_c = 3 \cdot 10^0$), indicated a Type 2a estuary with partially-mixed flow and low stratification. Under normal winter conditions, a similar classification was obtained with a p_e between $3 \cdot 10^{-2}$ and $7 \cdot 10^{-2}$ and a p_c between $3 \cdot 10^0$. However, under extreme discharge conditions, the water body at OUTER1 was classified as Type 2B, due to the increased stratification induced by the freshwater discharged into the Leschenault Estuary. Moreover, at spring tide the water body starts behaved like a fjord estuary of Type 3b. This could be due to the stagnant saline bed layer in the Bunbury Port (OUTER1) that was relatively unaffected at first by the intruding freshwater in the upper layers. The water body at BUnbury Port (OUTER1) was classified as a Type 2a estuary most of the year and became a Type 2b/3b estuary under the extreme peak flow event. The dominant processes at the Bunbury Port (OUTER1) for the upstream salt transport were advection and diffusion most of the analysed year and the current direction reversed over the vertical (Figure 6.77). Under peak river flow conditions, advection dominated the salt transport, with a contribution of over 99% (Hansen and Rattray Jr, 1966).

The 'Cut'

Waters at the 'Cut' (ESTUARY1) are indicated by squares and classified as Type 2a/2b depending on the conditions (Figures 6.83 and 6.84). For peak river flow conditions, a much higher stratification parameter was obtained with values between 0.4 and 1 and circulation parameters varied between 3 and 10 (Figure 6.83). Under peak river flow conditions, the water body at the 'Cut' (ESTUARY1) behaves as a Type 2b estuary (Figure 6.83). The same estuary type was applicable at neap tide in winter (Figure 6.83). Less pronounced stratification was observed both for winter and summer springs, resulting in a Type 2a classification (Figure 6.83). Under extreme flow conditions, the stratification intensified and the water body acted as a salt wedge (Type 4), with a thin layer of freshwater flowing on top of deeper saline waters (Figure 6.83). This particularly happened in the Koombana Bay under extreme flow conditions. Nevertheless, waters at the 'Cut' (ESTUARY1) behaved most of the time as Type 2a/2b, with partially-mixed flow and low to high stratification depending on the season (Figure 6.83).

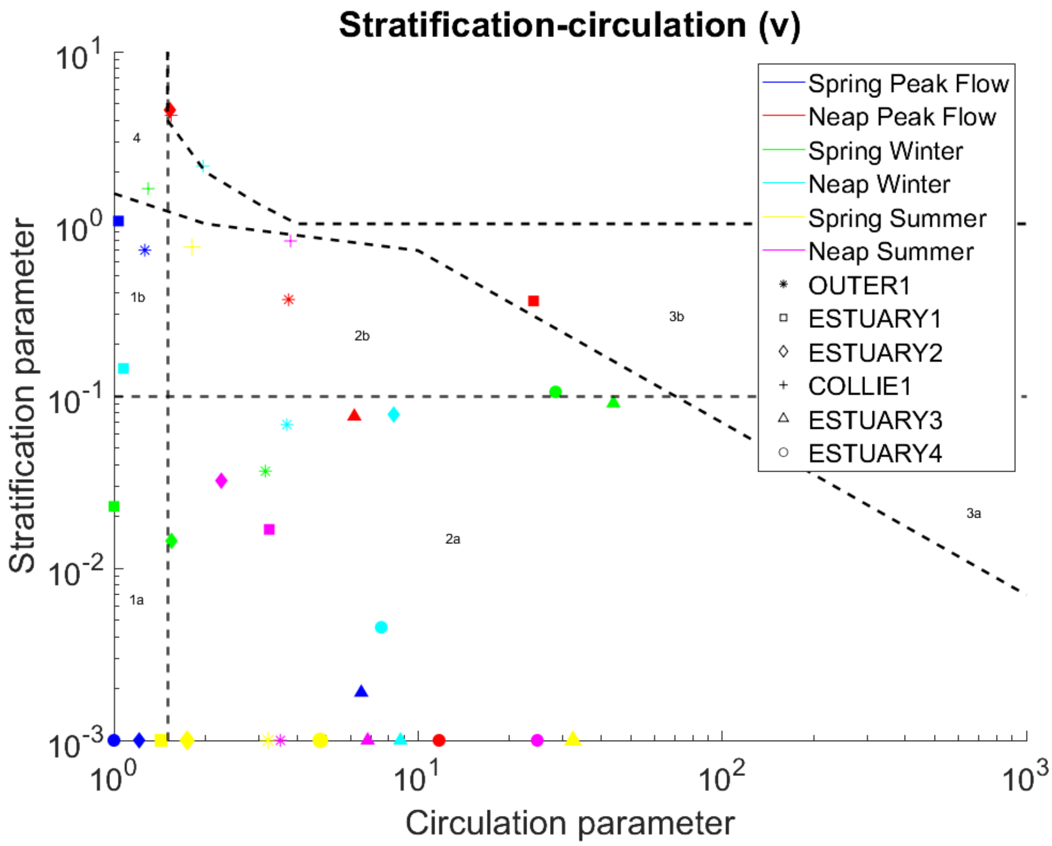

Figure 6.84: Circulation-stratification diagram for the y-component of the current velocity

Southern Basin

Waters in the southern basin (ESTUARY2) are indicated by diamonds and were the most dynamic in the Leschenault Estuary (Figures 6.83 and 6.84). For neap tide during the peak river flow event, the circulation parameter was small ($< 10^1$ for u and around 1.5 for v) and the stratification was above 1 (Figures 6.83 and 6.84). This indicated a Type 4 (salt-wedge) estuary. Under the same peak river flow conditions at spring tide, the water body was well-mixed, indicating a Type 1a estuary (Figures 6.83 and 6.84). The water body in the southern basin (ESTUARY2) in winter and summer were classified as Type 2a (Figures 6.83 and 6.84), with a partially-mixed flow and low stratification. The southern basin was dynamical, and the estuary classification varied between Types 1a, 2a and 4.

Collie River

Collie River waters (COLLIE1) are indicated by plus-symbols and had a consistent estuary classification of Type 2b/4 under normal winter and summer conditions (Figures 6.83 and 6.84). The stratification parameter was around 1 or higher, which lies on the transition between Type 2b and Type 4 (Figures 6.83 and 6.84). The Collie River (COLLIE1) also had a salt-wedge behaviour, with saline ocean water penetrating the Collie River near the bed and freshwater flowing out on top. The flow velocities were reversed over depth and the stratification was high. Type 4 was also applicable at neap tide under extreme discharge conditions (Figures 6.83 and 6.84). At spring tide under peak river flow conditions however, the halocline was displaced outside of the river mouth, generating a well-mixed water body. In this situation, the estuary had a Type 1a classification (Figures 6.83 and 6.84).

Central & Northern Basin

Central basin waters (ESTUARY3) and northern basin waters (ESTUARY4) are indicated by triangles and circles, respectively, and the currents flow mainly along the v-direction, i.e. the longitudinal flow prevails. Central basin waters (ESTUARY3) and northern basin waters (ESTUARY4) were classified as Type 2a for most of the time (Figure 6.84) and were partially-mixed with relatively low stratification. However, one exception occurred at the northern basin (ESTUARY4) at spring tide under peak flow conditions, as the circulation parameter fell below the transition zone of 1 to 2, resulting in negligible stratification (Figure 6.84). The water body at peak flow spring in the northern basin (ESTUARY4) was classified as Type 1a, indicating well-mixed conditions (Figure 6.84).

6.6 Salt transport

According to Dyer (1974), the salinity distribution in an estuary is an equilibrium between advection and diffusion. The amount of salt in an estuary therefore represents the level of mixing between fresh and marine waters (Miranda and Castro Filho, 1996). The salt flux and transport can be used to determine the driving forces of the transport of other substances (Miranda and Castro Filho, 1996). The salt transport was decomposed, explained in Section 2.1.1, to determine the physical processes of the salt transport between the Leschenault Estuary and the ocean. The salt flux components were calculated by using the equations from Table 2.1. The input for these equations was retrieved from cross-sections at the ‘Cut’ and the central basin (cross-sectional slice at ESTUARY3) by using the map-files of DFM. To filter the tidal and sub-tidal effects, time-averaged periods were considered that are significantly long (Hunkins, 1981). Therefore, the time-averaged periods are taken over the whole winter (1-June-2011 to 31-August-2011), summer (1-December-2011 to 29-February-2011) and year (1-June-2011 to 1-April-2012). The salt flux represent laterally and depth-averaged values, with the u-direction (east (+) and west (-)) as the governing flow direction at the 'Cut' and the v-direction (north (+) and south (-)) as the governing flow direction at the central basin. The salt components are summarized in Tables 6.3 and 6.4. The directions of the components are reasonably aligned, which could indicate that the time-averaged salt fluxes are reliable.

6.6.1 The 'Cut'

Winter

The dominant parcel of the salt transport in winter was the non-tidal advective component A (freshwater discharge), with a value of -4.77 kg/s (Table 6.3), indicating a salt flux directed out of the estuary. This was due to the high freshwater discharge flowing into the Leschenault Estuary in winter. The advective Stokes wave transport (component B) was directed landward, indicating a diffusive process due to a progressive tidal wave (De Miranda et al., 2017), and had a value of 0.606 kg/s (Table 6.3). The sum of component A and B was negative, which means they decrease the salinity values in the estuary and sharpen the salinity gradient between the ocean and the estuary. Component C (topographic trapping) was the second most important salt flux component with a value of 3.54 kg/s (Table 6.3). It is suggested that this was due to the phase lag of the tidally-driven salinity S_t compared to the tidally driven flow velocity u_t of less than 90° (De Miranda et al., 2017). Water became entrapped inside the estuary and was released out of the estuary at a later stage than the tide. The longitudinal salinity gradient induced by this process, generated a dispersive transport of salt into the estuary (De Miranda et al., 2017). The negative sign and low value of component D (gravitational circulation; -0.066 kg/s) (Table 6.3), could mean that the 'Cut' was less stratified than expected. It is therefore suggested that component D would be higher along transects nearby river mouths, as the salt transport generated by gravitational circulation is mostly high for partially-mixed and stratified estuaries, where the increased discharge drives a bottom current up the estuary carrying salt (De Miranda et al., 2017). Salt transport due to bathymetric tidal pumping (component E), was of the same order of magnitude as the Stokes drift in winter and was directed landward (Table 6.3). According to Hunkins (1981), these effects are not seasonally varying and maintain their direction and order of magnitude through the year (De Miranda et al., 2017). In the Leschenault Estuary they are of minor importance. The components of least importance are F and G, which was possibly due to the small amplitude of the tidal wave (Table 6.3). The total salt transport in winter was directed seaward indicating a loss of salt out of the estuary in winter, decreasing the estuarine salinities. There was an agreement within 43% between the total salt flux calculated by Equation 2.12 and the total salt flux calculated by summing up components A to G, which could indicate other factors had significant influence on the salt flux at the 'Cut' in winter (De Miranda et al., 2017).

Summer

The dominant parcel of the salt transport in summer was component B (Stokes drift) with a value of -1.1 kg/s (Table 6.3), indicating an advective salt flux directed out of the estuary (De Miranda et al., 2017). This salt flux generated by the Stokes drift has an opposite direction to its propagation and is known as the Stokes drift phenomenon (De Miranda et al., 2017). Due to the arid climate in summer the influence of component A (freshwater discharge) was less significant and the direction was seaward (pushing salt out of the estuary) (Table 6.3). Component A is the second most important factor in the salt transport in summer. The third most important was component C (topographic trapping), with a value of around 0.26 kg/s and was directed landward (Table 6.3). The influence of the gravitational circulation in summer was two orders of magnitude smaller than in winter and negative, indicating a well-mixed estuary with salt pushed out of the estuary by the gravitational circulation. Component E, F and G are all one order of magnitude smaller than in winter (Table 6.3). The total salt transport in summer was negative and three times higher than the winter average. This could be explained by the hypersaline character of the estuary that increased the salt content in the estuary. This abundance of salt in the estuary could then possibly flow out of the estuary mainly due to increased flow near surface and the Stokes drift. There was an agreement within 1% between the total salt flux calculated by Equation 2.12 and the total salt flux calculated by summing up components A to G, confirming that the various terms omitted were of negligible effect in summer (De Miranda et al., 2017).

Component	Physical process	Winter	Summer	Full period
A	Freshwater discharge	-4.77	$-3.02 \cdot 10^{-1}$	-2.30
B	Stokes drift/progressive tidal wave	$6.06 \cdot 10^{-1}$	-1.10	-1.17
C	Topographic trapping	3.54	$2.60 \cdot 10^{-1}$	1.85
D	Gravitational circulation	$-6.60 \cdot 10^{-2}$	$-1.00 \cdot 10^{-3}$	$-2.07 \cdot 10^{-2}$
E	Bathymetric tidal pumping	$3.59 \cdot 10^{-1}$	$1.37 \cdot 10^{-2}$	$1.57 \cdot 10^{-1}$
F	Tidal shear	$1.38 \cdot 10^{-2}$	$3.60 \cdot 10^{-3}$	$7.60 \cdot 10^{-3}$
G	Wind fluctuations	$1.70 \cdot 10^{-3}$	$6.60 \cdot 10^{-5}$	$9.51 \cdot 10^{-4}$
Total	Eq. 2.26	$-3.17 \cdot 10^{-1}$	-1.12	-1.48
Total	Eq. 2.12	$-5.50 \cdot 10^{-1}$	-1.13	-1.54

Table 6.3: Salt flux components in kg/s at transect the ‘Cut’ in winter [1 Jun 2011 - 1 Sep 2011], summer [1 Dec 2011 - 1 Mar 2012] and the whole year [1 Jun 2011 - 1 Apr 2012]

Whole year

Component A (freshwater discharge) was dominant over the year (-2.30 kg/s), followed by component C (topographic trapping; 2.85 kg/s) and B (Stokes drift; -1.17 kg/s). The Leschenault Estuary can therefore be classified as a freshwater dominated estuary, with a significant influence of a counteracting dispersive salt flux induced by topographic trapping and a supporting advective seaward salt transport driven by Stokes drift (De Miranda et al., 2017). Component D (gravitational circulation) was less of importance, which indicated the well-mixed character of the ‘Cut’. Bathymetric tidal pumping (component E) came in fourth place being also significant. Components F and G were negligibly small.

The total salt flux was negative, caused by the incomplete 10-month period that was considered. For a 12-month period the total salt flux would have been 0 (Hunkins, 1981). There was an agreement within 6% between the total salt flux calculated by Equation 2.12 and the total salt flux calculated by summing up components A to G, confirming that the various terms omitted were of negligible effect for the full 10-month period (De Miranda et al., 2017).

6.6.2 Central Basin

Winter

At the central basin, the dominant physical process influencing the salt flux in winter was the northward Stokes drift (component B), with an opposite direction to the prevailing northerly winds in winter (0.0614 kg/s; Table 6.4). The freshwater discharge (component A) was the second most important physical process, generated by the southern rivers (0.0319 kg/s; Table 6.4). The freshwater discharge and the Stokes drift both transported salt towards the north. Third was the influence by bathymetric tidal pumping (component E), followed by topographic trapping (C) and tidal shear (component F), which were all an order of magnitude lower than th freshwater discharge and Stokes drift (Table 6.4). Gravitational circulation (component D) and wind fluctuations had a minor role in the salt flux dynamics in winter.

Component	Physical process	Winter	Summer	Full period
A	Freshwater discharge	$3.19 \cdot 10^{-2}$	$1.14 \cdot 10^{-1}$	$6.98 \cdot 10^{-2}$
B	Stokes drift/progressive tidal wave	$6.14 \cdot 10^{-2}$	$-1.50 \cdot 10^{-1}$	$-1.28 \cdot 10^{-1}$
C	Topographic trapping	$-4.10 \cdot 10^{-3}$	$-2.50 \cdot 10^{-3}$	$1.40 \cdot 10^{-3}$
D	Gravitational circulation	$8.67 \cdot 10^{-4}$	$-2.76 \cdot 10^{-5}$	$-2.84 \cdot 10^{-4}$
E	Bathymetric tidal pumping	$-6.40 \cdot 10^{-3}$	$-4.64 \cdot 10^{-4}$	$-8.43 \cdot 10^{-4}$
F	Tidal shear	$-2.10 \cdot 10^{-3}$	$3.67 \cdot 10^{-4}$	$-1.10 \cdot 10^{-3}$
G	Wind fluctuations	$2.70 \cdot 10^{-4}$	$-3.68 \cdot 10^{-4}$	$2.94 \cdot 10^{-4}$
Total	Eq. 2.26	$8.19 \cdot 10^{-2}$	$-3.89 \cdot 10^{-2}$	$-5.87 \cdot 10^{-2}$
Total	Eq. 2.12	$8.74 \cdot 10^{-1}$	$-3.87 \cdot 10^{-2}$	$-5.77 \cdot 10^{-2}$

Table 6.4: Salt flux components in kg/s at transect Central Basin in winter [1 Jun 2011 - 1 Sep 2011], summer [1 Dec 2011 - 1 Mar 2012] and the whole year [1 Jun 2011 - 1 Apr 2012] (north (+); south(−))

Summer

In summer, the physical process governing the salt flux at the central basin also was the Stokes drift (component B) (-0.15 kg/s; Table 6.4). However, the Stokes wave transport was southward in summer, opposite to the prevailing southerly winds in summer. The freshwater discharge (component A) was the second most important physical process, generated by the southern rivers (0.114 kg/s; Table 6.4). The freshwater discharge and the Stokes drift had counteracting directions. Third was the influence topographic trapping (C), being two orders of magnitude lower than the two most dominant processes (Table 6.4). Components D, F and G had a minor role in the salt flux dynamics.

Whole year

During the whole year, the southward Stokes drift transport was the main salt component of the salt flux (-0.128 kg/s; Table 6.4). This is in line with the summer and winter period. The second and third most important salt flux were the freshwater discharge (0.0698 kg/s) and topographic trapping (0.0014 kg/s) respectively (Table 6.4), also in line with summer and winter. The other component were negligibly small. It could thus be suggested that the salt dynamics in the central basin were less prone to seasonal variations, with the Stokes drift, being the most important physical driver.

7

Scenario: Preston River alignment

The case study of the Preston River alignment was added to this thesis to evaluate the methodology proposed in this thesis and to give management of the Leschenault Estuary information related to hydrodynamical changes due to the Preston River alignment. Similar methodologies can be used to investigate other estuaries.

7.1 Model set-up

The same model set-up was applied to the Preston River alignment scenario (as is summarized in Chapter 4). However, due to the Preston River alignment, a new model grid was generated. Figure 7.1 (left) shows the initial design of the Preston River alignment proposed by the Bunbury Port Authority in Bunbury Port Authority (2013). However, as can be seen in Figure 7.1 (left), the river mouth was only shifted by approximately 600 m. Several tests have been performed in the calibration phase considering different positions of the river mouth, which had similar outcomes. The resolution of the grid around the mouth is in the order of hundred meters, which means the new river mouth is only located 6 grid cells to the right. This minor alteration of the grid would likely not change the outcomes, and therefore could not be used to validate the methodology. An additional alignment has been proposed and designed, shown in Figure 7.1 (right). A gradual descent of the bed level from the river bed towards the Bunbury Port was applied.

7.2 Water property anomalies

Modelled temperature, salinity, water level and flow velocity results of the Preston River alignment were used to evaluate the changes in the water properties induced by the alignment. The temporal changes at the different stations are presented as well as the time-averaged values, to visualise the horizontal and vertical changes spatially.

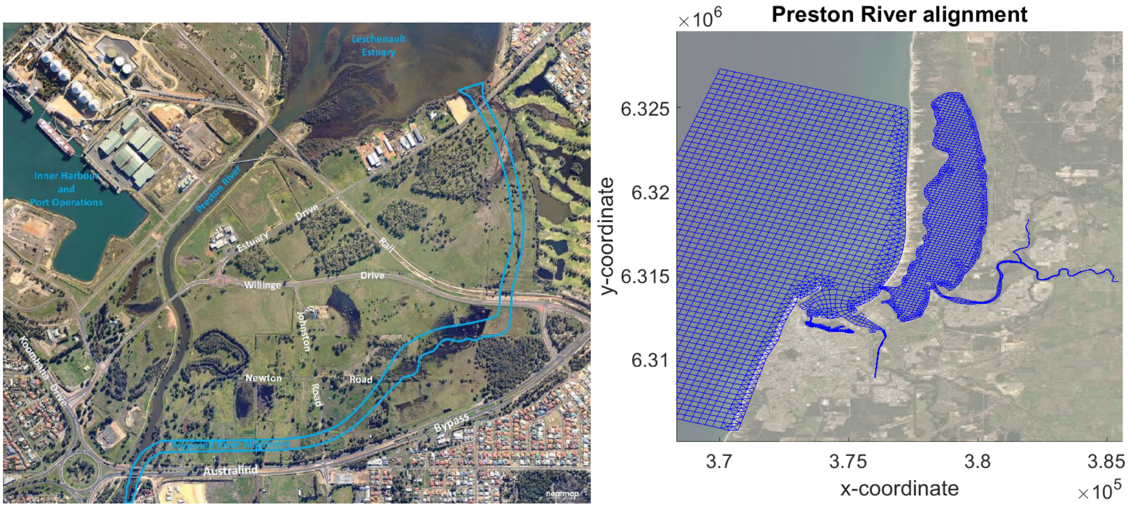

Figure 7.1: Initial design of the Preston River alignment (Bunbury Port Authority, 2013) (left) and model grid of the Preston River alignment in D-Flow FM (right)

7.2.1 Local anomalies

The same observation stations were adopted in this Chapter as in Chapter 6, namely OUTER1, ESTUARY1, ESTUARY2, COLLIE1, ESTUARY3 and ESTUARY4. The median anomalies of temperature, salinity, water level and flow velocity are summarised in Table 7.1, 7.2 and 7.3, which contain annual, winter and summer averages, respectively. The term anomaly means a departure from a reference value or long-term average, i.e. a positive temperature anomaly indicates that the observed temperature was warmer than the reference value, while a negative anomaly indicates that the observed temperature was cooler than the reference value. The anomalies were calculated by extracting the data of the initial model from the modelled data of the Preston River alignment model. The annual average of the temperature anomaly in the estuary was small, varying between -0.16 $°C$ and 0.20 $°C$. Averaged water level and flow velocity values were also small. However, the full period averaged salinity anomaly was considerable at Bunbury Port (OUTER1) and the southern basin (ESTUARY2), ranging between -2.53 PSU to 3.08 PSU. The highest salinity anomalies were obtained in winter, with varying anomalies between -4.51 PSU and 5.55 PSU. Furthermore, the temporal anomalies were applied to assess the short-term changes in temperature and salinity. The temporal water level and flow velocity anomalies are less significant and are therefore added to Appendix F.1.

	OUT1	EST1	EST2	COL1	EST3	EST4
Temperature [$°C$]	-0.16	0.07	0.20	-0.15	0.02	0.0003
Salinity [PSU]	-2.53	1.06	3.08	0.14	0.88	0.91
water level [m]	0.004	-0.002	-0.003	-0.001	-0.002	-0.002
Vel-mag [m/s]	0.005	0.001	-0.003	0.0007	-0.0005	0.0001

Table 7.1: Median values of full period anomalies of Preston River alignment scenario

	OUT1	EST1	EST2	COL1	EST3	EST4
Temperature [$°C$]	-0.13	0.15	0.4	0.08	0.04	-0.002
Salinity [PSU]	-4.51	1.94	5.55	0.28	1.22	0.76
water level [m]	0.008	-0.004	-0.005	-0.002	-0.003	-0.003
Vel-mag [m/s]	0.003	0.003	-0.002	0.001	-0.001	-0.00003

Table 7.2: Median values of winter anomalies of Preston River alignment scenario

	OUT1	EST1	EST2	COL1	EST3	EST4
Temperature [$°C$]	-0.17	0.01	0.01	-0.27	0.006	0.001
Salinity [PSU]	-0.26	0.09	0.20	-0.11	0.20	0.34
water level [m]	0.0005	-0.0003	-0.0003	-0.0002	-0.0003	-0.0004
Vel-mag [m/s]	0.006	-0.0002	-0.001	0.0003	-0.00001	0.0002

Table 7.3: Median values of summer anomalies of Preston River alignment scenario

Temperature

As can be observed in Figure 7.2 and 7.3, the Preston river alignment scenario presented much higher water temperature fluctuations than the initial conditions. Temperatures showed higher temporal variability, what could result in complications for the ecology. The higher fluctuations could be caused by the lower freshwater input, which have decreased the circulation and turbulent mixing in the estuary. The water body was therefore more influenced by atmospheric forcing, which caused the increased fluctuation. Another hypothesis is the increased influence of tidal stirring in the estuary, which could explain the diurnal fluctuations. Temperature anomalies had the same order of magnitude for all observation points and varied between -2 $°C$ and 2 $°C$.

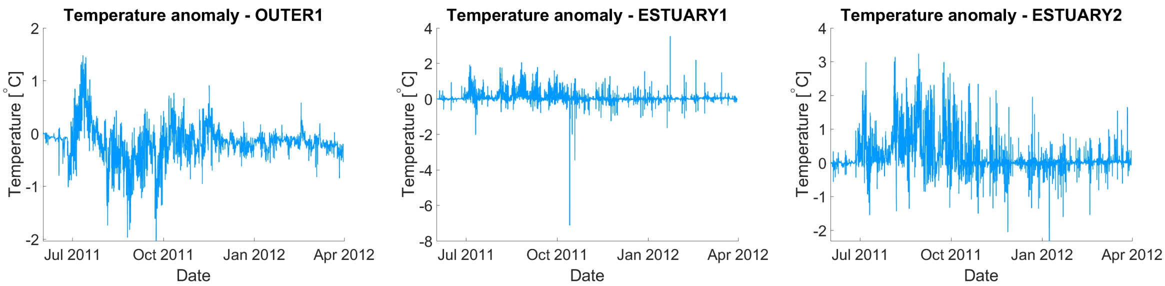

Figure 7.2: Temperature anomaly at observation point OUTER1 (left), ESTUARY1 (centre) and ESTUARY2 (right)

Salinity

Temporal salinity anomalies were even more accentuated than temperature anomalies, and reached values of up to 25 at the southern basin (ESTUARY2) (Figure 7.4, right). A clear distinction can be made between the winter and summer seasons. In winter, the anomaly had values around 25 and in summer the anomalies were small (oscillating around 0). In

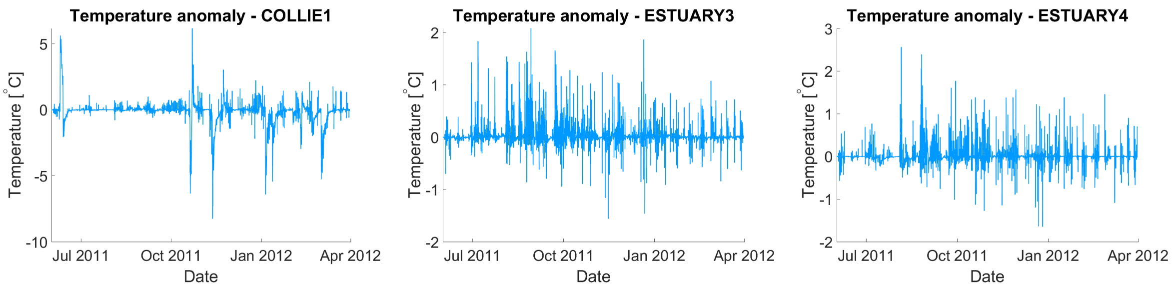

Figure 7.3: Temperature anomaly at observation point COLLIE1 (left), ESTUARY3 (centre) and ESTUARY4 (right)

summer, as freshwater discharge is reduced, the river realignment did not cause much change to the system. However, the increased freshwater input in winter drastically altered the estuarine dynamics. The southern stations (ESTUARY1 and ESTUARY2) were the most susceptible to changes, due to the Preston River alignment. The salinity at these stations was greatly increased, due to the lower river discharge. Obviously, the salinity at Bunbury Port (OUTER1) decreased due to the new freshwater input of the Preston River alignment (Figure 7.4, left). The southern basin water (ESTUARY3), was less affected by the alignment (Figure 7.5, centre). Even less affected were the Collie River (COLLIE1) and the northern basin (ESTUARY4), due to their remote location compared to the other stations (Figure 7.5, left and right).

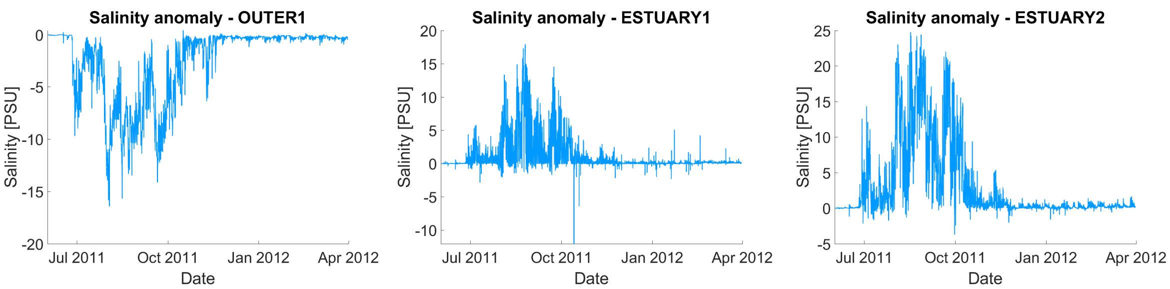

Figure 7.4: Salinity anomaly at observation point OUTER1 (left), ESTUARY1 (centre) and ESTUARY2 (right)

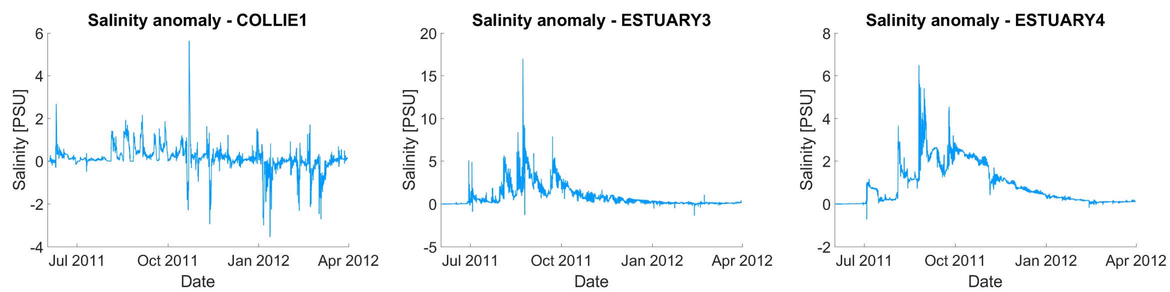

Figure 7.5: Salinity anomaly at observation point COLLIE1 (left), ESTUARY3 (centre) and ESTUARY4 (right)

7.2.2 Horizontal variation

Figures 7.6 and 7.7 show the winter and summer spatially-averaged anomalies. Temperature anomalies occurred mainly in the southern basin and in the Bunbury Port and varied between -0.2 $°C$ and 0.2 $°C$ (Figure 7.6). The rest of the estuary was unaffected, excepting the Collie River that became warmer in winter and colder in summer (Figure 7.6). Major salinity anomalies were observed for the winter scenario (Figure 7.7). The highest changes in salinity occurred in the Bunbury Port and the southern basin but salinity values were changed throughout the estuary in winter (Figure 7.7). In summer, the alterations were less evident and occurred mainly in the southern basin and to a lesser extent in the northern regions of the estuary (Figure 7.7). In the northern regions higher salinities occurred, indicating more hypersaline waters in summer after the Preston River alignment (Figure 7.7). In winter, salinity anomalies varied between -2 and 2 and in summer between -1 and 1 (Figure 7.7).

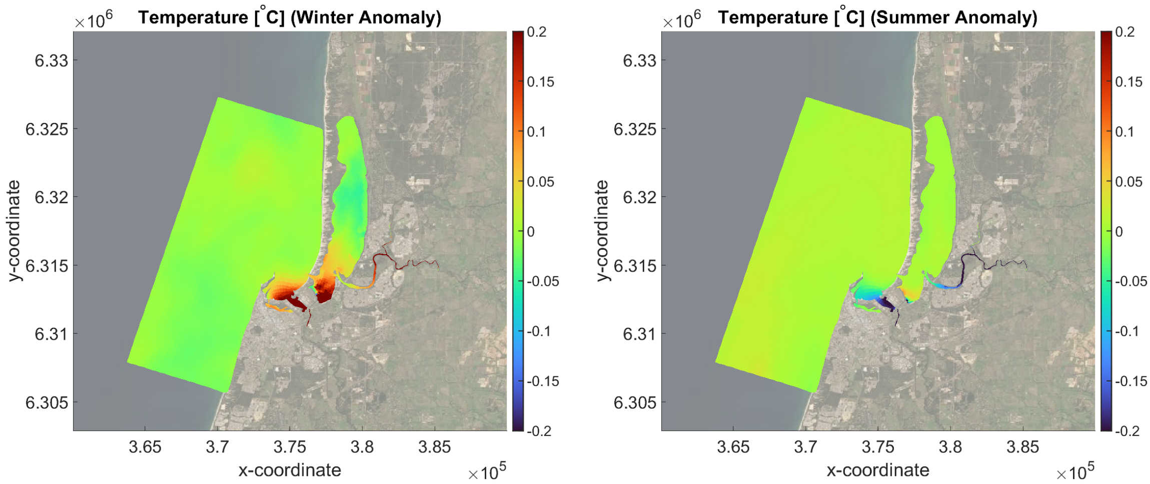

Figure 7.6: Mean winter (left) and summer (right) temperature anomaly

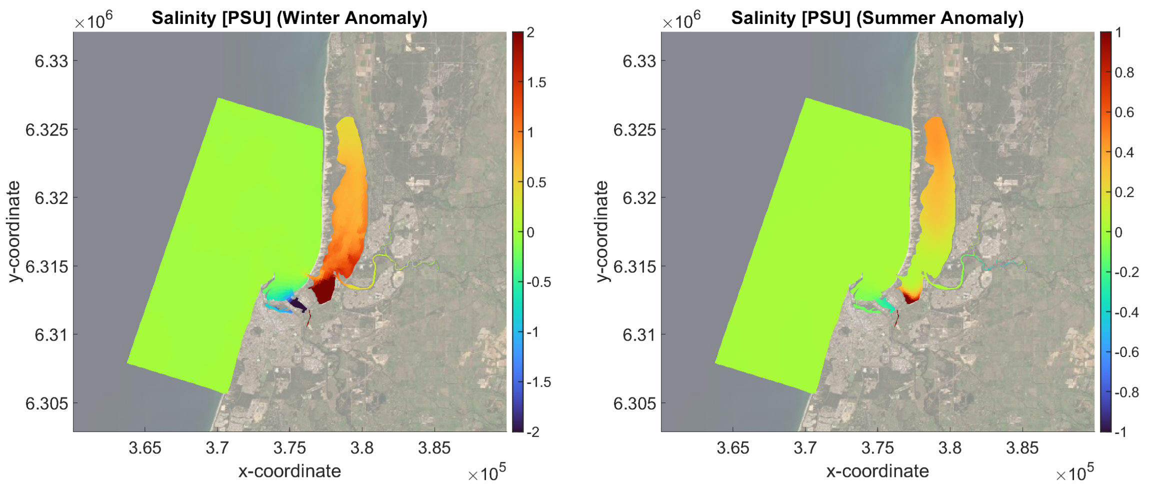

Figure 7.7: Mean winter (left) and summer (right) salinity anomaly

7.2.3 Vertical variation

To assess the spatially varying temperature and salinity anomalies vertically similar longitudinal profiles were used as in Chapter 6. The anomalies were averaged over the winter and summer periods.

Vertical temperature anomalies - Cut-Collie

Figure 7.8 shows the averages of winter and summer temperature anomalies for a longitudinal profile between the 'Cut' and the Collie River (Cut-Collie) (Figure 6.41). In winter, the average anomaly varied from 0 $°C$ in the ocean to 0.2 $°C$ in the Collie River (Figure 7.8, left). In summer, this variation lied between -0.2 $°C$ in the Collie River to 0 $°C$ in the Koombana Bay (Figure 7.8, right). Therefore, the Collie River was most susceptible to variations in water temperature. Furthermore, the upper layers in the 'Cut' were also prone to heating in winter, increasing the temperature stratification inside the 'Cut'.

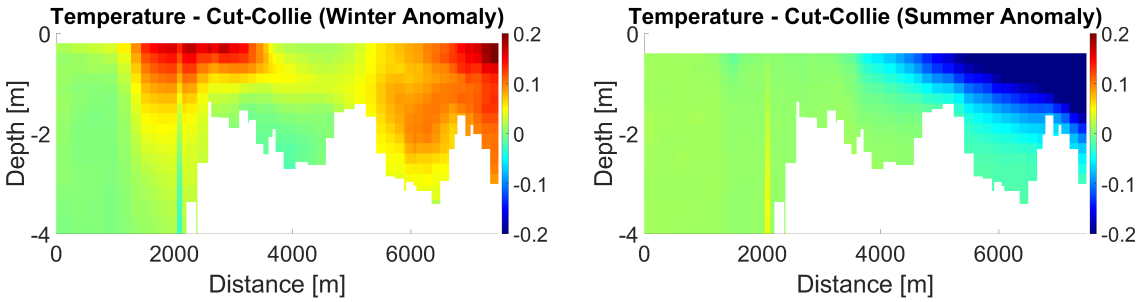

Figure 7.8: Longitudinal profile with averaged temperature anomalies in $°C$ between the mouth of the Leschenault Estuary and the Collie River- winter (left) and summer (right))

Vertical temperature anomalies - Cut-Preston

Figure 7.9 shows the average winter (left) and summer (right) temperature anomalies means of the Cut-Preston profile. In winter, the average water temperature anomalies varied from -0.2 $°C$ to 0.2 $°C$ in the southern basin (Figure 7.9, left) and in summer between -0.2 and 0 $°C$ (Figure 7.9, right). In summer, almost no change in temperature was observed in the southern basin (Figure 7.9, right). However, in winter the upper layers of the southern basin increased considerably in temperature in winter (Figure 7.9, left). Besides, a decrease in temperature was observed in the bottom layers of the southern boundary. This could indicate that the colder ocean water intruded the southern basin of the estuary along the bed in contrast with the central and northern basins.

Vertical temperature anomalies - Cut-Parkfield

Figure 7.10 shows the average winter (left) and summer (right) temperature anomalies for the Cut-Parkfield longitudinal section. In summer, no changes in temperature were observed in the Leschenault Estuary (Figure 7.10, left), which indicates the low influence of the Preston River alignment on the hydrodynamics of the northern regions. In winter, water temperatures were slightly reduced in the central and northern basin (Figure 7.10, right). In the 'Cut', higher temperatures were observed in the upper layers of up to 0.2 $°C$ (Figure 7.10).

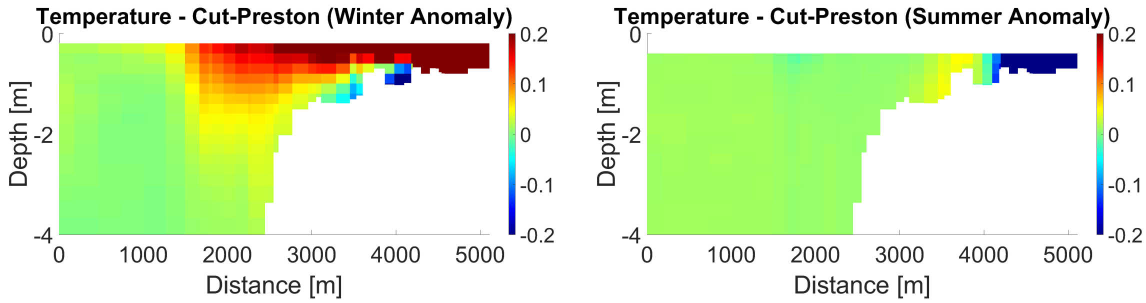

Figure 7.9: Longitudinal profile with averaged temperature anomalies in $^{\circ}C$ between the mouth of the Leschenault Estuary and the Preston River- winter (left) and summer (right))

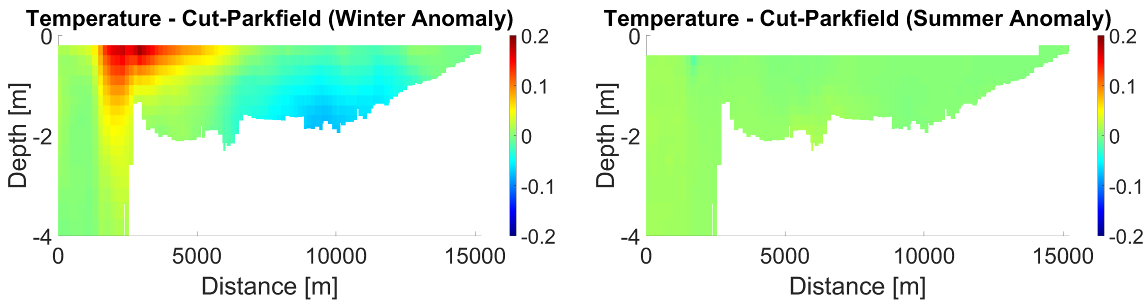

Figure 7.10: Longitudinal profile with averaged temperature anomalies in $^{\circ}C$ between the mouth of the Leschenault Estuary and the Parkfield Drain - winter (left) and summer (right))

Vertical temperature anomalies - Bunbury Port-Preston

Figure 7.11 shows the average winter (left) and summer (right) temperature anomalies for the longitudinal profile along Koombana Bay, Bunbury Port and the newly aligned Preston River. In summer, lower temperatures were observed throughout the Bunbury Port, with anomalies reaching values of -0.2 $^{\circ}C$ (Figure 7.11, right). In winter, higher temperature values were observed for the lower reaches of the Bunbury Port and lower values for the upper layer (Figure 7.11, left).

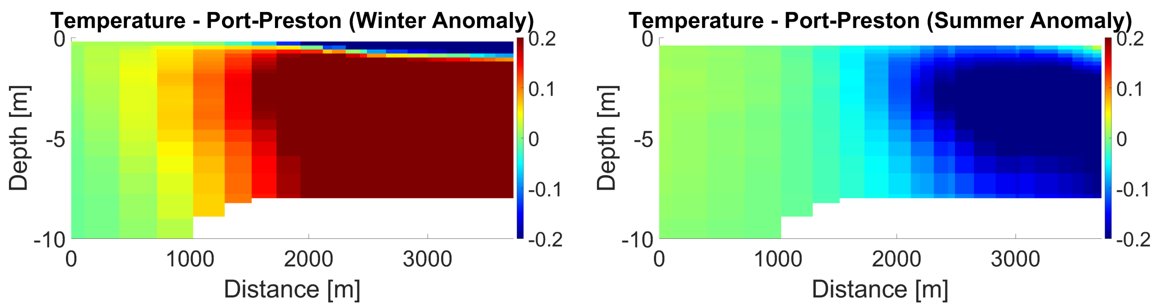

Figure 7.11: Longitudinal profile with averaged temperature anomalies in $^{\circ}C$ between the Koombana Bay and the newly aligned Preston River - winter (left) and summer (right))

Vertical salinity anomalies - Cut-Collie

Figure 7.12 shows the average winter (left) and summer (right) salinities along the Cut-Collie longitudinal profile. The summer anomalies were negligible in the Collie River and for the rest of the longitudinal profile (Figure 7.12, right). In winter, much higher salinity values were obtained at the 'Cut' and near the bed of the Collie River (Figure 7.12, left). This could indicate more saline ocean water intrusion in the Collie River and therefore more stratification. Changes in salinity varied between 0.5 in the Collie River to 1.5 in the 'Cut' (Figure 7.12).

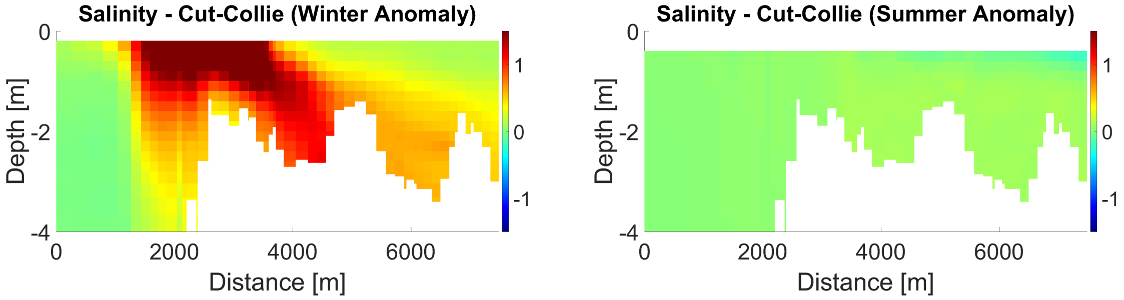

Figure 7.12: Longitudinal profile with averaged salinity anomalies in PSU between the mouth of the Leschenault Estuary and the Collie River- winter (left) and summer (right))

Vertical salinity anomalies - Cut-Preston

Figure 7.13 shows the average winter (left) and summer (right) salinity anomalies along the Cut-Preston longitudinal profile. A clear increase in salinity was observed throughout the southern basin in summer, with values exceeding 1.5 (Figure 7.13, right). Furthermore, this increase was observed all the way into the Koombana Bay. In winter, considerably less change in salinity occurred (Figure 7.13, left).

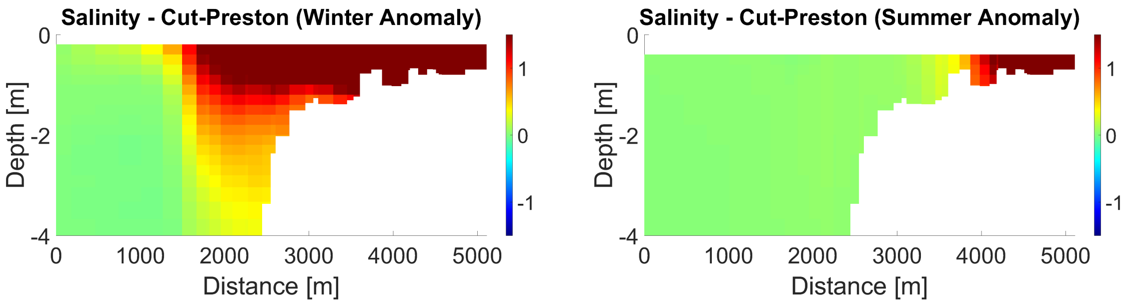

Figure 7.13: Longitudinal profile with averaged salinity anomalies in PSU between the mouth of the Leschenault Estuary and the Preston River- winter (left) and summer (right))

Vertical salinity anomalies - Cut-Parkfield

Figure 7.14 shows the average winter (left) and summer (right) salinity anomalies for the Cut-Parkfield longitudinal profile. In summer, the salinities in the estuary remained more or less the same but increased in the northern regions (Figure 7.14, right). This suggests that the hypersaline character of the estuary became more pronounced. In winter, the salinity rose in the entire estuary due to the lower freshwater input (Figure 7.14, left).

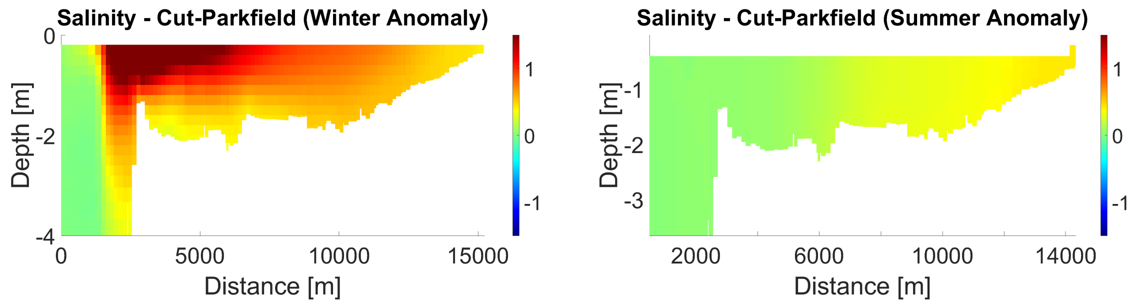

Figure 7.14: Longitudinal profile with averaged salinity anomalies in PSU between the mouth of the Leschenault Estuary and the Parkfield Drain - winter (left) and summer (right))

Vertical salinity anomalies - Bunbury Port-Preston

Figure 7.15 shows the average winter (left) and summer (right) salinity anomalies for the Koombana Bay - Bunbury Port - Preston River profile. The salinities in the Bunbury Port decreased in summer and winter, due to the new freshwater input of the Preston River (Figure 7.15). However, in winter the salinity only decreased in the upper layers and increased in the lower layers, indicating reduced vertical mixing in winter at Bunbury Port (Figure 7.15, left).

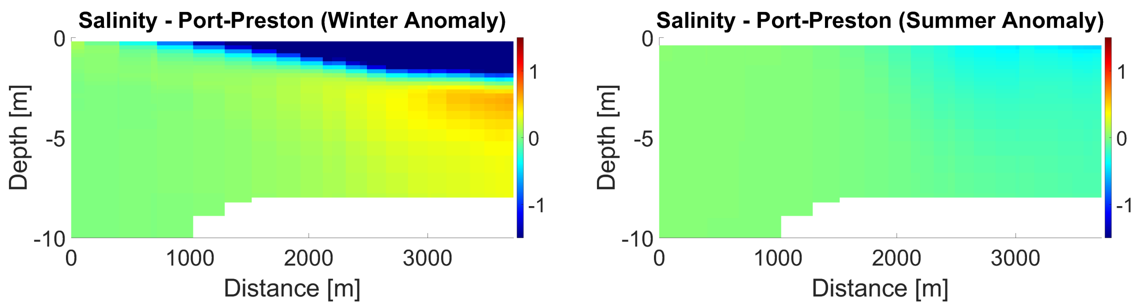

Figure 7.15: Longitudinal profile with averaged salinity anomalies in PSU between the Koombana Bay and the newly aligned Preston River - winter (left) and summer (right))

7.3 Estuarine classification

The changes in the governing hydrodynamic processes of the Leschenault Estuary and the influence of their physical drivers were assessed by the proposed classification techniques. The most effective methods to evaluate the governing processes are the Richardson theory, the stratification-circulation diagram and the decomposition of the salt transport.

7.3.1 Richardson

To assess the change in stratification the Richardson layer number was calculated for the Preston River alignment scenario and compared with the initial Richardson values of Section 6.5.2.

Bunbury Port

At Bunbury Port (OUTER1) the stratification regime was significantly changed (Figure 7.16, left). In winter, the water body at Bunbury Port (OUTER1) was more stable in the vertical (Figure 7.16, left), with values far above the transition zone, indicating a highly stratified water column. In summer, the situation remained unchanged, with partially-mixed to stratified conditions at neap tide and increased mixing at spring tide (Figure 7.16, left). Under peak river flow conditions, the water body at Bunbury Port (OUTER1) was highly stratified, with almost no vertical mixing (Figure 7.16, left), similar to the initial situation.

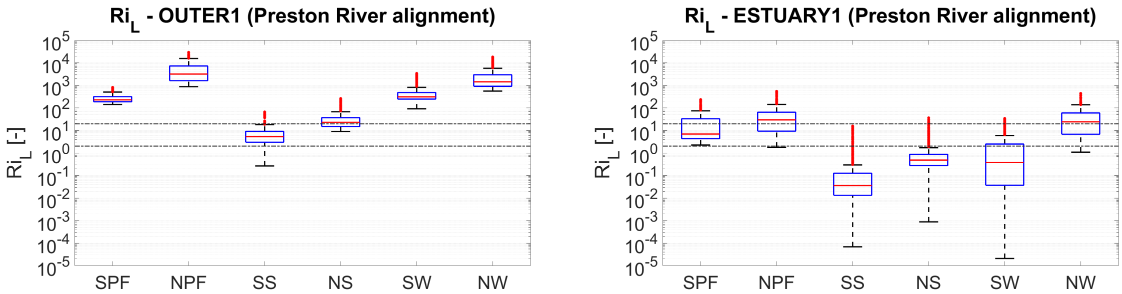

Figure 7.16: Richardson layer number for the Preston River alignment scenario at Bunbury Port (OUTER1) (left) and the 'Cut' (ESTUARY1) (right); SPW = Spring Peak Flow, NPW = Neap Peak Flow, SS = Spring Summer, NS = Neap Summer, SW = Spring Winter and NW = Neap Winter; $Ri_L < 2$ = well-mixed, $2 \leq Ri_L \leq 20$ = partially-mixed and $Ri_L > 20$ = highly stratified

The 'Cut'

At the 'Cut' (ESTUARY1), the stratification weakened, indicated by lower Richardson numbers (Figure 7.16, right). In winter, the water body at the 'Cut' (ESTUARY1) changed for the spring tidal cycle to a well-mixed flow, with $Ri_L < 2$. At winter neap tide, the water body at the 'Cut' (ESTUARY1) remained the same, with partially-mixed to stratified flows (Figure 7.16, right). In summer, a similar regime occurred at the 'Cut' (ESTUARY1), with even higher mixing (Figure 7.16, right). During the peak river flow event, a reduced stratification regime was found, with stratified to partially-mixed conditions (Figure 7.16, right).

Southern Basin

At the southern basin (ESTUARY2) less stratification was observed along the water column than in the initial situation (Figure 7.17, left). In winter, the stratification reduced significantly, resulting in higher vertical instability at spring tide ($Ri_{L,median} < 2$) (Figure 7.17, left). During the winter neap, also less stratification was observed, indicated by lower Richardson numbers (Figure 7.17, left). In summer, the water body remained well-mixed during spring and also became well-mixed during neap after the alignment of the Preston River ($Ri_L < 2$) (Figure 7.17, left). During the peak discharge event, the reduced freshwater input in the Leschenault Estuary increased mixing at the southern basin (ESTUARY2) during spring, indicating a higher influence of tidal stirring (Figure 7.17, left). At neap tide, the water body became less stratified and partially-mixed (Figure 7.17, left).

Collie River

The situation at COLLIE1 remained unaffected by the Preston River alignment and had similar stratification regimes as the situation without alignment (Figure 7.17, right).

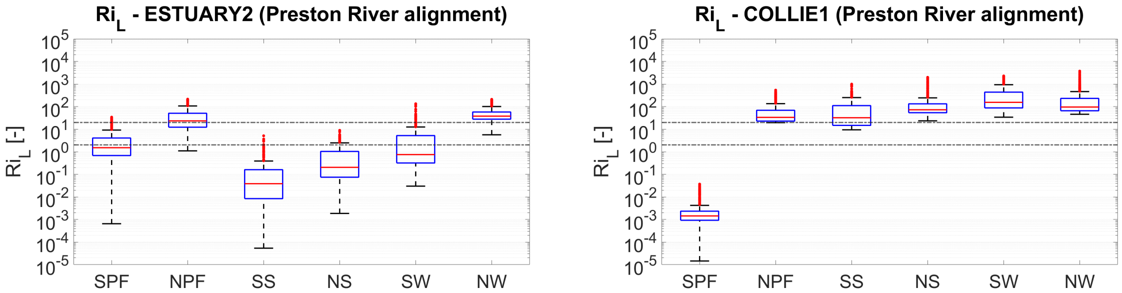

Figure 7.17: Richardson layer number for the Preston River alignment scenario at the southern basin (ESTUARY2) (left) and the Collie River (COLLIE1) (right); SPW = Spring Peak Flow, NPW = Neap Peak Flow, SS = Spring Summer, NS = Neap Summer, SW = Spring Winter and NW = Neap Winter; $Ri_L < 2$ = well-mixed, $2 \leq Ri_L \leq 20$ = partially-mixed and $Ri_L > 20$ = highly stratified

Central & Northern Basin

At the central basin (ESTUARY3), the stratification regimes were more or less unaffected by the Preston River alignment (Figure 7.18, left). However, for the peak discharge conditions the stratification decreased due to the reduced freshwater input caused by the alignment, resulting in well-mixed flows. Only during peak flow neap, the waters at the central basin became slightly partially-mixed (Figure 7.18, left). For the winter and summer situations, the stratification was already very low and remained unchanged, indicating well-mixed conditions, excepting partially-mixed conditions during winter neap (Figure 7.18, left). At the northern basin (ESTUARY4), the situation was totally unchanged, indicating that the stratification in the northern parts of the estuary was unaffected by the Preston River alignment (Figure 7.18, right).

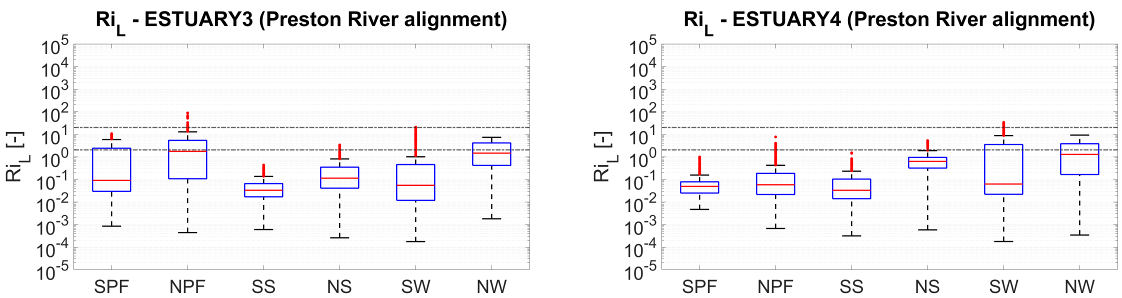

Figure 7.18: Richardson layer number for the Preston River alignment scenario at the central basin (ESTUARY3) (left) and the northern basin (ESTUARY4) (right); SPW = Spring Peak Flow, NPW = Neap Peak Flow, SS = Spring Summer, NS = Neap Summer, SW = Spring Winter and NW = Neap Winter; $Ri_L < 2$ = well-mixed, $2 \leq Ri_L \leq 20$ = partially-mixed and $Ri_L > 20$ = highly stratified

7.3.2 Stratification-circulation diagram

The circulation and stratification diagram was applied to the Preston River alignment scenario to assess the impact on the circulation and stratification regime of the Leschenault Estuary. The results for u- and v-directions are shown in Figure 6.83 and 6.84 and were compared with the initial results of Section 6.5.4.

Bunbury Port

Waters at the Bunbury Port (OUTER1) are indicated by asterisks in Figures 7.19 and 7.20. The circulation and stratification regime in the Bunbury Port (OUTER1) changed drastically after the Preston River alignment. During the peak discharge event, the water body at Bunbury Port (OUTER1) acted as a salt wedge Type 4 estuary, with a higher order of stratification and negligible mixing. In winter, the stratification was one order of magnitude lower and the water body behaved more like a Type 2b estuary. Under summer conditions, the stratification was even further reduced and had a Type 2a classification. The water in the Bunbury Port thus behaved as a partially-mixed estuary with low to high stratification under normal conditions, and occasionally as a salt-wedge estuary under peak discharge conditions.

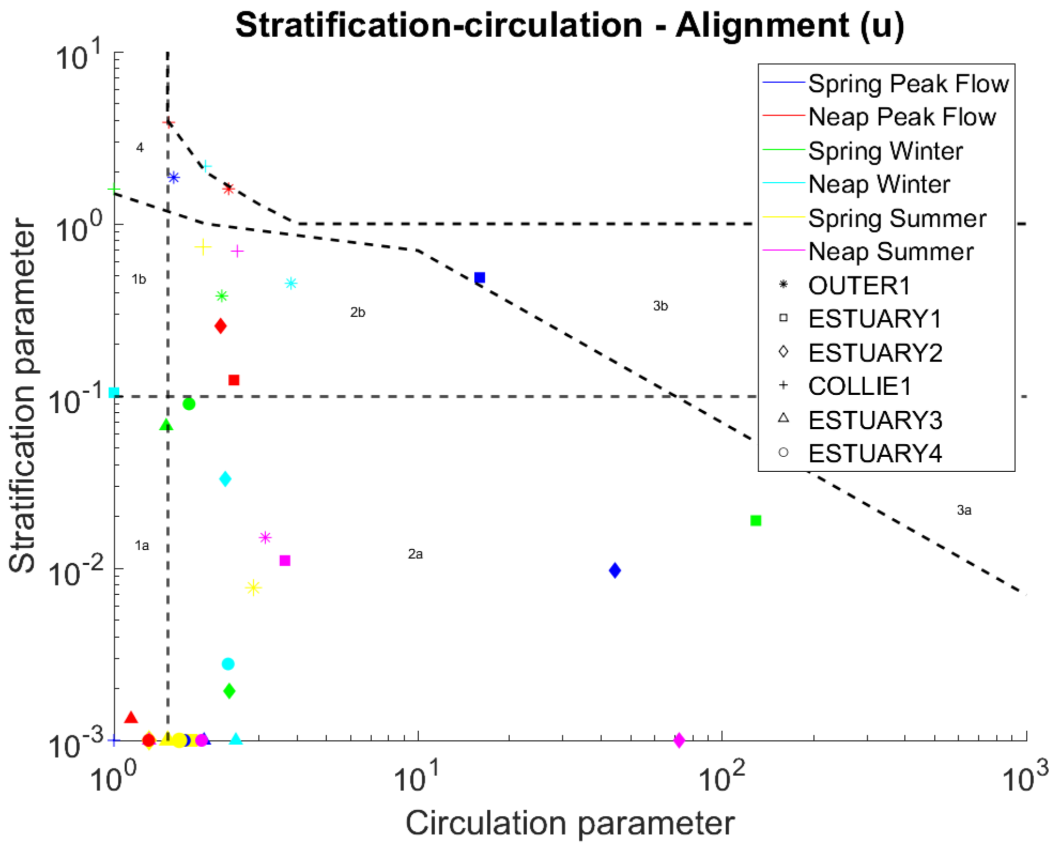

Figure 7.19: Circulation-stratification diagram for the u-component of the current velocity - Preston River Alignment

The 'Cut'

Waters at the 'Cut' (ESTUARY1) are indicated by squares in Figures 7.19 and 7.20. The water body first had a Type 2a classification for normal summer conditions and winter conditions at spring tide, a Type 2b classification for winter and peak discharge conditions at neap tide and a Type 4 classification for peak discharge conditions at spring tide. After the Preston River alignment, the stratification dropped drastically for all conditions. Under peak river flow conditions, the water body at the 'Cut' (ESTUARY1) was classified as Type 2b. Under normal winter and summer conditions, less stratification was observed at the 'Cut' (ESTUARY1), resulting in a Type 2a estuary.

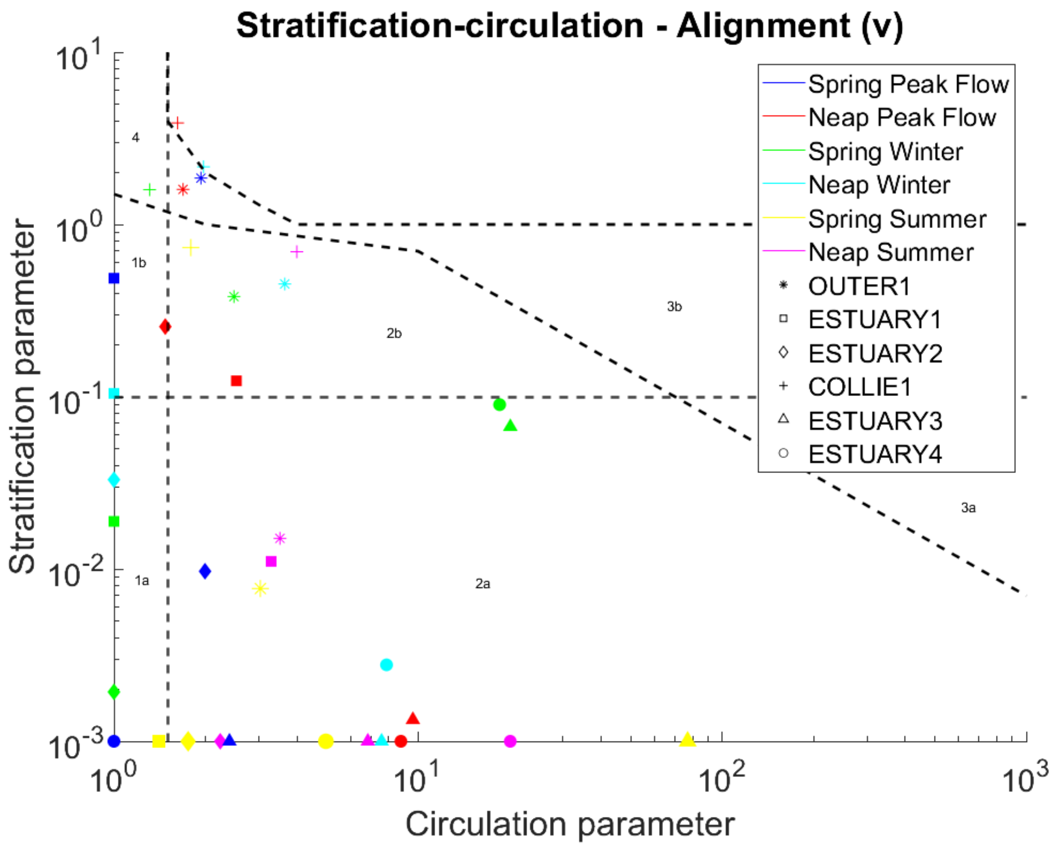

Figure 7.20: Circulation-stratification diagram for the v-component of the current velocity - Preston River Alignment

Southern Basin

Southern basin (ESTUARY2) waters, indicated by diamonds in Figures 7.19 and 7.20, were the most dynamical of the Leschenault Estuary for the initial situation, with classifications varying between Types 1a, 2a and 4. After the Preston River alignment, the waters in the southern basin became less dynamical (Figures 7.19 and 7.20). In summer, the estuary class behaved as Type 2a, with negligibly small stratification and partially-mixed circulations. In winter and during the peak discharge event at spring tide, the estuary class was also Type 2a, with more pronounced stratification and a partially-mixed water body. Only at neap tide during peak flow, the stratification became high enough for Type 2b.

Collie River

Collie River waters (COLLIE1), indicated by plus-symbols in Figures 7.19 and 7.20, were more or less unaffected by the Preston River alignment. Collie River waters (COLLIE1) were classified as Type 1a estuaries for peak discharge conditions at spring tide, a Type 4 estuary for normal winter conditions and peak discharge conditions at neap tide and a Type 2b estuary for normal summer conditions. After the Preston River alignment the classifications remained the same (Figures 7.19 and 7.20).

Central & Northern Basin

Water bodies at the central (ESTUARY3) and northern basin (ESTUARY4), indicated by triangles and circles respectively, maintained the same classification after the Preston River alignment (Figures 7.19 and 7.20). However, both stations showed a considerable decrease in stratification. After the Preston River alignment, the circulations at the central (ESTUARY3) and northern basin (ESTUARY4) were still well-mixed with a bidirectional flow pattern (Type 2a; (Figures 7.19 and 7.20)). Further, the water became well-mixed at the northern basin (ESTUARY4) during the peak discharge event (Figures 7.19 and 7.20).

7.4 Salt transport

To analyse the effects of the Preston River alignment on the dominant physical processes governing the salt transport at the 'Cut' and the central basin, the results of Tables 6.3 and 6.4 were compared with the results of the Preston River alignment scenario, listed in Tables 7.4 and 7.5. The same winter, summer and annual (10 months) averages were considered as in Section 6.6.

Component	Physical process	Winter	Summer	Full period
A	Freshwater discharge	-2.85	$-4.39 \cdot 10^{-1}$	-1.36
B	Stokes drift/progressive tidal wave	$6.41 \cdot 10^{-1}$	-1.10	-1.19
C	Topographic trapping	1.93	$2.17 \cdot 10^{-1}$	1.04
D	Gravitational circulation	$-7.05 \cdot 10^{-2}$	$-9.50 \cdot 10^{-4}$	$-1.89 \cdot 10^{-2}$
E	Bathymetric tidal pumping	$1.10 \cdot 10^{-1}$	$1.39 \cdot 10^{-2}$	$4.63 \cdot 10^{-2}$
F	Tidal shear	$1.09 \cdot 10^{-2}$	$3.30 \cdot 10^{-3}$	$3.30 \cdot 10^{-3}$
G	Wind fluctuations	$9.56 \cdot 10^{-4}$	$8.75 \cdot 10^{-5}$	$3.03 \cdot 10^{-4}$
Total	Eq. 2.26	$-2.22 \cdot 10^{-1}$	-1.31	-1.48
Total	Eq. 2.12	$-2.24 \cdot 10^{-1}$	-1.32	-1.49

Table 7.4: Salt flux components in kg/s at transect the 'Cut' in winter [1 Jun 2011 - 1 Sep 2011], summer [1 Dec 2011 - 1 Mar 2012] and whole year [1 Jun 2011 - 1 Apr 2012]

7.4.1 The 'Cut'

After the Preston River alignment, the influence of the freshwater discharge (component A) was reduced. However, it remained the most dominant process in winter and over the year (10 months). The salt flux A was around 40% less in winter and the whole year (10 months) compared to the situation with original Preston River location. In summer however, the component A increased by 45%. The Stokes wave transport (component B), was unaffected by the Preston River alignment, because no alterations were applied to the tidal forcing. Coincidentally with the decreased influence of the freshwater discharge, the effect of topographic trapping (component C) on the salt transport was also reduced. The lessened freshwater discharge decreased the accumulation of water in the estuary, weakening the longitudinal salinity gradient. In winter, the salt flux C of the river alignment scenario was 45% lower than the initial situation. In summer, the reduction was 17% and over the year 44%. The tidal correlation between the freshwater discharge and topographic trapping can thus easily be noticed. With regard to the gravitational circulation (component D), its impact on the salt transport increased with the higher salt flux in winter by 7% and decreased in summer and the whole year by 6% and 9% respectively. However, the influence of the steady shear dispersion was minor compared to components A, B and C. Components E, F and G, maintained their minor role on the salt transport. After the alignment of the Preston River, components A, B and C still had a dominant role on the salt transport. The influence of the Stokes drift on the salt transport remained equal, while the influence of the freshwater discharge and topographic trapping decreased by 40% and 45% respectively. This means the Stokes drift became relatively more important after the alignment of the Preston River compared to the freshwater discharge and topographic trapping. The Stokes wave transport and the freshwater discharge were both oriented seaward.

Component	Physical process	Winter	Summer	Full period
A	Freshwater discharge	$2.63 \cdot 10^{-2}$	$1.26 \cdot 10^{-1}$	$7.40 \cdot 10^{-2}$
B	Stokes drift/progressive tidal wave	$6.42 \cdot 10^{-2}$	$-1.47 \cdot 10^{-1}$	$-1.31 \cdot 10^{-1}$
C	Topographic trapping	$-1.30 \cdot 10^{-3}$	$-1.7 \cdot 10^{-3}$	$1.80 \cdot 10^{-3}$
D	Gravitational circulation	$3.04 \cdot 10^{-4}$	$-1.17 \cdot 10^{-4}$	$-8.90 \cdot 10^{-5}$
E	Bathymetric tidal pumping	$-4.60 \cdot 10^{-3}$	$-4.98 \cdot 10^{-4}$	$-1.00 \cdot 10^{-3}$
F	Tidal shear	$-2.00 \cdot 10^{-3}$	$4.28 \cdot 10^{-4}$	$-6.69 \cdot 10^{-4}$
G	Wind fluctuations	$2.50 \cdot 10^{-4}$	$-3.67 \cdot 10^{-4}$	$2.46 \cdot 10^{-4}$
Total	Eq. 2.26	$8.32 \cdot 10^{-2}$	$-2.33 \cdot 10^{-2}$	$-5.75 \cdot 10^{-2}$
Total	Eq. 2.12	$8.75 \cdot 10^{-2}$	$-2.29 \cdot 10^{-2}$	$-5.65 \cdot 10^{-2}$

Table 7.5: Salt flux components in kg/s at transect Central Basin in winter [1 Jun 2011 - 1 Sep 2011], summer [1 Dec 2011 - 1 Mar 2012] and whole year [1 Jun 2011 - 1 Apr 2012]

7.4.2 Central Basin

After the Preston River alignment, the directions of the salt flux and the order of dominance remained the same, indicating no major changes in the salt flux dynamics at the central basin. The influence of the Stokes drift (component B) was similar after the Preston River alignment and remained the most dominant process. The salt flux driven by the freshwater discharge (component A), was around 18% less in winter, but 11% and 6 % higher in summer and the whole year (10 months) respectively. The freshwater discharge maintained its second most dominant position. Topographic trapping was decreased by 70% and 30% in winter and summer respectively but increased over the whole year by 30%, and remained the third most important salt flux at the central basin. Bathymetric tidal pumping (component) had a substantial impact on the salt transport in winter and over the whole year but had a less significant role in summer. Gravitational circulation played a minor role on the salt transport overall. However, due to the Preston River alignment the gravitational circulation salt flux became three times higher. Other salt flux components were negligible.

Part IV

Evaluation

The study conducted for this thesis is thoroughly discussed to outline the general importance of this research but also to summarize the assumptions that have been made and the major questions that remain. Besides, the final conclusions and recommendations for follow-up studies are presented.

Chapter 8: Discussion

Chapter 9: Conclusion & recommendations

8

Discussion

As estuaries are prone to climate change and human interference, good water quality management is vital for the existence of these fragile ecosystems. One of the tools that can be used in supporting management decisions is a 3D-hydrodynamic numerical model, which can simulate water quality properties such as temperature and salinity. The measurements and model results presented in this thesis contributed to the understanding of the governing processes of the Leschenault Estuary's physical dynamics. Furthermore, the model was used to identify the consequences of a potential management intervention, the Preston River alignment. In this chapter, a reflection and insights on the modelling of such systems is provided. Furthermore, the results on the physical processes in the Leschenault Estuary are discussed and further generalised.

8.1 Numerical modelling aspects

The hydrodynamic modelling package, used in this study is the D-Flow FM module of the numerical modelling package Delft3D-FM developed by Deltares. Several assumptions were made in this study, which may affect the results.

The bed level in the DFM-model is generated by interpolating the bathymetry data on the unstructured grid. To guarantee the depth in the estuary and the rivers, the bathymetry data was averaged by using the minimum value in a certain range. This leads to higher than observed depths, but this approach was adopted to improve the salt transport distributions in the rivers.

A spatially uniform atmospheric forcing has been imposed to the model. Available spatially variable data were adopted from an atmospheric model with 10 km grid resolution. As the domain of the Leschenault Estuary is around 10x20km, the meteorological spatial variations were not significant. The measured meteorological forcing was applied instead. Atmospheric variations on a scale of 10 km were negligible, and therefore assumed to be almost constant in an area of 10x20 km.

The tidal forcing at the western boundary had a tidal and sub-tidal component. At first, the sub-tidal component was generated by filtering the tidal signal from the observed water level at the Bunbury Port. However, the correct execution of this process is quite challenging and prone to errors. Therefore, the sub-tidal forcing from the OFAM-Bluelink-model was applied to the DFM-model. The same tidal components as the CSIRO model were adopted but using the phases and amplitudes inferred from the Bunbury Port tidal gauge measurements (Australian Hydrographic Office). It could be argued if this method is going to generate realistic results in future models. To improve the water level and the current velocities, usually current forcing is added to the boundaries. However, the water level results showed a good agreement with the observed data, which diminished the need for adding current velocities to the boundaries. Moreover, the model used to develop the current velocity was the same as for the atmospheric forcing. The coarse resolution could therefore cause unrealistic circulations and flow velocities in the high resolution model.

The main drivers of the salt transport in the D-Flow FM module were the horizontal and vertical eddy diffusivity parameters. Very gentle modifications of these parameters resulted in completely different circulation and stratification regimes inside the estuary. A sensitivity analysis has been conducted to find the best performing value for these parameters. Some studies suggest that an increase in the horizontal diffusivity would increase the salt transport along the estuary. Less information is available for the order of magnitude of horizontal and vertical diffusivities in shallow and small estuaries like the Leschenault Estuary. The DFM-manual stated that the order of magnitude of the vertical eddy diffusivity parameter for highly stratified estuaries with only small vertical mixing is 10^{-4}. However, the best performing vertical eddy diffusivity parameter for the Leschenault Estuary, was two orders of magnitude smaller (10^{-6}).

8.2 Insights on the Leschenault Estuary case

The Leschenault Estuary behaved mainly as a partially-mixed estuary with low to high stratification, and occasionally as a well-mixed or salt-wedge-like estuary. Therefore, the Leschenault Estuary is a very dynamic water body encompassing different regimes depending on location and season. This is line with earlier studies (Semeniuk et al., 2000) (Charteris and Deeley, 2000) (Gillibrand et al., 2012). The general water circulation is the classical estuary circulation driven by gravitational circulation, with saline ocean waters intruding the estuary near the bed and brackish estuarine waters flowing out on top. In summer, the estuary presented an inverse circulation, with hypersaline estuarine waters flowing out of the estuary near the bed and ocean waters intruding the estuary on top. Again, this is in line with theory and earlier studies (Gillibrand et al., 2012). However, this pattern was not found at the 'Cut', which could be explained by the dynamic conditions in the southern basin (i.e., more vertical mixing). The cross-section at the 'Cut' showed two main circulation patterns, a horizontal and a vertical two-layered current velocity structure, depending on the conditions. Highest velocities in the horizontal two-layered structure were found at the south side of the 'Cut'. However, no changes in direction were observed at the cross-section over the lateral axis. The dominant processes with regard to salt transport at the 'Cut' were the freshwater discharge, the Stokes drift and the topographic trapping. Besides, the northern and central basins were less stratified than the southern basin, which could indicate the higher influence of tidal stirring in these parts. This is emphasized by the measurements conducted in 2020. Whereas earlier studies (Charteris and Deeley (2000) and Gillibrand et al. (2012)) stated that the tidal phase lag and attenuation inside the

Leschenault Estuary were accentuated, recent measurements showed a minor phase lag and relatively less attenuation. This could indicate a higher influence of the tides in the northern regions. However, due to an overestimation of the dimensions of the 'Cut' in the model, the attenuation and the phase lag in the DFM-model were less than observed. Still, the modelled phase lag was more realistic than shown by earlier models (Charteris and Deeley, 2000) (Gillibrand et al., 2012), which confirmed the reliability of the model.

8.3 Insights on the physical drivers of the hydrodynamics of the Leschenault Estuary

Ryan et al. (2003) classified the Leschenault Estuary as wave-dominated, based on morphological characteristics. However, freshwater discharge and tides play a dominant role in the Leschenault Estuary, especially in the southern basin and the 'Cut'. In the central and northern basins, the waters are shallower and stagnant, and therefore more susceptible to winds, waves and Coriolis. At the central basin, the Stokes drift transport is the dominant physical process driving the salt transport, confirming the findings of Ryan et al. (2003). In the northern basin and near the estuary's boundaries, winds have a substantial effect on the current directions and magnitudes. It is also assumed that Coriolis can play an important role in the water circulations in these areas.

8.4 Insights on the Preston River alignment scenario

The hydrodynamic changes in the Leschenault Estuary dynamics due to the Preston River alignment met the expectations. Due to the reduced freshwater discharge in the main estuarine body, salinities increased considerately. Much higher salinity values were observed in winter than in the initial situation. Temperature changes were less significant, but can be significant during short periods of time. The circulation-stratification regime drastically changed in the Bunbury Port and southern basin due to the alignment, in line with the expectations. The freshwater influence increased in the Bunbury Port resulting in higher stratification and greater seasonal variability. Further, the freshwater influence decreased in the southern basin, reducing the stratification and seasonal variations. The central and northern basin remained more or less unaffected by the intervention, what confirmed the lower influence of the freshwater discharge on the northern regions. The same applies to the Collie River, which had its hydrodynamics unaffected in its hydrodynamic regime. Regarding the salt flux, the influence of the freshwater discharge was significantly reduced compared to the influence of the Stokes drift. This makes sense as the tidal amplitude has not changed and the freshwater discharge was reduced in the estuary. The topographic trapping was also dependent on the freshwater input at the Leschenault Estuary, being therefore, reduced by the same order of magnitude. This indicates the Stokes wave transport became relatively more important in the main body of the estuary.

The methods and models used in this thesis have proved to be reliable and valuable assets for management. A follow-up research on the physics of the Leschenault Estuary is therefore recommended. These easy-to-apply methods could also be applied to other estuarine systems and could be very valuable for management.

9

Conclusion & Recommendations

The objective of this study is formulated as follows:

> "Improve the understanding of the processes governing the hydrodynamics in the Leschenault Estuary relevant for management purposes, and to forecast changes in water quality and enhance environmental regulatory decision-making, by using efficient and easy-to-apply methods for the observed and modelled data"

What are the governing hydrodynamic processes of the Leschenault Estuary and their main physical drivers? The processes governing the hydrodynamics in the Leschenault Estuary are internal circulation, stratification and turbulence. These were predominantly driven by the freshwater discharge and tides. The importance of both physical processes on the advective and diffusive terms depends on the seasonal conditions and the specific location. In general, three different conditions can be distinguished: normal summer conditions, normal winter conditions and peak river discharge conditions. Under normal summer conditions, the freshwater input was drastically lower than under normal winter conditions. This means that the influence of the freshwater input is reduced and the effect of tidal stirring is increased (i.e., more vertical mixing), with diffusive processes being dominant in summer. In winter, the freshwater input increased, consequently increasing the stratification and the importance of advective processes. Occasionally, peak flow events occurred, pushing the salt wedge out of the rivers and partially out of the estuary. In this case, the flow became unidirectional and well-mixed at certain locations.

Besides the distinction between seasonal conditions, the Leschenault Estuary can be spatially subdivided in four different areas (river, southern basin, central basin and northern basin) based on the governing hydrodynamic processes and their physical drivers. Firstly, the rivers are predominantly driven by the freshwater discharge. However, due to tidal forcing, the saline ocean water is able to penetrate upriver along the bed leading to strong stratification. The freshwater flows out of the estuary on top of this saline ocean water layer. At the front of this salt wedge high entrainment mixing occurs. However, both layers are mostly driven by advection. Secondly, the southern basin has the most dynamic regime influenced by the northern regions, the Preston River, the Collie River and the Cut. The governing hydrodynamic processes are therefore highly variable in this region and diffusive and advective processes can dominate depending on the circumstances. Central basin waters are less prone to stratification induced by the Collie and Preston River. In an event of peak river discharge, less saline waters can intrude the central basin, causing more stratification and disrupting the general circulation patterns. Two circulation patterns are observed in the central basin: the classical estuary circulation and the inverse estuary circulation. The former is observed in the Leschenault Estuary under normal winter conditions and the latter under normal summer conditions driven by the hypersaline conditions in the northern basin. The northern basin becomes hypersaline in summer due to the reduced depth, low freshwater discharge from the Parkfield Drain and its remote position. The main physical drivers in the northern basin were tides, winds, Coriolis and evaporation. The importance of tides in the central and northern basin was higher than concluded in earlier studies that estimated a higher than observed phase lag and tidal attenuation of the tide (Charteris and Deeley, 2000) (Gillibrand et al., 2012). Winds mostly affected shallower areas in the northern basin and near the estuary's boundaries. The same areas might also be influenced by Coriolis, however the influence of winds was assumed to be dominant over Coriolis.

What are efficient classification techniques for management and how can the Leschenault Estuary be classified?

The stratification-circulation diagram of Hansen and Rattray Jr (1966) was applied to classify the water bodies at the five distinct stations in the Leschenault Estuary. The stratification-circulation diagram provides a first, simplified approach to classify and compare different estuaries. However, care should be taken in the application of the diagram and complementary methods are required to confirm the findings. Therefore, the Richardson layer number, TS-diagrams and vertical distribution profiles were also used to understand the estuarine physical dynamics. The water body at the 'Cut' was classified as a partially-mixed and weakly stratified estuary (Type 2a) under summer conditions and winter spring tide conditions and as a partially-mixed and strongly stratified estuary (Type 2b) under winter neap and peak discharge neap conditions. The water body at the 'Cut' (ESTUARY1) can occasionally be classified as a salt-wedge estuary under peak discharge conditions at spring tide. A clear difference between spring and neap tide is noticed when assessing the winter scenario. At spring tide, the tidal forcing was stronger and therefore tidal stirring was more pronounced. In this case, the stratification becomes less at the 'Cut'. At neap tide, the tidal forcing was weaker, increasing the dominance of the freshwater input and the stratification. In the southern basin, the water body was the most dynamic and could not be classified to a single regime. The classification varied between well-mixed and weakly stratified (Type 1a), partially-mixed and weakly stratified (Type 2a) and highly stratified with almost no vertical mixing (Type 4) in this region. The regime at the Collie River varied between partially-mixed to highly stratified, with well developed gravitational circulation. Occasionally, the river can transform into a well-mixed, freshwater body during peak river discharge. The northern regions were classified as Type 2a, indicating a partially-mixed water body with low stratification and reversed flow over the depth. The classification methods used in this thesis successfully determined the hydrodynamic regimes both in space and time. The efficient well-performing methods are therefore recommended for water quality management.

What are the main physical drivers of the salt transport in the Leschenault Estuary?

A clear difference could be distinguished between the physical drivers of the salt transport at the 'Cut' and the central basin. Over the whole year, the main physical process that influenced the salt transport at the 'Cut', was the freshwater discharge. The advective salt flux of the freshwater discharge was negative, and therefore seaward. The second most important process was the topographic trapping, which is tidally correlated. An increased water level due to the tides corresponded to increased trapping of water in the Leschenault Estuary and therefore more dispersion. Increased freshwater discharge also increased the accumulation of water in the estuary, generating higher flushing times and therefore more diffusive mixing of salt. The salt flux by topographic trapping was transporting salt into the estuary. The third process, Stokes drift, had a similar order of magnitude as the previous two processes. At the 'Cut', the Stokes drift was directed oppositely to the landward wave propagation, driving salt out of the estuary. The other salt flux components (gravitational circulation, bathymetric tidal pumping, tidal shear and wind fluctuations) played a minor role in the salt balance of the 'Cut'. In winter, the influence of the freshwater discharge was dominant increasing the salt flux due to topographic trapping. In summer, the Stokes drift was the main driver of the salt transport and generated a seaward salt flux. The dominant physical driver of the salt transport over the whole year at the central basin was the Stokes drift, followed by the freshwater discharge and topographic trapping. The salt flux driven by the freshwater discharge was northward, caused by the southern rivers. The Stokes wave transport was southward in summer, coincident with the prevailing northerly winds. Topographic trapping also counteracted the freshwater discharge and transported salt southward by dispersion. Gravitational circulation played a minor role on the salt flux dynamics at the central basin, indicating less developed gravitational in the central and northern basin. Other components also played a minor role on the salt transport at the central basin.

How will the Preston River Alignment change the hydrodynamics, the classification and the salt transport in the Leschenault Estuary and which conclusion can be drawn from these changes on a management level?

The Preston River alignment had a significant impact on the characteristics of the Leschenault Estuary leading to higher fluctuations of temperature and salinity inside the estuary. Compared to the initial situation, the annually averaged temperature increased only slightly ($< 0.20\ °C$) but the temperatures could rise or fall temporally and locally up to $5\ °C$. With regard to salinity, local and temporal changes of -15 to +25 were observed, compared to the initial situation. In winter, the lower freshwater supply in the Leschenault Estuary due to the Preston River alignment, drastically changed the temperature and salinity values. In summer, minor changes in salinity were observed. The southern basin was the most affected area in the estuary, showing much higher salinity variations both during winter and summer (average salinity anomalies of 1-2). Also in the Bunbury Port, the regime changed drastically. In summer, the water body was partially-mixed with low stratification. In winter, the water body was partially-mixed with high stratification, and under peak discharge, a salt wedge estuary developed in the Bunbury Port. At the 'Cut', the water body after the river alignment was classified as partially-mixed and highly stratified under extreme river discharge and partially-mixed and weakly stratified under normal conditions. The water body at the 'Cut' thus becomes much less dynamic after the Preston River alignment. The southern basin was partially-mixed with low to high stratification after the alignment. The water bodies in the Collie River and in the central and northern basins were less influenced by the alterations and maintained their stratification-circulation regime. With regard to the driving forces of the salt transport, no major changes were observed in the relative influence of the different components. The dominant process driving the salt transport at the 'Cut' was the freshwater discharge, followed by topographic trapping and Stokes drift. However, the effect of the freshwater discharge and the topographic trapping became relatively weak compared with the effect of the Stokes drift. The physical drivers of the salt transport at the central basin were not affected by the Preston River alignment, indicating the weak influence of the southern rivers on salinity at the central and northern basins. From a management perspective it is relevant to note that despite the Preston River alignment, the Collie River and the central and northern basin remained more or less unaffected in terms of stratification-circulation regime. However, higher salinity and temperature fluctuations were observed in winter, which could have detrimental effects on the ecology. Also the regimes of the Bunbury Port, southern basin and the 'Cut' were drastically altered. This stresses the need for an ecological evaluation of this potential intervention.

9.1 Recommendations

This study recommends the use of efficient classification methods to evaluate the governing hydrodynamic processes of an estuary and to unravel its main physical drivers. Besides, the successful use of D-Flow FM to develop a 3D-numerical model promotes the application of Delft3D-FM packages for follow-up studies. Besides the hydrodynamics, morphodynamics could be modelled in order to expand the overall knowledge in the dynamics of systems like the Leschenault Estuary.

In the model set-up, waves have been left out of the calculations, because no wave data was available for the 2011/2012 period. As the Leschenault Estuary is very shallow (<0.5 m) at some points, it is suggested that the waves will increase the vertical mixing in these shallow zones. The wave data from Feb 2020 - Apr 2020, gave some insight in the order of magnitude of the wave height, which is less than 10 cm in this period. This indicates, the waves will not have a significant effect on most parts of the estuary. However, these waves were measured for summer/autumn conditions and higher waves could occur in winter. The influence of waves in winter should be evaluated in the future, particularly in the shallow and stagnant regions of the estuary.

The tidal and sub-tidal forcing of the western boundary in the DFM-model have been obtained by combining the input used in the CSIRO-model and observed data of the Australian Hydrographic Office. While developing the DFM-model several attempts were done to filter the tidal signal from the observed water level at the Bunbury Port. This process was quite challenging and prone to errors. Instead, a combination between the sub-tidal input of the CSIRO-model and the tidal constituents minus J1 and MSM of the CSIRO-model was used with the measured tidal phase and amplitude of the Australian Hydrographic Office. This solution was found after a thorough calibration process, but it is arguable if this solution will work for other periods of time. Improving the filter methods to extract the sub-tidal component from the measured level is recommended.

The modelled evaporation did not match well to the measured evaporation and future improvements in the representation of this process are recommended. Different methods were applied to the model and the model presented in this thesis used the composite model, which considers humidity, cloudiness, air temperature and water temperature. Besides, model 1 was used with prescribed evaporation on the rainfall input, which resulted in very different temperature outcomes than observed. The impact of evaporation seems to be rather insignificant for most parts of the estuary. However, the stagnant and shallow northern parts are likely to be more prone to evaporation. Correcting the evaporation rates could improve the representation of the hydrodynamics of the northern regions.

In addition to the evaporation, the calculation of the water temperature should also be investigated. Throughout the calibration process the temperature results did not improve and remained the same. This indicates that the water temperature is most importantly affected by atmospheric forcing. The atmospheric forcing has not been altered during the process, and should be calibrated in future studies. Besides, the use of spatially variable atmospheric data improve the temperature results. However, it is arguable if the resolution of the existent models will be fine enough to generate more realistic results than the measured data.

In the sensitivity analysis, the diffusivity and viscosity had significant impact on the salinity values in the model. However, less data were available about these parameters. Eventually, a much lower vertical eddy diffusivity was applied to the model than literature suggested. Calibration of these values are time consuming, and measurement of the diffusivity in the field would be advisable. Therefore it is suggested to conduct measurements on the diffusivity and viscosity in the estuary.

The tidal phase lag between the Bunbury Port and the Leschenault Estuary is about 1-2 hours, which is less than previous studies assumed. Moreover, the attenuation is also less than previous studies assumed. However, the modelled water level results were not dampened at all in the DFM-model. This could probably be due to the dimensions of the Cut or the Leschenault Estuary in general. A bathymetric survey of the Cut would provide a more reliable result.

The decomposition of the salt fluxes highlighted the main physical processes affecting the salt transport at the 'Cut'. The salt transport could also be investigated at different cross-sections inside the estuary since physical drivers varied spatially. The classification methods provided in this thesis are valuable tools for management.

The influence of winds and Coriolis was not investigated thoroughly in this study, but could be important drivers of the Leschenault Estuary hydrodynamics. Coriolis and winds are likely to be dominant drivers of the water circulation in shallow and stagnant regions of the estuary. It is therefore recommended to research their influences.

Bibliography

Ahmad, L., Kanth, R. H., Parvaze, S., and Mahdi, S. S. (2017). *Experimental Agrometeorology: A Practical Manual.* Springer.

Andutta, F. P., de Miranda, L. B., Schettini, C. A. F., Siegle, E., da Silva, M. P., Izumi, V. M., and Chagas, F. M. (2013). Temporal variations of temperature, salinity and circulation in the peruípe river estuary (nova viçosa, ba). *Continental Shelf Research*, 70:36–45.

Arulananthan, K. (2000). Salinity measurements and use of the practical salinity scale (pss). *Journal of the National Aquatic Resources Research and Development Agency of Sri Lanka*, 36:80–92.

Association, A. P. H., Association, A. W. W., Federation, W. P. C., and Federation, W. E. (1915). *Standard methods for the examination of water and wastewater*, volume 2. American Public Health Association.

Beardsley, R., Limeburner, R., and Rosenfeld, L. (1983). Introduction to the code-2 moored array and large-scale data report whoi technical report 85-35. *Woods Hole Oceanographic Institution: Woods Hole, MA, USA.*

Berlamont, J. (2020). Bed roughness and friction factors in estuaries.

Bosboom, J. and Stive, M. J. (2012). *Coastal dynamics I: lectures notes CIE4305.*

Bowden, K. (1963). The mixing processes in a tidal estuary. *International Journal of Air and Water Pollution*, 7(4–5):343–356.

Boyd, R., Dalrymple, R., and Zaitlin, B. (1992). Classification of clastic coastal depositional environments. *Sedimentary Geology*, 80(3-4):139–150.

Bunbury Port Authority (2013). Realignment of preston river.

Cameron, W. and Pritchard, D. (1963). Estuaries. in 'the sea, vol. 2'.(ed. mn hill.) pp. 306–324.

Charteris, A. and Deeley, D. (2000). Hydrodynamics of leschenault inlet, western australia. *Journal of the Royal Society of Western Australia*, 83:251.

Cossu, R., Wells, M. G., and Wåhlin, A. (2010). Influence of the coriolis force on the velocity structure of gravity currents in straight submarine channel systems. *Journal of Geophysical Research: Oceans*, 115(C11).

CWT (2004). Electrical conductivity/salinity fact sheet. *The Clean Water Team Guidance Compendium for Watershed Monitoring and Assessment, Division of Water Quality, factsheet*, 3(3.0).

Damara, W. (2016). Shire of harvey coastal hazard risk management and adaptation plan - coastal hazards assessment - part two.

Davies, J. (1964). A morphogenic approach to world shorelines. *Zeitschrift fur Geomorphologie*, 8:127–142.

De Miranda, L. B., Andutta, F. P., Kjerfve, B., and de Castro Filho, B. M. (2017). *Fundamentals of estuarine physical oceanography*, volume 8. Springer.

Deltares (2020). *D-Flow Flexible Mesh*. Deltares.

DWER (2020). Data sets.

Dyakonova, T. and Khoperskov, A. (2018). Bottom friction models for shallow water equations: Manning's roughness coefficient and small-scale bottom heterogeneity. In *Journal of Physics: Conference Series*, volume 973, page 012032. IOP Publishing.

Dyer, A. (1974). A review of flux-profile relationships. *Boundary-Layer Meteorology*, 7(3):363–372.

Dyer, K. and New, A. (1986). Intermittency in estuarine mixing. In *Estuarine variability*, pages 321–339. Elsevier.

Dyer, K. R. (1977). *Lateral circulation effects in estuaries*. National Academy of Sciences.

Encyclopaedia Britannica (2015). The editors of encyclopaedia britannica. *Encyclopaedia Britannica*.

Feng, M., Weller, E., and Hill, K. (2009). The leeuwin current. *A Marine Climate Change Impacts and Adaptation Report Card for Australia*, pages 1–11.

Fischer, H. B. (1976). Mixing and dispersion in estuaries. *Annual review of fluid mechanics*, 8(1):107–133.

Fondriest Environmental, Inc. (2014). Conductivity, salinity and total dissolved solids, fundamentals of environmental measurements.

Fugate, D. and Jose, F. (2019). Forces in an estuary. *Oceanography*, 32(1):231–236.

Geyer, W. (1997). Influence of wind on dynamics and flushing of shallow estuaries. *Estuarine, coastal and shelf science*, 44(6):713–722.

Gillibrand, P., Andrewartha, J., and Herzfeld, M. (2012). *Numerical hydrodynamic modelling of the Leschenault Estuary*.

Google. Google earth pro images.

Hansen, D. V. and Rattray Jr, M. (1966). New dimensions in estuary classification 1. *Limnology and Oceanography*, 11(3):319–326.

Hardisty, J. (2007). *Estuaries: monitoring and modeling the physical system.* Number 551.4618 H3. Wiley Online Library.

Hayes, M. (1979). Barrier island morphology as a function of tidal and wave regime. in: Leatherman sp (ed) barrier islands. *Academic Press, New York*, 1:27.

Heggie, D., Skyring, G., Berelson, W., Longmore, A., and Nicholson, G. (1999). Sediment-water interaction in australian coastal environments: implications for water and sediment quality.

Huang, R. (2015). Oceanographic topics| surface/wind driven circulation.

Hugues-dit-Ciles, J., Kelsey, P., Marillier, B., Robb, M., Forbes, V., and McKenna, M. (2012). Leschenault estuary water quality improvement plan. *Perth, WA: Department of Water.*

Hunkins, K. (1981). Salt dispersion in the hudson estuary. *Journal of Physical Oceanography*, 11(5):729–738.

Ji, Z.-G. (2012). River fate and transport. In *Transport and Fate of Chemicals in the Environment*, pages 219–240. Springer.

Ji, Z.-G. (2017). *Hydrodynamics and water quality: modeling rivers, lakes, and estuaries.* John Wiley & Sons.

Ketchum, B. H. and Rawn, A. (1951). The flushing of tidal estuaries [with discussion]. *Sewage and Industrial Wastes*, pages 198–209.

Kjerfve, B. (1986). Comparative oceanography of coastal lagoons. In *Estuarine variability*, pages 63–81. Elsevier.

Kothandaraman, C. (2006). *Fundamentals of heat and mass transfer.* New Age International.

Kundu, P., Cohen, I., and Dowling, D. (2016). Fluid mechanics.

Lawrence, M. G. (2005). The relationship between relative humidity and the dewpoint temperature in moist air: A simple conversion and applications. *Bulletin of the American Meteorological Society*, 86(2):225–234.

List, E., Koh, R. C., Imberger, J., et al. (1979). Mixing in inland and coastal waters. Technical report.

Liu, L. (2018). Application of a hydrodynamic and water quality model for inland surface water systems. *Applications in Water Systems Management and Modeling*, page 87.

McKenna, M. (2004). *The Leschenault Inlet/Estuary : a changing environment / [prepared by Mike McKenna].* Dept. of Environment [Perth, W.A.].

McKenna, M. (2007). *The Leschenault Estuarine System, South-Western Australia: Condition Statement and Recommendations for Management.* Department of Water.

Miranda, L. B. d. and Castro Filho, B. M. d. (1996). On the salt transport in the cananéia sea during a spring tide experiment. *Rev. bras. oceanogr*, pages 123–133.

Nichols, M. and Biggs, R. (1985). Estuaries in: Davis ra (ed) coastal sedimentary environments, 77–186.

NRMRL (U.S.) and EMPACT Program (U.S.) (2002). *Developing and Implementing an Estuarine Water Quality Monitoring, Assessment, and Outreach Program: The MYSound Project.* U.S. Environmental Protection Agency, National Risk Management Research Laboratory, Office of Research and Development.

Pachauri, R. K., Allen, M. R., Barros, V. R., Broome, J., Cramer, W., Christ, R., Church, J. A., Clarke, L., Dahe, Q., Dasgupta, P., et al. (2014). *Climate change 2014: synthesis report. Contribution of Working Groups I, II and III to the fifth assessment report of the Intergovernmental Panel on Climate Change.* Ipcc.

Pawlowicz, R. (2013). Key physical variables in the ocean: temperature, salinity, and density. *Nature Education Knowledge*, 4(4):13.

Pearce, A., Hart, A. M., Murphy, D., and Rice, H. (2015). *Seasonal Wind Patterns Around the Western Australian Coastline and Their Application Fisheries Analysis.* Department of Fisheries.

Pepper, I. L., Gerba, C. P., and Brusseau, M. L. (2011). *Environmental and pollution science.* Elsevier.

Potter, I. C., Chuwen, B. M., Hoeksema, S. D., and Elliott, M. (2010). The concept of an estuary: a definition that incorporates systems which can become closed to the ocean and hypersaline. *Estuarine, Coastal and Shelf Science*, 87(3):497–500.

Prichard, D. (1955). Estuarine circulation patterns. *Proc. Amer. Sco. Civil Eng.*, 81:1–11.

Pritchard, D. W. (1952). Estuarine hydrography. In *Advances in geophysics*, volume 1, pages 243–280. Elsevier.

Pritchard, D. W. (1954). A study of the salt balance in a coastal plain estuary. *J. mar. Res*, 13(1):133–144.

Pritchard, D. W. (1967). What is an estuary: physical viewpoint. American Association for the Advancement of Science.

Reddy, P. J. R. (2005). *A text book of Hydrology.* Firewall Media.

Ryan, D. A., Heap, A. D., Radke, L., and Heggie, D. T. (2003). Conceptual models of australia's estuaries and coastal waterways. *Applications for coastal resource management.*

Scully, M. E., Friedrichs, C., and Brubaker, J. (2005). Control of estuarine stratification and mixing by wind-induced straining of the estuarine density field. *Estuaries*, 28(3):321–326.

Semeniuk, V., Semeniuk, T., and Unno, J. (2000). The leschenault inlet estuary: an overview. *Journal of the Royal Society of Western Australia*, 83:207.

Sverdrup, H. U., Johnson, M. W., Fleming, R. H., et al. (1942). *The Oceans: Their physics, chemistry, and general biology*, volume 7. Prentice-Hall New York.

Thomas, M. D., De Boer, A. M., Johnson, H. L., and Stevens, D. P. (2014). Spatial and temporal scales of sverdrup balance. *Journal of Physical Oceanography*, 44(10):2644–2660.

Thomson, C., Kilminster, K., Hallett, C., Valesini, F., Hipsey, M., Trayler, K., Gaughan, D., Summers, R., Syme, G., and P, S. (2017). Research and information priorities for estuary management in southwest western australia. page 87.

Tomczak, M. (1998). Shelf and coastal oceanography.

Tomczak, M. and Godfrey, J. (1994). Regional oceanography: an introduction pergamon. *New York*.

Van Leussen, W. and Dronkers, J. (1988). Physical processes in estuaries: An introduction. In *Physical processes in estuaries*, pages 1–18. Springer.

van Rijn, L. (2013). Basic hydrodynamic processes in the coastal zone.

Willmott, C. J., Ackleson, S. G., Davis, R. E., Feddema, J. J., Klink, K. M., Legates, D. R., O'donnell, J., and Rowe, C. M. (1985). Statistics for the evaluation and comparison of models. *Journal of Geophysical Research: Oceans*, 90(C5):8995–9005.

Wooltorton, S. (2013). A sense of home: a cultural geography of the leschenault estuary district: Report.

Appendix A

Literature review

A.1 Oceanic influence

The definition of an estuary stated by Potter et al. (2010) in Section 2.2.1 already implied that estuarine hydrodynamics are affected by oceans. The dynamics of shallow waters can therefore not be understood without any knowledge of the physical principles of the deep ocean. According to Tomczak and Godfrey (1994) a basic understanding of the oceanic hydrodynamics can be obtained by considering the interior pressure field, the Coriolis force and friction. These forces are the main ingredients of the most important theories of the oceanic hydrodynamics, namely geostrophic flow, Ekman layer transport and the Sverdrup balance.

A.1.1 Oceanic forcing

In Section 2.1 it became clear that hydrodynamics are mainly driven by the interior pressure field in the water column. As oceans are deep, the vertical pressure gradient in oceans is mainly dependent on the water depth and thus on the weight above a certain point in the water column (Tomczak and Godfrey, 1994). The vertical pressure gradient is therefore not of importance in deep oceans, as it does not initiate motion of water. On the contrary, horizontal pressure gradients are causing large scale circulations in oceans and can be due to thermohaline forcing and spatially varying water levels (Tomczak and Godfrey, 1994). The second important force, the Coriolis force, is the deflection of moving objects due to the Earth's rotation to the right on the Northern Hemisphere and to the left on the Southern Hemisphere (Ji, 2017). The Coriolis force is only of importance in large water bodies that are wide enough to allow a force normal to the water bodies axis (Ji, 2017). The last important force is friction, which is an essential force which governs the transfer of momentum from the atmosphere to the ocean (Tomczak, 1998). Friction is the main force behind the generation of waves and wind-driven currents on all kinds of water bodies (Tomczak and Godfrey, 1994).

A.1.2 Geostrophic flow

In deep oceans the effect of friction on currents is mostly negligible (Tomczak and Godfrey, 1994). Currents are therefore driven by a balance between the Coriolis force and the horizontal pressure gradient (Ji, 2017). This is called the geostrophic balance, which is depicted in Figure A.1. As can be seen in Figure A.1, geostrophic currents flow along isobars, with the low pressure zone on its right on the Southern Hemisphere and with the low pressure zone on its left on the Northern Hemisphere. An isobar is a line connecting points of equal atmospheric pressure (Reddy, 2005). Moreover, according to Tomczak and Godfrey (1994), the isopycnals, lines connecting points of equal density, slope upwards right of the direction of flow on the Southern Hemisphere and left of the direction of flow on the Northern Hemisphere.

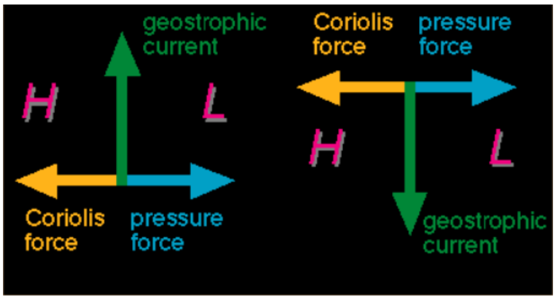

Figure A.1: Geostropic balance on Southern (left) and Northern (right) Hemisphere (Tomczak, 1998)

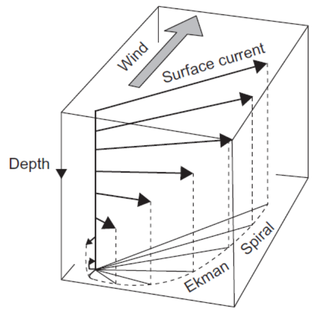

Figure A.2: Ekman layer balance on Northern Hemisphere, the reverse applies on Southern Hemisphere (Huang, 2015)

A.1.3 Ekman layer

The Ekman layer can be defined as a boundary layer of an ocean where the Coriolis force is balanced by a frictional force (Huang, 2015). In Figure A.4, the Surface Ekman layer is depicted generated by a wind stress on the ocean's surface. A frictional stress on the surface counteracts the winds stress, which subsequently causes the transfer of momentum from the atmosphere to the ocean (Tomczak and Godfrey, 1994). The earth's rotation results in a force called the Coriolis force, perpendicularly directed to the wind stress and causes the surface current to bend 45° from the wind direction (Tomczak and Godfrey, 1994).
In Figure A.2 it can clearly be seen that the current deflects further from the wind direction down the water column. As is mentioned by Huang (2015) the Ekman layer can occur in a water column as long there is a horizontal frictional stress. To satisfy the balance between Coriolis and friction, the interior pressure field is assumed to be equal (Huang, 2015). This means the balance assumes that there is no stratification in the water column and the surface is horizontal (Tomczak and Godfrey, 1994). According to Tomczak and Godfrey (1994), this is often satisfied as wind is causing turbulent mixing in the surface layer, resulting in a balance between friction and Coriolis. The average transport of water in the Ekman layer is pointed perpendicular and to the right of the wind direction on the Northern Hemisphere and to the left of the wind direction on the Southern Hemisphere, as is depicted in Figure A.2. It should be noted that this mechanism applies to a relationship

between the wind direction and the direction of the Ekman layer transport and not the current in the Ekman layer (Tomczak and Godfrey, 1994).

A.1.4 Sverdrup balance

The Sverdrup balance can best be described as a balance between the wind stress curl, which is the rotation in the wind field around the vertical axis, and the depth-integrated transport of water in oceans (Thomas et al., 2014). It combines the frictional, pressure and Coriolis force, into a single balance and is the main theory behind the large scale oceanic circulation (Tomczak and Godfrey, 1994). It states that friction is only of importance in the Ekman layer and friction is zero below the Ekman layer (Tomczak and Godfrey, 1994). Two important phenomena are caused by wind and drive the oceanic circulation, namely Ekman pumping and Ekman suction, shown in Figure A.3. In case of Ekman pumping, wind is causing surface divergence (an area where the water surface is depressed), which raises the water from the interior layer up into the Ekman layer in a process called upwelling (Encyclopaedia Britannica, 2015). In case of Ekman suction, wind is causing surface convergence (an area where water flows meet and result in an accumulation of water), which pushes the water from the Ekman layer down the water column in a process called downdwelling (Encyclopaedia Britannica, 2015).

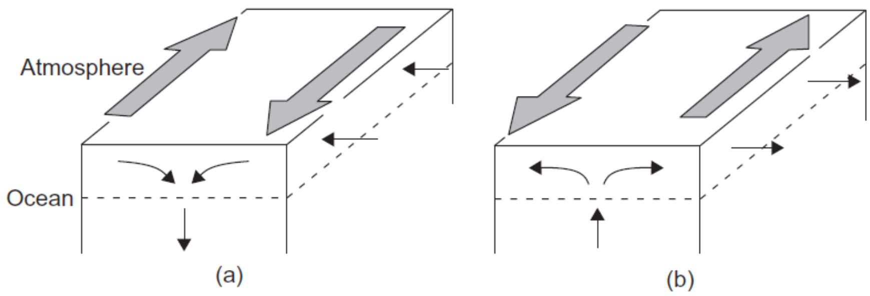

Figure A.3: (a) Ekman pumping (b) Ekman suction; on Northern Hemisphere (Huang, 2015)

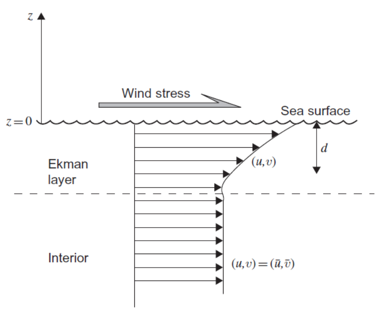

Figure A.4: The Surface Ekman layer produced by a wind stress on the surface (Huang, 2015)

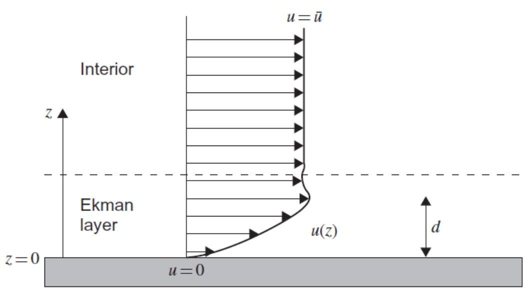

Figure A.5: The Bottom Ekman layer generated by a frictional force at the bottom (Huang, 2015)

A.1.5 Friction

As any layer with a horizontal frictional stress can in theory be an Ekman layer according to Huang (2015), the bottom layer can also be called an Ekman layer. In Figure A.5, the Bottom Ekman layer is depicted for an idealised situation with a flat bottom and an uniform flow in a rotating framework. Tomczak and Godfrey (1994) explained that the Ekman spiral depicted in Figure A.2, can be observed in water depths of 1.25 times the Ekman layer height. In water depths of 1 to 0.5 times the Ekman layer height, the current is getting more in line with the wind direction as the influence of Coriolis becomes less and the influence of the wind stress and the frictional stress becomes more in shallower depths (Tomczak and Godfrey, 1994). The deformation of the Ekman layer spiral over different depths is depicted in Figure A.6. In water bodies with water depths of 0.2 times the Ekman layer height, the Coriolis effect becomes negligibly small and the current is controlled by the wind stress and bottom friction (Tomczak and Godfrey, 1994). In this case, the Ekman layer transport is directed in the direction of the wind.

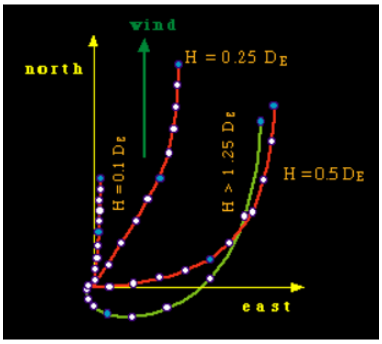

Figure A.6: Ekman layer transport for different depths (Tomczak, 1998)

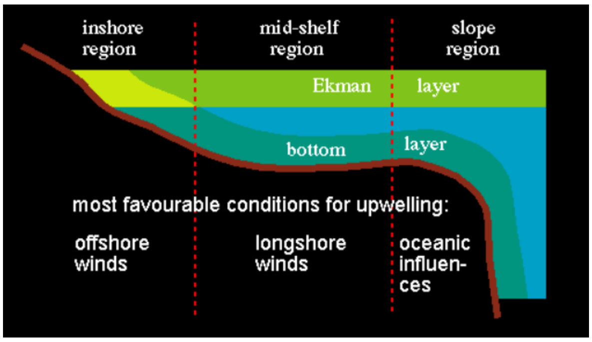

Figure A.7: Different coastal zones based on their upwelling dynamics (Tomczak, 1998)

A.1.6 Downdwelling and upwelling

The upwelling and downdwelling processes in the deep ocean have already been expounded in Section A.1. However, the impact of downdwelling and upwelling is an order of magnitude higher in coastal regions and the driving forces differ from the deep ocean (Tomczak, 1998). As can be seen in Figure A.7, the coast can be divided in three regions according to Tomczak (1998), the inshore region, the mid-shelf region and the slope region. The inner shore is the region where the Ekman current is directed in the direction of the wind as is explained in Section 2.2.2. The dominant process controlling upwelling and downdwelling in the inner region is therefore offshore and onshore wind respectively (Tomczak, 1998). In case of downdwelling an onshore wind is causing an onshore surface current and an offshore bottom current. This means warmer and fresher surface water is transported to the coast and pushed to the bottom near the coast, where it is transported offshore. In an upwelling event, offshore wind is producing surface water movement away from the coast and an onshore bottom current. This means saltier and colder water is transported from the bottom layer to the surface layer near the coast. In contrast, the warmer and fresher surface water is moved away from the coast. In the mid-shelf region, the influence of the frictional stress in the bottom layer becomes less noticeable, which means the Ekman spiral is present here.

In the mid-shelf region, the upwelling and downdwelling are mainly driven by alongshore winds (Tomczak, 1998). In this situation transport of water is deflected to the right of the wind direction on the Northern Hemisphere and to the left on the Southern Hemisphere. It therefore depends on the wind direction if upwelling or downdwelling is experienced. The most outer region, the slope region, experience downdwelling and upwelling affected by winds also, but has some additional drivers (Tomczak, 1998). The first mechanism is dynamic uplift, which is a shift of the thermocline's position caused by variations of the position of a current or eddy formations (Tomczak, 1998). The second mechanism explained by Tomczak (1998) is tidal pumping, which is the amplification of the tidal current and causes significant turbulence.

A.1.7 Sea level variation

Tomczak (1998) explained that the presence of coasts obstruct the free flow of oceanic currents, which results in the accumulation of water near coasts. Whereas accumulations of water in deep oceans is usually of small duration due to Ekman pumping, the presence of coasts allow longer periods of accumulations due to the supportive character of the coast (Tomczak, 1998). This accumulation of water along the coast, lead to sea level variations and thus horizontal pressure gradients. Subsequently, the horizontal pressure gradients indicate the presence of alongshore currents. According to van Rijn (2013), four types of currents exist in the vicinity of the coastal zone: tide-, wind-, density- and wave-induced currents. Wave-induced currents are out of the thesis' scope, but are of significant importance in the hydrodynamics of estuaries. Tidal currents have briefly been explained in Section 2.2.2. However, it should be noted that tidal currents are affected by processes like refraction, reflection, damping, Coriolis and shoaling, which have impact on the amplitude and propagation of the tidal waves (van Rijn, 2013). Due to reflection and Coriolis the tidal currents propagate around a amphidromic point in amphidromic systems and due to shoaling and bottom friction the tidal amplitude is increased (van Rijn, 2013). Wind generated currents can be subdivided in two categories as is explained by van Rijn (2013): local wind drift currents and large-scale circulation systems. Tomczak (1998) defined local wind generated currents as currents generated by sea level set-up and large scale wind generated circulations as Kelvin waves and coastal trapped waves.

A.2 Geomorphic classifications

Geomorphology is "the study of the nature and history of landforms and the processes which create them" (Ryan et al., 2003). The advantage of geomorphic characteristics is that they are easily observed by the eye and provides a fundament for biological and ecological research (Ryan et al., 2003). One of the first estuarine classifications was conducted by Pritchard (1952, 1967) as is stated in De Miranda et al. (2017) and considered these geomorphic characteristics to categorize estuaries. This lead to the classification of estuaries into fjords, coastal plains, bar built estuaries (coastal lagoons) and tectonically created estuaries (De Miranda et al., 2017). Boyd et al. (1992) defined a more extensive geomorphic classification system based on the three driving forces of coastal geomorphology: waves, tides and river discharge. This resulted in the process-based triangular diagram depicted in Figure A.8. Here, seven different estuary types can be distinguished based on their fluvial power and their relative power between waves and tides (Boyd et al., 1992). Ryan et al. (2003) used this process-based framework in their conceptual model to classify Australia's coastal waterways. The conceptual model developed by Ryan et al. (2003), used in Chapter 3, combines geomorphic, environmental and climatic classification systems to describe the hydrodynamics, morphodynamics and nutrients dynamics of the coastal waterways. In this way it is easier for managers to make well-founded decisions. However, between the geomorphic classified coastal waterways, but even in a single coastal waterway, the hydrodynamics like circulation patterns, mixing processes and salinity stratification are highly variable (De Miranda et al., 2017). This underlines the need for hydrodynamic classification systems to be able to really understand the dynamics of estuaries.

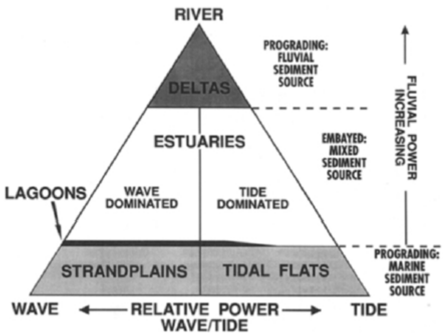

Figure A.8: Estuarine classification (Boyd et al., 1992)

Appendix B

Data

B.1 Tidal constituents

	2016		2017		2018		2019		2020	
Constituent	A [m]	ϕ [°]	A [m]	ϕ [°]	A [m]	ϕ [°]	A [m]	ϕ [°]	A [m]	ϕ [°]
K1	0.175	301.6	0.175	301.6	0.175	301.6	0.175	301.5	0.175	301.5
O1	0.12	288.5	0.12	288.5	0.2	288.5	0.12	288.5	0.12	288.5
SA	0.111	69.9	0.111	70.2	0.111	69.7	0.111	70	0.109	70.2
M2	0.057	299.6	0.057	299.7	0.057	299.7	0.057	299.6	0.057	299.5
S2	0.052	300.7	0.052	300.8	0.052	300.8	0.052	300.7	0.052	300.6
P1	0.051	291.2	0.051	291.3	0.051	291.3	0.051	291.2	0.051	291.2
Q1	0.03	278	0.03	278.1	0.03	278.1	0.029	278.2	0.029	278.3
SSA	0.028	156	0.028	156	0.027	154.9	0.027	155.2	0.027	155.3
S1	0.022	44.2	0.022	44.2	0.022	44.2	0.022	44.3	0.022	44.2
N2	0.02	341.9	0.02	342.2	0.019	342.4	0.019	342.4	0.019	342.4
2MS6	0.008	75.7	0.008	75.4	0.008	75.6	0.008	75.8	0.008	75.8
MU2	0.008	322.7	0.008	322.7	0.008	322.6	0.008	322.7	0.008	322.8
M4	0.007	283.3	0.007	283.4	0.007	283.4	0.007	283.3	0.007	283.2
MF	0.006	91.5	0.006	84.5	0.006	86.6	0.006	89.1	0.006	85.8
MSF	0.005	296.9	0.006	289	0.006	296	0.006	296.7	0.005	290.8
2N2	0.005	314.3	0.005	314.5	0.005	314.7	0.005	314.9	0.005	314.9
MM	0.005	246.9	0.005	256.1	0.005	252	0.005	240.9	0.005	235.5
MS4	0.005	6	0.005	6.3	0.005	6.2	0.005	5.8	0.005	5.8
L2	0.004	281	0.004	280.9	0.004	281	0.004	281.2	0.004	281.6
NU2	0.003	340.6	0.003	340.9	0.003	342.4	0.003	341.5	0.003	341.8
T2	0.002	298.5	0.002	297.5	0.002	299.2	0.002	298.8	0.002	299

Table B.1: Amplitude (A) and Phase(°) measured by DWER of all tidal constituents present at Bunbury Port

Constituent	A [m]	ϕ [°]
J1	0.008	333
K1	0.168	298
K2	0.016	288
M2	0.054	292
MF	0.033	73
MM	0.017	200
MSF	0.028	321
MSM	0.033	34
MU2	0.008	301
N2	0.018	337
O1	0.12	283
P1	0.051	290
Q1	0.032	269
S2	0.048	293

Table B.2: Amplitude (A) and Phase(°) calculated by Gillibrand et al. (2012) of the major tidal constituents present at the Bunbury Port

Appendix C

Model set-up

C.1 Output parameters

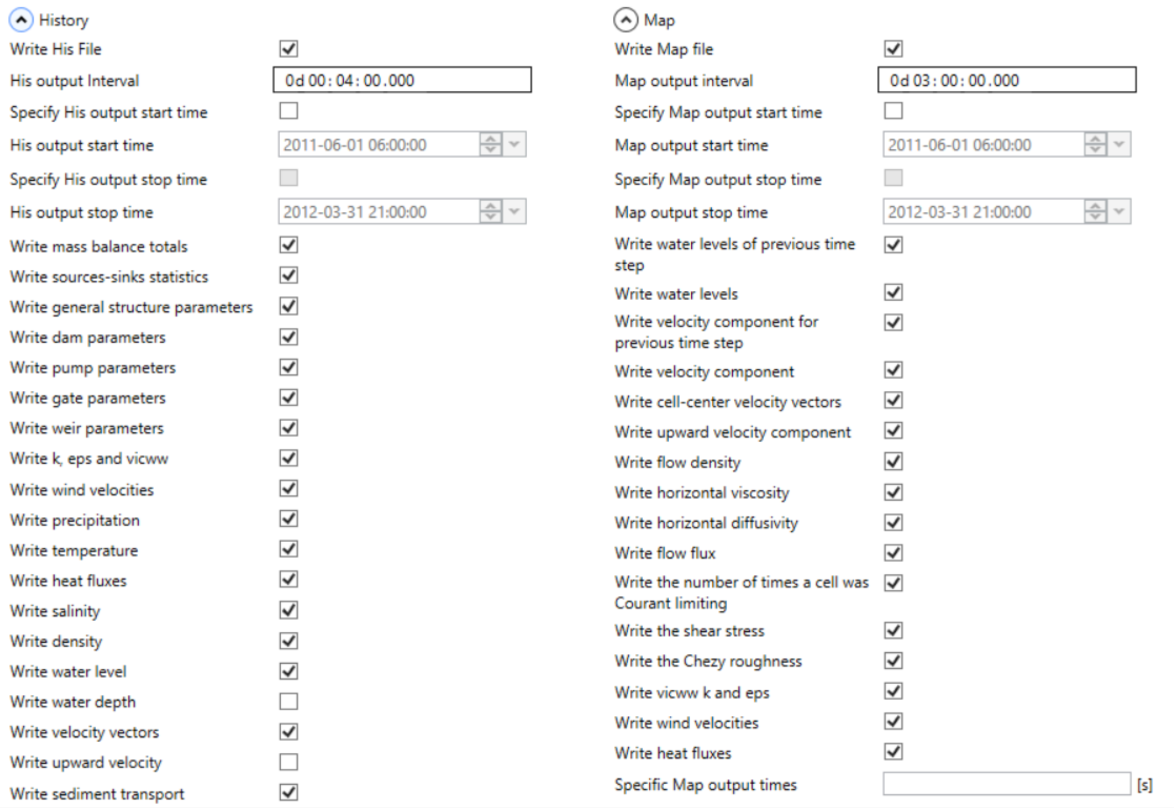

Figure C.1: Output parameters page 1

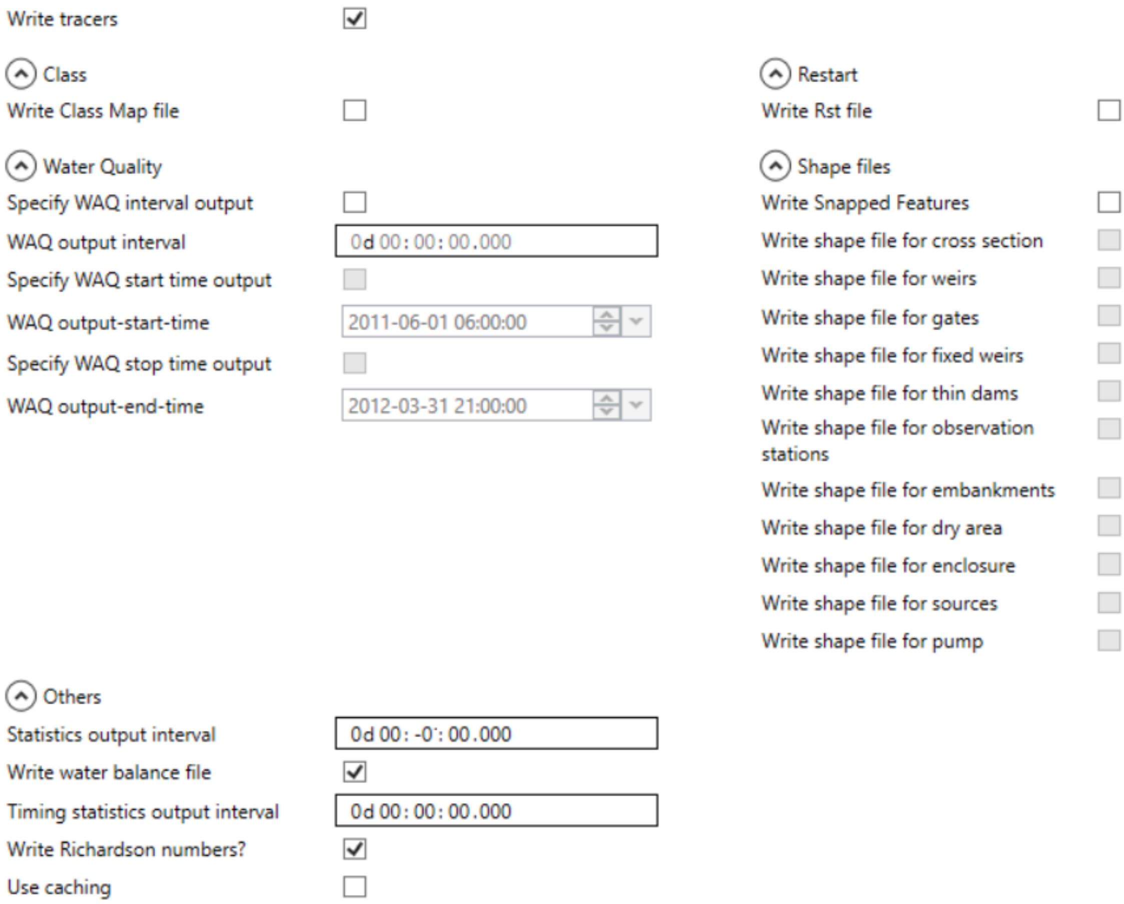

Figure C.2: Output parameters page 2

C.2 Miscellaneous

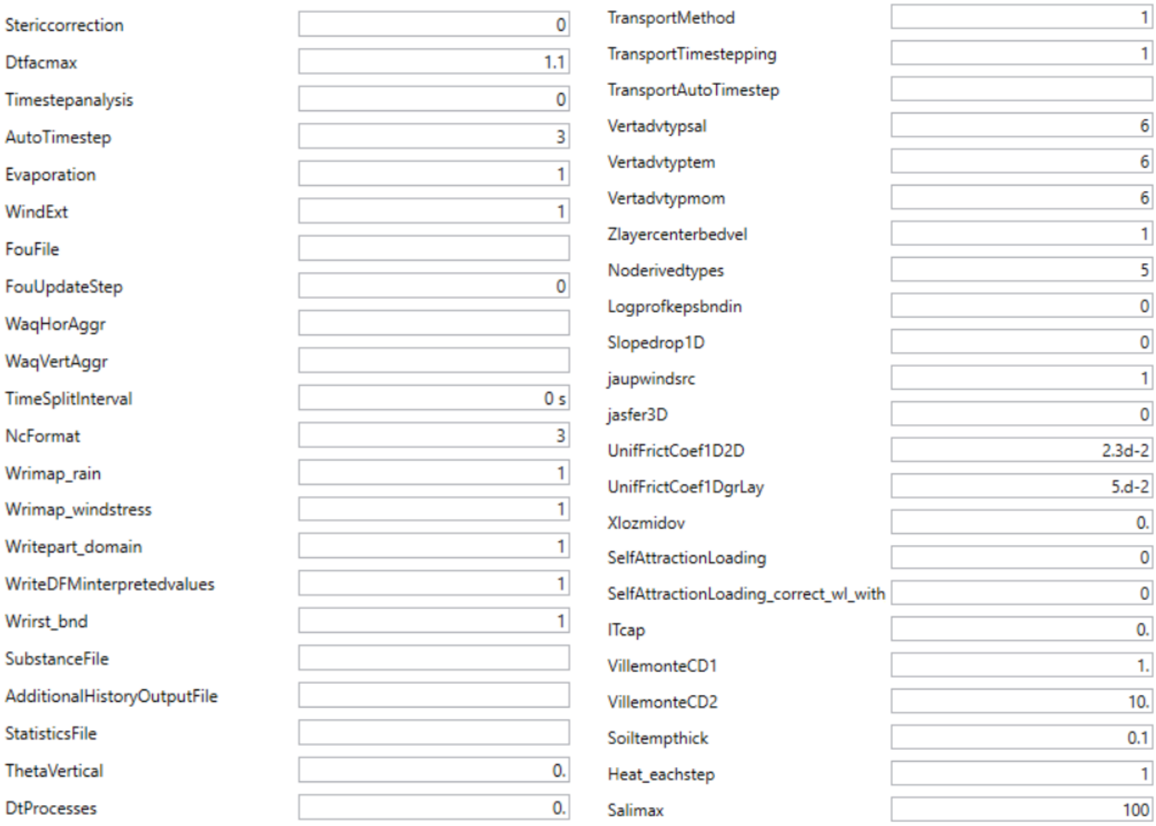

Figure C.3: Miscellaneous page 1 (left) and miscellaneous page 2 (right)

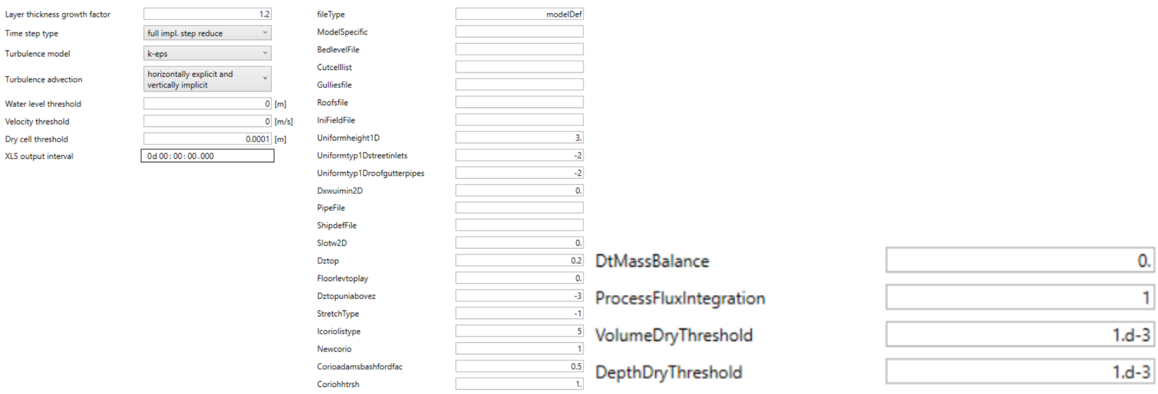

Figure C.4: Miscellaneous page 3 (left) and miscellaneous page 4 (right)

Appendix D

Calibration & validation

D.1 CSIRO-model validation

The CSIRO-model of 2012, expounded in Gillibrand et al. (2012), is calibrated and validated against observed data collected at six different observation locations, which are also considered in this research. However, the naming of the observation points is different: Bunbury is OUTER1, Collie is COLLIE1, Cut is ESTUARY1, Estuary 3 is ESTUARY4, Estuary 6 is ESTUARY3 and South Estuary is ESTUARY2. The modelled waterlevel is validated at one observation point, Bunbury. The modelled salinity and temperature are validated at six observation points, namely: Collie (bed and surface), Cut, Estuary 3, Estuary 6 and South Estuary.

D.1.1 CSIRO waterlevel

The waterlevel data at the Bunbury Port, generated with the CSIRO-model, is depicted in Figure D.1 and is validated against observed data. The index of agreement of Willmott et al. (1985) is 0.99 and the RMSE is 0.05 m. The modelled waterlevel of the CSIRO-model is therefore in good agreement with the observed data.

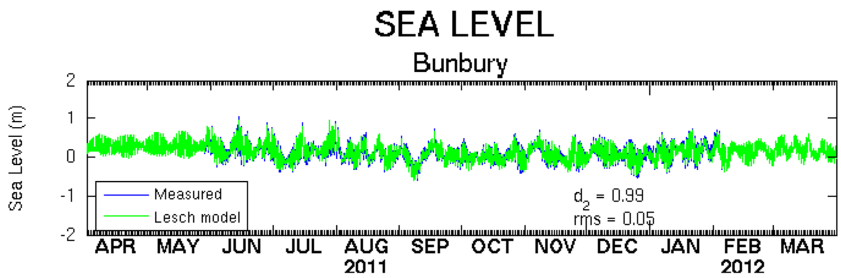

Figure D.1: CSIRO-model waterlevel at Bunbury Port validated against observed data

D.1.2 CSIRO salinity

The CSIRO salinity output correctly simulates the main physics of the estuarine salinity as can be seen in Figure D.2. However, the saline ocean water does not seem to penetrate all the way up the Collie River. Gillibrand et al. (2012) blamed this on the coarse vertical resolution of the model grid in the rivers. A vertical grid size of 0.5 *m* is considered in the CSIRO-model, while the river is less than a meter deep at some points. Besides, the salinity in the central and northern basin (Estuary 6 and Estuary 3 respectively) is lower than the observed data. Gillibrand et al. (2012) blamed this on the overestimation of the freshwater discharge of the Parkfield Drain. Overall, the index of agreement is around 0.8 and a RMSE of 2-6 PSU (10-25% of the weighted average) in the estuary. For the Collie River these values are higher indicating a worse agreement.

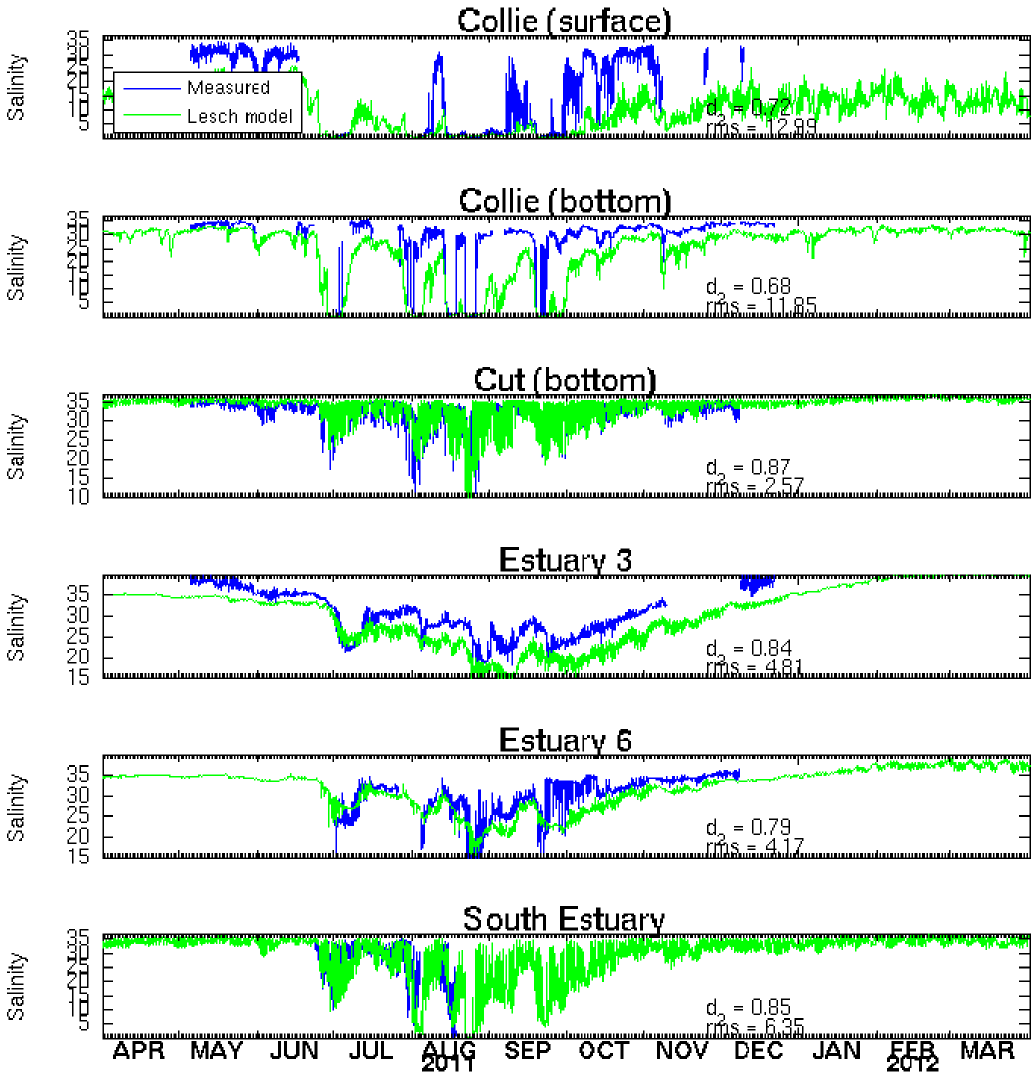

Figure D.2: CSIRO-model salinity at Bunbury Port validated against observed data

D.1.3 CSIRO temperature

The CSIRO-model temperature output is in good agreement with the observed temperature data as can be seen in Figure D.3. The index of agreement of Willmott et al. (1985) is typically higher than 0.9 and the RMSE is around 1 °C (less than 10% of the weighted average). This emphasizes the reliability of the model in simulating the temperature correctly.

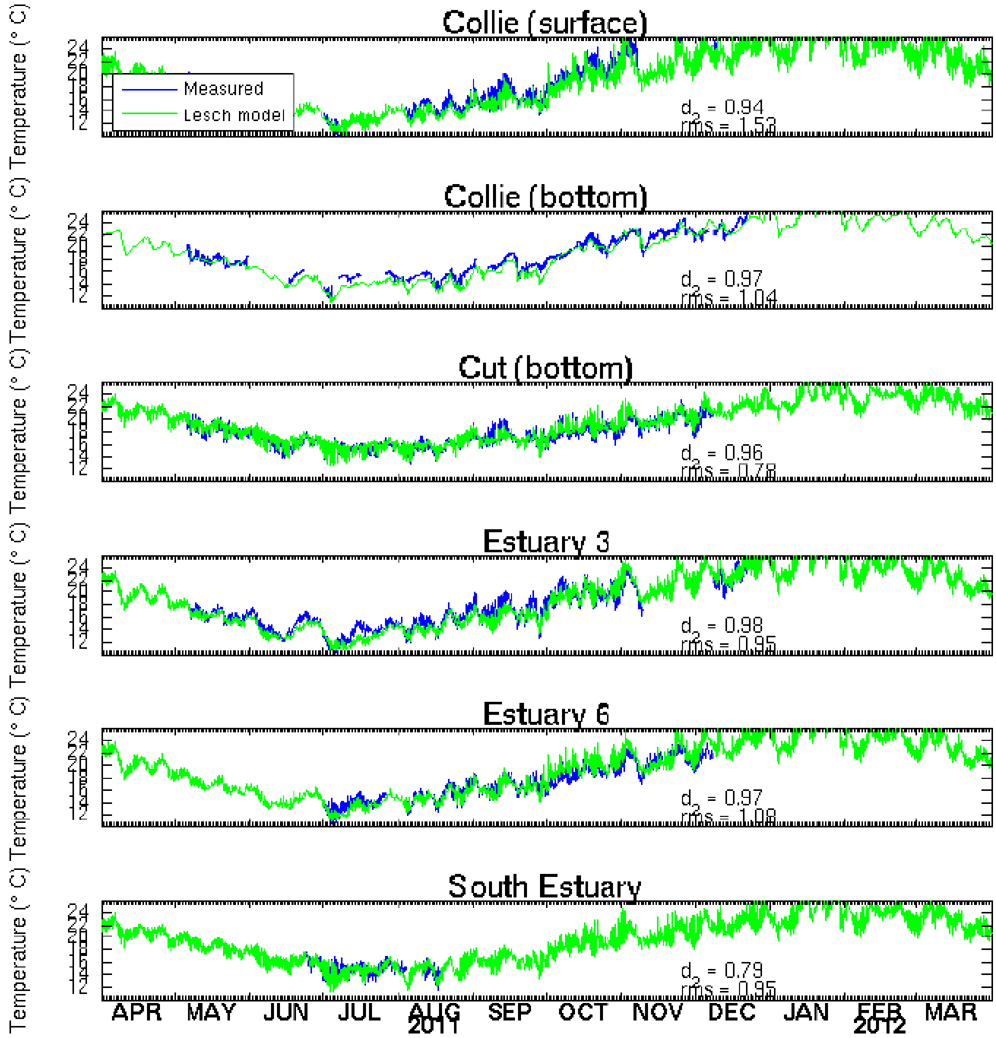

Figure D.3: CSIRO-model temperature at Bunbury Port validated against observed data

D.2 Salinity

The modelled salinity was validated against salinity data collected at six different observation points: ESTUARY1 (Figure D.4), ESTUARY2 (Figure D.5), ESTUARY3 (Figure D.6), ESTUARY4 (Figure D.7), COLLIE1BED (Figure D.8) and COLLIE1SURFACE (Figure D.9).

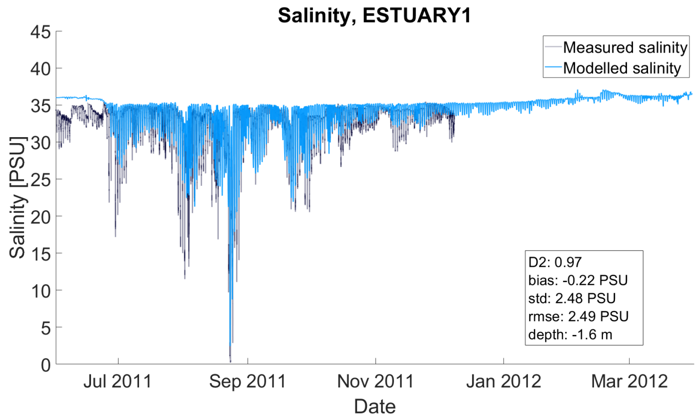

Figure D.4: Modelled and observed salinity values for observation point ESTUARY1

Salinity - ESTUARY1

The simulated salinity at ESTUARY1 was in good agreement with the observed data (Figure D.4). The d_2 was equal to 0.97 and RMSE to 2.49 PSU (less than 10% of the weighted average). Compared to the CSIRO-model (d_2 of 0.87 and RMSE of 2.57 PSU) the DFM-output is in better agreement with the observed data.

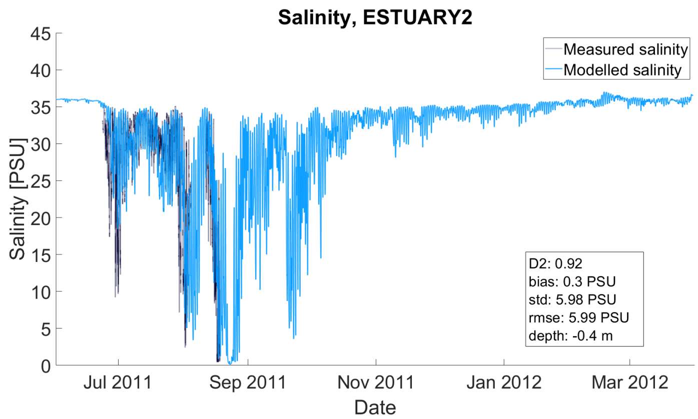

Figure D.5: Modelled and observed salinity values for observation point ESTUARY2

Salinity - ESTUARY2

The salinity generated with the DFM-model at observation point ESTUARY2 was also in good agreement with the observed data (Figure D.5). However, less observed data were available, what reduced the reliability of the statistics. The d_2 was equal to 0.92 and RMSE to 5.99 PSU (around 20% of the weighted average). Compared to the CSIRO-model (d_2 of 0.85 and RMSE of 6.35 PSU) the DFM-output presented a better agreement with the observed data.

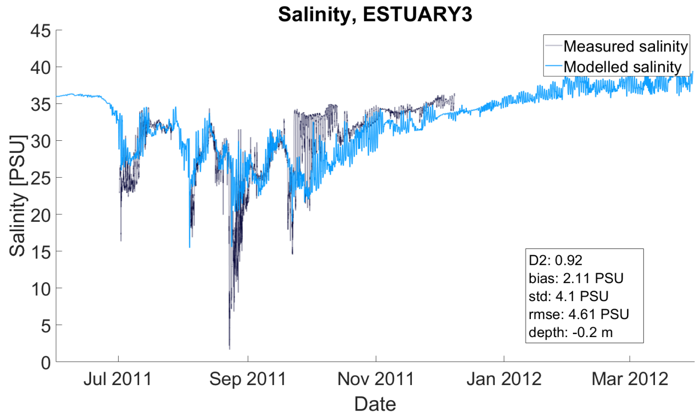

Figure D.6: Modelled and observed salinity values for observation point ESTUARY3

Salinity - ESTUARY3

The modelled salinity at ESTUARY3 represents the general variability of the observed salinity (Figure D.6). However, the second half of the dataset has lower salinity values than observed, which could indicate an excess of freshwater discharge or an underestimation of the evaporation in the central basin. The d_2 was equal to 0.92 and the RMSE to 4.61 PSU (around 15% of the weighted average). Compared to the CSIRO-model (d_2 of 0.79 and RMSE of 4.17 PSU), the DFM-output had similar performance.

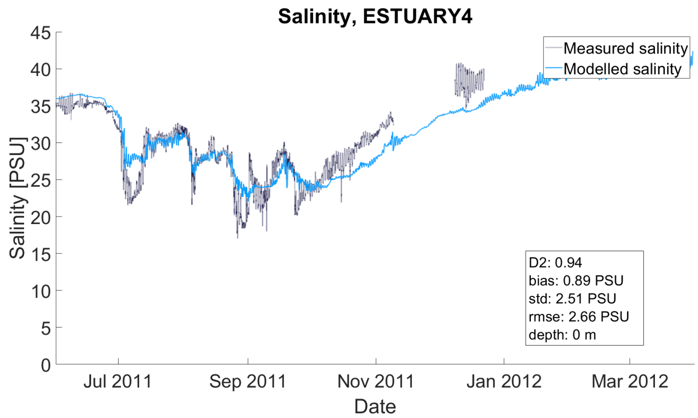

Figure D.7: Modelled and observed salinity values for observation point ESTUARY4

Salinity - ESTUARY4

The modelled salinity at observation point ESTUARY4 compared well with the observed data (Figure D.7). Similarly to ESTUARY3, the salinity values were underestimated from the beginning of November 2011 until March 2012. The d_2 was equal to 0.94 and the RMSE to 2.66 PSU (less than 10% of the weighted average). Compared to the CSIRO-model (d_2

of 0.84 and RMSE of 4.81 PSU) the DFM-output performed better. It can clearly be seen that in the first half of the period the salinity matched well the observed data. In the second half of the year, the salinity was underestimated. This could possibly indicate that the model is underestimating the evaporation in summer or the freshwater input is too high in summer.

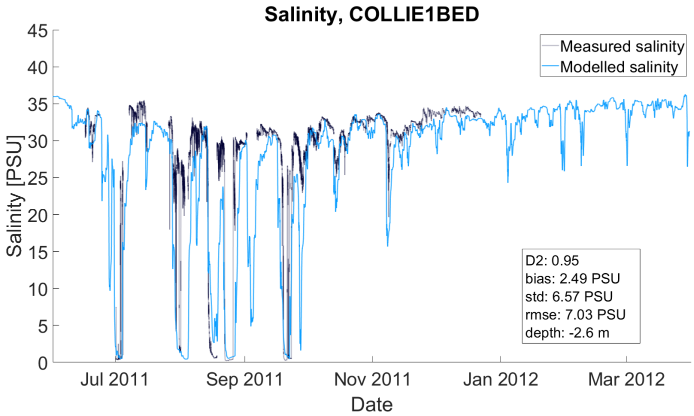

Figure D.8: Modelled and observed salinity values for observation point COLLIE1BED

Salinity - COLLIE1BED

At observation point COLLIE1BED the modelled salinity data matched the observed data well (Figure D.8). Despite some errors, the modelled salinity shows the same variability as the observed data. Gillibrand et al. (2012) concluded that due to the highly dynamic character of the Collie River it is difficult to correctly model the salinity inside the Collie River. Small errors in the input of the model can lead to major errors in the model output of the Collie River. The d_2 was equal to 0.95 and the RMSE to 7.03 PSU (around 25% of the weighted average). Compared to the CSIRO-model (d_2 of 0.68 and RMSE of 11.85 PSU) the DFM-output represented a great improvement. This can clearly be seen by comparing Figure D.8 with Figure D.2.

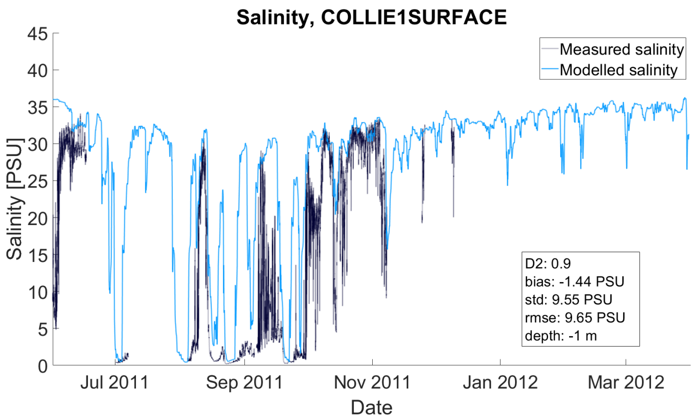

Figure D.9: Modelled and observed salinity values for observation point COLLIE1SURFACE

Salinity - COLLIE1SURFACE

The modelled salinity of observation point COLLIE1SURFACE sufficiently matches the observed data as can be seen in Figure D.9 (right). The same difficulties were encountered for this observation point as for COLLIE1BED. The d_2 was equal to 0.9 and the RMSE to 9.65 PSU (around 33% of the weighted average). Compared to the CSIRO-model (d_2 of 0.72 and RMSE of 12.99 PSU) the DFM-output is in much better agreement with the observed data.

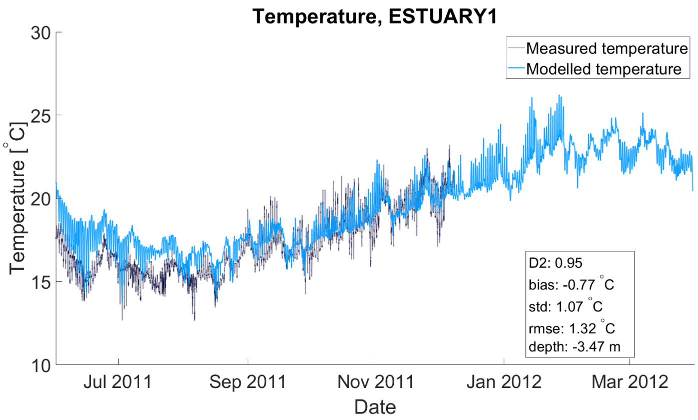

Figure D.10: Modelled and observed temperature values for observation point ESTUARY1

D.3 Temperature

The modelled temperature were validated against data collected at observation point ESTUARY1, ESTUARY2, ESTUARY3, ESTUARY4 , COLLIE1BED and COLLIE1SURFACE.

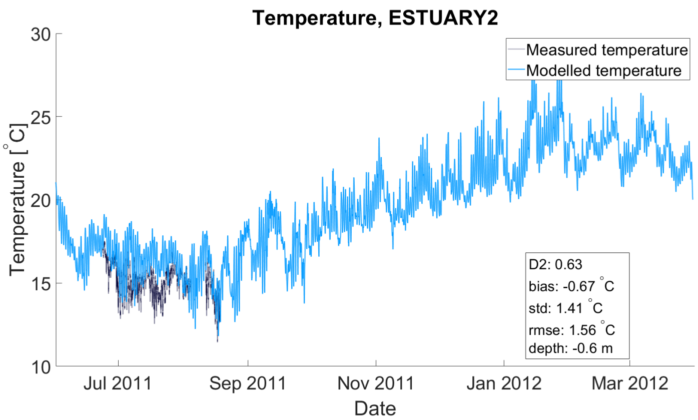

Figure D.11: Modelled and observed temperature values for observation point ESTUARY2

Temperature - ESTUARY1

The modelled temperature at ESTUARY1 matched the observed data well (Figure D.10). Temperature was slightly overestimated in the first two months, probably because of the initial conditions. A good agreement was observed for the remaining period. The d_2 was equal to 0.95 and the RMSE to 1.32 °C (less than 10% of the weighted average). These results were similar to the CSIRO-model (d_2 of 0.96 and RMSE of 0.78 °C).

Temperature - ESTUARY2

The temperature generated with the DFM-model at ESTUARY2 was slightly overestimated (Figure D.11). Due to the limited amount of data collected at this point, the reliability of the statistics is small. The d_2 was equal to 0.63 and the RMSE to 1.56 °C (less than 10% of the weighted average). Compared to the CSIRO-model (d_2 of 0.79 and RMSE of 0.95 °C) the DFM-output was slightly worse.

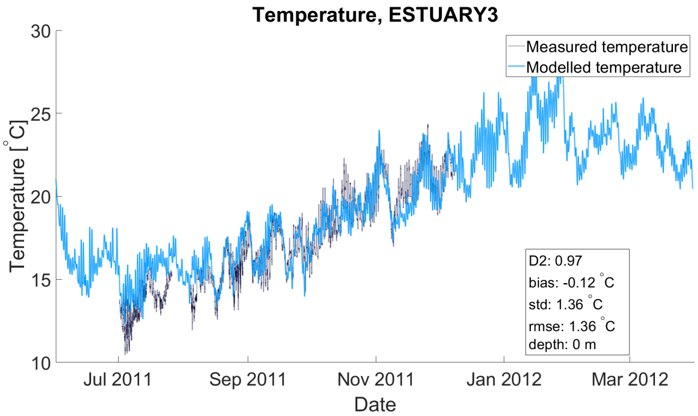

Figure D.12: Modelled and observed temperature values for observation point ESTUARY3

Temperature - ESTUARY3

The temperature modelled at ESTUARY3 agreed well with the observations (Figure D.12). The temperature was only momentarily overestimated around August. The d_2 was equal to 0.97 and the RMSE to 1.36 °C (less than 10% of the weighted average), with similar performance to the CSIRO-model (d_2 of 0.97 and RMSE of 1.08 °C).

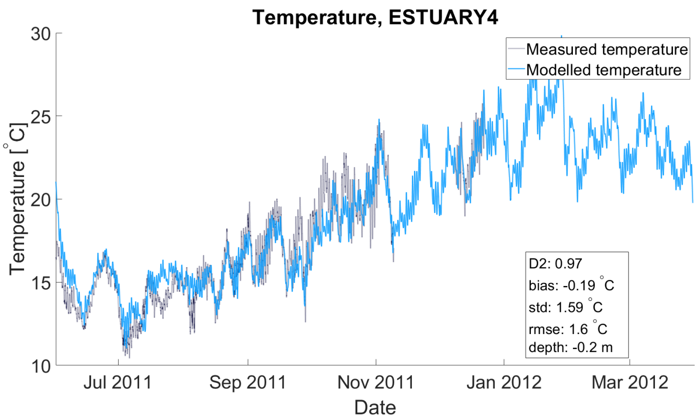

Figure D.13: Modelled and observed temperature values for observation point ESTUARY4

Temperature - ESTUARY4

The modelled temperature at ESTUARY4 matched the observations well (Figure D.13). The temperature was overestimated around August. The d_2 was equal to 0.97 and the RMSE to 1.6 °C (less than 10% of the weighted average), similarly to CSIRO-model performance (d_2 of 0.98 and RMSE of 0.95 °C).

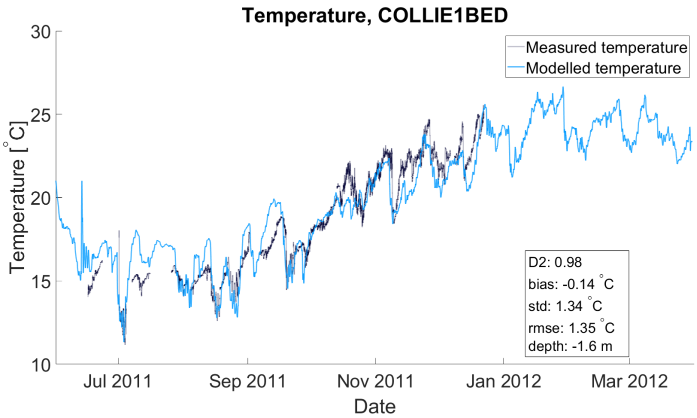

Figure D.14: Modelled and observed temperature values for observation point COLLIE1BED

Temperature - COLLIE1BED

Despite a slight overestimation of the temperature at the beginning of the considered period and a slight underestimation at the end of the period, the DFM-model temperature at COLLIE1SURFACE showed a good agreement with the observed data (Figure D.14). The d_2 was equal to 0.98 and the RMSE to 1.35 °C (less than 10% of the weighted average). Compared to the CSIRO-model (d_2 of 0.97 and RMSE of 1.04 °C) the DFM-output had similar performance.

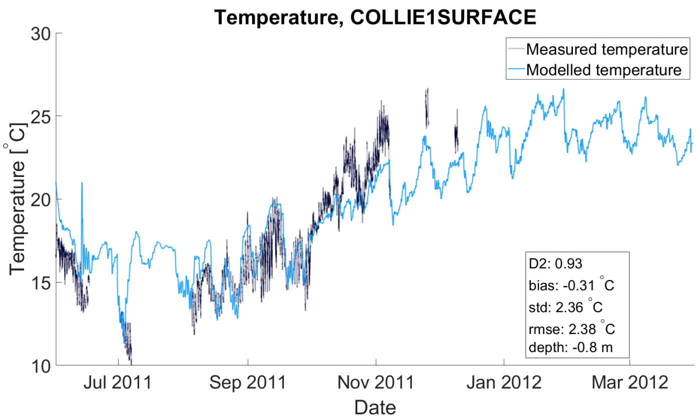

Figure D.15: Modelled and observed temperature values for observation point COLLIE1SURFACE

Temperature - COLLIE1SURFACE

The temperature of the DFM-model at COLLIE1SURFACE is shown in Figure D.15 (right). The temperature is quite off at the beginning, which is probably due to the overestimation of the initial water temperature. In the second half of the considered period the temperature was underestimated. The d_2 was equal to 0.93 and RMSE to 2.38 °C (less than 15% of the weighted average). Compared to the CSIRO-model (d_2 of 0.94 and RMSE of 1.53 °C) the DFM-output performed slightly worse.

Appendix E

Model results

E.1 Tidal analysis

Charteris and Deeley (2000) and Gillibrand et al. (2012) both discovered a tidal phase lag between the ocean and the estuary. Charteris and Deeley (2000) found a phase lag of 4 and 7 hours between the high and low water levels in the ocean and the Leschenault estuary respectively. Gillibrand et al. (2012) found a phase lag of 2 and 6 hours between the Bunbury Harbour and the Leschenault Estuary for high and low water respectively. Charteris and Deeley (2000) also described the restrictive character of the 'Cut', which damps the tidal wave inside the estuary and the rivers. In Figure E.1, E.2, E.3 and E.4, the water levels at OUTER1 and ESTUARY4 are presented for a typical neap tidal cycle in winter, spring tidal cycle in winter, neap tidal cycle in summer and spring tidal cycle in summer, respectively. The ebb water levels show a phase lag of approximately 1 to 2 hours between the Bunbury Harbour and the Leschenault Estuary. The flood water levels show a phase lag of approximately 0 to 1 hours between the harbour and the estuary. The tidal wave does not seem to be dampened significantly by the estuary's entrance. The verified modelled salinity values of the estuary in Chapter 5, indicate that the salt transportation is correctly modelled. This could therefore indicate that the tidal wave propagation in the CSIRO-model was underestimated due to an overpronounciation of the tidal damping and restriction of the 'Cut'. Tides play a dominant role in the hydrodynamics of the Leschenault Estuary.

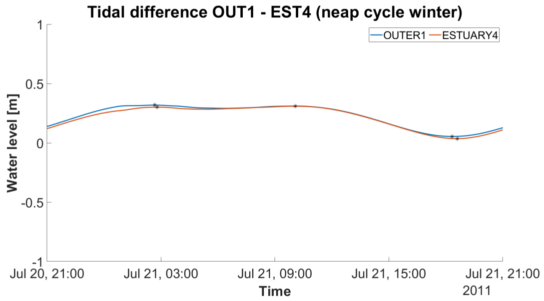

Figure E.1: Tidal difference between OUTER1 and ESTUARY4 (neap tidal cycle in winter), the black asterisks indicate the maximum troughs and crests

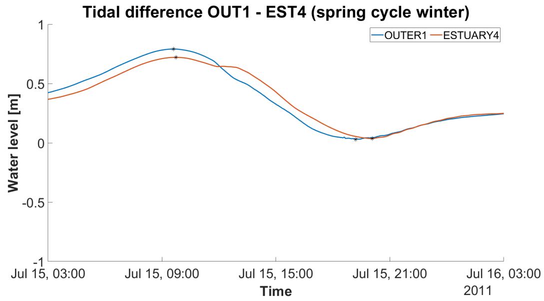

Figure E.2: Tidal difference between OUTER1 and ESTUARY4 (spring tidal cycle in winter), the black asterisks indicate the maximum troughs and crests

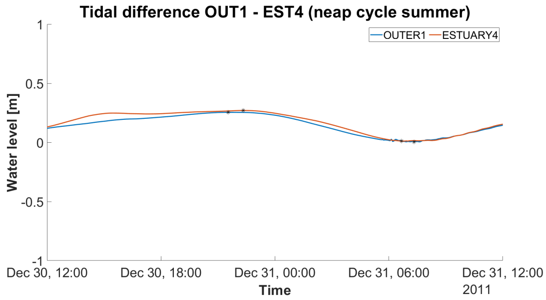

Figure E.3: Tidal difference between OUTER1 and ESTUARY4 (neap tidal cycle in summer), the black asterisks indicate the maximum troughs and crests

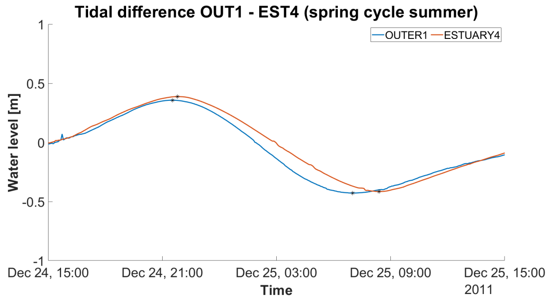

Figure E.4: Tidal difference between OUTER1 and ESTUARY4 (spring tidal cycle in summer), the black asterisks indicate the maximum troughs and crests

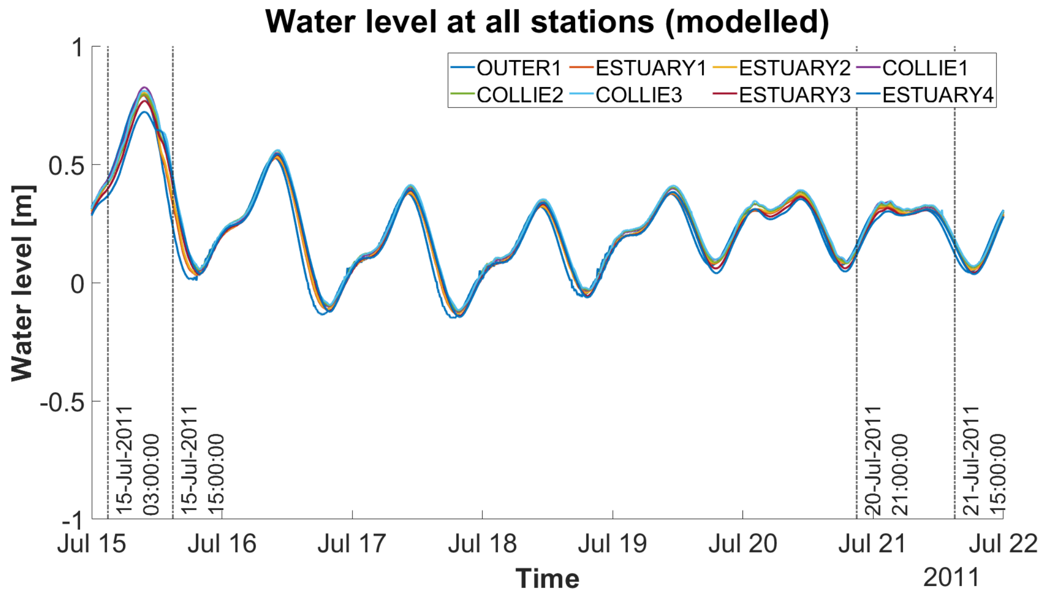

Figure E.5: Water levels at all stations in the Leschenault Estuary during a typical winter period

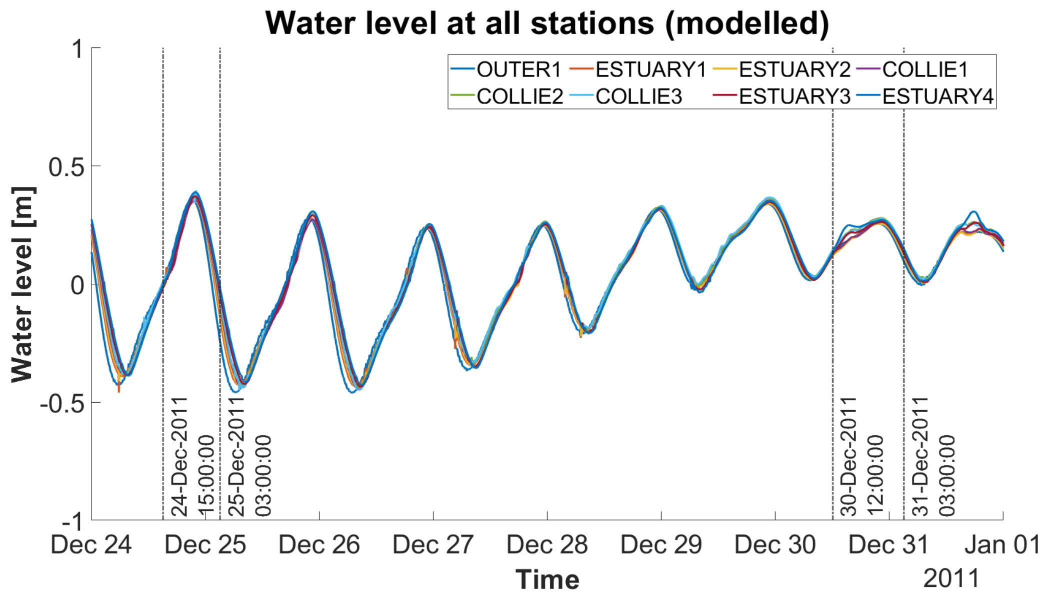

Figure E.6: Water levels at all stations in the Leschenault Estuary during a typical summer period

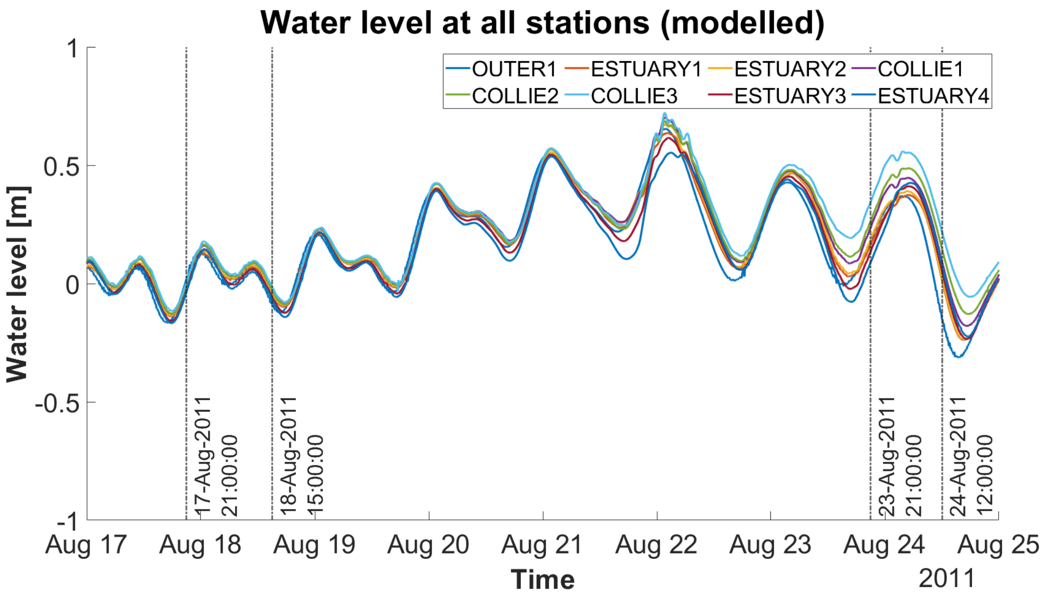

Figure E.7: Water levels at all stations in the Leschenault Estuary during a peak flow neap-spring period

Appendix F

Scenario: Preston River Alignment

F.1 Water property anomalies

F.1.1 Waterlevel

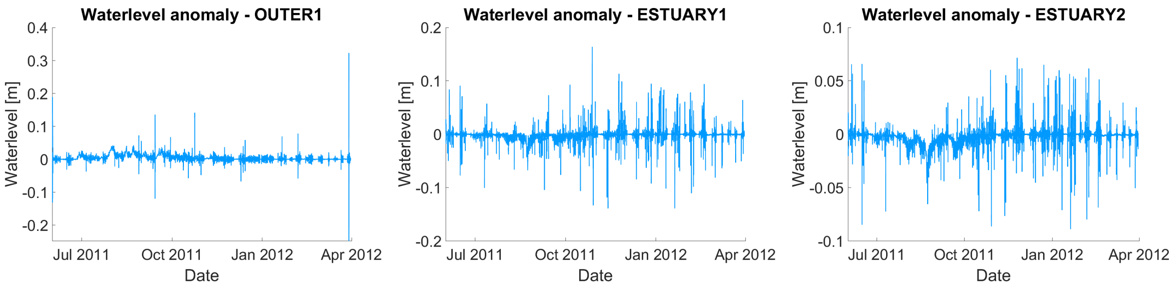

Figure F.1: Waterlevel anomaly at observation point OUTER1 (left), ESTUARY1 (centre) and ESTUARY2 (right)

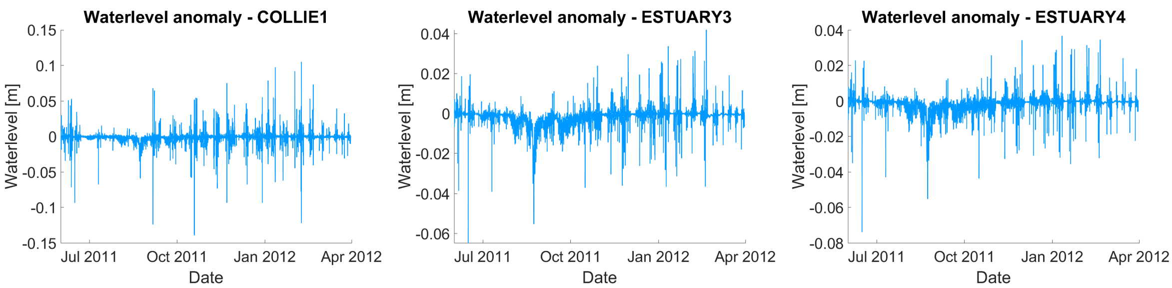

Figure F.2: Waterlevel anomaly at observation point COLLIE1 (left), ESTUARY3 (centre) and ESTUARY4 (right)

F.1.2 Velocity magnitude

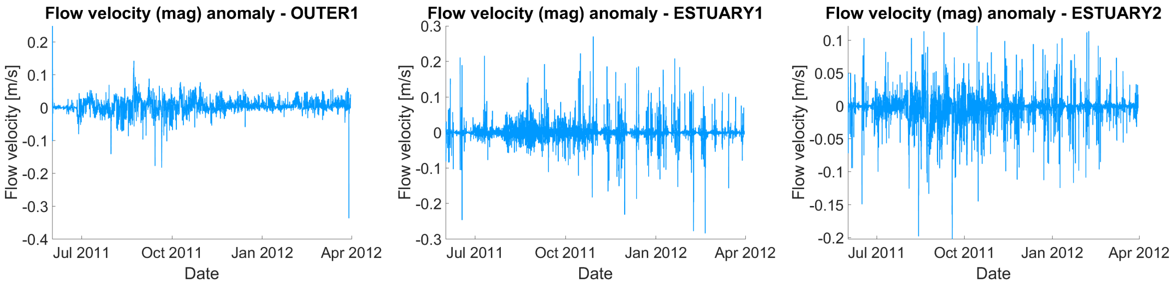

Figure F.3: Velocity magnitude anomaly at observation point OUTER1 (left), ESTUARY1 (centre) and ESTUARY2 (right)

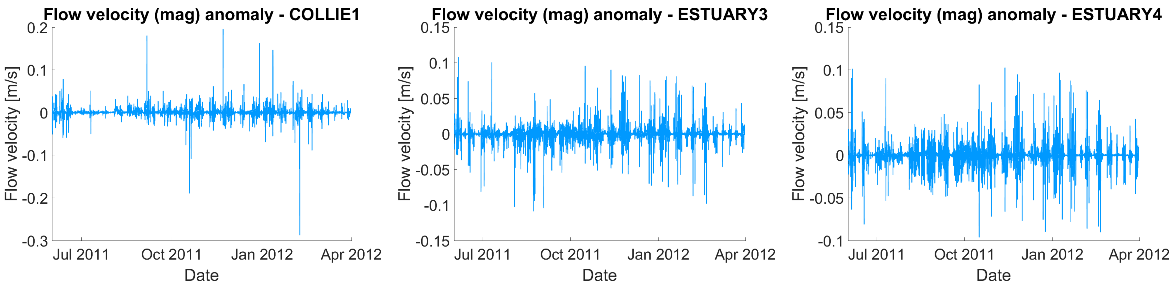

Figure F.4: Velocity magnitude anomaly at observation point COLLIE1 (left), ESTUARY3 (centre) and ESTUARY4 (right)